



Faculty of Pharmaceutical, Biomedical and Veterinary Sciences
Department of Pharmaceutical Sciences
Medicinal Chemistry

**Design, synthesis and evaluation of novel
activity-based probes and inhibitors for
trypsin-like serine proteases**

Focus on Dry eye disease (DED) and Irritable bowel
syndrome (IBS)

**Ontwerp, synthese en evaluatie van nieuwe activity-
based probes en inhibitoren voor trypsin-like serine
proteasen**

Focus op droge ogen (DED) en prikkelbare darmsyndroom (IBS)

PhD thesis submitted for the degree of doctor in pharmaceutical sciences
at the University of Antwerp to be defended by

Alba Ramos Llorca

Promotors:

Prof. Koen Augustyns

Prof. Pieter Van Der Veken

Antwerp, 2023

Members of the jury:

- Prof. dr. K. Augustyns (promotor)
- Prof. dr. P. Van Der Veken (promotor)
- Prof. dr. P. Cos (chair of the IDC and chair of the jury)
- Prof. dr. I. De Meester (internal member of the jury)
- Prof. dr. R. Leurs (external member of the jury)
- Prof. dr. S. Verhelst (external member of the jury)

Financial support:

This project has received funding from the European Union's Horizon 2020 research and innovation program under the Marie Skłodowska-Curie grant agreement No 765608 and from the Research Fund Flanders grant agreement FWO-SBO S 001017N and by the University of Antwerp SEP-BOF grant number 44875.

The cover of this doctoral thesis was designed by Dr. Clara Borràs Eroles (@lacienciaclara).

© 2023 Alba Ramos Llorca

Alle rechten voorbehouden. Niets uit deze uitgave mag worden vermenigvuldigd en/of openbaar gemaakt worden door middel van druk, fotokopie, microfilm, elektronisch of op welke andere wijze ook zonder voorafgaandelijke schriftelijke toestemming van de uitgever.

All rights reserved. No part of the publication may be reproduced in any form by print, photoprint, microfilm, electronic, or any other means without written permission from the publisher.

“Tot està per fer i tot és possible”
Everything is yet to be done and everything is possible
- *Miquel Martí i Pol, Catalan poet*

Table of contents

Table of contents	I
List of abbreviations	VII
Amino acid codes	XI
Chapter 1 Introduction	3
1.1 Proteases	3
1.2 Serine proteases	4
1.2.1 Mechanism: Peptide bond cleavage	4
1.2.2 Substrate specificity.....	5
1.3 Serine proteases in immune responses and inflammation.....	6
1.3.1 Neutrophil proteases	7
1.3.2 Mast cells proteases	8
1.3.3 Natural killer cells proteases.....	9
1.3.4 Other serine proteases.....	9
1.4 Introduction to activity-based protein profiling.....	11
1.5 Design of activity-based probes	12
1.5.1 Selectivity enhancing group or ligand and linker	14
1.5.2 Linker.....	16
1.5.3 Reporter tag.....	16
1.5.4 Warhead	19
1.6 Diphenyl phosphonate ABPs	23
Chapter 2 Objectives	29
2.1 Unraveling the potential role of serine proteases in inflammatory conditions.....	30
2.2 Design, synthesis, and characterization of activity-based probes for biomarker identification.....	31

2.3 Design, synthesis, and characterization of novel trypsin-like serine protease inhibitors	32
Chapter 3 Proteases and their potential role as biomarkers and drug targets in Dry eye disease and ocular surface dysfunction	37
3.1 Abstract	37
3.2 Introduction.....	37
3.3 Proteases and Dry eye disease.....	40
3.3.1 Matrix metalloproteases.....	41
3.3.2 Serine proteases	43
3.3.3 Cysteine proteases.....	44
3.4 Protease-activated receptors and Dry eye disease	45
3.5 Protease inhibitors and Dry eye disease.....	48
3.5.1 MMP-9 inhibitors	48
3.5.2 Serine protease inhibitors.....	48
3.6 Conclusions and Future Directions/Perspectives	51
Chapter 4 Serine proteases and their potential role as biomarkers and therapeutic targets of Irritable bowel syndrome.....	57
4.1 Irritable bowel syndrome and visceral hypersensitivity	57
4.2 Serine proteases in IBS and visceral hypersensitivity	59
4.3 Protease-activated receptors (PARs) in visceral hypersensitivity in IBS.....	60
4.4 Serine proteases inhibitors in IBS and visceral hypersensitivity.....	61
4.5 Conclusions.....	64
Chapter 5 The proof of concept: the inhibitor UAMC-00050.....	69
5.1 Introduction.....	69
5.1.1 Dry eye disease and UAMC-00050	70
5.1.2 Irritable bowel syndrome and UAMC-00050.....	71
5.2 Results and discussion.....	72
5.2.1 Up-scaled chemical synthesis.....	72

5.2.1 Evaluation of UAMC-00050 enantiomers.....	74
5.3 Conclusions and future perspectives.....	76
5.4 Experimental section	77
5.4.1 Chemistry.....	77
5.4.2 Development of biochemical protocols	80
Chapter 6 Chemically diverse activity-based probes with unexpected inhibitory mechanisms targeting trypsin-like serine proteases	95
6.1 Abstract.....	95
6.2 Introduction	96
6.3 Results and discussion	99
6.3.1 Chemical synthesis.....	99
6.3.2 Biochemical characterization	105
6.3.3 Labeling and detection of recombinant proteases.....	119
6.3.4 Labeling of mast cell supernatants and functional proteomic profiling.....	121
6.4 Conclusions	122
6.5 Experimental section	124
6.5.1 Chemistry.....	124
6.5.2 Determination of IC_{50} values.....	153
6.5.3 Kinetic experiments and determination of k_{app} , K_1 , and K_i^*	155
6.5.4 Determination of inhibition type	156
6.5.5 Labeling and detection of recombinant proteases.....	156
6.5.6 Primary human mast cells culture	156
6.5.7 Mast cell degranulation assay.....	157
6.5.8 Measurement of protein concentration	157
6.5.9 Measurement of proteolytic activity	157
6.5.10 Functional proteomic profiling of mast cell supernatants.....	158
6.5.11 Detection of tryptase in mast cell supernatants.....	158
6.6 Supplementary information	160
6.6.1 Chemical synthesis.....	160

6.6.2 <i>Biochemistry evaluation</i>	169
Chapter 7 From ABPs to small molecules: novel inhibitors UAMC-0004206 & UAMC-00042067	193
7.1 Introduction.....	193
7.2 Results and discussion.....	195
7.2.1 <i>Chemistry</i>	195
7.2.2 <i>Biochemical characterization</i>	196
7.3 Conclusion and future perspectives.....	199
7.4 Experimental section.....	201
7.4.1 <i>Chemistry</i>	201
7.4.2 <i>Biochemical characterization</i>	205
7.4.3 <i>Physicochemical properties</i>	208
7.5 Supplementary data	209
Chapter 8 Conclusions and future perspectives	215
8.1 Activity-based probes for biomarker identification.....	216
8.2 Novel trypsin-like serine protease inhibitors	220
Chapter 9 Summary	225
Chapter 10 Samenvatting	233
References	241
Scientific Curriculum Vitae	281
Acknowledgments	287

List of abbreviations

A	ABP	Activity-based probes
	ABPP	Activity-based protein profiling
	ADDE	Aqueous deficient dry eye
	AMC	7-amino-4-methyl coumarin
B	BAC	Benzalkonium chloride
	BBI	Bowman-Birk inhibitors
	Boc	<i>tert</i> -butyloxycarbonyl group
C	CatG	Cathepsin G
	ChTryp	Chymotrypsin
	ClpP	Caseinolytic protease proteolytic subunit
	CTLs	Cytotoxic T lymphocytes
	CyA	Cyclosporin A
D	DCM	Dichloromethane
	DED	Dry eye disease
	DEWS	Dry eye workshop
	DMP	Dess martin periodinane
	DPP	Diphenyl phosphonate
	DRGs	Dorsal root ganglia
E	ECM	Extracellular matrix
	EDE	Evaporative dry eye
	ELISA	Enzyme-linked immunosorbent assay
	eq.	Equivalents
F	FDA	Food and Drug Administration
	FP	Fluorophosphonate
G	GPCR	G protein-coupled receptor
	GrA	Granzyme A

H	HCE	Human corneal epithelial cells
	HPLC	High-performance liquid chromatography
	HRMS	High-resolution mass spectrometry
	HyCoSuL	Hybrid combinatorial substrate library
	Hz	Hertz

I	i.c	Intracolonic
	i.p	Intraperitoneal
	IBS	Irritable bowel syndrome
	IBS-C	Irritable bowel syndrome – constipation
	IBS-D	Irritable bowel syndrome – diarrhea
	IBS-M	Irritable bowel syndrome – mixed
	IBS-U	Irritable bowel syndrome – untyped
	IC ₅₀	Half-maximal inhibitory concentration
	ICAM-1	Intracellular adhesion molecule-1
	ICAT	Isotope-coded affinity tag labeling
	IEC	Ion-exchange chromatography
	IL	Interleukin
	IMC	Imaging mass cytometry
	INF	Interferon
	IP ₃	Inositol 1,4,5-triphosphate
	Irrev.	Irreversible inhibition
	IT-DED ³	Integrated Training of Dry Eye Disease Drug Development
	iTRAQ	Isobaric tag for relative and absolute quantitation

J	JNK	C-Jun N-terminal kinase
----------	-----	-------------------------

K	K ₁	Slow-binding first step equilibrium constant
	k _{app}	Apparent second-order rate constant
	KI*	Overall slow-binding equilibrium constant
	KLK	Kallikreins
	K _m	Michaelis-Menten's constant

	KO	Knock-out
	k_{obs}	Observed rate constant of inactivation
	k_{off}	Off rate constant
L	LFA	Lymphocyte function-associated antigen
	LIOS	Latvian Institute of Organic Synthesis
M	MAPK	Mitogen-activated protein kinase
	MGD	Meibomian gland dysfunction
	MMP	Matric metalloprotease
	MS	Mass spectrometry
N	NE	Neutrophil elastase
	NET	Neutrophil extracellular trap
	NF κ B	Nuclear factor kappa beta
	NK	Natural killer cells
	NMR	Nuclear magnetic resonance
	NSP4	Neutrophil serine protease 4
	NSSDE	Non-Sjögren syndrome dry eye
O	OSDI	Ocular surface disease index
P	PAI	Plasminogen activator inhibitors
	PAR	Protease-activated receptor
	PBMC	Peripheral blood mononuclear cells
	PBS	Phosphate buffer saline
	PET	Positron emission tomography
	PIP ₂	Phosphatidylinositol 4,5-bisphosphate
	pNA	<i>para</i> -nitroaniline
	ppm	Part per million
	PR3	Proteinase-3
	PS-SCL	Positional scanning synthetic combinatorial libraries
R	Rev.	Slow-binding reversible inhibition

S	SBTI	Soybean trypsin inhibitor
	SERPINA3K	Serine protease inhibitor A3K
	SILAC	Stable isotope labeling by amino acids in cell culture
	SPECT	Single photon emission calculated tomography
	SSDE	Sjögren syndrome dry eye

T	TCEP	Tris(2-CarboxyEthyl)Phosphine
	TFAA	Trifluoroacetic anhydride
	TFOS	Tear Film and Ocular Society
	THF	Tetrahydrofuran
	TIMPs	Tissue inhibitors of MMPs
	TLC	Thin-layer chromatography
	TNBS	2,4,6-trinitrobenzene sulphonic acid
	TNF	Tumor necrosis factor
	tPA	Tissue-type plasminogen activator

U	UAMC	Laboratory of Medicinal Chemistry University of Antwerp
	uPA	Urokinase plasminogen activator
	uPAR	uPA receptor
	UPLC	Ultra high performance liquid chromatography

V	VMR	Visceromotor response
----------	-----	-----------------------

Amino acid codes

A	Ala	Alanine
C	Cys	Cysteine
D	Asp	Aspartic acid
E	Glu	Glutamic acid
F	Phe	Phenylalanine
G	Gly	Glycine
H	His	Histidine
I	Ile	Isoleucine
K	Lys	Lysine
L	Leu	Leucine
M	Met	Methionine
N	Asn	Asparagine
P	Pro	Proline
Q	Gln	Glutamine
R	Arg	Arginine
S	Ser	Serine
T	Thr	Threonine
V	Val	Valine
W	Trp	Tryptophan
Y	Tyr	Tyrosine

CHAPTER 1

INTRODUCTION TO SERINE PROTEASES AND
ACTIVITY-BASED PROBES

Chapter 1 Introduction

1.1 Proteases

Proteases, also known as proteolytic enzymes, catalyze the hydrolysis of peptides or proteins by cleaving peptide bonds, thereupon releasing amino acids or smaller peptides. These are encoded by about 2 to 4% of the total genes in all kinds of organisms.¹ Proteolytic enzymes greatly interest biomedical research due to their involvement in many physiological processes. Proteases are present among others in cell-cycle regulation, cell death, wound healing, food digestion, and immune and inflammatory responses.^{2,3} Noteworthy, peptide bond cleavage is an irreversible process and must be highly regulated. In a healthy organism, protease activity is controlled at three levels: (i) expression, (ii) activation by post-translational modifications, and (iii) endogenous inhibitors.⁴ Protease dysfunction can play a role in different pathologies.⁵

Based on different criteria, proteases can be classified into diverse groups. The broadest classification clusters proteases based on the position of the cleaved peptide bond into two major groups: exopeptidases and endopeptidases. Exopeptidases exclusively cleave peptide bonds from the N-terminal or C-terminal end, known as aminopeptidases and carboxypeptidases, respectively.⁶ Conversely, endopeptidases cleave any bond within the target molecule. However, the most widely used classification of peptidases is based on their catalytic mechanism.⁷ The proteases are grouped based on the catalytic element present in the active site. Following this principle, they divide into seven types: serine, cysteine, threonine, aspartic, glutamic, metallo- and asparagine. Both metallo- and serine proteases are the most abundant types.⁸

This research has focused on the potential role of serine proteases in Dry Eye Disease (DED) and Irritable Bowel Syndrome (IBS). Both disorders are characterized by the activation of immune pathways and the release of pro-inflammatory mediators. Therefore, the

following sections will highlight the role of serine proteases in immune responses and inflammation.

1.2 Serine proteases

Serine proteases are essential in many physiological processes and have been widely studied by drug discovery researchers. This family accounts for over 40% of all proteases described in humans.⁹ Most serine proteases share an active site formed by a catalytic triad, in which the primary amino acid and nucleophile is a serine. An aspartate and a histidine accompany the serine. However, serine proteases evolved through time, and different families with distinctive catalytic triads can be distinguished. Following the MEROPS classification, the families are built based on sequence similarity. Up to the date of writing (July 2022), 85 families have been described for the serine proteases. The S1 family is the most prominent family, populated entirely by endopeptidases.^{2,10} Chymotrypsin was the first protease belonging to the S1 family, which structure was determined in 1967 by Matthews B.W. *et al.*¹¹ Consequently, most research papers take its sequence numbering as a model. Accordingly, the amino acids corresponding to the catalytic triad are Asp102, His57, and Ser195.¹² Likewise, this numbering will be used in this thesis.

1.2.1 Mechanism: Peptide bond cleavage

The mechanism of peptide bond cleavage catalyzed by serine proteases is characterized by two phases: acylation and deacylation (**Figure 1.1**). First, during the acylation process, the catalysis of the peptide bond cleavage occurs due to enhancing the Ser195 nucleophilicity by hydrogen bond interactions with Asp102 and His57. Then, there is a nucleophilic attack by the serine hydroxyl on the carbonyl of the substrate forming a tetrahedral intermediate. The oxyanion hole, formed by backbone amides of Gly193 and Ser195, helps stabilize the tetrahedral intermediate. In the following step, the tetrahedral intermediate is broken, leading to a primary amine displacement and formation of the acyl-enzyme complex. The

amine displacement is possible due to a hydrogen transfer from the imidazolium ion of His57 to the substrate amide. Subsequently, during the deacylation process, a water molecule interacts with His57 allowing the formation of a second tetrahedral intermediate. In the last step, a carboxylic acid is formed, and the catalytic triad is regenerated.¹³

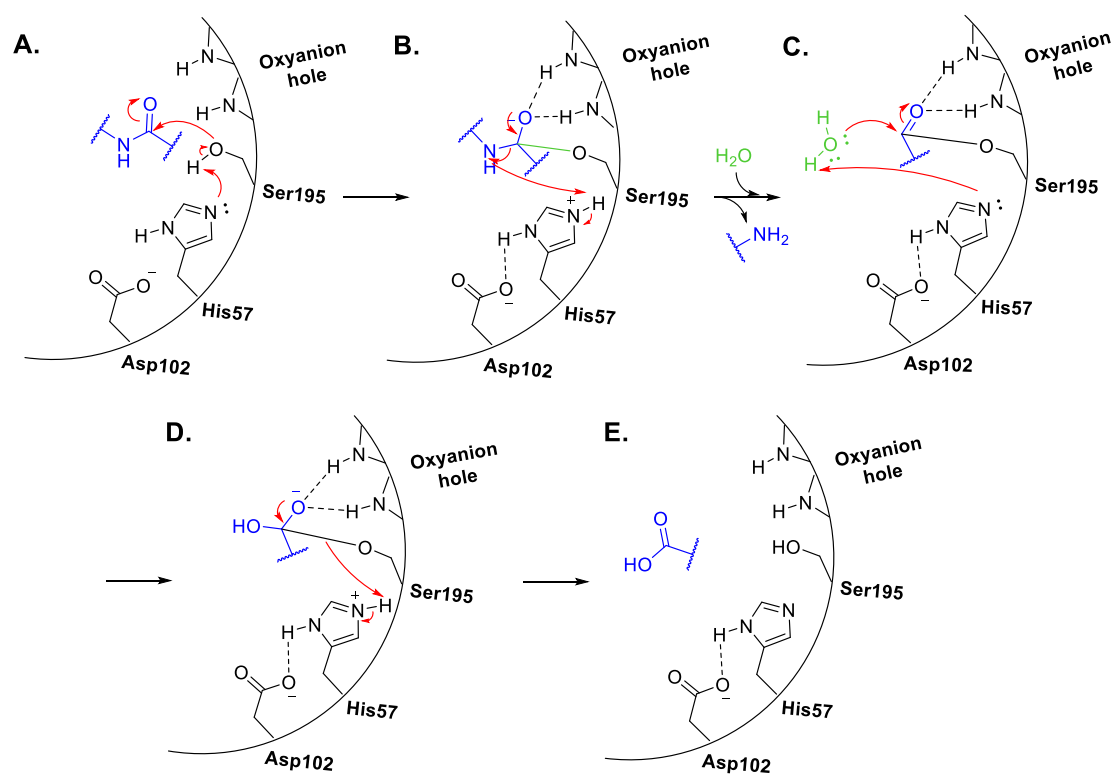


Figure 1.1 Peptide bond cleavage mechanism catalyzed by the serine protease catalytic triad.

1.2.2 Substrate specificity

Although the serine protease S1 family shares the same peptide bond cleavage mechanism, they can be further classified by their substrate specificity. The specificity of a serine protease is determined by the preferred amino acid sequence that will fit into the specificity pocket of the active site, also known as P1.¹⁴ There are three main subfamilies: trypsin-, chymotrypsin-, and elastase-like serine proteases. Amino acid 189, placed at the bottom of the P1 pocket, is crucial for specificity between trypsin- and chymotrypsin-like serine proteases. An Asp189 in the trypsin-like proteases shifts the specificity towards positively charged residues such as Arg or Lys. In contrast, chymotrypsin-like proteases prefer hydrophobic amino acids due to their interaction with Ser189. Consistently, at the

entrance of the P1 pocket in the first two subfamilies, there are Gly216 and Gly226. However, elastase-like proteases have bulkier amino acids, generally Val216 and Thr226. Therefore, the specificity of the last subfamily is shifted towards small and non-polar residues, such as Val or Ala (**Figure 1.2**).¹⁵

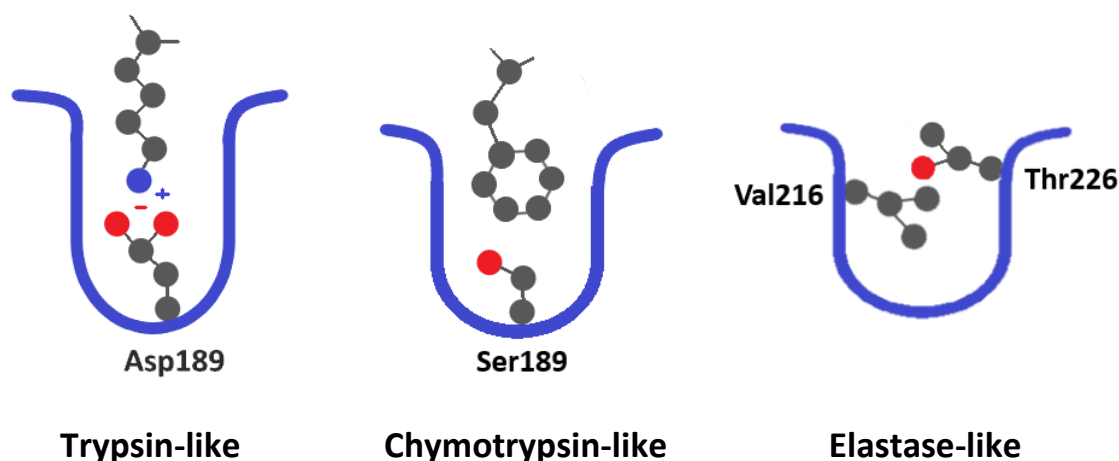


Figure 1.2 Serine proteases differ in their amino acid specificity. Trypsin-like proteases prefer positively charged residues, chymotrypsin-like proteases prefer hydrophobic residues, while elastase-like proteases prefer small non-polar residues.

1.3 Serine proteases in immune responses and inflammation

Serine proteases are involved in different physiological processes related to immune responses, such as inflammation, tissue remodeling, programmed cell death, or pathogen clearance.¹⁶ Most serine proteases are expressed as zymogens or inactive forms and activated *a posteriori*.¹⁷ Moreover, the activity of serine proteases is typically regulated by endogenous serine protease inhibitors, known as serpins. Serpins are proteins with a well-conserved structure. However, they can undergo genetic mutations which impede their function.¹⁸

Due to the involvement of serine proteases in human pathologies, they have been considered potential biomarkers and drug targets for different pathologies such as cancer, lung, cardiovascular, or intestinal disorders.¹⁶ This research will focus on the role of serine proteases in inflammation and immune responses. An in-depth discussion on the potential

role of serine proteases as biomarkers and therapeutic targets is provided in **Chapter 3** (DED) and **Chapter 4** (IBS).

Some serine proteases are directly expressed in cells of the immune system (**Figure 1.3**). For example, tryptase and chymase in mast cells, neutrophil proteases in neutrophils, and granzymes in natural killer cells (NK) and cytotoxic T lymphocytes (CTLs). Furthermore, proteases are supplied by the pancreas, epithelium, or macrophages.¹⁹

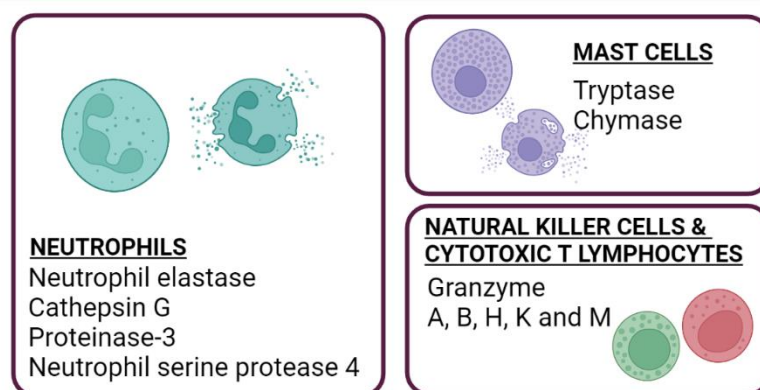


Figure 1.3 Serine proteases are directly released by immune cells. Neutrophil elastase, cathepsin G, proteinase-3, and neutrophil serine protease 4 by neutrophils; tryptase and chymase by mast cells; and granzymes by natural killer cells and cytotoxic T lymphocytes.

The following sections discuss the different proteases released by immune cells and their roles in immunity and inflammation. Further details are given for those proteases mentioned later in the following chapters.

1.3.1 Neutrophil proteases

Neutrophils are one of the first immune cells to arrive at the site of inflammation. These immune cells express different serine proteases, primarily neutrophil elastase (NE), cathepsin G (CatG), proteinase-3 (PR3), and neutrophil serine protease 4 (NSP4), and in a minor quantity, granzyme A (GrA).²⁰ Proteases are secreted to the medium upon neutrophil degranulation.²¹ However, protease activity is further regulated by post-translational modifications and zymogen activation.²² Neutrophil proteases are essential for defending the organism against bacterial infections by forming neutrophil extracellular traps (NETs).

Additionally, neutrophil proteases play a role in the degradation of extracellular matrix (ECM) components, activation of pro-inflammatory cytokines, and increased permeability in epithelial cells.^{23,24} Further, in this thesis, NE and CatG are mentioned giving special attention to CatG.

In human, CatG has simultaneous trypsin- and chymotrypsin-like substrate specificity. Thus, it has a preference for Lys and Arg and also Phe in P1. However, its preference lies more toward large hydrophobic residues.²⁵ Apart from activating pro-inflammatory cytokines and chemokines, CatG promotes inflammation by activating cell surface receptors such as protease-activated receptor (PAR)-2 and PAR-4.²³ More details about PARs will be given later in this thesis. Last, CatG is related to several autoimmune diseases, such as rheumatoid arthritis or type 1 diabetes mellitus patients.²⁶

1.3.2 Mast cells proteases

Mast cells are immune cells related to allergic reactions due to the efflux of histamine upon activation. Their degranulation occurs by different stimuli, especially by high-affinity IgE cross-linking.²⁷ Upon release of histamine and heparin, blood vessels are dilated, and inflammation is induced. Moreover, they are also related to wound healing and pathogen defense.²⁸ Trypsin and chymase are the two main serine proteases stored in mast cells. However, other non-specific mast cell serine proteases are also stored, including CatG.^{29,30}

Trypsin is a trypsin-like serine protease, thus, its P1 specificity is for Arg and Lys. Noteworthy, its specificity overlaps with other trypsin-like serine proteases such as trypsin and challenges the design of highly selective inhibitors.³¹ The structure of trypsin is formed by four monomers placed in a rectangular frame with the four active sites facing a central pore. Trypsin activity is only present when the tetramer structure is established and normally stabilized by heparin.³² There are two main types of trypsin, α -trypsin and β -trypsin.³³ However, only β -trypsin is released in its active form upon degranulation. Trypsin plays a role in the degradation of ECM components, the expression and secretion

of inflammatory chemokines and cytokines, and the migration and activation of immune cells.³⁴ Furthermore, tryptase also acts as a signaling molecule by activating PARs.³⁵ As previously mentioned, the presence of tryptase activity has been commonly correlated with allergic reactions. Moreover, it is considered to play a pro-inflammatory role in pulmonary conditions such as asthma.³⁶ It has also been associated with kidney, cardiovascular, and intestinal diseases or autoimmune diseases such as multiple sclerosis or arthritis.^{37–40}

1.3.3 Natural killer cells proteases

NK and CTLs are responsible for defending the organism by killing infected cells. One of their mechanisms of apoptosis induction is mediated by their granule-associated enzymes, known as granzymes.⁴¹ Degranulation of NK and CTLs occurs upon recognition of an infected cell, thereupon releasing granzymes and perforin, which assist the delivery of granzymes into the infected cell.⁴² Among the five released granzymes, GrA with trypsin-like specificity is the most studied.⁴³ It has been suggested that GrA plays a pro-inflammatory role by releasing cytokines or remodeling ECM components.^{44,45} Its presence has been described not only in microbial infections but also in rheumatoid arthritis, several inflammatory lung diseases, or celiac disease.^{46–50}

1.3.4 Other serine proteases

This section mentions other trypsin-like serine proteases used during this PhD thesis.

1.3.4.1 *Trypsin*

Trypsin is a pancreatic protease that gives name to the trypsin-like serine protease family. In humans, the pancreas secretes three types of trypsin: trypsin-1, trypsin-2, and trypsin-3. The three isoforms are structurally similar. Nevertheless, trypsin-3 is resistant to endogenous trypsin inhibitors such as soybean trypsin inhibitor (SBTI) and α 1-antitrypsin inhibitor.^{51,52} In addition to its digestive role, trypsin can activate pro-enzymes and is crucial in wound healing by helping detach adherent cells.⁵³ However, dysregulation of trypsin

levels has been associated with some disorders. For example, it has been described as a specific biomarker in pancreatitis, cystic fibrosis, and biliary cirrhosis.^{54–56}

1.3.4.2 *Thrombin*

Thrombin plays pivotal roles in the coagulation cascade. It is synthesized by the liver and secreted to the circulation as a zymogen, known as prothrombin, activated by the prothrombinase complex.⁵⁷ As part of the coagulation cascade, thrombin has two major and antagonistic functions. First, it is a procoagulant factor by converting fibrinogen into fibrin clots. Opposite, it acts as an anticoagulant through activation of protein C.⁵⁸ Moreover, it can activate cellular responses by activating PAR receptors. However, upregulated thrombin activity has been correlated with cardiovascular and neurodegenerative diseases or intestinal disorders.^{59–62}

1.3.4.3 *Urokinase plasminogen activator*

Urokinase plasminogen activator (uPA) is a trypsin-like serine protease belonging to the plasminogen activator system together with tissue-type plasminogen activator (tPA), the uPA receptor (uPAR), and plasminogen activator inhibitors (PAIs).⁶³ The expression and secretion of uPA occur in different human cell types. Its role is related to cell migration and tissue remodeling. Furthermore, uPA can activate uPAR, which activates MMPs and leads to the degradation of ECM components. Also, it activates signaling cascades by converting plasminogen into plasmin.⁶⁴ Generally, it has been of interest as a therapeutic target for many cancer types for its role in promoting tumor growth.⁶⁵ Additionally, uPA is of interest in other diseases such as chronic dermal ulcers or rheumatoid arthritis.^{66,67}

1.4 Introduction to activity-based protein profiling

Proteomics is the large-scale characterization and analysis of proteins in cells, tissue, or organisms. The aim is not restricted to identifying proteins but includes studying their location and function.^{68,69} Most proteomic techniques focus on the expression, location, and function of the studied proteins. For instance, traditional methods, such as two-dimension gel electrophoresis coupled to mass spectrometry (MS) or chromatography-based methods, such as ion-exchange chromatography (IEC), were later complemented by other methods suitable for high-throughput screening.⁶⁸ For example, protein microarrays were implemented for protein expression analysis, but exploring the function remained challenging.⁷⁰ Other techniques such as isotope-coded affinity tag labeling (ICAT), stable isotope labeling with amino acids in cell culture (SILAC), or isobaric tag for relative and absolute quantitation (iTRAQ) were developed for quantitative proteomics.^{71,72} However, protein expression does not take into account protein activity. Post-translational modifications, such as zymogen activation or interaction with other proteins or small molecules, regulate the activity of proteins.¹⁴ Therefore, there was a lack of tools able to study active proteins rather than their expression. Hence, activity-based protein profiling (ABPP) was designed to overcome this problem and distinguish between active and inactive proteins.⁷³ During the last decades, it has been used for different families of enzymes but especially proved to be effective for studying proteases.⁷⁴

ABPP uses chemical probes, known as activity-based probes (ABP), which react covalently with the active form of the target enzyme. These allow detection, visualization, or affinity purification of the labeled enzymes (**Figure 1.4**).⁷⁵ The applications of ABPs include identifying enzyme targets, visualization *in vivo*, and discovering biomarkers or new inhibitors.^{76–78}

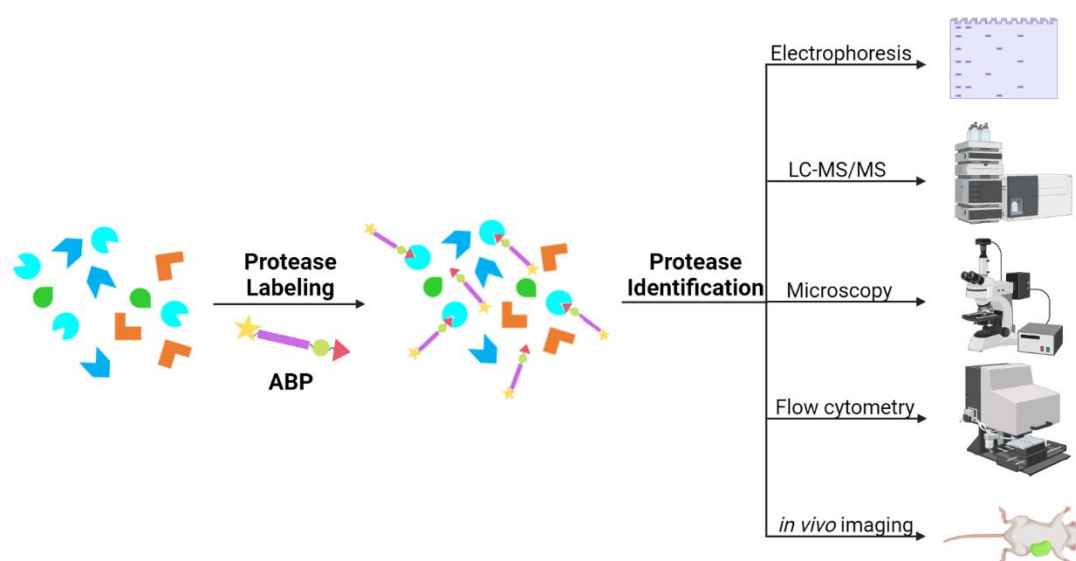


Figure 1.4 General representation of protease labeling with an activity-based probe and the different analysis methods that can be used depending on the reporter tag.

1.5 Design of activity-based probes

The general structure of an ABP consists of four parts: (i) a selectivity enhancing group that targets a specific enzyme family; (ii) a reporter tag used for visualization or isolation, (iii) a warhead or reactive group; and (iv) a linker to connect the three other components.^{79,80} A representation of the general structure is depicted in **Figure 1.5**. The following section aims to develop each part by giving specific examples of developed ABPs targeting trypsin-like serine proteases, and several published ABPs are depicted in **Figure 1.6**.

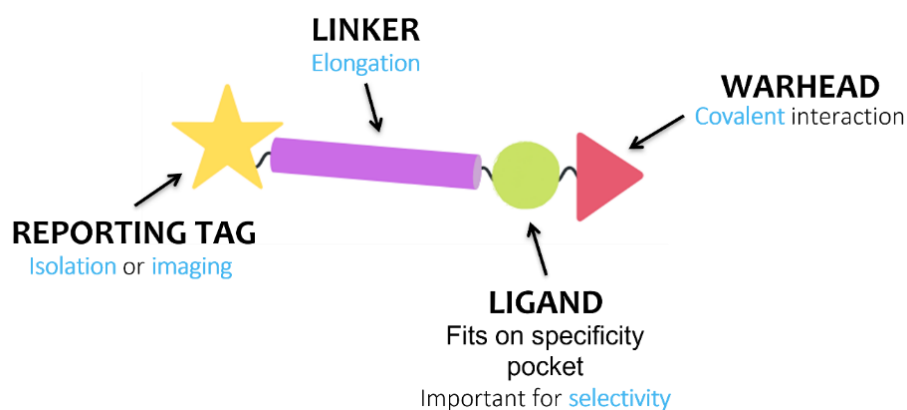


Figure 1.5 Activity-based probe (ABP) – General structure

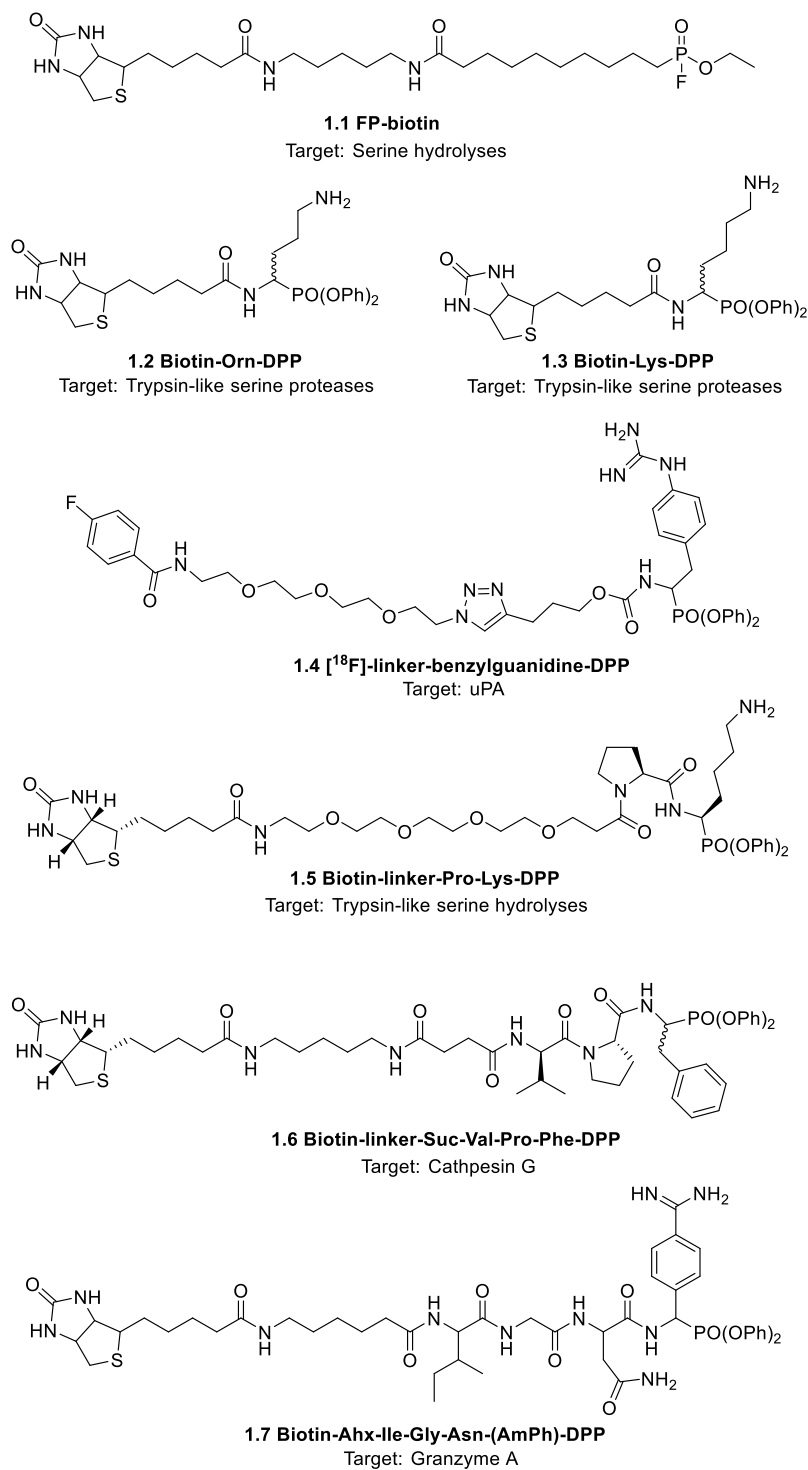


Figure 1.6 A selection of previously reported ABPs with electrophilic phosphorus and their target enzymes. The stereochemistry shown is based on the source literature.

1.5.1 Selectivity enhancing group or ligand and linker

The selectivity enhancing group allows the ABP to target a protease or a family of proteases. Structural elements are added to increase the affinity of the probe for the active site of the targeted enzyme.⁸¹ Most ABPs, previously reported, are based on a short peptidic sequence mimicking the protease substrate specificity.⁸² Moreover, the ligand design allows to achieve different degrees of selectivity. Thus, ABPs with a higher selectivity will target specifically one protease. In contrast, broad selectivity ABPs can be used to label a wide range of proteases simultaneously, for example, a specific protease family.⁸³

As mentioned previously, even though serine proteases share the same peptide hydrolysis mechanisms, different subfamilies can be distinguished when focusing on the selectivity pockets, as depicted in **Figure 1.2**. Moreover, the area surrounding the active site and the P1 pocket is formed by other subpockets or fingerprints (P2, P3, P4, etc.) (**Figure 1.7**).⁸⁴ These are characteristic of each protease and are critical to achieving selectivity in a specific family (e.g., for trypsin over other trypsin-like serine proteases). When designing ABPs resembling the peptidic chain, frequently, these incorporate the amino acids from the substrate specificity of the protease under study.⁸⁵ However, when ABPs do not mimic the peptide structure, it is more challenging to achieve selectivity.⁸⁶ Later in this research, we will focus on peptidic ABPs.

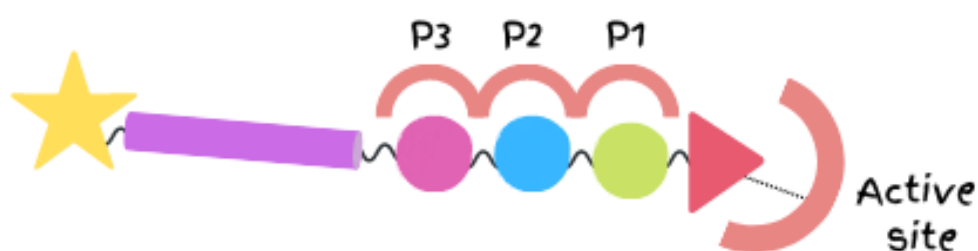


Figure 1.7 Schematic representation of an activity-based probe (ABP) with an enhancing selectivity peptidic chain fitting in the P1 pocket and P2 and P3 subpockets

The first ABPs targeting serine proteases showed a broad reactivity, as it was designed to target serine hydrolases, including proteases and esterases, lipases, and amidases.^{87–89} These probes did not have a selectivity enhancing group, and their wide-ranging reactivity generated complex activity profiles, sometimes difficult to analyze (**1.1**). Later, the peptidic ABPs were designed with natural amino acids as enhancing selectivity moieties. For instance, lysine and ornithine were widely used to target trypsin-like serine proteases (**1.2-1.3**).^{90,91} Haedke *et al.* created an ABP library with different substrate specificities to target trypsin, chymotrypsin, and elastase-like proteases.⁹² Recently, Ferguson *et al.* designed ABPs for trypsin-like serine proteases based on an arginine moiety targeting the P1 pocket.⁹³ Alternatively, non-natural amino acids mimicking substrate specificity can be used. For example, Ides *et al.* introduced benzyl guanidine as a basic polar moiety in P1 to target uPA (**1.4**).⁹⁴

Pan *et al.* included ABPs targeting the P2 pocket. They suggested that the incorporation of the P2 element enhances selectivity and potency. Introducing a P2 proline to a lysine probe increased the overall inhibitory potency (**1.5**), while an asparagine resulted in selectivity towards trypsin.⁹¹ To target specifically one protease, longer peptidic ABPs have been reported. Grzywa *et al.* developed ABPs targeting neutrophil proteases with diverse peptidyl chains. An ABP with the sequence Tag-Linker-Suc-Val-Pro-Phe^P(O-C₆H₅)₂ (**1.6**) achieved absolute selectivity for CatG over NE and PR3.⁹⁵ Recently, Lovell *et al.* reported selective ABPs for different families of kallikreins (KLK). These probes consisted of small peptides which included non-natural amino acids, such as phenyl guanidine, to mimic arginine.⁹⁶

Achieving selectivity for one protease by substrate specificity is challenging due to the close resemblance and overlap between closely correlated proteases.⁹⁷ Several techniques have been described to elucidate the substrate specificity of related proteases. For example, scanning all the natural amino acids in a specific position while maintaining the rest unvaried. This technique is known as Positional Scanning Synthetic Combinatorial Libraries (PS-SCLs).⁹⁸ Later, this approach was expanded to unnatural amino acids. This method is

called Hybrid Combinatorial Substrate Library (HyCoSuL).⁹⁹ These techniques could elucidate specific characteristics of a targeted protease to design selective ABPs.

1.5.2 Linker

The linker or spacer adds separation between the warhead and the reporter tag. The primary function of the linker is to avoid steric hindrance between the different parts of the probe. Structurally, the linker can chemically differ from a simple alkyl chain to more complex polyethyleneglycol chains with different lengths.⁷⁴

The 6-aminohexanoic acid linker has been used to develop ABP targeting different serine proteases. For example, Kasperkiewicz *et al.* developed ABP targeting neutrophil proteases with a long alkyl chain as a linker.¹⁰⁰ Likewise, Kolt *et al.* and Mahrus *et al.* designed probes targeting GrA (**1.7**).^{101,102} Because of the high hydrophobicity of the linker, these probes lack good solubility and cell permeability. Alternatively, the use of polyethyleneglycol chains can help to overcome this problem. Ferguson *et al.* recently reported ABPs targeting trypsin-like serine proteases with a linker formed by four ethylene glycol moieties.⁹³ Other linker approaches include the use of small amino acid sequences. However, this can interfere with the specificity of the probe. For example, Kahler *et al.* used a three amino acid linker with an ABP targeting serine proteases.¹⁰³

1.5.3 Reporter tag

The reporter tag enables the detection and visualization of the targeted proteases and enrichment purification and identification of the labeled protease. The selection of the reporter tag will influence the analytical technique used for detection. Thus, different tags are used depending on the end application of the ABP. Three main reporter tags are commonly used in ABPP: fluorophores, radioisotopes, and affinity tags. The three can be used to visualize labeled proteases in SDS-PAGE electrophoresis. However, while fluorophores are used in microscopy and flow cytometry, radioisotopes are widely used for *in vivo* detection.¹⁰⁴ On the other hand, affinity tags are used for protein isolation and

identification. The most commonly used affinity tag is biotin, which can be used in avidin pull-down assays.¹⁰⁵ The biotinylated labeled proteases are bound to streptavidin beads and eluded for SDS-PAGE or LC-MS/MS analysis.¹⁰⁶ Because of the strong interaction of biotin and the streptavidin beads, harsh conditions are needed for elution or digestion. Usually, part of the labeled proteases are discarded, and contaminants such as natural biotinylated proteins are found in the final samples.⁸¹ Desthiobiotin can be used instead. This is a non-sulfur biotin analog with a lower affinity for streptavidin. Therefore, the conditions needed for dissociation are more suitable for the stability of the enzymes, and fewer contaminants are present in the final sample.^{107,108}

Radioisotopes can be used for positron emission tomography (PET) or single photon emission calculated tomography (SPECT).^{94,109} For example, the radiolabeled [¹⁸F] probe (1.5) developed by Ides *et al.* targeting uPa was evaluated by *ex vivo* and *in vivo* PET imaging. It showed promising results in a human breast cancer model.⁹⁴ Other radioisotopes used in ABPs include ¹²⁵I, ³H, and ¹¹¹In. Unfortunately, the half-life time of radioisotopes reduces their applications significantly. Alternatively, stable isotopes can be used as reporter tags. Poreba *et al.* used stable metal isotope probes analyzed by mass cytometry and imaging mass cytometry (IMC) to study human neutrophil elastase.¹¹⁰ Another technique to quantify stable isotope labeled probes is SILAC.¹¹¹

Fluorophores are widely used as reporting tags. There are diverse fluorophores available with different absorption and emission wavelengths. For example, fluorescent ABPs targeting serine proteases have been developed with Cy5 as a reporter tag. Cy5 is a near-infrared fluorophore suited for *in vivo* imaging. With the synthesized probes, Edgington *et al.* detected proteases in gel with complex proteomes and luminal colon fluids from a mouse acute colitis model.¹¹² The fluorophore BODIPY was used by Schulz-Fincke *et al.* to label human leukocyte elastase and visualize it in SDS-page gels.¹¹³

Even though the drawbacks of biotin as a reporter tag are mentioned previously, there are many examples of its use in ABPP. For instance, Shannon *et al.* identified several

endogenous serine proteases from the S1 family from the mouse pancreas proteome after treatment with a biotinylated sulfonyl fluoride probe and enrichment on streptavidin beads.¹¹⁴ Likewise, Haedke *et al.* developed diphenyl phosphonate probes and demonstrated their ability to be utilized for mass spectrometry target identification in rat pancreas lysates.⁹² Moreover, proteases labeled with biotin probes can be visualized by SDS-PAGE. For example, Pan *et al.* identified β -tryptase and CatG from degranulated mast cells.⁹¹

Furthermore, a reporter tag with dual functionality has been used, where a fluorescence and a biotin affinity tag allows the enrichment with avidin beads and visualization with a fluorescent scanner.¹¹⁵

Traditionally, reporter tags have been introduced by peptidic coupling. For example, Pan *et al.* used peptidic coupling to connect the enhancing selectivity moieties, targeting trypsin-serine proteases and the linker-reporter tag.⁹¹ Bulky reporter tags, especially biotin, present low cell permeability, adding challenges for their use *in vitro* or *in vivo*. Alternatively, ABPs can be designed with a smaller tag which does not influence their physicochemical properties.¹⁰⁴ Furthermore, these may allow the incorporation of the reporter tag of choice after forming the covalent bond with the enzyme. Click chemistry is used for this purpose, where the probe bears an azide or an alkyne group, and the reporter tag the complementary functionality.¹¹⁶ The Huisgen cycloaddition reaction between an azide and an alkyne occurs with copper catalysis in aqueous media. This approach allows the use of different reporter tags, as the pair azide/alkyne can be incorporated into biotin, fluorophores, or radioisotopes (**Figure 1.8**).^{116,117} This technique was first used in the field of enzyme activity profiling by Speers *et al.*, as they synthesized a rhodamine-alkyne tag clicked to an azide phenyl sulfonate ester to label glutathione S-transferases in human breast cancer lines.¹¹⁶

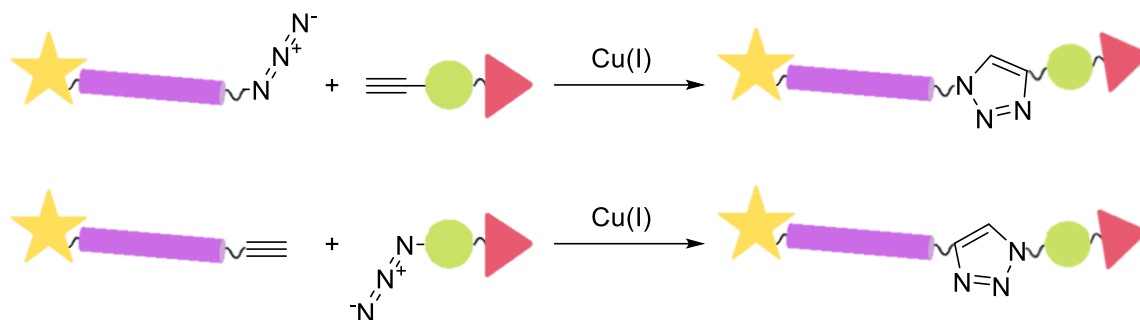


Figure 1.8 Huisgen cycloaddition reaction between an azide and an alkyne catalyzed by copper. This reaction is also known as "click chemistry". The alkyne and azide can be in both linker and selectivity-enhancing groups.

1.5.4 Warhead

The warhead can form a covalent link between the ABP and the active site of the enzyme. In designing the ABP, it is essential to consider the catalytic mechanism of the desired target enzyme. Most warheads have electrophilic character. Therefore, when targeting serine proteases, the reactive group should create a covalent interaction with the nucleophilic serine in the active site (**Figure 1.9**).¹¹⁸ The first probe designed to target serine hydrolases was based on a fluorophosphonate (FP) warhead.⁸⁷ As mentioned, FP probes have a broad reactivity with all serine hydrolase families, including proteases, lipases, esterases, and amidases. Even though FPs showed potential by reacting only with the active enzymes, they have a wide-ranging reactivity and display little selectivity. Moreover, they are highly toxic due to their interaction with acetylcholinesterase.¹¹⁹ Later, other phosphorylated ABPs were developed, such as mixed alkyl-aryl phosphonate esters, phosphoramidates, phosphinates, and α -amino diphenyl phosphonates.^{90,92,103,120} The latest nowadays is the most used warhead for serine proteases ABPs. Especially the high selectivity for this family makes it the perfect reactive group. Warheads not based on an electrophilic phosphorus have also been developed. For example, there are ABPs based on isocoumarin, oxolactams, chloromethyl ketone, sulfonyl fluorides, or sulfonyloxyphtalimides.^{86,114,121–124}

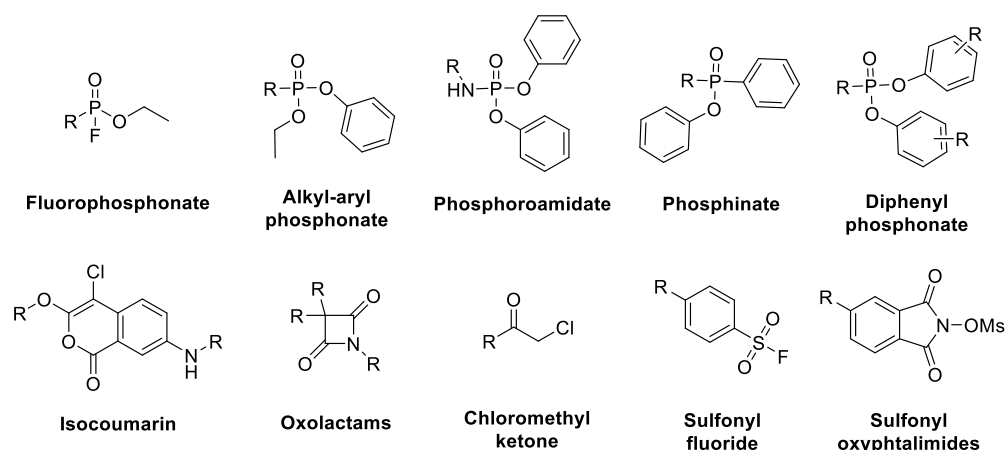


Figure 1.9 Serine protease ABPs warheads

The group of Medicinal Chemistry at the University of Antwerp (UAMC) has extensive experience developing diphenyl phosphonate inhibitors targeting different serine protease families, for example, dipeptidyl peptidases, kallikrein, caseinolytic protease proteolytic subunit (ClpP), or trypsin-like serine proteases, such as uPa.^{125–129} Moreover, several diphenyl phosphonate ABPs have also been developed for uPa.^{94,130}

1.5.4.1 Diphenyl phosphonates

α -amino diphenyl phosphonates are well-studied compounds targeting serine proteases. This warhead is highly interesting due to its lack of reactivity with other protease families, such as cysteine or threonine. Moreover, they are not reactive with acetylcholine esterases.¹¹⁸

Inhibitors bearing a diphenyl phosphonate warhead were first described by J. Oleksyszyn *et al.* in 1979, and later, many medicinal chemists got interested in these.¹³¹ Diphenyl phosphonates have improved selectivity, stability, and toxicity over other phosphorylated warheads and are efficient serine proteases inhibitors.¹³² The phosphonate warhead forms a covalent and irreversible bond with the serine of the catalytic triad, demonstrated by trypsin and thrombin X-Ray structures and a CatG crystal structure.^{133,134} The covalent bond has a tetrahedral structure resembling the peptide bond cleavage transition state described in **Figure 1.1**. Therefore, these inhibitors have been classified as transition state-analog or mechanism-based inhibitors.¹³⁵ The general structure of a diphenyl phosphonate

inhibitor is depicted in **Figure 1.10**. The selectivity enhancing group is placed at R^1 and fits into the P1 pocket. Whereas the extension of the peptidic chain and, typically, the linker and reporter tag on an ABP would be placed in R^2 . Additionally, not only the two phenoxy groups are essential to give an electrophilic character to the phosphorus atom, but also adding electron-withdrawing substituents in R^3 will increase the phosphorus electrophilicity and, therefore, the enzymatic inhibition.¹³⁶

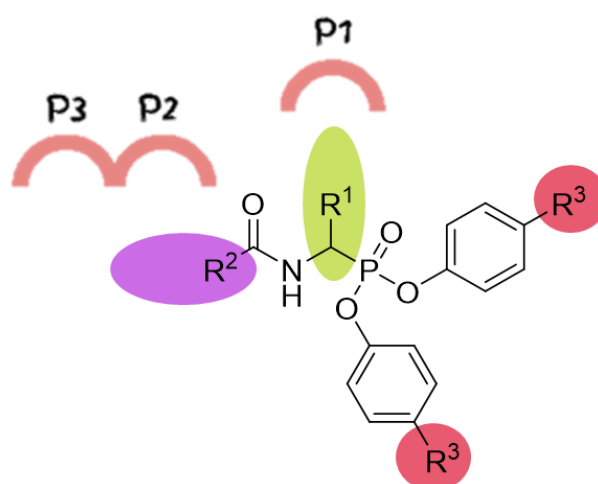


Figure 1.10 General structure of a diphenyl phosphonate inhibitor, focus on the three variable parts

The inhibitory mode of action involves the formation of a covalent bond between the electrophilic phosphorus and the serine of the enzyme catalytic triad. To begin, the serine, backed by the other two catalytic triad residues, attacks the electrophilic phosphorus. Then, by the formation of hydrogen bonds, with the oxyanion hole, the phosphonyl is stabilized. Consequently, it leads to a pentacoordinate transition state with a negatively charged phosphonyl. A phenolate will leave to recover the tetrahedral conformation, forming an irreversible covalent bond. Slowly, the enzyme-inhibitor complex will undergo aging, and the other phenolate group will hydrolyze (**Figure 1.11**).

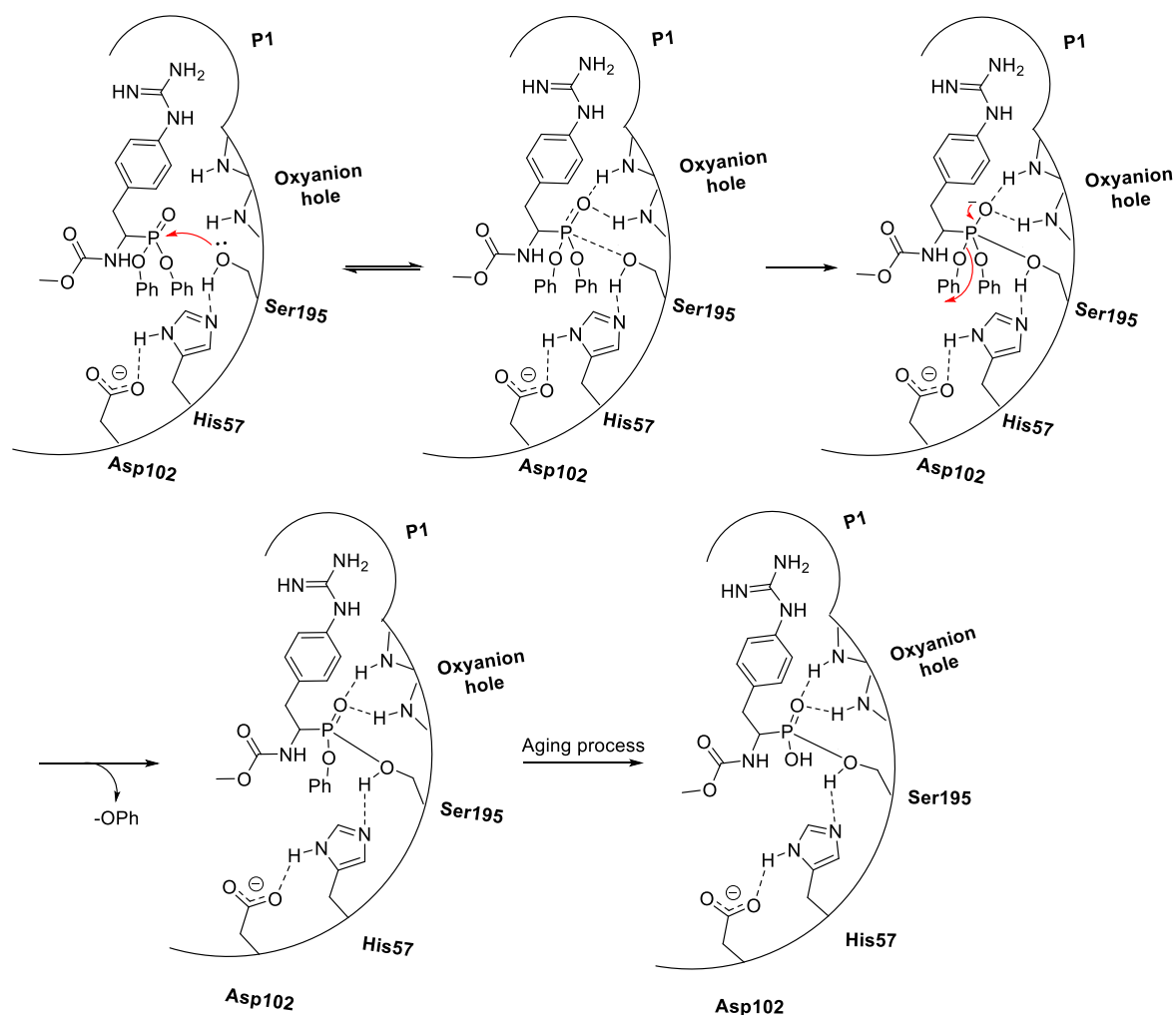
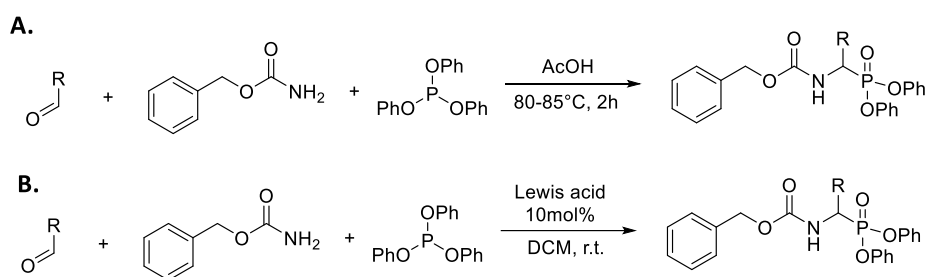


Figure 1.11 Inhibition mechanism of α -amino diaryl phosphonates, reference compound: UAMC-0000139.¹³⁷

The synthesis of α -amino diaryl phosphonates is based on a one-pot three-component reaction known as the Birum-Oleksyszyn reaction. The three components used are benzyl carbamate, an aldehyde, and triphenyl phosphite. However, over the years, different carbamates and phosphites have been used. The mechanism of the reaction required the condensation of the starting materials with acetic acid at 80-85°C (**Scheme 1.1a**). The product was isolated by crystallization in methanol. Even though the first yields described were modest, ranging from 35 to 55%.¹³¹ Later, higher yields, up to 93%, using the same conditions have been reported.^{138,139} Despite the ease of the reaction procedure and the higher yields described, there is a considerable drawback. The reaction is limited to the use of aldehydes over other carboxyls, such as ketones. Moreover, acetic acid makes the reaction inaccessible for acid-labile protecting groups. In 2005, Van Der Veken *et al.*

reported the replacement of acetic acid for a Lewis acid, such as tin chloride. The Lewis acid-catalyzed reaction can be performed at room temperature in dichloromethane (**Scheme 1.1b**). By substituting acetic acid for a Lewis acid, not only a greater yield was achieved, but also the scope of the reaction was opened to acid-labile protecting groups, for example, *tert*-butyloxycarbonyl group (Boc), and also to ketones instead of aldehydes.¹⁴⁰



Scheme 1.1 Birum-Oleksyszyn reaction. a) Initial conditions with acetic acid,¹³¹ b) Lewis acid-catalyzed reaction.¹⁴⁰

1.6 Diphenyl phosphonate ABPs

The rationale behind the first reported ABPs for serine proteases bearing a diphenyl phosphonate was the biotinylation of previously synthesized inhibitors. For example, Abuelyaman *et al.* described two peptidic inhibitors and the respective biotin ABPs targeting chymotrypsin. Surprisingly, the biotin analogs displayed higher inhibitory potencies.¹⁴¹ Likewise, Hawthorne *et al.* developed biotinylated analog compounds with ornithine (**1.2**) and lysine (**1.3**) targeting the trypsin-like serine protease family. However, the biotin was directly attached to the α -carbon by a peptide bond, and subsequently, the inhibitory potency was reduced significantly.⁹⁰ Later, these probes were improved by adding a linker by Pan *et al.*, who also incorporated proline in the P2 position. These were used to visualize recombinant proteases and proteases released from mast cells.⁹¹ The sequence Pro-Lys phosphonate has also been used with a Cy5 fluorophore for *ex vivo* and *in vivo* protease visualization in a pancreatitis model.¹¹²

Efforts have been put into developing probes targeting the different neutrophil proteases.¹⁰⁰ For example, a phosphonate tripeptide with sequence Val-Pro-Val^P(OPh-*p*-SCH₃)₂ equipped with a BODIPY tag was used for selective NE imaging by SDS-PAGE and fluorescence analysis.¹¹³ A small peptide with sequence Val-Pro-Phe phosphonate coupled with a biotin tag was reported to be a highly sensitive probe for detecting CatG in western blots and high-throughput 96-well active site-based ELISA.¹⁴² Peptidyl di(chlorophenyl) phosphonate compounds were biotinylated to act as ABPs to target PR3.¹⁴³ Kasperkiewicz *et al.* developed diphenyl phosphonate ABPs to target the latest discovered NSP4.¹⁴⁴

Studying the substrate specificity of different human granzymes, Mahrus *et al.* developed selective probes for GrA and B. The probes were small peptides targeting the subpockets P1 to P4. In the case of GrA, 4-amidinophenyl was used for P1 to target the trypsin-like specificity. These probes were used in cell assays to demonstrate the role of GrA and B in NK cell-mediated lysis of target cells.¹⁰²

The group UAMC has previously developed ABPs to target uPa with different reporter tags, including rhodamine, BODIPY, biotin, Cy5, and 4-fluorobenzamide.¹³⁰ All these probes had a benzyl guanidine moiety targeting the P1 pocket of uPa. This was also used for radiolabeling with ¹⁸F for PET imaging.⁹⁴ Later, they developed a ¹¹¹In probe with a DOTA chelator for SPECT imaging.¹⁰⁹ However, the stability and the pharmacokinetic properties of the tracers were not favorable or moderate for tumor uptake. For instance, the fluorinated probe showed slow blood clearance and low plasma stability, whereas the indium probe proved useful in two tumor models at 95 h post-injection. Unfortunately, there was a high uptake in non-invaded lymph nodes. Thus, the authors suggest the modification of the linker and visualization tag to improve the pharmacokinetic profile and stability of the tracer.⁹⁴

The diphenyl phosphonate warhead has been validated as a powerful tool for the development of potent and selective serine protease inhibitors and ABPs. Their specific reactivity with the serine in the active site and their good physicochemical and

pharmacokinetic properties endorse the use of these compounds for the detection of active proteases *in vitro* and *in vivo* assays.¹²⁸ Further development of diphenyl phosphonate ABPs targeting trypsin-like serine proteases will be discussed in **Chapter 6**.

CHAPTER 2

OBJECTIVES

Chapter 2 Objectives

As described in **Chapter 1**, proteases are abundant enzymes in all organisms and are responsible for peptide bond hydrolysis. Proteolytic activity is tightly regulated under healthy conditions. However, dysregulation is known to play a role in different pathologies, making them potential biomarkers and therapeutic targets. The first objective of this work was the study of the potential role of serine proteases, more specifically, trypsin-like serine proteases, in different inflammatory pathologies. This is described for Dry eye disease (DED) and Irritable bowel syndrome (IBS) in **Chapter 3** and **Chapter 4**, respectively. Proof of concept on the potential therapeutic role of trypsin-like serine proteases is given in **Chapter 5** by the study of previously reported inhibitor UAMC-00050. Further, this doctoral thesis in **Chapter 6** focuses on the development of an extensive library of activity-based probes (ABPs) as a tool to identify and visualize proteases in complex proteomes. Finally, novel inhibitors for trypsin-like serine proteases were developed and characterized in **Chapter 7**. The overview of the subjects covered in this doctoral thesis is depicted in **Figure 2.1**.

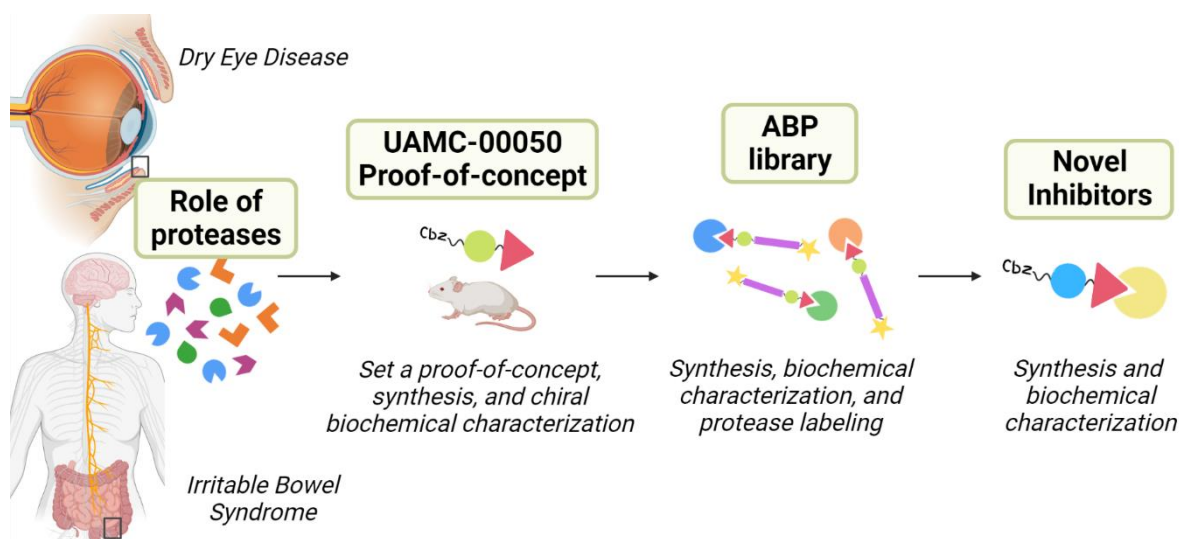


Figure 2.1 Overview of the subjects covered in this doctoral thesis

2.1 Unraveling the potential role of serine proteases in inflammatory conditions

DED is a multifactorial ocular surface disease characterized by inflammation and tissue damage.¹⁴⁵ The pathophysiology of DED is defined by the vicious cycle of DED, characterized by ocular surface disruption and hyperosmolarity. These lead to the release of pro-inflammatory cells and cytokines.¹⁴⁶ To date, the diagnosis and treatment of DED present many challenges for clinicians. Therefore, there is a need to identify new biomarkers and potential therapeutic targets. The study of proteases in DED in the last decades has been focused on the role of metalloproteases (MMPs), especially MMP-9. The involvement of MMP-9 in the pathophysiology of DED and its use as a biomarker has been widely studied.¹⁴⁷ However, studies involving other families of proteases are found in minor quantities. This study aimed to set a hypothesis on the role of different families of proteases in the pathophysiology of DED to open the possibility for new research on identifying new biomarkers. This part of the work was done as part of the Marie Skłodowska-Curie Actions consortium, the Integrated Training of Dry Eye Disease Drug Development (IT-DED³).¹⁴⁸

IBS is a gut-brain interaction disorder characterized by abdominal pain. Visceral hypersensitivity, in its turn, is the major contributing factor that characterizes abdominal pain.¹⁴⁹ Its pathophysiology is triggered by a disturbance of sensitization pathways at different levels.¹⁵⁰ The role of serine proteases in the intestinal tract and their potential role in IBS and visceral hypersensitivity has been previously reported.¹⁵¹ However, their role still needs to be fully understood. This study aimed to illustrate the potential roles of serine proteases on the pathophysiology of visceral hypersensitivity and IBS, together with their potential as therapeutic targets. This part of the work was done as part of the FWO-SBO project TRP-sensation.¹⁵²

2.2 Design, synthesis, and characterization of activity-based probes for biomarker identification

Previously, the laboratory of Medicinal Chemistry developed a multi-target trypsin-like serine protease diaryl phosphonate inhibitor known as UAMC-00050. This inhibitor is characterized by an α -amino diaryl phosphonate warhead which can form a covalent bond with the serine of serine proteases in the active site. α -amino diaryl phosphonates are a class of compounds that selectively inhibit serine proteases. These have been widely used in medicinal chemistry projects to design and synthesize inhibitors and develop ABPs.

The racemic mixture of UAMC-00050 was used prior to this doctoral thesis to set proof of concept of the potential use of serine proteases as a therapeutic target for DED and IBS.

Even though the promising proof-of-concept that UAMC-00050 had in DED and IBS models, the specific proteases that are upregulated in these pathologies still need to be elucidated. Therefore, the primary objective of this doctoral thesis was to develop a proteomic tool to determine protease activity in biological samples. In recent decades, protease activity has been studied by activity-based protein profiling (ABPP). ABPP is a proteomic tool that uses chemical probes that react covalently with the active form of a target enzyme to identify enzymatic activity, making them attractive for target and biomarker identification.

ABPs targeting serine proteases have been developed previously with different reactive groups. Interestingly, the α -amino diaryl phosphonate warhead has proven to be one of the most promising warheads for this family. Most diaryl phosphonate ABPs targeting trypsin-like serine proteases in literature mimic the natural basic amino acids ornithine, arginine, and lysine. However, we aim to move away from this approach and design several synthetic analogs to improve potency and selectivity.

Furthermore, the newly synthesized probes had to be fully biochemically characterized in a panel of trypsin-like serine proteases. This was performed by in-house developed

biochemical protocols. Their IC_{50} values set a preliminary cut-off value and give a first evaluation of the compound affinity for the specific enzyme. However, the newly synthesized probes were designed to be irreversible compounds. Thus, IC_{50} values are not suitable for affinity description. Kinetic studies complemented the biochemical characterization to determine their kinetic constants and mechanism of inhibition. The latter had to be further corroborated by another experimental setting. To validate the mechanism of inhibition, jump dilutions were performed.

We aimed to label proteases to describe the potential of the newly synthesized ABPs to identify active trypsin-like serine proteases participating in physiological processes. The ABPs were used first to label recombinant proteases and later for proteases released from degranulated mast cells.

2.3 Design, synthesis, and characterization of novel trypsin-like serine protease inhibitors

The last goal of this doctoral thesis arose from the results observed during the characterization of the ABPs developed in **Chapter 6**. We described high-affinity probes with different inhibitory mechanism than the inhibitor UAMC-00050. Interestingly, a set of probes with phenyl guanidine as a side chain emerged as a good starting point for inhibitor development. Thus, we developed and characterized two new inhibitors with phenyl guanidine as a side chain and an α -amino diaryl phosphonate warhead. Moreover, the new inhibitors were fully characterized in the same panel of trypsin-like serine proteases as the probes. Finally, a preliminary study of their physicochemical properties was performed to determine their suitability for *in vivo* use.

CHAPTER 3

PROTEASES AND THEIR POTENTIAL ROLE AS BIOMARKERS AND DRUG TARGETS IN DRY EYE DISEASE AND OCULAR SURFACE DYSFUNCTION

Published as:

Alba Ramos-Llorca, Camilla Scarpellini, Koen Augustyns.

Proteases and their potential role as biomarkers and drug targets in Dry Eye Disease and Ocular Surface Dysfunction. *International Journal of Molecular Sciences*, **2022**, 23, 9795

Responsible for literature search, creation of images, and writing of the manuscript.

Chapter 3 **Proteases and their potential role as biomarkers and drug targets in Dry eye disease and ocular surface dysfunction**

3.1 Abstract

Dry eye disease (DED) is a multifactorial disorder that leads to ocular discomfort, visual disturbance, and tear film instability. DED is accompanied by an increase in tear osmolarity and ocular surface inflammation. The diagnosis and treatment of DED still present significant challenges. Therefore, novel biomarkers and treatments are of great interest. Proteases are present in different tissues on the ocular surface. In a healthy eye, proteases are highly regulated. However, dysregulation occurs in various pathologies, including DED. With this review, we provide an overview of the implications of different families of proteases in the development and severity of DED, along with studies involving protease inhibitors as potential therapeutic tools. Even though further research is needed, this review aims to give suggestions for identifying novel biomarkers and developing new protease inhibitors.

3.2 Introduction

DED, defined by the Tear Film and Ocular Society (TFOS) in the Dry Eye Workshop II (DEWS) report, is a multifactorial disease of the ocular surface defined by the disruption of homeostasis of the tear film. The ocular signs accompanying DED are tear film instability and hyperosmolarity, ocular surface inflammation and damage, and neurosensory abnormalities.¹⁴⁵ Consequently, some symptoms patients describe are dryness, itching, redness, visual disturbance, and ocular fatigue. The impact of DED on the quality of life increases with the disease severity.¹⁵³ In general, DED affects the ability to perform daily activities and work, and in more severe cases, it can instigate mood alterations and depression.¹⁵⁴ The prevalence of DED ranges from 5% to 50%, depending on the studied

population.¹⁵⁵ However, prevalence studies can differ due to a lack of heterogeneity in the description of DED and whether the study is based on the symptoms or the signs of the patients.¹⁵⁶ Risk factors for DED include sex and race.¹⁵⁷ Furthermore, the constant use of screens, wear of contact lenses, environmental conditions, and use of medication are also considered risk factors.¹⁵⁸ Thus, with the current general population lifestyle, the prevalence is expected to increase in the following years. For instance, during the recent COVID-19 pandemic, a rise in patients with DED symptoms was described. This increase is correlated to wearing a face mask, also known as mask-associated dry eye. The misplacement of the face mask potentially displaces the air around the eyes and increases the evaporation of tears.^{159,160}

DED patients can be broadly divided into evaporative dry eye (EDE) and aqueous deficient dry eye (ADDE).¹⁶¹ They are not exclusive; thus, patients can present characteristics of the two simultaneously. EDE is associated with the dysregulation of the lipid layer of the tear film. This leads to excessive evaporation of the aqueous layer, causing hyperosmolarity and inflammation of the ocular surface.¹⁶² This DED type is commonly associated with meibomian gland dysfunction (MGD). The meibomian glands are responsible for segregating lipids towards the eyelid margin to form the tear film lipid layer. In patients with MGD, the quantity and quality of the lipids are decreased.¹⁶³ Thus, MGD can lead to DED. On the contrary, ADDE is correlated with reduced aqueous production by the lacrimal system or the accessory glands.¹⁶⁴ ADDE, in itself, can be divided into Sjögren syndrome dry eye (SSDE) and non-Sjögren syndrome dry eye (NSSDE).¹⁴⁵ Sjögren syndrome is an autoimmune disease affecting the exocrine glands, specifically the salivary and lacrimal glands, resulting in dryness of mucosal surfaces.¹⁶⁵ The DED pathophysiology can be described by the vicious circle of dry eye.¹⁶⁶ The ocular surface disruption leads to osmotic stress. Then, hyperosmolarity initiates stress-related signaling pathways and the release of inflammatory cells and cytokines.¹⁴⁶ Among the activated signaling pathways, there are the nuclear factor kappa beta (NFκB), the mitogen-activated protein kinase (MAPK), and the c-Jun N-terminal kinase (JNK).¹⁶⁷

The current diagnosis of DED is based on questionnaires handed to patients. The Ocular Surface Disease Index (OSDI) is the most widespread and widely used, which assesses symptoms, environmental triggers, and the impact on quality of life. Other tests widely performed by clinicians include tear film breakup time, fluorescein breakup time, and the Schirmer test.¹⁶⁸ Tear film biomarkers for DED are proinflammatory cytokines and chemokines, such as interleukin-6 (IL-6), tumor necrosis factor-alpha (TNF- α), IL-1 β , interferon-gamma (INF- γ), and IL-8.¹⁶⁹ Other biomarkers include matrix metalloprotease-9 (MMP-9) and vascular endothelial growth factor. A limitation of biomarker identification is the variability among different collection methods and instruments.¹⁷⁰

The most common treatment is artificial tear substituents. These bring momentary relief by diluting inflammatory markers. However, artificial tears do not have an anti-inflammatory effect; therefore, they do not tackle the main trigger of DED.^{171,172} Cyclosporin A (CyA) was the first approved drug by the Food and Drug Administration (FDA, USA) to treat specifically DED. CyA is an immunomodulatory drug that reduces many inflammatory markers. Unfortunately, many patients do not respond to CyA or have significant side effects.¹⁷³ Xiidra, a competitive antagonist of lymphocyte function-associated antigen-1 (LFA-1), was approved in 2016. It takes up to 3 months to reduce the symptoms, and many patients experience side effects.¹⁷⁴ Finally, topical corticosteroids, such as Eysuvis, approved in 2020, can only be used for short periods due to steroid side effects.¹⁷⁵

To date, the diagnosis and treatment of DED present many challenges. Thus, there is a significant interest in identifying new potential biomarkers and developing new therapies.

In a healthy eye, proteases and endogenous protease inhibitors are in equilibrium in the tear film. On the contrary, the imbalance of their levels can induce different pathologies.¹⁷⁶ Proteases destroy peptides or proteins by cleaving peptide bonds through hydrolysis.¹⁷⁷ Their function is essential in living organisms.¹⁷⁸ Proteases are encoded by about 2% to 4% of the total genes in all kinds of organisms.⁸ The MEROPS database (12.0 release), an

information source about all peptidases and their inhibitors, includes more than 5000 proteases.² Based on their catalytic mechanism, they are divided into seven families: aspartic, cysteine, glutamic, metallo-, asparagine, serine, and threonine proteases.¹⁰ Metallo- and serine proteases are the most abundant families.⁸

Proteolytic enzymes have raised a great interest in biomedical research due to their involvement in many physiological processes. Proteases are relevant in regulating many diverse biological processes.¹⁷⁹ For example, they modulate protein-protein interactions, cell division and replication, wound repair, blood coagulation, digestion, immunity, and inflammation.^{180,181} Due to their role in pivotal biological functions, the malfunction or alteration of their expression is correlated with pathological conditions, such as cancer, inflammatory, cardiovascular, and neurodegenerative disorders.¹⁷⁸ Proteases can also act in signaling pathways by activating protease-activated receptors (PARs).¹⁸²

Recently, studies involving proteases in the ocular surface have focused on matrix metallo-, serine, and cysteine proteases.¹⁸³ In particular, for DED, the role of MMP-9 has been widely studied.¹⁶⁹ Even though the role of other proteases is less well established, there is evidence that serine and cysteine proteases also play a role in the immunity and inflammation of DED.^{184,185}

This review assesses the role of proteases and PARs in ocular surface dysfunction and concentrates more specifically on their potential role as biomarkers and therapeutic targets in DED. Protease inhibitors with the potential to mitigate symptoms of DED are also discussed.

3.3 Proteases and Dry eye disease

Proteases play pivotal roles in inflammation and are considered therapeutic targets and biomarkers for different pathologies. Different reviews can be found on this subject.^{178,186,187} The correlation between DED and inflammation and the involvement of

proteases in inflammatory events show the potential for proteases to become new drug targets or biomarkers for DED. The following section describes the different families of proteases linked to ocular surface disorders. We summarize their role in inflammation and immunity and their involvement in various pathologies, specifically in DED (**Figure 3.1**).

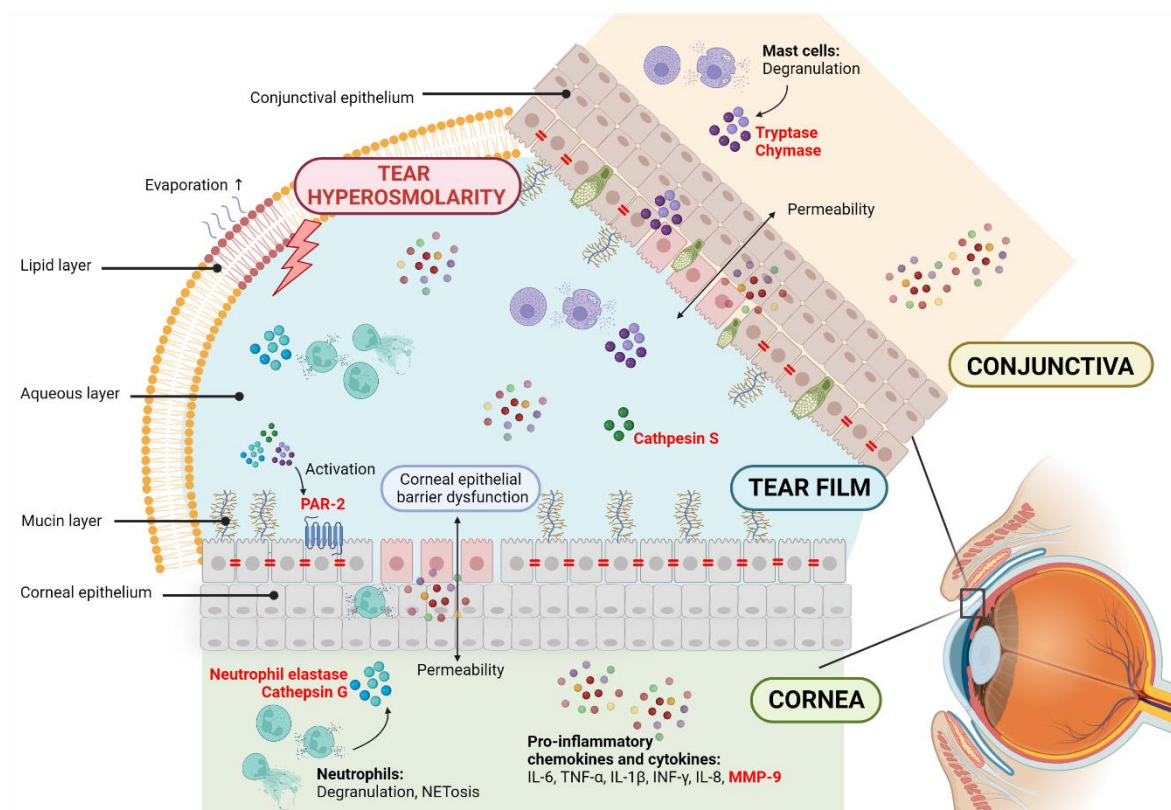


Figure 3.1 Potential contribution of proteases in Dry eye disease (DED). The disruption of homeostasis of the tear film is accompanied by tear instability and hyperosmolarity, and ocular surface inflammation and damage. DED is related to corneal epithelial barrier dysfunction, allowing permeability and cell circulation to the tear film. This elevates the production of proinflammatory chemokines and cytokines, including the metalloprotease MMP-9. Neutrophils and mast cells are innate immune cells in the cornea and conjunctiva that, upon degranulation, release biological mediators to the environment, including serine proteases. Cathepsin S is a cysteine protease found in the tears of Sjögren syndrome patients. Proteases are known to promote the expression and activation of proinflammatory cytokines and impact the degradation of extracellular matrix components and the loss of epithelial barrier function. Proteases are also known for activating protease-activated receptors (PARs) and starting intracellular signaling. PAR-2 is expressed in corneal epithelial cells. In red, the proteases and protease-activated receptors are highlighted.

3.3.1 Matrix metalloproteases

MMPs are calcium-dependent proteases that contain a zinc atom. They are responsible for tissue remodeling and extracellular matrix degradation.^{188,189} MMPs can be found as secreted or transmembrane proteases. However, they are synthesized as inactive

zymogens and activated by different proteases through a process called cysteine switch.¹⁹⁰ Under healthy physiological conditions, the activity of MMPs is further regulated by their endogenous inhibitors, known as tissue inhibitors of MMPs (TIMPs). The equilibrium between MMPs and TIMPs is crucial to control their activity.¹⁹¹

MMPs have been shown to affect inflammatory pathways and immune responses in different pathologies, including DED. The involvement of MMPs in DED has been extensively studied. For example, in an experimental dry eye model, the expression of several MMPs (MMP-1, 10, 3, and 9) increased under desiccating stress conditions.¹⁹² In many reports, the critical role of MMP-9 in response to hyperosmolar stress in DED is described.¹⁴⁷

The expression of MMP-9 has been studied in several experimental DED animal models. For instance, DED was induced in C57BL6 mice by scopolamine hydrobromide and exposure to airflow,¹⁹³ or extra orbital lacrimal gland removal;¹⁹⁴ Balb/C mice were treated with benzalkonium chloride (BAC);¹⁹⁴ or in New Zealand white rabbits, DED was induced by concanavalin A.¹⁹⁵ In all these experimental settings, the expression of MMP-9 was enhanced, tear production was reduced, and corneal epithelial damage could be measured.^{193–195} Interestingly, the induction of DED to MMP-9 knockout mice improved resistance to corneal epithelial barrier damage.¹⁹⁶

Clinical studies report the use of MMP-9 as a DED biomarker due to a direct correlation between its upregulation and the development and severity of the disease.^{197–199} Moreover, Kook *et al.*, in a study involving 63 SSDE patients, determined that the concentration of tear MMP-9 combined with tear osmolarity may help determine the severity of SSDE.²⁰⁰ An immunoassay called InflammDry is commonly used clinically to measure MMP-9 levels and discriminate between DED and non-DED patients.²⁰¹

3.3.2 Serine proteases

Serine proteases are named after the presence of a nucleophilic serine in the active site. The active site is composed of a catalytic triad, which is conserved among most of the proteases of this family.⁹ Serine proteases can be further divided by their substrate specificity in chymotrypsin-, trypsin- and elastase-like serine proteases.¹⁵ They are an abundant proteolytic enzyme family that plays pivotal roles in critical physiological processes. Their upregulation leads to different malfunctions and pathologies.²⁰² Most of the serine proteases are secreted to the extracellular milieu. However, a reduced number can be found intracellularly or membrane-bound.²⁰³ In a healthy environment, endogenous inhibitors, known as SERPINS, regulate serine protease activity.¹⁸

Some serine proteases are directly involved with the immune system and secreted by immune cells. For instance, neutrophil proteases are expressed in granulocytes, granzymes in lymphocytes, and tryptase and chymase in mast cells.¹⁶ These promote pro-inflammatory cytokine expression and MMP-9 activation and impact the degradation of extracellular matrix components and the loss of epithelial barrier function. There is evidence of their contribution to several diseases, such as arthritis, asthma, irritable bowel syndrome, and multiple sclerosis.^{204,205} Serine proteases and their endogenous inhibitors have been found in the tear fluid on the ocular surface.²⁰⁶ While studies that focus on the presence of serine proteases in DED patients are lacking, the dysregulation of expression of related immune cells hypothesizes that serine proteases might be secreted upon degranulation to the extracellular milieu.

Neutrophils are an innate immune cell type known to act upon infection or injury. Additionally, they play roles in adaptive immunity by interacting with T and B cells.²⁰⁷ They play a role in other autoimmune diseases, such as rheumatoid arthritis.²⁰⁸ Upon degranulation, serine proteases (cathepsin G, neutrophil elastase, and proteinase-3) are released.²⁰⁹ Evidence suggests that neutrophils play a role in DED. Their presence has been described in several studies.^{210,211} Recently, Postnikoff *et al.* described an increase of the

receptor CD66b in DED patients, a secondary marker of neutrophil degranulation.²¹² Moreover, hyperosmolarity may promote neutrophil extracellular trap (NET) formation. NETs are defense structures formed after neutrophils release chromatin.²¹³ NETs can obstruct the ducts of meibomian glands, causing MGD.²¹⁴ As mentioned earlier, MGD is the main cause of EDE.

Mast cells in the conjunctiva play pivotal roles in allergic conjunctivitis inflammation.²¹⁵ Upon activation, mast cells undergo degranulation and release mediators, such as histamine, tryptase, and chymase. Tryptase and chymase directly degrade extracellular matrix components.²¹⁶ Tryptase is a trypsin-like serine protease and is only present in mast cells, making it the perfect indicator of mast cell degranulation.²¹⁷ Li *et al.* studied the effect of tryptase on the corneal epithelial barrier function and described that human corneal epithelial cells (HCE) exposed to tryptase expresses MMP-9, and the corneal epithelial barrier is disturbed.²¹⁸ Similarly, Ebihara *et al.* described that chymase could also decrease the barrier function in HCE.²¹⁹ It is known that patients who suffer from ocular allergy can develop DED.²²⁰ Their close relation derives the hypothesis that mast cell proteases might be present in patients with both conditions.

Studies demonstrate the presence of immune cells on the ocular surface. However, further studies are needed to determine the presence of serine proteases released by neutrophils and mast cells in patients and validate their therapeutic potential for treating DED.

3.3.3 Cysteine proteases

Cysteine proteases, similar to serine proteases, are named after having cysteine as a nucleophile in their active site. They are divided into different clans based on sequence homology.²²¹ The most abundant is clan C1, which includes papain and calpain proteases.²²² Most cathepsins belong to this clan, excluding cathepsins A and G, which belong to the serine proteases, and cathepsin D and E, belonging to aspartic proteases. Cathepsins are lysosomal proteases, playing essential roles in the extracellular matrix.

Cystatins regulate cathepsin activity. Their role is to mediate the release of proteases from lysosomes and protect the tissues from invading microorganisms or parasites.²²³

Cathepsins play roles in arthritis, osteoporosis, Alzheimer's disease, cancer, and apoptosis.²²⁴ Focusing on the eye, cathepsins are found in the cornea, retinal pigment epithelial cells, optic nerve, and choroid.²²⁵ However, their role in health and disease has not been investigated in depth.

Cathepsin S has been correlated with SSDE. It is known for protein and extracellular matrix degradation, thus facilitating cell migration and infiltration.²²⁶ Cathepsin S is stored in lysosomes as a zymogen and activated in late endosomes or lysosomes.²²⁷ Li *et al.* were the first to identify the upregulation of cathepsin S expression and activity in lacrimal gland acinar cells and subsequently in tears of NOD mice, a mice model of SSDE.²²⁸ Later, Hamm-Alvarez *et al.* further studied the clinical potential of cathepsin S as a biomarker for SSDE. They found that the activity of cathepsin S is higher in SSDE patients compared with healthy controls or patients with NSSDE or other autoimmune diseases.²²⁹ Cathepsin S may also affect the quality of tears by degradation of other tear proteins.²³⁰ Yu *et al.* recently investigated the cathepsin S activity in age-related DED. Interestingly, they found a significant increase in cathepsin S expression and activity in aged C57BL/6J mice compared with young ones. Thus, an aged ocular surface might be prone to an increase in this protease. Although cathepsin S is not upregulated in all DED patients, it could be an interesting biomarker to discriminate between SSDE and NSSDE and also for age-related DED.

3.4 Protease-activated receptors and Dry eye disease

Proteases are also known for their role in activating PARs.²³¹ These belong to the seven-transmembrane G protein-coupled receptors (GPCRs). Thus, PARs are cell-surface proteins composed of seven transmembrane domains and three extracellular and three intracellular loops.²³² PARs differ from other GPCR receptors due to their activation by proteases instead

of activation by a ligand. Especially serine proteases can cleave their N-terminal exodomain by proteolysis. The new N-terminal sequence, acting as a tethered ligand, interacts with extracellular loop-2, leading to a conformational change of the receptor.²³³ After that, intracellular signaling starts (**Figure 3.2**). However, this can vary from the receptor subtype, the protease responsible for activation, and the activated pathway. Contrarily, some proteases can inactivate PARs by cleaving the N-terminus in a different position.²³⁴ Currently, four subtypes of PARs are described from PAR-1 to PAR-4.²³¹ The functions and proteases that can cleave and activate them differ from subtypes.²³⁵ This section focuses on PAR-2 since only studies on this receptor could be found with interest in the ocular surface.

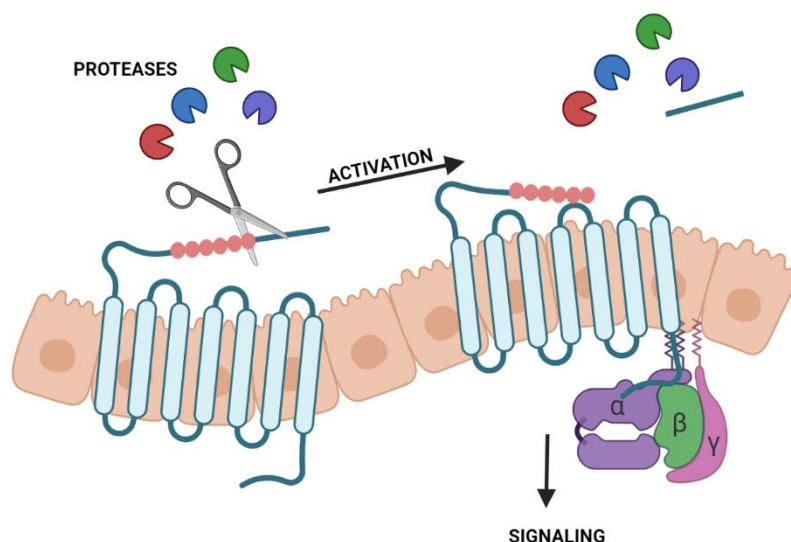


Figure 3.2 Activation of protease-activated receptors (PARs) by proteases. Proteases cleave the N-terminal exodomain of a specific PAR. The new N-terminal acting as a tethered ligand interacts with the extracellular loop-2, starting intracellular signaling.

The canonical activation of PAR-2 can be performed by several trypsin-like serine proteases, including trypsin, thrombin, tryptase, matriptase, plasmin, and some kallikreins. After activation, PAR-2 couples with $G_{\alpha_q/11}$, which leads to the hydrolysis of phosphatidylinositol 4,5-bisphosphate (PIP_2), and the Ca^{2+} /inositol 1,4,5-triphosphate (IP_3)/PKC signaling pathway is initiated.²³⁶ This pathway leads to the activation of NF κ B, which induces NF κ B-dependent genes' induction of proinflammatory cytokines and intracellular adhesion

molecule-1 (ICAM-1).²³⁷ The canonical activation of PAR-2 has also been related to MAPK signaling and subsequent inflammatory response. Other proteases can activate PAR-2 in a biased manner, initiating different signaling pathways.²³⁸ For instance, studies demonstrated that biased activation by neutrophil elastase activates MAPK.²³⁹ The activation of MAPK and NF κ B is also associated with DED inflammatory response.²⁴⁰

PARs have been widely studied and demonstrated to be potential drug targets and valuable biomarkers for many pathologies. For instance, PAR-2 is correlated with visceral hypersensitivity in irritable bowel syndrome;²⁴¹ in the cardiovascular system, it is associated with vascular inflammation,²⁴² and airway proteases and PARs have been proposed as therapeutic targets for various lung diseases.²⁴³

While the presence of PARs has been widely studied in diverse human tissues and pathologies, not much is known about their expression and function in the different human eye tissues. The involvement of PARs in DED was never mentioned until recently when Joossen *et al.* described a significant increase in PAR-2 expression on the corneal tissue of untreated dry eye rats.¹⁸⁵ Several studies indicate the expression of PAR-1 and PAR-2 in HCE.^{218,244,245} Lang *et al.* also demonstrated that a specific activation of PAR-2 by trypsin and thrombin increased the production of the proinflammatory cytokines IL-6, IL-8, and TNF- α by HCE.²⁴⁴ These cytokines are also found on the tear film of DED patients. Li *et al.* postulated that tryptase activates PAR-2 in HCE, compromising the barrier function and triggering the expression of MMP-9,²¹⁸ another DED biomarker. Cathepsin S can activate PAR-2 in a distinctive site compared with the serine proteases, which proved to cause inflammation and neuropathic pain.²⁴⁶ Klinngam *et al.* showed that the increased secretion of IL-6, IL-8, TNF- α , IL-1 β , and MMP-9 in HCE treated with cathepsin S is correlated with PAR-2 expression.²⁴⁷

Although little is known about the function of PAR-2 in DED, studies demonstrating their presence in corneal epithelial cells and their ability to increase the levels of

proinflammatory cytokines support the hypothesis of the participation of these receptors in DED inflammatory responses.

3.5 Protease inhibitors and Dry eye disease

Only a limited number of papers on this subject are reported. However, with evidence that proteases play a role in the pathophysiology of DED, protease inhibitors could potentially be new therapeutics. This section summarizes the studies and results with protease inhibitors in DED animal models (**Table 3.1**).

3.5.1 MMP-9 inhibitors

Mori *et al.* studied PES_103, a synthetic water-soluble small molecule targeting the catalytic domain of MMP-9. They administered 0.1% PES_103 to an experimental reduced lacrimation mice model twice a day. This treatment showed an increase in tear production.²⁴⁸ In another study, a divalent PAMAM-based MMP-9 inhibitor showed increased tear production in an experimental rabbit dry eye model, in which the administration of atropine sulfate by ocular instillations induced DED. Moreover, there was no sign of corneal damage.²⁴⁹ Similarly, RSH-12, an MMP-9 peptide inhibitor, showed reduced signs of DED in a rabbit model. Treatment for 7 days showed an increase in tear volume and a decrease in tear breakup time.²⁵⁰

3.5.2 Serine protease inhibitors

The serine protease inhibitor A3K (SERPINA3K) belongs to the endogenous serine protease inhibitor family. SERPINA3K has effects on other ocular treatments, such as corneal injury.²⁵¹ A study by Hu *et al.* described a reduced TNF- α -induced disruption of the rabbit corneal endothelial barrier.²⁵² Z. Lin *et al.* studied the effect of the inhibitor on dry eye and squamous metaplasia, an ocular surface pathology commonly occurring under prolonged tear deficiency conditions.²⁵³ This study used a mouse animal model, where DED was induced by BAC.²⁵⁴ Both BAC and SERPINA3K were administered twice a day for 16 days.

Mice treated with SERPINA3K showed a significant reduction in DED development. They showed minor epithelial damage and reduced inflammatory response in the cornea. They postulate that SERPINA3K can decrease DED severity by reducing TNF- α .

PEDF is a 50 kDa glycoprotein belonging to the serpin family.²⁵⁵ In the eye, it is expressed in multiple tissues, such as the cornea, retina, choroid, and ciliary muscles.²⁵⁶ Singh *et al.* first demonstrated that treatment with recombinant PEDF in a dry eye model inhibits the maturation of corneal dendritic cells, reduces Th17 generation, and suppresses the expression of proinflammatory cytokines on the ocular surface. The mice received 1 μ l of 100 μ g/ml topical recombinant murine PEDF via ocular surface instillations three times a day for 7 days. DED was induced in mice in a controlled environment chamber.²⁵⁷ A subsequent study postulates that PEDF reduces DED severity by significantly reducing corneal fluorescein staining scores.²⁵⁸

Recently, Joossen *et al.* described a serine protease inhibitor, UAMC-00050, to treat inflammation in DED.¹⁸⁵ UAMC-00050 is a synthetic diaryl phosphonate small-molecule inhibitor that targets several trypsin-like serine proteases.¹²⁸ They reported in vivo studies carried out in a rat animal model, where DED was induced by the surgical removal of the exorbital lacrimal gland.²⁵⁹ The animals were treated for 24 days, twice a day. UAMC-00050 at a concentration of 5 mM appeared to be the most promising treatment compared with cyclosporin A and vehicle animals. Fluorescein scores showed that UAMC-00050 reduces tissue damage significantly, and the expression of inflammatory cytokines, IL-1 α and TNF- α , were significantly reduced. UAMC-00050, at a concentration of 5 mM, was able to reduce inflammatory cell infiltration (CD3⁺ and CD45⁺) and MMP-9 activity. The accumulation of pro-MMP9 and the decrease in active MMP-9 could show that serine proteases have a role in activating MMP-9 in DED.¹⁸⁵

Table 3.1 Protease inhibitors and the effect they have in a specific experimental setting.

Inhibitor	Target	Experimental Setting	Effect ^a
PES_103 ²⁴⁸	MMP-9	Dry eye mice model Transdermal scopolamine patches	↑ Tear production
Divalent PAMAM ²⁴⁹	MMP-9	Dry eye rabbit model Atropine sulfate	↑ Tear production ↓ Corneal damage
RSH-12 ²⁵⁰	MMP-9	Dry eye rabbit model Atropine sulfate	↑ Tear volume ↓ Tear breakup time
SERPINA3K ²⁵³	Serine proteases	Dry eye mice model BAC induced	↓ Epithelial damage ↓ TNF- α
PEDF ^{257,260}	Serine proteases	Dry eye mice model Controlled environment chamber	↓ DCs, Th17 ↓ Proinflammatory cytokines ↓ Fluorescein score
UAMC-00050 ¹⁸⁵	Serine proteases	Dry eye rat model Surgical removal exorbital lacrimal gland	↓ IL-1 α , TNF- α , MMP-9 ↓ CD3+, CD45+

^a An up-facing arrow (↑) represents an increase, whereas a down-facing arrow (↓) corresponds to a reduction.

3.6 Conclusions and Future Directions/Perspectives

Tear proteins are a good indicator of health and disease on the ocular surface. The metalloprotease MMP-9 has been widely studied as a biomarker of DED, and it is commonly used in clinical settings to diagnose DED. There is enough evidence that not only MMP-9 is a relevant protease in DED pathophysiology. Furthermore, protease inhibitors could be used as a potential treatment for DED, which would tackle inflammation directly. However, there is a lack of studies focused on different protease families, such as the serine or cysteine proteases. Even though the tear proteome is very complex, identifying upregulated proteases in DED patients could open a window for new biomarkers and potentially new protease inhibitors as a novel DED treatment.

Several techniques can monitor and quantify protein expression in complex proteomes, for example, the enzyme-linked immunosorbent assay (ELISA) or protein microarrays.^{261,262} However, these techniques analyze protein expression rather than activity. The activity of proteins is regulated by post-translational modifications, such as zymogen activation or interaction with other proteins or small molecules.¹⁴ Therefore, it is of interest to identify active proteases. Activity-based protein profiling (ABPP) is a proteomic tool that uses activity-based probes (ABPs) to identify active enzymes in a complex proteome. The reactive group of the probe interacts with the active site of the protease, and later, it is identified by electrophoresis or mass spectrometry (**Figure 3.3**).⁷⁵ Peng *et al.* published an interesting review on the prospective application of ABPP with ocular proteases.²⁶³

After identifying upregulated proteases in DED, efforts could be moved to the design of selective inhibitors for a specific protease with therapeutic potential. Other techniques, such as X-ray crystallography, can determine the protease structure and, together with molecular docking, help to design novel inhibitors.^{262,264}



Figure 3.3 Tear protease identification by activity-based protein probes (ABPs). Proteases present in DED patients are labeled with an ABP for a specific protease family. The reactive group of the ABP would bind to the active enzymes. The bound proteases can be isolated and analyzed by electrophoresis and/or mass spectrometry.

CHAPTER 4

SERINE PROTEASES AS POTENTIAL
BIOMARKERS AND THERAPEUTIC TARGETS OF
IRRITABLE BOWEL SYNDROME

Chapter 4 **Serine proteases and their potential role as biomarkers and therapeutic targets of Irritable bowel syndrome**

4.1 Irritable bowel syndrome and visceral hypersensitivity

Irritable bowel syndrome (IBS) is a disorder affecting the gut-brain axis characterized by abdominal pain, in association with alterations in bowel habits in the absence of major histological abnormalities in the intestine.²⁶⁵ The Rome IV criteria set the standards for diagnosis. The minimal symptoms are abdominal pain and changes in stool frequency and/or form. However, other common symptoms include gas, bloating, and cramping. These symptoms must be recurring at least once a week during the last three months, and the symptoms-onset must be ongoing for at least six months.¹⁴⁹ Due to its chronic character, IBS significantly impacts the quality of life and is linked to substantial patient and healthcare costs.²⁶⁶ Following the Rome IV criteria, IBS affects, on average, 4% of the population worldwide.²⁶⁷ Noteworthy, this prevalence is higher in females than in the male population in most regions.²⁶⁸ Potential risk factors include diet, genetics, disturbances in the gut microbiome, gastrointestinal infection, and physiological factors such as stress or depression.^{269,270}

IBS patients can be divided into three subtypes based on stool type, a predominance of diarrhea (IBS-D), constipation (IBS-C), or mixed (IBS-M), when a patient cannot be clearly classified, it is considered as untyped (IBS-U).²⁷¹ The diagnosis of IBS is based on a physical and psychological evaluation of the patient and several laboratory studies such as blood or stool tests. Moreover, complementary tests for other pathologies are routine, such as serological testing for coeliac disease.²⁷² The treatment of IBS mainly focuses on targeting the motility disturbances exclusively. These are primarily symptomatic therapies. However, only a limited amount of treatments focus on abdominal pain.²⁷³ Unfortunately,

effective treatment is still lacking, and the diagnosis is not always accurate, and therefore, further research in identifying new biomarkers and novel therapies is an absolute priority.

IBS is a multifactorial disorder, and its pathophysiology is still under debate. Several mechanisms contribute to the development of IBS, including microbiome alteration, intestinal barrier disruption, activation of immune cells, altered bowel motility, or sensitization of visceral nociceptors.¹⁸⁶ The mechanism characterizing abdominal pain is visceral hypersensitivity, an increased perception of stimuli in the gastrointestinal tract.¹⁵⁰ This occurs by a disturbance of sensitization pathways at different levels. Mechanical, thermal, or chemical information in the gut wall is sensed by primary afferent neurons whose cell bodies are located at the dorsal root ganglia. This information is translated to different cerebral somatosensory areas through secondary neurons in the spinal cord. The signal is then interpreted and perceived as harmful due to cognitive and emotional biasing.^{150,274,275} Furthermore, there is evidence that gastrointestinal inflammation plays a role in visceral hypersensitivity. Activated inflammatory cells release inflammatory mediators such as histamine, cytokines, serotonin, or proteases at the peripheral level. It is known that these mediators can sensitize peripheral neurons, hence contributing to visceral hypersensitivity.²⁷⁶

Proteases, as mentioned in **Chapter 1**, are enzymes that catalyze the hydrolysis of peptide bonds.² They are present in high concentrations in the gastrointestinal tract, where they have essential functions in digestion.²⁰³ However, during inflammation, epithelial and immune cells release proteolytic enzymes, which can disrupt the intestinal barrier and activate signaling pathways.²⁷⁷ Moreover, it is known that proteases can mediate visceral hypersensitivity by activating protease-activated receptors (PAR).²⁷⁸ Despite different families of proteases, serine proteases are suggested to play a role in the development and severity of IBS and visceral hypersensitivity.¹⁶ Thus, the following sections focus on the involvement of serine proteases and PARs in the pathophysiology of visceral hypersensitivity in IBS and the therapeutic potential of serine protease inhibitors (**Figure 4.1**).

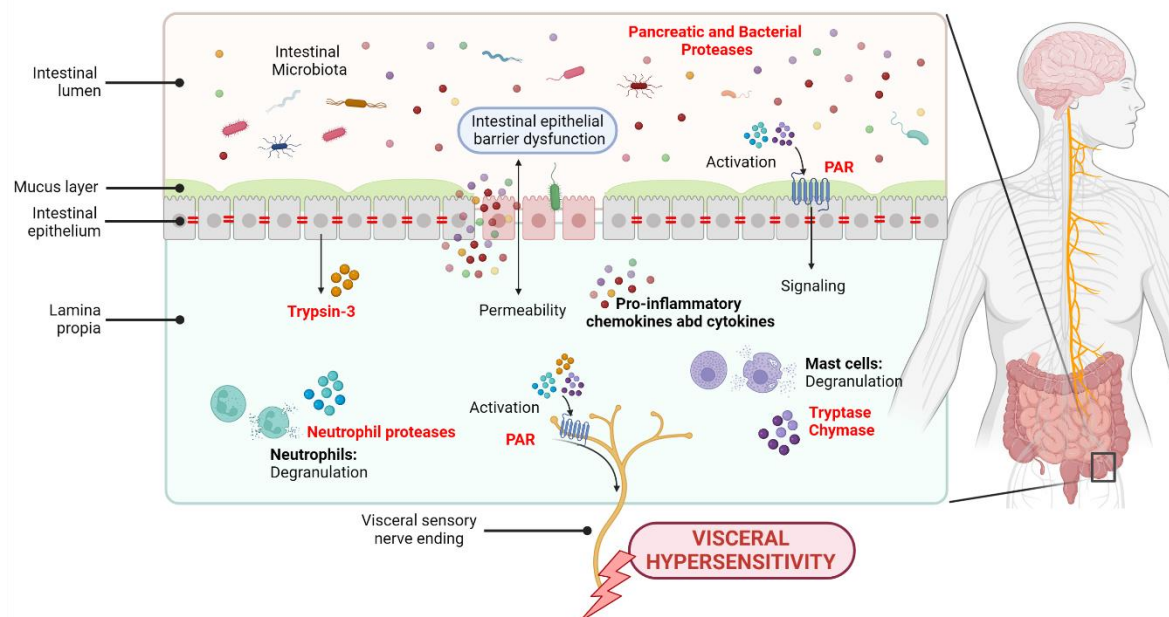


Figure 4.1 Potential contribution of serine proteases in Irritable bowel syndrome (IBS) and visceral hypersensitivity. IBS is a gut-brain disorder occurring in the intestinal walls. Lumen proteases contribute to intestinal epithelial barrier dysfunction, allowing permeability and cell circulation to the lamina propria. Neutrophils and mast cells are innate immune cells present in the intestine wall that, upon degranulation, release serine proteases (neutrophil elastase, cathepsin G, trypsin, chymase). Furthermore, proteases from immune cells and trypsin-3 expressed by epithelial cells can signal to visceral nociceptors and mediate visceral hypersensitivity via protease-activated receptors (PARs). PARs are expressed in intestinal epithelial cells and visceral sensory nerve endings. In red, the proteases and PARs are highlighted.

4.2 Serine proteases in IBS and visceral hypersensitivity

Proteases are abundant in the gastrointestinal tract and are secreted by the pancreas, microbiota, macrophages, and epithelial and inflammatory cells such as neutrophils or mast cells.²⁰³ For instance, a correlation between mast cell infiltration in the bowel wall and the development and severity of abdominal pain in IBS has been described.²⁷⁹ Mast cells are immune cells that undergo degranulation and secrete pro-inflammatory mediators upon activation.²⁸⁰ Recently, Aguilera-Lizarraga *et al.* provided evidence that mast cells in the rectal mucosa of IBS patients are more prone to degranulate with IgE stimulation by food antigens, thus releasing proteases.²⁸¹ Trypsin- $\alpha\beta 1$ and - $\beta 2$, herein referred to as trypsin, are trypsin-like serine proteases restricted to mast cells. An upregulated trypsin expression has been found in colonic biopsies of IBS patients.^{40,282,283} Likewise, trypsin-3 is expressed by the intestinal epithelium, and its expression has been found higher in IBS colonic biopsies compared to healthy controls.²⁸² Recently, Buhner *et al.* described the

upregulation of elastase-like proteases in colonic biopsies supernatants from IBS patients.²⁸³ Additionally, elevated trypsin-serine protease activity was measured in both colon biopsies and feces in several studies.^{284,285} Noteworthy, fecal protease activity might not help sensitize intestinal nociceptors; however, it might play a role in intestinal epithelial barrier dysfunction.²⁸⁶

Studies demonstrate the presence of elevated expression and activity of serine proteases in IBS patients. However, there is a need for tests that can identify which proteases are involved unambiguously due to a lack of selectivity of these techniques. Activity-based probes (ABPs) can help to elucidate this uncertainty. The warhead of the ABP can react covalently with the target enzyme, which can be identified by mass spectrometry after purification. This technique has already been used in the field of IBS proteases.²⁰⁵

4.3 Protease-activated receptors (PARs) in visceral hypersensitivity in IBS

PARs are cell-surface signaling proteins belonging to the seven-transmembrane G protein-coupled receptors (GPCRs).²³² Similarly to a few GPCRs, such as rhodopsin and some hormone receptors, the receptor agonist is embedded within its structure. Contrary to other GPCRs, though, PARs are activated by cleavage of the N-terminal exodomain by proteases, especially serine proteases, thereby revealing a tethered ligand. For more details on the activation of PARs by serine proteases, refer to **Section 3.4**. Moreover, PARs can be activated by peptides mimicking the tetrahedral ligand sequence.

To date, four different types of PARs are described, from PAR-1 to PAR-4, and they are expressed in different kinds of cells in the intestine, including epithelial cells and neurons.²⁸⁷ Noteworthy, the activation of the different PARs affects visceral hypersensitivity differently. While activation of PAR-4 has an antinociceptive effect (reduction of pain), the activation of PAR-2 induces pronociceptive effects, thus increasing the perception of pain. In mice, PAR-1 has been reported to have an antinociceptive effect,

while in humans, there is growing evidence that this receptor may be the most important member of this GPCR family in mediating visceral hypersensitivity.¹⁸⁶

Several studies demonstrate the involvement of PARs in visceral hypersensitivity. The antinociceptive properties of PAR-1 have been evaluated by the administration of PAR-1 agonists TFFLR-NH₂ and thrombin to capsaicin-evoked visceral nociception male ddY mice and carrageenan-induced male Wistar rats, observing a suppression of visceral pain.^{288,289} Likewise, activation of PAR-4 by agonist AYPGKF-NH₂ or cathepsin G reduced visceral hypersensitivity in C57BL/6J mice infused with IBS-D fecal supernatants.²⁹⁰ Contrary, Kawabata *et al.* and Coelho *et al.* demonstrated that treating male Wistar rats with PAR-2 agonist SLIGRL-NH₂ or trypsin increases visceral hypersensitivity.^{291,292} The involvement of PAR-2 has been further evaluated by experimental knock-out (KO) models. Valdez-Morales *et al.* demonstrated that neuronal excitability of colonic dorsal root ganglia (DRGs) was enhanced in C57BL/6 wild-type mice but not in PAR-2-KO mice.²⁴¹

Even though agonists/antagonists of PARs can reduce visceral hypersensitivity, these compounds have not reached the clinic so far. One of the main reasons being that while the interaction site between proteases and PARs is high affinity, the interaction site of the receptor with its tethered ligand is intrinsically low affinity. Thus, serine protease inhibitors have been put forward in recent years as an alternative to target abdominal pain in IBS.

4.4 Serine proteases inhibitors in IBS and visceral hypersensitivity

Even though the role of serine proteases in the pathophysiology of IBS has been widely studied, the identity of dysregulated proteases participating in the pathophysiology of IBS remains elusive. Consequently, the research for effective serine protease inhibitors with a therapeutic role in IBS is limited. To date, no protease inhibitors are in clinical trials or have been marketed for IBS (September 2022). Nevertheless, serine protease inhibitors have been used in preclinical studies. This section summarizes the studies and results with protease inhibitors in IBS and visceral hypersensitivity (**Table 4.1**).

Table 4.1 Protease inhibitors and the effect they have in a specific experimental setting.

Inhibitor	Target	Experimental setting	Effect
Nafamostat mesylate (or FUT-175)	Serine proteases	IBS mice model	↓ Visceral hypersensitivity
		I.c.colonic IBS supernatants ²⁹³	↓ Neurons sensitization
		IBS mice model	↓ Visceral hypersensitivity
	Serine proteases	I.c.fecal IBS-D supernatants ²⁹⁴	↓ Visceral hypersensitivity
		Post-colitis rat model	↓ Visceral hypersensitivity
		TNBS-induced (i.p.) ²⁹⁵	↓ Visceral hypersensitivity
	Serine proteases	Neonatal acetic acid mice model ²⁹⁶	↓ Visceral hypersensitivity
		Acute restraint stress rat model ²⁹⁷	↓ Visceral hypersensitivity
		Post-colitis rat model	↓ Visceral hypersensitivity
UAMC-00050	Trypsin-like serine proteases	TNBS-induced (i.p.) ²⁹⁵	↓ Visceral hypersensitivity
		Post-colitis rat model	↓ Trypsin-like serine protease activity
		TNBS-induced (i.c.) ²⁹⁸	↓ Visceral hypersensitivity ↑ Colonic compliance
UAMC-001162	Trypsin-like serine proteases	Neonatal acetic acid mice model ²⁹⁶	↓ Visceral hypersensitivity
		Post-colitis rat model	↓ Visceral hypersensitivity
		TNBS-induced (i.p.) ²⁹⁵	↓ Visceral hypersensitivity
Bowman-Birk inhibitors	Trypsin-like serine proteases	Post-colitis rat model	↓ Fecal protease activity
		TNBS-induced ²⁹⁹	↓ Fecal protease activity
		Acute restraint stress rat model ³⁰⁰	↓ Fecal protease activity

^a An up-facing arrow (↑) represents an increase, whereas a down-facing arrow (↓) corresponds to a reduction

^b i.p.: intraperitoneal ; i.c.: intracolonic

Nafamostat mesylate, also known as FUT-175, is a synthetic serine protease inhibitor with broad specificity.^{301,302} Cenac *et al.* induced visceral hypersensitivity to male C57BL/6 mice by an intracolonic infusion of supernatants from biopsies of IBS patients. When these supernatants were previously treated with nafamostat, visceral hypersensitivity was significantly decreased. Moreover, they demonstrated a reduced sensitization of mice neurons after treating the supernatants with nafamostat.²⁹³ Similar results were observed by Wang *et al.*, with the difference that mice were infused with IBS-D fecal supernatants.²⁹⁴ Moreover, the Laboratory of Experimental Medicine and Pediatrics (Division of Gastroenterology) at the University of Antwerp demonstrated that a single intraperitoneal injection of nafamostat in a post-colitis rat model could significantly attenuate visceral hypersensitivity. Colitis was induced in male Sprague-Dawley rats by an intrarectally 2,4,6-trinitrobenzene sulphonic acid (TNBS) enema containing 4 mg of TNBS in 50% ethanol.²⁹⁵ Recently, they corroborated these findings in a neonatal acetic acid mouse model. Hypersensitivity was induced in C57BL/6 mice by an intracolonic infusion of 20 μL of a 0.5% acetic acid solution in 0.9% NaCl.²⁹⁶ A closely structurally related serine protease inhibitor, camostat mesylate or FOY-305, was tested in female Sprague-Dawley rats. Intragastric pretreatment with camostat mesylate could lower visceral hypersensitivity induced by acute restraint stress.²⁹⁷

Diaryl phosphonates were described as irreversible inhibitors and have been widely studied for different targets.³⁰³ UAMC-00050 and UAMC-001162 were developed by the Laboratory of Medicinal Chemistry at the University of Antwerp as trypsin-like serine protease inhibitors with a broad spectrum. These compounds were studied in two animal models of IBS. First, the effect of UAMC-00050 and UAMC-001162 was tested in the post-colitis TNBS-induced model described before, together with nafamostat mesylate. Both successfully reversed visceral hypersensitivity with a dose of 1 $\text{mg}\cdot\text{kg}^{-1}$ and 2.5 $\text{mg}\cdot\text{kg}^{-1}$, respectively.²⁹⁵ When UAMC-00050 is administered intracolonicly, higher concentrations are needed [5 $\text{mg}\cdot\text{kg}^{-1}$].²⁹⁸ These results were recently confirmed in the neonatal acetic acid-induced mouse model.²⁹⁶

Last, Moussa *et al.* studied the effect of a soy extract characterized by the presence of isoflavones and trypsin-like protease inhibitors known as Bowman-Birk inhibitors (BBI) in female Wistar rats. The first study induced hypersensitivity with an intracolonic TNBS dose of 80 mg·kg⁻¹ in 50% ethanol.²⁹⁹ In a consequent analysis, hypersensitivity was caused by acute stress.³⁰⁰ They postulate that the treatment with soy extract reduces hypersensitivity. However, they correlate this effect to the isoflavones, as the treatment with an estrogen receptor antagonist reversed these observations. However, they also observe a decrease in fecal proteolytic activity, which correlates with BBI inhibitory potency.^{299,300}

4.5 Conclusions

The involvement of proteases in the pathophysiology of IBS and visceral hypersensitivity has been explored in recent years. Proteases have been suggested as potential novel biomarkers for IBS, and protease inhibitors are a promising novel therapeutic strategy to explore.

Nevertheless, further research is needed to unravel the role of proteases. The main limitation is the little knowledge of the specific proteases dysregulated in IBS and visceral hypersensitivity. Under healthy conditions, proteases have many important physiological roles, such as functions in the coagulation cascade, and their inhibition could generate severe problems, such as unintended bleeding.³⁰⁴ Thus, it is important to unambiguously characterize the upregulated protease activity in IBS patients. Furthermore, further research to design specific and selective inhibitors targeting these proteases is needed to minimize the side effects.

CHAPTER 5

THE PROOF OF CONCEPT: THE INHIBITOR UAMC-00050

Responsible for the development of biochemical protocols and characterization of the molecules.

The upscaled synthesis is based on:

Davide Ceradini, Pavel Cacivkins, Alba Ramos-Llorca, Kirill Shubin.

Improved Synthesis of the Selected Serine Protease uPA Inhibitor UAMC-00050, a Lead Compound for the Treatment of Dry Eye Disease. *Org. Process Res. Dev.*, **2022**, 26, 10, 2937-2946.

Chapter 5 The proof of concept: the inhibitor UAMC-00050

5.1 Introduction

Diaryl phosphonates have been described as irreversible serine protease inhibitors, which can form a covalent bond with the serine alcohol in the active site. UAMC-00050 is a small diaryl phosphonate inhibitor developed by the laboratory of Medicinal Chemistry of the University of Antwerp (UAMC) (**Figure 5.1**). Initially, it was designed as a highly potent and irreversible inhibitor for uPA ($IC_{50} = 0.0042 \mu\text{M}$).¹²⁹ Later, a multi-target inhibition profile was described, achieving nanomolar potencies for matriptase ($IC_{50} = 0.0025 \mu\text{M}$) or KLK4 and 8 ($IC_{50} = 0.0016 \mu\text{M}$) and submicromolar potencies for tryptase ($IC_{50} = 0.028 \mu\text{M}$).¹⁸⁵ Many of the proteases inhibited, such as tryptase, cathepsin G, or thrombin, are involved in inflammatory and extracellular matrix degradation processes. Such processes also occur in Dry eye disease (DED) and Irritable bowel syndrome (IBS), as mentioned in **Chapters 3** and **4**. UAMC-00050 has been tested previously in DED and IBS models, and the results were published before this PhD started.^{185,295} In the following sections, the results are summarized.

In this chapter, we describe a new synthetic route on a larger scale and the biochemical evaluation of the two enantiomers of UAMC-00050. Moreover, the experimental section gives a detailed explanation of all the biochemical methods developed during this PhD.

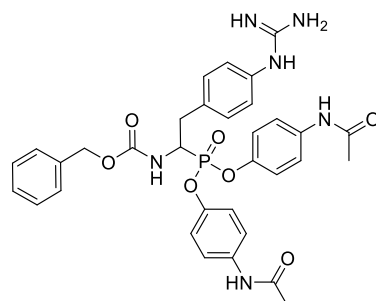


Figure 5.1 UAMC-00050 structure

5.1.1 Dry eye disease and UAMC-00050

DED is a multifactorial disease of the ocular surface accompanied by disruption of the tear film homeostasis. The symptoms of DED are tear film instability and hyperosmolarity. The diagnosis and treatment are still challenging. Moreover, the prevalence is expected to keep rising in the following years.^{145,305} Because proteases may play a role in DED, it was hypothesized that UAMC-00050 could become a potential treatment. The effect of UAMC-00050 in a DED animal model was evaluated after local application in a teardrop formulation. The detailed results can be found in Joossen C. *et al.*¹⁸⁵

DED was induced in female Wistar rats by removing the exorbital lacrimal gland. The animals were treated with two concentrations of UAMC-00050 (0.5 mM and 5 mM), and the results were compared with animals treated with vehicle and cyclosporin A (CyA). UAMC-00050 at a concentration of 5mM proved to be the best-performing treatment in this experimental setting.

UAMC-00050 [5mM] showed the lowest fluorescein scores, indicating reduced tissue damage, while vehicle and CyA did not show a significant reduction. Likewise, the best results of inflammatory cytokines concentration in tear fluid were observed on UAMC-00050 [5mM] treated animals. They showed the lowest concentrations of Interleukin (IL)-1 α and tumor necrosis factor (TNF)- α .

They studied the expression of trypsin, which was increased in the conjunctival and corneal tissue of animals with DED. As expected, UAMC-00050 did not reduce the trypsin expression as it only inhibits its activity.

This study can be used as a preliminary proof-of-concept of the involvement of trypsin-like serine proteases in ocular inflammation and DED and the potential of UAMC-00050 and serine protease inhibitors as a potential treatment.

5.1.2 Irritable bowel syndrome and UAMC-00050

IBS is a disorder of the gut-brain axis accompanied by abdominal pain and alteration of stool frequency and/or form.¹⁴⁹ This disorder affects 4% of the world population, with a higher prevalence in females. The costs related to the diagnosis and the non-effective treatment create a heavy burden for patients and healthcare systems. Visceral hypersensitivity and intestinal permeability contribute to the pathophysiology of IBS, and proteases have been suggested as mediators of these processes. Therefore, the effect of the serine protease inhibitor UAMC-00050 was studied in two animal models of IBS as a potential therapeutic treatment. The detailed results can be found in Ceuleers *et al.* (2018, 2022) and Hanning *et al.*^{295,296,298}

First, the effect of UAMC-00050 was studied in a rat model of post-inflammatory IBS. Colitis was induced in male Sprague-Dawley rats by an intrarectally 2,4,6-trinitrobenzene sulphonic acid (TNBS) enema containing 4 mg of TNBS in 50% ethanol. Visceral hypersensitivity was monitored by the visceromotor response (VMR) 3 days post-colitis. VMR is the nociceptive reflex in which abdominal muscles contract in response to colorectal balloon distension.³⁰⁶ The animals were treated with an intraperitoneal injection 30 min prior to the VMR experiment with different concentrations of UAMC-00050, UAMC-001162, and nafamostat. UAMC-00050 [$1 \text{ mg}\cdot\text{kg}^{-1}$] restored sensitivity to normal values and had no effect in control animals. Moreover, they demonstrated that the expression of trypsin-3 and trypsinase are upregulated in post-colitis rats. However, UAMC-00050 does not alter their expression as it only inhibits protease activity.²⁹⁵

In the same animal model, Hanning *et al.* administered intracolonicly different concentrations of UAMC-00050 30 min prior to the VMR experiment. They demonstrated that local administration of UAMC-00050 [$5 \text{ mg}\cdot\text{kg}^{-1}$] reduces trypsin-like serine protease activity on colon tissue. Moreover, visceral hypersensitivity was normalized to control values when treated with UAMC-00050 [$2.5 \text{ mg}\cdot\text{kg}^{-1}$] and even lower with a higher concentration [$5 \text{ mg}\cdot\text{kg}^{-1}$].²⁹⁸

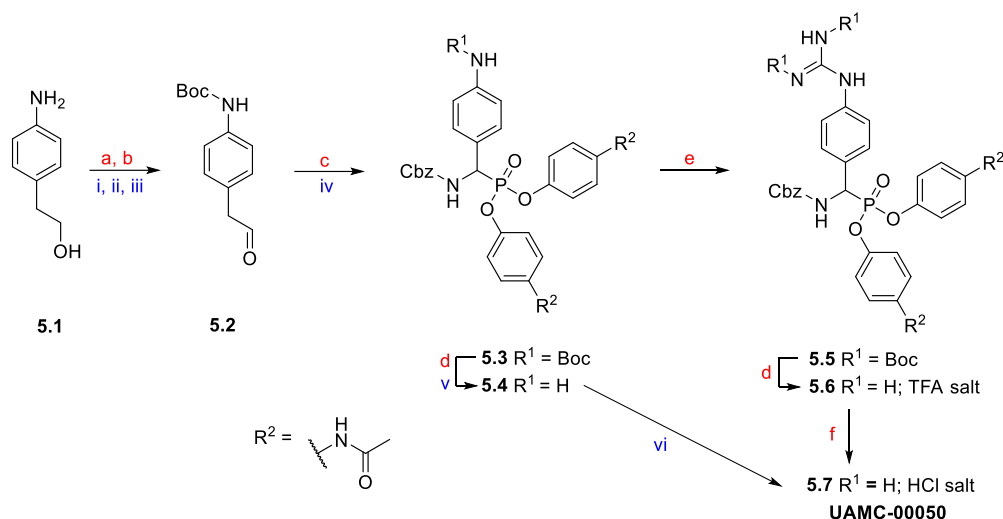
Recently, Ceuleers *et al.* (2022) corroborated the potential of UAMC-00050 as a promising compound for the treatment of visceral pain in a neonatal acetic acid-induced mouse model. IBS was induced in C57BL/6 mice by an intracolonic infusion of 20 μL of a 0.5% acetic acid solution in 0.9% NaCl. The animals were treated with a single intraperitoneal injection of UAMC-00050 or nafamostat 30 min prior to the VMR experiment. Administration of UAMC-00050 [$2 \text{ mg}\cdot\text{kg}^{-1}$] could completely reverse visceral hypersensitivity to control values.²⁹⁶

Analyzing all these studies on the effect of UAMC-00050 in different IBS animal models, we can conclude that serine protease inhibitors potentially reduce visceral hypersensitivity in these experimental settings. Thus, proving that serine proteases play a pivotal role in developing this pathology and giving evidence that serine protease inhibitors may be a potential therapeutic strategy for treating abdominal pain.

5.2 Results and discussion

5.2.1 Up-scaled chemical synthesis

The upscaled chemical synthesis of UAMC-00050 to a 10 g scale was performed by PhD student Davide Ceradini at the Latvian Institute of Organic Synthesis (LIOS) in Riga, Latvia, where I did an academic secondment for one month within the IT-DED³ consortium. The synthetic route is depicted in **Scheme 5.1**. In red are the conditions used in the previous synthetic route, and in blue are the new conditions.



Scheme 5.1 Synthesis of UAMC-00050 – Old synthetic route vs. New up-scaled route

Old synthetic route: (a) Boc_2O , Et_3N , dioxane, rt; (b) DMP, DCM, 0°C to rt (60% - 2 steps); (c) Benzyl carbamate, diaryl phosphite, $\text{Cu}(\text{OTf})_2$, CH_3CN , rt, 16 h (20%); (d) TFA/DCM (1:2) rt, 3 h (>90%); (e) N, N'-Bis-Boc-1-Guanylpurazole, Et_3N , CH_3CN , 36 h (40%); (f) DOWEX 1x8 Cl, $\text{EtOH}/\text{H}_2\text{O}$ (2:1), rt, 32 h (>90%).

New up-scaled route: (i) Boc_2O , EtOAc , rt (99%), (ii) NaOCl , TEMPO, KBr , Toluene/ EtOAc (1:1), 0°C ; NaHSO_3 , EtOH , rt (80%); (iii) Na_2CO_3 , $\text{EtOAc}/\text{H}_2\text{O}$, rt (89%); (iv) Benzyl carbamate, triaryl phosphite, $\text{Y}(\text{OTf})_3$, $\text{CH}_3\text{CN}/\text{THF}$ (1:1), TFAA, rt (44%); (v) HCl 4N dioxane, rt (99%); (vi) NH_2CN , $\text{Sc}(\text{OTf})_3$, $\text{CH}_3\text{CN}/i\text{PrOH}$ (1:1), rt (72%).

The entire description and optimization can be found in Ceradini *et al.*³⁰⁷ In summary, the old synthetic route showed several problems regarding yield, hazardous reagents, environmental footprint, and process scalability. An optimized process for the scalable multigram preparation of the α -aminophosphonate UAMC-00050 was developed. Environmental unfriendly solvents were removed (e.g., DCM), and hazardous reagents were replaced with more handleable compounds and more efficient atom economy (e.g., N, N'-Bis-Boc-1-Guanylpurazole). Furthermore, every reaction was investigated to obtain the maximum yield, and all the flash chromatography purifications were replaced with plug filtration and slurry purifications. The key step of the route, the Birum-Oleksyzyn reaction, a three-component reaction between an aldehyde, a carbamate, and a phosphite, was widely investigated. Trifluoroacetic anhydride (TFAA) proved to be an essential additive, improving the reactivity of the diaryl phosphite and increasing the reaction yield. The overall yield was increased from 3% in the discovery route to 22% in the process development route.

5.2.1 Evaluation of UAMC-00050 enantiomers

UAMC-00050 is synthesized as a mixture of enantiomers with two configurations of the α -carbon of the phosphonate. Noteworthy, it has been used as a racemic mixture in previous studies, as the enantioselective synthesis of this compound is not available. However, it was previously reported by Walker *et al.* that serine protease inhibition depends on the configuration of the phosphonate. This is explained by the fact that the phosphonate (R)-isomer directly compares with the (S)-isomer of natural amino acids.³⁰⁸ Thus, only the (R)-isomer is expected to exhibit inhibition.

PhD student Davide Ceradini at LIOS separated the two enantiomers of intermediate **5.5** by preparative HPLC with a CHIRALPAK IG column (250x30 nm-5 μ m) (**Figure 5.2**). Followed by the removal of the Boc-protection to achieve the two enantiomers of UAMC-00050 (**5.7**). However, the absolute configuration was not determined. Therefore, we call them enantiomer 1 (E1) and 2 (E2).

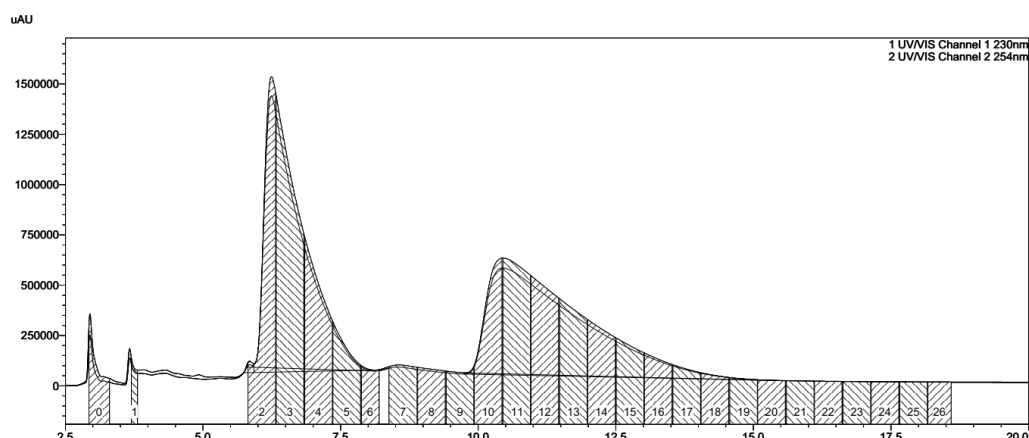


Figure 5.2 Chiral chromatogram of the racemic mixture of intermediate **5.5** with the two enantiomers

The racemic mixture of UAMC-00050 and the two enantiomers were biochemically evaluated in β -tryptase and urokinase plasminogen activator (uPA) at UAMC. Their half-maximal inhibitory concentration (IC_{50}) values were determined, and the kinetic progress curves were measured to determine the inhibition mechanism (**Table 5.1**).

Table 5.1 Biochemical evaluation of racemic mixture of UAMC-00050 and the two enantiomers in uPA and β -tryptase

#	β -tryptase	uPA ^a	β -tryptase	uPA ^a
	IC ₅₀ (μ M) ^b		k _{app} (M ⁻¹ s ⁻¹) ^c	
UAMC-00050 R (5.7)	0.023 \pm 0.004	0.0042 \pm 0.0006	Rev.	49x10 ⁴ \pm 39x10 ³ Irrev.
UAMC-00050 E1 (5.8)	0.161 \pm 0.04	0.0193 \pm 0.0008	N.D.	26x10 ³ \pm 20x10 ² Irrev.
UAMC-00050 E2 (5.9)	0.006 \pm 0.001	0.0023 \pm 0.0004	Rev.	97x10 ⁴ \pm 90x10 ³ Irrev.

^a Panel of serine proteases abbreviations: urokinase plasminogen activator (uPA)

^b Half maximal inhibitory concentration (IC₅₀) value is the concentration of inhibitor required to reduce the enzyme activity to 50% after a 15 min preincubation with the enzyme at 37 °C and activity measurements as mentioned in the Experimental section. IC₅₀ values are calculated from two independent experiments; when SD was higher than three times the average value, a third independent experiment was run (mean \pm SD).

^c k_{app} values are calculated from two independent experiments; when SD was higher than three times the average value, a third independent experiment was run (mean \pm SD)

The IC₅₀ of the enantiomers show that the enantiomer E2 has a higher inhibitory potency than the other enantiomer and the racemic mixture in both enzymes. Surprisingly, the other enantiomer was also an inhibitor despite being less potent. In the study published by Walker *et al.*, they encountered similar observations.³⁰⁸ For tryptase, UAMC-00050 E2 is 4- and 27-fold more potent than the racemic mixture and E1, respectively, whereas, for uPA, the differences are 2- and 8-fold.

The kinetic curves showed that the racemic mixture and the two enantiomers behave in the same manner. For β -tryptase, UAMC-00050 has a reversible mechanism. Contrary, it inhibits uPA irreversibly. For the latter, the second-order rate constant (k_{app}) was determined. The k_{app} values show a similar trend to the IC₅₀. The enantiomer E2 (k_{app} = 97x10⁴ M⁻¹ s⁻¹) is 2-fold more potent than the racemic mixture (k_{app} = 49x10⁴ M⁻¹ s⁻¹) and 37-fold more potent than E1 (k_{app} = 26x10³ M⁻¹ s⁻¹).

5.3 Conclusions and future perspectives

UAMC-00050 is a diaryl phosphonate inhibitor developed by UAMC.¹²⁸ It is a multi-target trypsin-like serine protease inhibitor with a high affinity for different proteases within this enzymatic family. Previously, it showed promising results in animal models of DED and IBS. Moreover, it served as a proof of concept that serine protease inhibitors might be a therapeutic agent for these diseases. Unfortunately, UAMC-00050 inhibits broadly trypsin-like serine proteases; therefore, it is impossible to establish which serine proteases play a role in these diseases. Further evaluation is needed to unravel this aspect. Later, UAMC-00050 could be further optimized to gain selectivity towards those targets.

Within the collaboration of the IT-DED³ consortium, the synthetic route of UAMC-00050 was modified to a scale of 10.0 g in LIOS, Riga (Latvia). This new synthetic pathway is more efficient and greener and is translatable to other diaryl phosphonates that might be of interest in the future.

Up to date, only the racemic mixture of UAMC-00050 has been evaluated. During the PhD, the two enantiomers of UAMC-00050 were available for biochemical evaluation, and their IC_{50} and kinetic progress curves were measured. Surprisingly, both enantiomers showed inhibitory potency towards β -tryptase and uPA. However, enantiomer E1, with supposedly the (R)-configuration, displayed higher affinity. It is known that the (R)-configuration of the diphenyl phosphonates resembles the (S)-configuration of natural amino acids. Therefore, it is supposed to fit better on the active site of serine proteases. However, determination of the absolute configuration should be done to prove this.

The study of UAMC-00050 on trypsin-like serine proteases and in pathology models opens future research toward the determination of which serine proteases are involved in DED and IBS and the development of new serine protease inhibitors as therapeutic agents for these diseases.

5.4 Experimental section

5.4.1 Chemistry

The synthesis of UAMC-00050 with the old synthetic route was already reported.¹²⁸ In this section, the synthesis performed at LIOS (Riga, Latvia) for a scale of 10.0 g is described.

Unless otherwise specified, all commercially available reagents were used as received. ¹H, ¹³C, and ³¹P NMR spectra were obtained on a 400 MHz Bruker Avance 400 spectrometer at 400, 101, and 162 MHz, respectively. Chemical shifts (δ) are reported in parts per million (ppm) relative to the residual DMSO peak. Multiplicities are given as s (singlet), d (doublet), t (triplet), q (quartet), and m (multiplet). Complex splittings are described by a combination of these abbreviations, *i.e.*, dd (doublet of doublets). Reaction conversion was estimated by LC-MS on Waters Acquity UPLC H-class instrument, column Waters Acquity UPLC BEH-C18, 2.1 \times 50 mm, 1.7 μ m, eluent 5–95% CH₃CN in 0.1% aq. HCOOH; flow rate: 0.8 mL/min; detection Waters PDA Detector (200–300 nm). HPLC were recorded with Waters Alliance instrument equipped with 2695 separations module, consisting of quaternary pump, degasser, autosampler, and column heater, Waters 2489 dual wavelength absorbance detector was used for detection of analytes or Shimadzu Prominence-I LC-2030C, column prevail organic acid or Apollo C18-13, 4.6 \times 150 mm, eluent 25 – 95% or 40 – 95% CH₃CN in 0.1% aq. H₃PO₄; flow rate: 1.0 mL/min, temp. = 40 °C, detector at 254 nm. HRMS spectra were acquired on an electrospray ionization mass spectrometer with a TOF analyzer, using the following parameters: positive ionization mode, drying gas 10 mL/min and 325 °C, fragment or ionization 100 V.

Tert-butyl (4-(2-oxoethyl)phenyl)carbamate (5.2) (i) To a 500 mL flask equipped with a magnetic stirrer, were added **5.1** (10.0 g, 0.073 mol, 1.0 eq.), EtOAc (200 mL) and di-tert-butyl dicarbonate (17.50 g, 0.08 mol, 1.1 eq.). The mixture was stirred for 16 h at 20–25 °C, and then heptane (100 mL) was added to the reaction mixture. A silica pad with 180 g of silica gel was prepared in a 350 mL glass filter, the solution was poured on the filter and

washed with 500 mL of EtOAc/heptane 2:1, then the solvent was removed to yield tert-butyl (4-(2-hydroxyethyl)phenyl)carbamate (17.0 g, 0.072 mol, 99% yield) as a white solid. ^1H NMR (400 MHz, DMSO- d_6) δ (ppm) 9.20 (s, 1H), 7.35 (d, J = 8 Hz, 2H), 7.09 (d, J = 8 Hz, 2H), 4.95 (s, 1H), 3.56 (q, J = 8 Hz, 2H), 2.65 (t, J = 8 Hz, 2H), 1.47 (s, 9H). (ii) To a 500 mL flask equipped with a magnetic stirrer were added the Boc-protected alcohol (17.30 g, 0.073 mol, 1.0 eq.), dissolved in EtOAc (90.0 mL) and TEMPO (114 mg, 0.73 mmol, 0.01 eq.) dissolved in toluene (90.0 mL), then potassium bromide (869 mg, 7.3 mmol, 0.1 eq.) dissolved in NaHCO₃ sat. (67.0 mL). The mixture was vigorously stirred for 10 minutes in an ice bath, then sodium hypochlorite 13% (67.0 mL) was added dropwise in 5 minutes. The reaction was vigorously stirred for 10 min., then was quenched with sodium thiosulfate 10% (250.0 mL), the reaction mixture was washed with EtOAc (3 x 200 mL), and the combined organic layers were then washed with brine (500 mL), dried with Na₂SO₄ (250.0 g). The solvent was removed by rotary evaporation. The crude aldehyde was then dissolved in ethanol 96% (340.0 mL) in a 500 mL flask equipped with a magnetic stirrer. Sodium bisulfite (11.71 g, 0.113 mol, 1.5 eq.) dissolved in 20 mL of deionized water was added dropwise in 5 min., the mixture was stirred for 18 h at 20-25 °C and 1 h at 0 °C, and the solid was filtrated, washed with cold ethanol 96% (300 mL). And dried in a vacuum for 16 h to yield sodium 2-(4-((tert-butoxycarbonyl)amino)phenyl)-1-hydroxyethane-1-sulfonate (18.47 g, 0.058 mol, 80% yield) a white solid. ^1H NMR (400 MHz, D₂O) δ (ppm) 7.30 (d, J = 2 Hz, 4H), 4.61 (dd, J = 11.3 Hz, 1H), 4.32 (dd, J = 16.4 Hz, 1H), 2.88 (dd, J = 12.1 Hz, 1H), 1.50 (s, 9H). (iii) To a 500 mL flask were added the previous intermediate (19.68 g, 0.085 mol, 1.0 eq.) dissolved in deionized water (260 mL), sodium carbonate (17.20 g, 0.162 mol, 2.2 eq.), and EtOAc (300 mL), the mixture was stirred for 3 h at 20-25 °C, the solution was placed in a 1.0 L separation funnel and extracted with EtOAc (3 x 250 mL), the combined organic layers were washed with brine (400 mL) and dried on Na₂SO₄ (250 g), the solvent was removed with vacuum to yield **5.2** (17.79 g, 0.076 mmol, 89% yield) as pale yellow solid. ^1H NMR (400 MHz, DMSO- d_6) δ (ppm) 9.63 (t, J = 4 Hz, 1H), 9.32 (s, 1H), 7.43 (d, J = 8 Hz, 2H), 7.11 (d, J = 8 Hz, 2H), 3.66 (d, J = 4 Hz, 2H), 1.47 (s, 9H).

Tert-butyl 4-(2-(((benzyloxy)carbonyl)amino)-2-(bis(4-acetamidophenoxy)phosphoryl)ethyl)phenyl)carbamate (5.3) To a 500 mL flask equipped with a magnetic stirrer were added in this order: compound **5.2** (10.0 g, 0.043 mol, 1.0 eq.), yttrium triflate (2.30 g, 4.3 mmol) dissolved in dry-CH₃CN (130.0 mL), benzyl carbamate (6.50 g, 0.043 mol, 1.0 eq.), tris(4-acetamidophenyl) phosphite (23.00 g, 0.043 mol, 1.0 eq.), dry-THF (130.0 mL) and trifluoroacetic anhydride (5.98 mL, 0.043 mol, 1.0 eq.). The mixture was stirred for 4 h at 20-25 °C. The solvent was removed, and the residue was dissolved in a solution of EtOAc/ethanol 4:1 (500 mL). The organic phase was washed with NaOH 0.5 M (4 x 500 mL) and brine (500 mL). The organic layers were collected together, dried on Na₂SO₄ (300 g), and the solvent was removed with vacuum. A silica pad with 200 g of silica gel was packed in a 500 mL glass filter, and the residue was dissolved in a solution of heptane/EtOAc/ethanol 21:5:2 (250 mL). The mixture was poured through the filter and washed with EtOAc/heptane 2:1 (2000 mL) to collect fraction 1, the collection flask was changed, and the silica pad was washed with EtOAc/ethanol 3:1 (1000 mL) to collect fraction 2, the solvent was removed from fraction 2 to yield **5.3** as a yellow foamy solid. The crude product was dissolved in acetone (100 mL), and a solution of NaHCO₃ 0.5% (200 mL) was added dropwise. The solid was filtered, washed with MTBE (100 mL), and dried in vacuum overnight. The dry solid was suspended in EtOAc/acetone 19:1 (300 mL), stirred for 24 h, filtered, washed with EtOAc (100 mL), and dry in vacuum overnight to yield **5.3** (13.55 g, 0.019 mol, 44% yield) as white solid. ¹H NMR (400 MHz, DMSO-d₆) δ (ppm) 10.00 (s, 2H), 9.32 (s, 1H), 8.11 (d, *J* = 8 Hz, 1H), 7.57 (m, 4H), 7.39 (d, *J* = 8 Hz, 2H), 7.30 (m, 3H), 7.19 (d, *J* = 8 Hz, 2H), 7.12 (m, 6H), 4.97 (dd, *J* = 32.12 Hz, 2H), 4.42 (q, *J* = 12 Hz, 1H), 3.18 (d, *J* = 12 Hz, 1H), 2.90 (m, 1H), 2.04 (s, 6H), 1.49 (s, 9H).

4-(2-(((benzyloxy)carbonyl)amino)-2-(bis(4-acetamidophenoxy)phosphoryl)ethyl)benzenaminium chloride (5.4) In a 500 mL flask equipped with a magnetic stirrer, were added in this sequence: compound **5.3** (10.00 g, 0.014 mol, 1.0 eq.) and 4 M HCl in dioxane (150 mL), the solution was stirred for 3 h at 20-25 °C, and then the solvent was removed with vacuum. The residue was dissolved in dry-EtOH (100 mL), and the solution was added dropwise to 1000 mL of EtOAc, and the mixture was stirred for 30 min. at 20-25 °C, the

precipitate was filtered and dried in vacuum overnight to yield **5.4** (9.05 g, 0.014 mmol, 99% yield) as an off-white powder. ^1H NMR (400 MHz, DMSO- d_6) δ (ppm) 10.09 (d, $J = 4$ Hz, 2H), 9.76 (s, 2H), 8.17 (d, $J = 12$ Hz, 1H), 7.658 (m, 4H), 7.38-7.28 (m, 5H), 7.21 (t, $J = 8$ Hz, 5H), 7.09 (m, 4H), 4.96 (dd, $J = 20, 12$ Hz, 2H), 4.45 (m, 1H), 3.25 (m, 1H), 2.99 (m, 1H), 2.03 (s, 6H).

Benzyl (1-(bis(4-acetamidophenoxy)phosphoryl)-2-(4-guanidinophenyl)ethyl)carbamate (5.7) In a 50 mL flask were added compound **5.4** (5.00 g, 7.7 mmol, 1.0 eq.), Sc(OTf) $_3$ (377 mg, 0.77 mmol, 0.1 eq.) dissolved in 15.4 mL of dry-THF/abs-EtOH (2:1 v/v) and cyanamide (3.23 g, 77.0 mmol, 10.0 eq.). The flask was flushed with Argon for 10 min., and the solution was left to stir for 96 h. The solvent was removed, and the crude product was dissolved in 50 mL of abs-EtOH, dropped in 500 mL of *i*PrOAc at rt, and stirred for 1 h. The solid was filtered, washed with 250 mL of *i*PrOAc, and dried in vacuum overnight. The crude material was dissolved in 500 mL of deionized water/EtOH (10:1 v/v) and pre-loaded on a 300 g YMC-DispoPack AT reverse phase column. The column was eluted with deionized water/(CH $_3$ CN/EtOH 9:1) gradient 0-100%. The solid was collected from the selected tubes, and the solvent was removed with freeze-drying to yield **5.7** (3.64 g, 5.54 mmol, 72% yield). ^1H NMR (400 MHz, DMSO- d_6) δ (ppm) 10.04 (s, 2H), 8.44 (s, 1H), 8.18 (d, $J = 12$ Hz, 1H), 7.97 (s, 3H), 7.57 (m, 4H), 7.35 (d, $J = 8$ Hz, 2H), 7.29 (m, 3H), 7.19 (m, 2H), 7.10 (m, 6H), 4.97 (dd, $J = 20.12$ Hz, 2H), 4.46 (q, $J = 8$ Hz, 1H), 3.22 (m, 1H), 3.00 (m, 1H), 2.03 (s, 6H).

5.4.2 Development of biochemical protocols

For this chapter, UAMC-00050 was tested in recombinant uPA and β -tryptase. However, this section explains the development of all biochemical protocols for the trypsin-like serine proteases used during this doctoral thesis and utilized later in **Chapters 6** and **7**. These include trypsin-3, thrombin, and cathepsin G. Neutrophil elastase and chymotrypsin have also been used in **Chapter 6**. However, the measurements were performed by the Laboratory of Medical Biochemistry at the University of Antwerp and the Laboratory for Intestinal Neuroimmune Interactions at KU Leuven.

5.4.2.1 IC_{50} determination

The IC_{50} is the most used measure to define the inhibitory potency of a molecule. It describes the concentration needed to inhibit a specific biological process.³⁰⁹ In the case of enzymatic activity, the IC_{50} value is defined as the concentration of inhibitor required to reduce the enzyme activity to 50%.

Protocols to determine the inhibitory potency for uPA and tryptase were already present at UAMC. The IC_{50} values were determined using a spectrophotometric or fluorogenic assay. A summary of the conditions used in the original protocols is described in **Table 5.2**, and more details are given in the following discussion.

Table 5.2 Assay conditions of the original IC_{50} protocols for urokinase plasminogen activator (uPA) and tryptase present at the Laboratory of Medicinal Chemistry (UAMC).

Enzyme	Substrate	Buffer
uPA^a (~20 nM)	<i>pyro</i> -Glu-Gly-Arg-pNA (250 μ M)	50 mM HEPES (pH 8.1)
Tryptase (1:200)	Tosyl-Gly-Pro-Arg-pNA (0.5 mM)	50 mM Tris-HCl, 0.02% Triton-X (pH 8.0)

^a Abbreviations: Urokinase plasminogen activator (uPA)

The protocol to determine the inhibitory potency for uPA was used as previously described. However, the final substrate concentration was modified to the K_m value.³¹⁰

Final IC_{50} protocol for uPA: Enzymatic activity was measured for 30 min at 37 °C using uPA (recombinant urokinase plasminogen activator, HYPHEN BioMed) and chromogenic substrate *pyro*-Glu-Gly-Arg-pNA ($K_m = 80 \mu$ M) in HEPES buffer (50 mM HEPES) at pH 8.1 (25°C). The readout consisted of evaluating the protease-mediated release of the chromophore *para*-nitroaniline (pNA) from the substrate. Absorbance was monitored at $\lambda = 405$ nm. Each reaction mixture had a total volume of 200 μ L and contained the inhibitor in DMSO (5 μ L), the enzyme in buffer (145 μ L) at an approximate concentration of 20 nM, and the chromogenic substrate in water (50 μ L) at a final concentration of 80 μ M. The

inhibitor was preincubated for 15 min with the enzyme at 37 °C before adding the substrate.

To corroborate that the protocol was reproducible in my hands, the IC_{50} value of racemic UAMC-00050 was determined and compared to the previously published value ($IC_{50} = 4.2$ nM) (Figure 5.3).

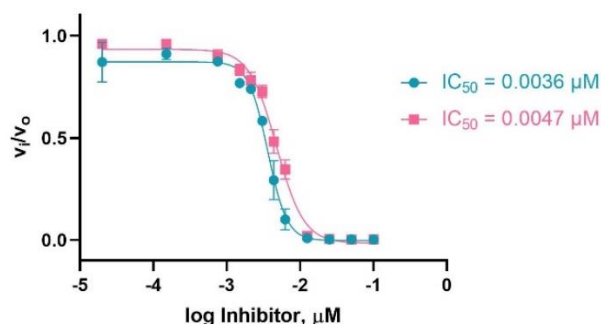


Figure 5.3 Determination of IC_{50} value of UAMC-00050 with two independent experimental results

The protocol to determine the inhibitory potency of trypsin already in place at UAMC did not have consistency and was not reproducible in my hands. The protocol used a stock solution of trypsin diluted 1:100 in 10 mM MES buffer and 2 M NaCl (pH 6.1). In a microplate were added 15 μL of inhibitor and 15 μL of trypsin and buffer (1:200). The buffer used was 50 mM Tris-HCl, 0.02% Triton-X (pH 8.0). After 15 min of incubation, 15 μL of Tosyl-Gly-Pro-Arg-pNA ($K_m = 1.5$ mM) were added with a final concentration of 0.5 mM. Suppliers of enzyme and substrate were not mentioned.

The first step to improving the protocol was decreasing the DMSO percentage. This was solved by increasing the concentration of the substrate stock solution. Next, to reduce pipetting errors, the volumes were increased for easier handling of the multi-channel pipette. Even though the protocol used more quantity of substrate and enzyme, therefore being more expensive, the assay was more reliable and reproducible. Last, the concentration of trypsin was modified to find the best readout possible with the least enzyme (final well concentration = 0.125 nM).

Despite the changes, the enzyme seemed to not be stable under the assay conditions, as the absorbance measured was close to the blank in some experiments. Tryptase is only active when it is presented as a tetramer structure. This structure is stabilized by heparin or high quantities of NaCl.³² After checking several protocols for tryptase in literature, the buffer was modified to 50 mM Tris 120 mM NaCl pH 8,0 + 0,1 mg/mL BSA + 50 µg/mL heparin.^{311–315}

Last, the chromogenic substrate was substituted with the fluorogenic Boc-Gln-Ala-Arg-AMC. The readout consisted of evaluating the protease-mediated release of the fluorophore 7-amino-4-methyl coumarin (AMC). The K_m of the substrate was measured by incubating the enzyme with different substrate concentrations ranging from 1 to 1000 µM and calculated by fitting the data to the Michaelis-Menten equation of GraphPad9.

Final IC₅₀ protocol for tryptase: Enzymatic activity was measured for 30 min at 37 °C using tryptase (recombinant tryptase β-2, EnzoLife Sciences) and fluorogenic substrate Boc-Gln-Ala-Arg-AMC ($K_m = 146 \mu\text{M}$) in Tris buffer (50 mM Tris, 120 mM NaCl, 0.1 mg/mL BSA, 0.1 mg/mL heparin) at pH 8.0 (25°C). Each reaction mixture had a total volume of 200 µL and contained the inhibitor in DMSO (5 µL), the enzyme in buffer (145 µL) at a concentration of 0.125 nM, and the fluorogenic substrate in buffer (50 µL) at a final concentration of 150 µM. The inhibitor was preincubated for 15 min with the enzyme at 37 °C before adding the substrate. The readout consisted of evaluating the protease-mediated release of the fluorophore AMC from the substrate. Fluorescence was monitored at an excitation of 380 nm and an emission of 460 nm.

The protocols for determining the IC₅₀ for trypsin-3 and thrombin were developed by the Laboratory for Intestinal Neuroimmune Interactions at KU Leuven and used at UAMC under the same conditions and reagents when needed. Before use, an already known IC₅₀ was determined to corroborate the reproducibility of the assay in my hands.

Final IC₅₀ protocol for trypsin-3: Enzymatic activity was measured for 30 min at 37 °C using trypsin-3 (recombinant trypsin-3, R&D) and fluorogenic substrate tosyl-Gly-Pro-Arg-AMC ($K_m = 22.5 \mu\text{M}$) in Tris buffer (100 mM Tris, 1 mM CaCl₂) at pH 8.0 (25°C). Each reaction mixture had a total volume of 200 μL and contained the inhibitor in DMSO (5 μL), the enzyme in buffer (145 μL) at a concentration of 1.5 nM, and the fluorogenic substrate in buffer (50 μL) at a final concentration of 25 μM . The inhibitor was preincubated for 15 min with the enzyme at 37 °C before adding the substrate. The readout consisted of evaluating the protease-mediated release of the fluorophore AMC from the substrate. Fluorescence was monitored at an excitation of 380 nm and an emission of 440 nm.

Final IC₅₀ protocol for thrombin: Enzymatic activity was measured for 30 min at 37 °C using thrombin (recombinant thrombin, R&D) and fluorogenic substrate Boc-Val-Pro-Arg-AMC ($K_m = 15 \mu\text{M}$) in TRIS buffer (50 mM Tris HCl, 50 mM Tris base, 10 mM CaCl₂, 150 mM NaCl) at pH 8.3 (25°C). Each reaction mixture had a total volume of 200 μL and contained the inhibitor in DMSO (5 μL), the enzyme in buffer (145 μL) at an approximate concentration of 0.5 nM, and the fluorogenic substrate in buffer (50 μL) at a final concentration of 15 μM . The inhibitor was preincubated for 15 min with the enzyme at 37 °C before adding the substrate. The readout consisted of evaluating the protease-mediated release of the fluorophore AMC from the substrate. Fluorescence was monitored at an excitation of 380 nm and an emission of 440 nm.

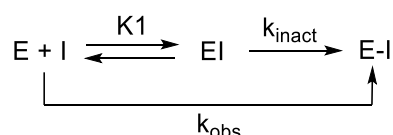
The protocol for determining of the IC₅₀ for cathepsin G was developed by the Laboratory of Medical Biochemistry at the University of Antwerp and used at UAMC under the same conditions and reagents when needed. The intensity of the readout of cathepsin G with the equipment available at UAMC was low, which induced a higher error in some assays. However, the concentrations were kept to compare the assays performed at the two laboratories. Before use, an already known IC₅₀ was determined to corroborate the reproducibility of the assay in my hands.

Final IC₅₀ protocol for cathepsin G: Enzymatic activity was measured for 30 min at 37 °C using cathepsin G (cathepsin G human neutrophil, Sigma-Aldrich) and fluorogenic substrate Suc-Ala-Ala-Pro-Phe-AMC ($K_m = 130 \mu\text{M}$) in Tris buffer (50 mM Tris, 120 mM NaCl) at pH 8.0 (25°C). Each reaction mixture had a total volume of 100 μL and contained the inhibitor in DMSO (5 μL), the enzyme in buffer (45 μL) at a concentration of 100 nM, and the fluorogenic substrate in buffer (50 μL) at a final concentration of 130 μM . The inhibitor was preincubated for 15 min with the enzyme at 37 °C before adding the substrate. The readout consisted of evaluating the protease-mediated release of the fluorophore AMC from the substrate. Fluorescence was monitored at an excitation of 380 nm and an emission of 440 nm.

IC₅₀ values were obtained by fitting the data with the four-parameter logistics equation using GraphPad Prism 9. The IC₅₀ determination was the average of two independent experimental results. This value was accepted when the standard deviation of the two independent experiments was lower than three times the IC₅₀. Contrary, a third independent experiment was performed.

5.4.2.2 Development of a protocol for determination of k_{app}

The k_{app} is used as a potency measurement for irreversible inhibitors. These display a time-dependent inhibition, and the IC₅₀ value is not the ideal measure to describe their inhibitory potency. Most irreversible inhibitors have a two-step mechanism depicted in **Scheme 5.2**, where EI represents the initial reversible enzyme-inhibitor complex, and E-I represents the irreversible complex. The reversible equilibrium constant K_1 describes the formation of EI, and the irreversible inactivation is described by k_{inact} . The overall process is defined by the observed rate constant (k_{obs}).³¹⁶



Scheme 5.2 Two-step mechanism for irreversible inhibitors

The general protocol for kinetic assays was previously reported in published papers by the University of Antwerp.^{126,129,310} Progress curves were recorded in pseudo-first-order conditions ($[I]_0 \gg [E]_0$) and with less than 10% conversion of the substrate during the entire time course. In these conditions, dA/dt decreases exponentially with time. For a simple pseudo-first-order inactivation process, the activity after incubation with inhibitor (v_i) varies with the inhibitor concentration (i), as described in the following equation:

$$v_i = v_0 \cdot e^{-kit}$$

where v_0 is the activity in the absence of an inhibitor, ki is the second-order rate constant of inactivation, and t is the time.

The inhibitor was mixed with the substrate and incubated for a period of 15 minutes. Then, the buffer solution with the enzyme was added at the time zero. The progress curves show the release of pNA or AMC as a function of time. Initially, no inhibitor is bound to the enzyme, and the tangent to the progress curve (dA/dt) is proportional to the free enzyme concentration. The free enzyme concentration decreases over time due to inhibitor binding kinetics. The progress curves were fitted with the integrated rate equation with GraFit7 to yield a value for k_{obs} , a pseudo-first-order rate constant.

$$A_t = A_0 + v_s \cdot t + (v_i - v_s) \cdot (1 - e^{-k_{obs} \cdot t}) / k_{obs}$$

where A_t is the absorbance or fluorescence at time t , A_0 is the absorbance or fluorescence at time zero, v_i is the initial rate, and v_s is the velocity at the steady-state. Finally, the k_{app} was calculated from the slope of the linear part of the plot of k_{obs} vs. the inhibitor concentration ($[I]_0$).

Progress curves of uPA using the same conditions used for the IC_{50} determination did not meet the acceptance requirements. The control did not show linearity throughout the assay time. Therefore substrate depletion was affecting the kinetic curves. To avoid a

substrate depletion higher than 10% and achieve a linear control, the concentration of uPA was reduced to half compared to the concentration used for IC₅₀ determination.

Final progress curve protocol for uPA: Progress curves were measured by the release of pNA for 1 hour at 37°C using uPA (recombinant urokinase plasminogen activator, HYPHEN BioMed) and chromogenic substrate *pyro*-Glu-Gly-Arg-pNA ($K_m = 80 \mu\text{M}$) in HEPES buffer (50 mM HEPES) at pH 8.1 (25°C). Absorbance was monitored at $\lambda = 405 \text{ nm}$. Each reaction mixture had a total volume of 200 μL and contained the inhibitor in DMSO (5 μL), the enzyme in buffer (145 μL) at an approximate concentration of 10 nM, and the chromogenic substrate in water (45 μL) at a final concentration of 80 μM . The inhibitor was mixed with the substrate and incubated for a period of 15 minutes. Then, the buffer solution with the enzyme was added at the time zero.

The progress curves for β -tryptase and trypsin-3 with the concentrations used for IC₅₀ determination did not show substrate depletion throughout the time course of the assay. Therefore, the same enzyme and substrate conditions were used.

Final progress curve protocol for tryptase: Progress curves were measured by the release of AMC for 1 hour at 37°C using tryptase (recombinant tryptase β -2, EnzoLife Sciences) and fluorogenic substrate Boc-Gln-Ala-Arg-AMC ($K_m = 146 \mu\text{M}$) in Tris buffer (50 mM Tris, 120 mM NaCl, 0.1 mg/mL BSA, 0.1 mg/mL heparin) at pH 8.0 (25°C). Fluorescence was monitored at an excitation of 380 nm and an emission of 460 nm. Each reaction mixture had a total volume of 200 μL and contained the inhibitor in DMSO (5 μL), the enzyme in buffer (145 μL) at a concentration of 0.125 nM, and the fluorogenic substrate in buffer (45 μL) at a final concentration of 150 μM . The inhibitor was mixed with the substrate and incubated for a period of 15 minutes. Then, the buffer solution with the enzyme was added at the time zero.

Final progress curve protocol for trypsin-3: Progress curves were measured by the release of AMC for 1 hour at 37°C using trypsin-3 (recombinant trypsin-3, R&D) and fluorogenic

substrate tosyl-Gly-Pro-Arg-AMC ($K_m = 22.5 \mu\text{M}$) in Tris buffer (100 mM Tris, 1 mM CaCl_2) at pH 8.0 (25°C). Fluorescence was monitored at an excitation of 380 nm and an emission of 440 nm. Each reaction mixture had a total volume of 200 μL and contained the inhibitor in DMSO (5 μL), the enzyme in buffer (145 μL) at a concentration of 1.5 nM, and the fluorogenic substrate in buffer (45 μL) at a final concentration of 25 μM . The inhibitor was mixed with the substrate and incubated for a period of 15 minutes. Then, the buffer solution with the enzyme was added at the time zero.

The protocol for determining the k_{app} for thrombin was developed together with the Laboratory for Intestinal Neuroimmune Interactions at KU Leuven and used at UAMC under the same conditions and reagents when needed. Before use, an already measured k_{app} was determined to corroborate the reproducibility of the assay in my hands. The data sets were processed and analyzed at UAMC. To avoid substrate depletion, the enzyme concentration had to be modified compared to the conditions used for IC_{50} determination.

Final progress curve protocol for thrombin: Progress curves were measured by the release of AMC for 1 hour at 37°C using thrombin (recombinant thrombin, R&D) and fluorogenic substrate Boc-Val-Pro-Arg-AMC ($K_m = 15 \mu\text{M}$) in Tris buffer (50 mM Tris HCl, 50 mM Tris base, 10 mM CaCl_2 , 150 mM NaCl) at pH 8.3 (25°C). Fluorescence was monitored at an excitation of 380 nm and an emission of 440 nm. Each reaction mixture had a total volume of 200 μL and contained the inhibitor in DMSO (5 μL), the enzyme in buffer (145 μL) at an approximate concentration 0.25 nM, and the fluorogenic substrate in buffer (50 μL) at a final concentration of 15 μM . The inhibitor was mixed with the substrate and incubated for a period of 15 minutes. Then, the buffer solution with the enzyme was added at the time zero.

The protocol for the determination of the k_{app} for cathepsin G was developed by the Laboratory of Medical Biochemistry at the University of Antwerp and used at UAMC under the same conditions and reagents when needed. Before use, an already measured k_{app} was determined to corroborate the reproducibility of the assay in my hands.

Final progress curve protocol for cathepsin G: Progress curves were measured by the release of AMC for 1 hour at 37°C using cathepsin G (cathepsin G human neutrophil, Sigma-Aldrich) and fluorogenic substrate Suc-Ala-Ala-Pro-Phe-AMC ($K_m = 130 \mu\text{M}$) in Tris buffer (50 mM Tris, 120 mM NaCl) at pH 8.0 (25°C). Fluorescence was monitored at an excitation of 380 nm and an emission of 440 nm. Each reaction mixture had a total volume of 100 μL and contained the inhibitor in DMSO (5 μL), the enzyme in buffer (45 μL) at a concentration of 100 nM, and the fluorogenic substrate in buffer (50 μL) at a final concentration of 130 μM . The inhibitor was mixed with the substrate and incubated for a period of 15 minutes. Then, the buffer solution with the enzyme was added at the time zero.

5.4.2.3 *Development of jump dilution protocol*

The kinetic progress curves can suggest the type of mechanism of inhibition. While an irreversible inhibitor will have a steady-state velocity equal to zero, for a reversible compound, the steady-state rate will differ from zero. Moreover, the plot of k_{obs} versus $[I]$ is a straight line for simple bimolecular reactions, and for an irreversible inhibitor, the line goes through the origin or close to it. However, the experimental error can be significant and is not proof of irreversibility. For a reversible reaction, the Y-intercept of the plot of k_{obs} versus $[I]$ is the off-rate constant (k_{off}). For slow-binding inhibitors, when the k_{off} is very slow, these can appear to be irreversible. Therefore, it is necessary to perform additional assays, such as jump dilutions, to corroborate the irreversible nature. These use an inhibitor concentration of 10-fold the IC_{50} for the incubation, and *a posteriori*, the reaction mixture is diluted 10-fold or 100-fold before adding the substrate. In the case of an irreversible inhibitor, enzymatic activity is not regained, whereas, in the case of a reversible compound, a slow release of the inhibitor and a gradual increase of the enzymatic activity rate is observed.^{316,317}

The protocols for the jump dilution assay used for uPA, β -tryptase, trypsin-3, and thrombin were developed at UAMC. While the buffer, substrate concentration, and pre-incubation period were kept like the previous assays, the desired enzyme concentration had to be determined not to observe residual enzymatic activity after the dilution. This was especially

challenging to obtain the desired readability within the detection limit of the spectrophotometer and not observe residual activity after the dilution. The pre-incubation enzyme concentration was 2.5x to 4x the one used in the previous assays. All protocols were validated by analyzing a compound with a known mechanism of inhibition.

The results of the jump dilutions of some compounds for Cathepsin G, shown in the experimental section of **Chapter 6**, have a different protocol. This was developed and performed by the Laboratory of Medical Biochemistry at the University of Antwerp. However, the rest of the jump dilutions for cathepsin G were measured at UAMC following a protocol similar to the other proteases. The concentrations used for enzyme and substrate were the same as the protocol developed by the Laboratory of Medical Biochemistry. To validate the protocol, the jump dilution of a compound analyzed by the Laboratory of Medical Biochemistry was also measured by the newly developed protocol.

Final jump dilution protocol: Progress curves were measured by the release of pNA or AMC for 16 hours at 37°C using the recombinant enzymes and substrates specified in the previous protocols. Absorbance and fluorescence were measured, as previously mentioned. Each reaction mixture had a total volume of 200 µL and contained the inhibitor in DMSO (5 µL), the enzyme in buffer (145 µL) at a concentration 2.5x to 4x the one used in previous assays and the chromogenic or fluorogenic substrate in buffer (50 µL) at a final concentration equal to the K_m . The inhibitor was preincubated for 15 min with the enzyme at 37 °C before dilution. The diluted reaction mixtures were allowed to reach equilibrium for 30 min before adding the substrate.

CHAPTER 6

CHEMICALLY DIVERSE ACTIVITY-BASED PROBES WITH UNEXPECTED INHIBITORY MECHANISMS TARGETING TRYPSIN-LIKE SERINE PROTEASES

Published as:

Alba Ramos-Llorca, Lisse Decraecker, Valerie Cacheux, Irena Zeiburlina, Michelle De bruyn, Louise Battut, Carlos Moreno-Cinos, Davide Ceradini, Eric Espinosa, Gilles Dietrich, Maya Berg, Ingrid De Meester, Pieter Van Der Veken, Guy Boeckxstaens, Anne-Marie Lambeir, Alexandre Denadai-Souza and Koen Augustyns.

Chemically Diverse Activity-Based Probes With Unexpected Inhibitory Mechanisms Targeting Trypsin-Like Serine Proteases. *Frontiers in Chemistry*, **2023**, 10, 1089959.

Responsible for chemical synthesis, biochemical and kinetic characterization of molecules, and writing of the manuscript.

Chapter 6 **Chemically diverse activity-based probes with unexpected inhibitory mechanisms targeting trypsin-like serine proteases**

6.1 Abstract

Activity-based probes (ABP) are molecules that bind covalently to the active form of an enzyme family, making them an attractive tool for target and biomarker identification and drug discovery. The present study describes the synthesis and biochemical characterization of novel ABPs targeting trypsin-like serine proteases. We developed an extensive library of ABPs with “clickable” affinity tags and a diaryl phosphonate warhead. A wide diversity was achieved by including natural amino acid analogs as well as basic polar residues as side chains. A detailed enzymatic characterization was performed in a panel of trypsin-like serine proteases. Their inhibitory potencies and kinetic profile were examined, and their IC_{50} values, mechanism of inhibition, and kinetic constants were determined. The ABPs with a benzyl guanidine side chain showed the highest inhibitory effects in the panel. Surprisingly, some of the high-affinity probes presented a reversible inhibitory mechanism. On the other hand, probes with different side chains exhibited the expected irreversible mechanism. For the first time, we demonstrate that not only irreversible probes but also reversible probes can tightly label recombinant proteases and proteases released from human mast cells. Even under denaturing SDS-PAGE conditions, reversible slow-tight-binding probes can label proteases due to the formation of high-affinity complexes and slow dissociation rates. This unexpected finding will transform the view on the required irreversible nature of ABPs. The diversity of this library of ABPs, combined with a detailed enzyme kinetic characterization, will advance their applications in proteomic studies and drug discovery.

6.2 Introduction

In recent years, many efforts have been carried out to study the expression and function of proteins in biological organisms. This provided new insights into the pathophysiology of different diseases and disorders. Activity-based protein profiling (ABPP) is a proteomics technique that uses activity-based probes (ABPs) to visualize and characterize enzyme activity within a complex proteome. These chemical probes are designed to react covalently with the active form of a target enzyme and allow their detection or isolation. Thus, ABPs give information about the activity level of an enzyme rather than its expression level.^{75,318} This feature represents a considerable advantage since protease activity is tightly regulated. All ABPs share a similar structure consisting of four parts: (i) a warhead or reactive group; (ii) a selectivity enhancing group that targets a specific enzyme family; (iii) a reporter tag used for visualization or isolation, and (iv) a linker or spacer to connect the three other components.^{79,80}

ABPs have the potential for target and biomarker identification in different pathologies.³¹⁹ The most common application for ABPs is detecting and visualizing active enzymes in biological samples, including *in vitro* samples, and visualization in animal models *in vivo*. However, uptake of the ABPs by living organisms can be problematic due to their bulkiness. Alternatively, conjugation with the reporter tag can be done *in situ* by click chemistry. The probe precursors are added to living cells or tissues and then undergo the reaction with a fluorophore or affinity label to yield the ABP. Subsequently, the probes can be visualized or identified by different techniques.^{74,320}

Different analytical tools can detect the complex enzyme-ABP. The method used depends on the reporter tag of choice. Fluorescent or radioactive labels could be detected by SDS-PAGE gel, imaging by microscopy, or flow cytometry.^{77,321,322} Whereas, Western blots are used for biotinylated probes.^{97,104} The latter can also be used to isolate or purify the targeted enzyme before detection. The strong interaction of biotin with immobilized avidin makes it a good strategy for enzyme affinity purification and mass spectrometry (MS)

detection, thereby allowing the unambiguous identification of active proteases.^{81,106} Unfortunately, the conditions needed to dissociate the biotin-avidin interaction are harsh and sometimes unsuitable for the analysis. Alternatively, desthiobiotin, an analog of biotin which does not contain sulfur, can be used. Desthiobiotin has a lower affinity with avidin, therefore the ABPs and enzymes can better tolerate the dissociation conditions.^{107,108}

ABPs have been designed for various enzyme families.^{323–325} Specifically, they have been widely studied for many proteases,⁷³ such as cysteine,^{326,327} metalloproteases,³²⁸ and serine proteases.¹¹⁴ Serine proteases represent one of the largest classes of proteases expressed in the human degradome. Unlike cysteine proteases, which are predominantly intracellular, most serine proteases are secreted enzymes, thereby active players in cell-to-cell communication in health and disease. Unambiguous identification of active serine proteases released by cells has been hindered by the limitations of classical studies based on enzymatic substrates and inhibitors due to the catalytic overlap among proteases, while the use of ABPs for this purpose has made its proof.²⁰⁵

The first probe targeting serine proteases was based on a fluorophosphonate warhead, designed to react covalently with the active site serine residue on serine hydrolases. However, it has a wide-ranging reactivity and did not show selectivity towards serine proteases.⁸⁷ Other warheads reported for this enzyme family include isocoumarins,¹²¹ sulfonyloxyphtalimides,¹²³ and diphenyl phosphonates.⁹⁴

Diphenyl phosphonate (DPP) is a well-studied reactive group. The phosphorus can react with the serine hydroxyl on the active site to form a covalent bond. Thus, it has the required characteristics to design selective and irreversible ABPs. Therefore, it was previously used to develop irreversible inhibitors and ABPs targeting serine proteases.^{128,132,138}

Within the human degradome, serine proteases can be divided into three main subfamilies known as trypsin-, chymotrypsin-, and elastase-like, depending on their substrate specificity. The specificity of a protease is determined by the preferred amino acid

sequence that will fit into the specificity pocket of the active site.¹⁵ In this study, we focus on trypsin-like serine proteases. These have an aspartic acid residue at the bottom of the primary substrate binding pocket (S1). Thus their preference is shifted towards basic and polar residues such as lysine or arginine.²⁰²

The first synthesized α -aminoalkyl diphenyl phosphonate ABPs targeting trypsin-like proteases were described by Hawthorne *et al.*⁹⁰ These were based on lysine (**Biotin-Lys-DPP**) and ornithine (**Bio-Orn-DPP**) as a selectivity enhancing group. Similarly, Pan *et al.* described a lysine ABP by adding a pegylated linker. Additionally, they described a promising ABP with two residues, lysine in P1 and proline in P2 (**Biotin-PK-DPP**).⁹¹ More recently, Reihill *et al.* described an arginine probe (**Biotin-Arg-DPP**) as an inhibitor for channel-activating proteases.^{93,329,330} Moreover, several “clickable” benzyl guanidine probes conjugated with different reporter tags were reported, for instance, biotin (**Biotin-p-guanidino-Phe-DPP**).¹³⁰ This was proven to be a potential Positron emission tomography (PET) imaging agent if coupled with a radioactive label.⁹⁴ (**Figure 6.1**)

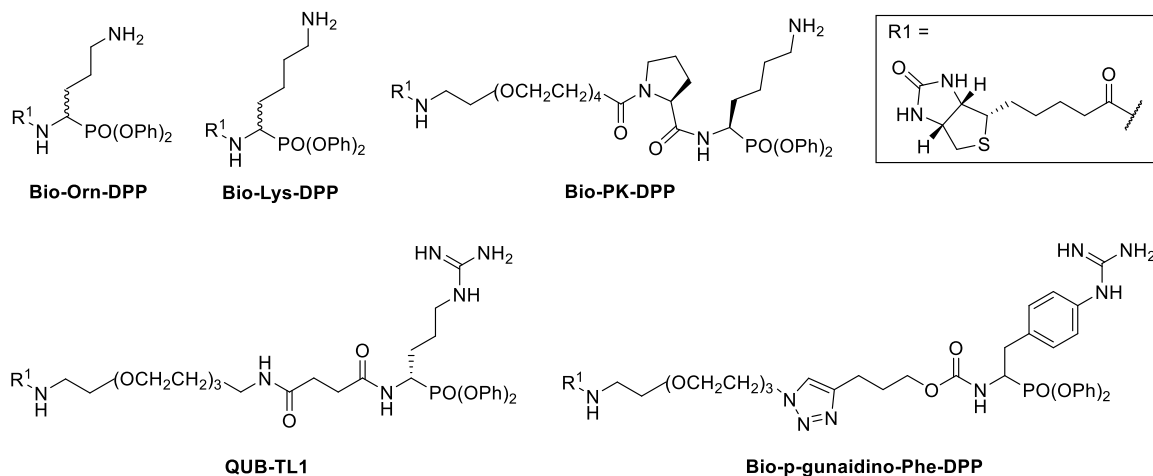


Figure 6.1 Chemical structure of published biotinylated ABPs targeting trypsin-like serine proteases. The stereochemistry shown is based on the source literature.

Driven by the need to identify new biomarkers in pathologies where serine proteases are upregulated and inspired by previously reported irreversible serine protease inhibitors and ABPs, this study reports the synthesis and characterization of a library of ABPs for trypsin-like serine proteases. The idea was to move away from the ABPs mimicking the natural

basic amino acids lysine and arginine and to design several different synthetic analogs to improve potency and selectivity. The ABPs described are based on a DPP warhead with a biotin or desthiobiotin tag attached by click chemistry. We performed an extensive biochemical characterization and demonstrated the ability of these ABPs to differently label trypsin-like serine proteases, both recombinant enzymes and also from degranulated mast cells. Thus, these ABPs have the potential to be used in more complex pathological samples to identify active trypsin-like proteases participating in physiological processes as well as dysregulated enzymes potentially promoting disease. Therefore, these could represent a valuable tool with translational prospects for target identification and biomarker discovery.

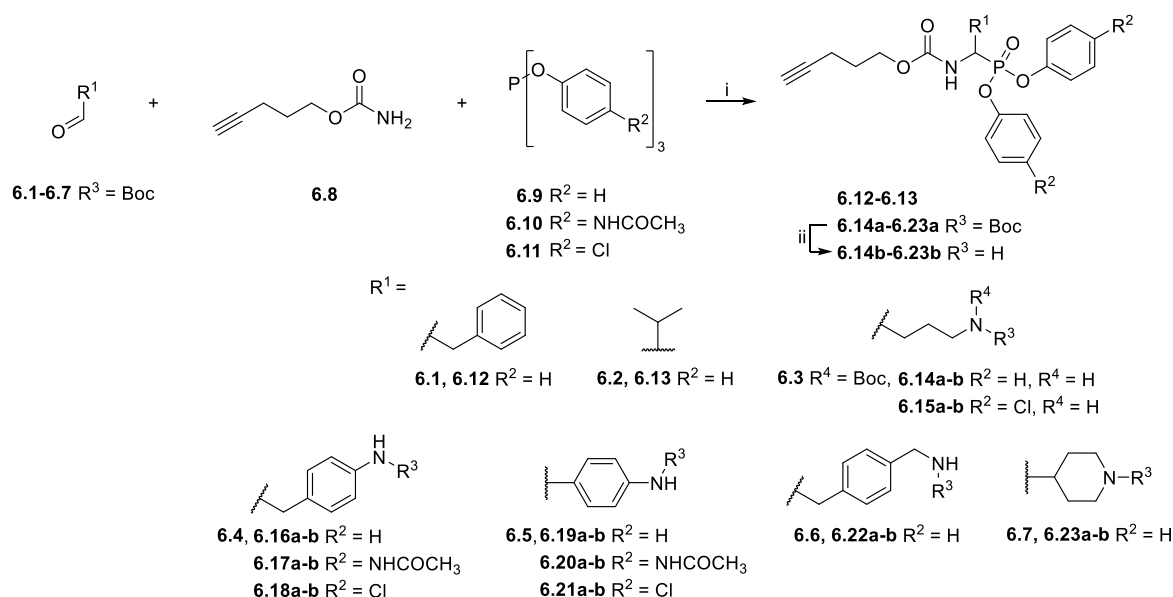
6.3 Results and discussion

6.3.1 Chemical synthesis

With the aim to achieve a range of chemical tools able to identify different trypsin-like serine proteases in complex proteomes, the first goal of this study was to obtain an extensive and diverse library of ABPs. Trypsin-like serine proteases interact favorably with basic and polar residues in the S1 pocket.¹⁵ Previously reported diaryl phosphonate ABPs targeting this family incorporated ornithine and the trypsin-like natural substrate, lysine.⁹¹ Other studies included benzyl guanidine as the selectivity enhancing moiety.⁹⁴ Pan *et al.* described a promising ABP for trypsin with a two amino acid diphenyl phosphonate with proline and lysine.⁹¹ To broaden the probe library, not only amino acids lysine and arginine were included but also other non-natural amino acid analogs with different polar and basic moieties and a two amino acid probe with proline and lysine. In addition to residues targeting the trypsin-like family, phenylalanine and valine were introduced to target chymotrypsin and elastase-like serine proteases.

Although diaryl phosphonate ABPs targeting serine proteases have been reported in the literature, this study aimed to develop a common and accessible synthetic strategy for a

wide-ranging library. Therefore, instead of adding the reporter tag by commonly used peptidic coupling,^{91,329} the pegylated linker was added by click-chemistry. More specifically, the Huisgen 1,3-dipolar cycloaddition between an azide and an alkyne forms a 1,2,3-triazole moiety.³³¹ This approach requires an initial probe bearing the warhead with a terminal alkyne. The synthetic strategy depicted in **Scheme 6.1** was inspired by the previously described route used for benzyl guanidine ABPs synthesis.^{94,130}



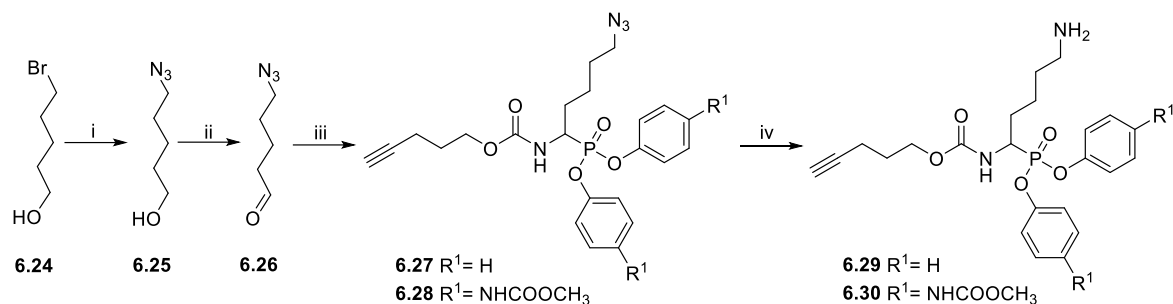
Scheme 6.1 General synthesis of diaryl phosphonate alkyne probes by the Birum-Oleksyszyn reaction; (i) Lewis acid, solvent, rt, 16h; (ii) TFA, DCM, rt, 2-5h or HCl (4M, dioxane), rt, 2-5h.

The primary step of the diaryl phosphonate probe synthesis is the Birum-Oleksyszyn reaction, first described by Oleksyszyn *et al.*¹³¹ in 1979 and later optimized by Van Der Veken *et al.*¹⁴⁰ in 2005. This is a three-component reaction involving an aldehyde, a carbamate, and a triaryl phosphite, catalyzed by an acid (**Scheme 6.1**). The product can contain an acid-labile Boc-protecting group if a Lewis acid is used as the catalyst instead of a Brønsted acid. The aldehyde carries the selectivity enhancing group targeting the enzyme S1 pocket. Thus, various aldehydes were used to extend the chemical space (**6.1-6.7**). The pent-4-yn-1-yl carbamate (**6.8**) was prepared from the corresponding alcohol to conjugate the precursor with the reporting tag (**Scheme S6.1**). To add further diversity, triaryl phosphites (**6.9-6.11**) with two different substituents in *para*-position were prepared from phosphorus trihalides (**Scheme S6.2-S6.3**).

The Birum-Oleksyszyn step required protected nitrogen aldehydes. Thus, for most products, the commercial alcohols were first protected with a Boc group, followed by Dess Martin periodinane (DMP) oxidation to achieve the desired aldehyde (**6.4-6.5, 6.7**) (**Scheme S6.4**). However, other protecting or oxidation strategies were needed for the aliphatic amines and the benzyl methyl amine.

The synthesis of 4-aminobutanal (**6.3**) required a double Boc protection of the corresponding alcohol before a Swern oxidation (**Scheme S6.5**). In contrast, the double Boc protection of 5-aminopentanal was insufficient to achieve yields higher than 5% in the Birum-Oleksyszyn reaction. It is suggested that the catalytic quantity of Lewis acid is enough to deprotect one of the Boc groups. Since Boc protection was not adequate, other synthetic strategies were assessed. The described synthesis of a diphenyl phosphonate probe with lysine and proline-lysine by Pan *et al.* was achieved by phthalimide protection.⁹¹ Unfortunately, in our hands, the phosphonate was readily hydrolyzed when deprotecting with hydrazine. A study by Hamilton *et al.* also postulated that they experienced inconsistency with hydrazine-mediated phthalimide deprotection.³³² Therefore, we explored a novel synthetic strategy with the use of an azide group instead of the primary amine. Hence, the desired lysine alkyne probes (**6.29b-6.30b**) were obtained from 5-azidopentanal (**6.26**), and the further reduction to a primary amine was best achieved with polymer-supported triphenylphosphine in THF (**Scheme 6.2**). The same synthetic strategy was used for the proline-lysine alkyne probe (**6.31b**). The proline and the alkyne were introduced by peptidic coupling (**Scheme S6.6**). A similar approach was used to obtain the benzylmethylamine aldehyde (**6.6**), as the corresponding alcohol was not commercially available (**Scheme S6.7**).

The Boc protecting groups of the diarylphosphonates were removed using acid treatment with hydrogen chloride in dioxane or trifluoroacetic acid in dichloromethane (DCM).



Scheme 6.2 Synthesis of alkyne probes with Lysine as selectivity enhancing moiety (i) NaN_3 , H_2O , $80\text{ }^\circ\text{C}$, 18 h; (ii) DMP, DCM, $0\text{ }^\circ\text{C}$ to rt, 4 h; (iii) phosphite 9 or 10, carbamate 8, Lewis acid, DCM, rt, 16 h; (iv) Polymer supported triphenylphosphine, THF, rt, 72 h.

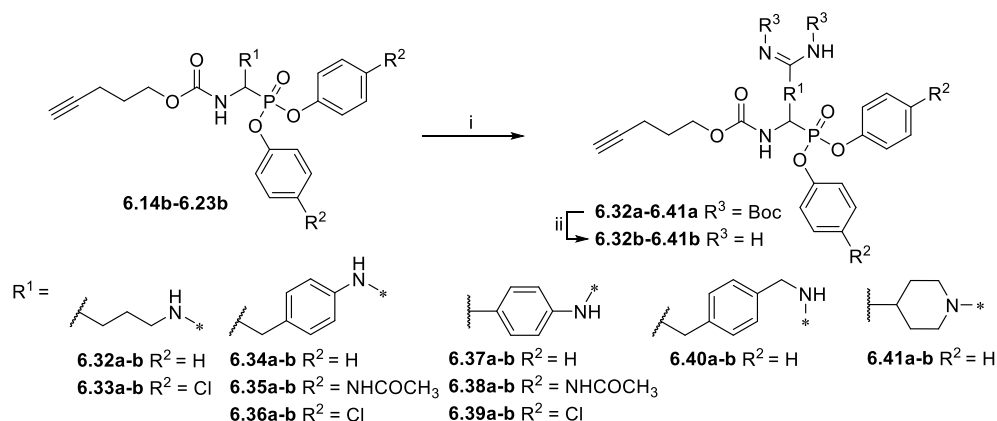
The previously reported synthesis of benzylamine alkyne probes **6.16** and **6.17** used $\text{Cu}(\text{OTf})_2$ as a catalyst in DCM and tetrahydrofuran (THF), respectively. However, for the synthesis of benzylamine 4-acetamidophenyl phosphonate (**6.17**), low yields were reported (<5%).¹³⁰ For the synthesis of this library, these catalyst and solvent combinations were kept. However, other Lewis acids and solvents were assessed when low yielding. A summary of the conditions used is shown in **Table 6.1**. For example, for the synthesis of **6.17**, the yield was increased from 5 to 19% when using $\text{BF}_3(\text{OEt})_2$ in acetonitrile (CH_3CN). For the benzylamine alkyne probe with unsubstituted diphenyl phosphonate (**6.16**), the combination of $\text{Cu}(\text{OTf})_2$ in DCM worked in a similar yield range as reported.¹³⁰ These conditions were used for all the unsubstituted products ($\text{R}^2 = \text{H}$). However, for substituted diaryl phosphonates, either $\text{Bi}(\text{OTf})_3$ in THF (**6.15**), $\text{BF}_3(\text{OEt})_2$ in CH_3CN (**6.17-6.18**, **6.28**), or $\text{Cu}(\text{OTf})_2$ in THF (**6.20-6.21**) were more successful. Interestingly, $\text{Bi}(\text{OTf})_3$ has recently been reported as one of the best-performing catalysts for the Birum-Oleksyszyn reaction in an extensive optimization of the synthesis of inhibitor UAMC-00050.^{128,333}

All the alkyne probes with a basic amine, except all the lysine analogs, were elongated for further chemical space exploration by adding a guanidine moiety. The protected guanidine was inserted with *N, N'*-bis(*tert*-butoxycarbonyl)-1-guanylpyrazole in a mixture of 1:1 of $\text{CH}_3\text{CN}/\text{DCM}$, reducing the previously reported reaction time from 3 days to 16 hours.¹³⁰ Later, the guanidine was deprotected by acid treatment before biochemical characterization (**6.32b-6.41b**) (**Scheme 6.3**).

Table 6.1 Birum-Oleksyszyn reaction conditions

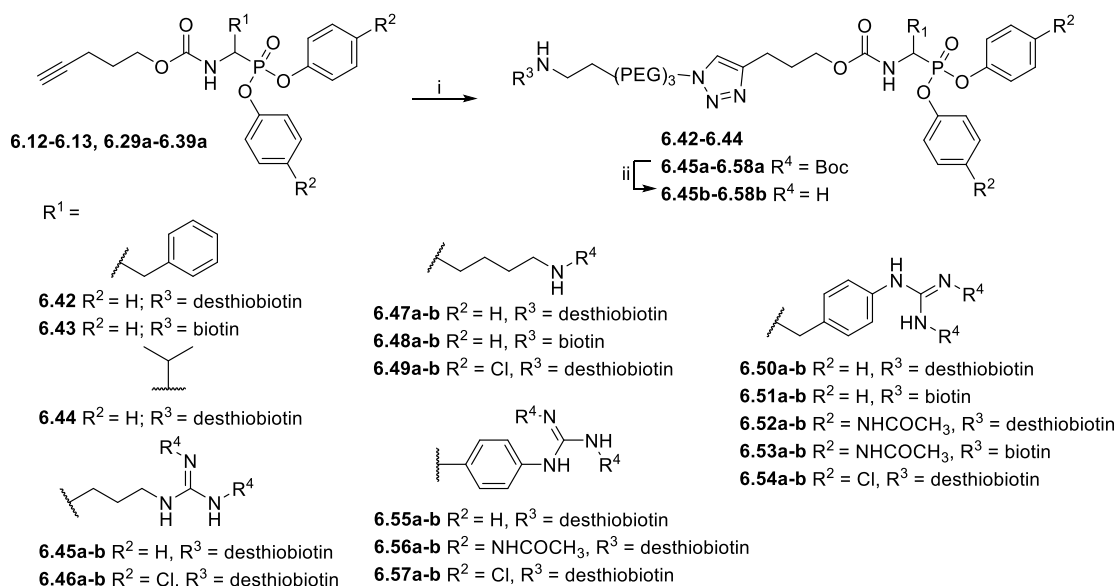
#	R ¹	R ²	Lewis acid	Solvent	Yield, % ^a
6.12		H	Cu(OTf) ₂	DCM	62
6.13		H	Cu(OTf) ₂	DCM	55
6.14		H	Cu(OTf) ₂	DCM	5
6.15		Cl	Bi(OTf) ₃	THF	10
6.16		H	Cu(OTf) ₂	DCM	29
6.17		NHCOCH ₃	BF ₃ (OEt) ₂	CH ₃ CN	19
6.18		Cl	BF ₃ (OEt) ₂	CH ₃ CN	10
6.19		H	Cu(OTf) ₂	DCM	50
6.20		NHCOCH ₃	Cu(OTf) ₂	THF	34
6.21		Cl	Cu(OTf) ₂	THF	41
6.22		H	Cu(OTf) ₂	DCM	45
6.23		H	Cu(OTf) ₂	DCM	46
6.27		H	Cu(OTf) ₂	DCM	71
6.28		NHCOCH ₃	BF ₃ (OEt) ₂	CH ₃ CN	59

^a Isolated yield



Scheme 6.3 Guanylation of alkyne probes; (i) *N, N'*-Bis-Boc-1-Guanylpurazole, Et_3N , $\text{DCM}/\text{CH}_3\text{CN}$ (1:1), rt, 16 h; (ii) TFA, DCM, rt, 2-5 h or HCl (4M, dioxane), rt, 2-5 h.

The obtained alkyne probes can be conjugated to different visualization tags such as rhodamine, biotin, BODIPY, or radiolabeled 4-fluorobenzamide. In this study, we used the affinity tags biotin and desthiobiotin. For the synthesis of the biotin and desthiobiotin probes, the alkyne probe reacted with an azide attached to the reporting tag by click chemistry (**Scheme 6.4**). This produced full-conversion reactions with easy purifications. When the precursors presented basic nitrogens, these had to be Boc-protected before the cycloaddition to allow easier purifications (**6.29a-6.39a**). In the last step, the clicked probes were deprotected by acid treatment (**6.45b-6.59b**).



Scheme 6.4 Synthesis of biotin and desthiobiotin probes by click chemistry with reporter tag azide; (i) Biotin/Desthiobiotin-(PEG)₃-Azide, $\text{CuSO}_4 \cdot 5 \text{H}_2\text{O}$, Ascorbic acid (Na salt), $\text{THF}/\text{H}_2\text{O}$ (1:1), rt, 16 h; (ii) TFA, DCM, rt, 2-5 h or HCl (4M, dioxane), rt, 2-5 h.

6.3.2 Biochemical characterization

The alkyne, biotin, and desthiobiotin probes were tested in a panel of different proteases. The probes were designed to target irreversibly different families of trypsin-like serine proteases. In addition, to test their selectivity, chymotrypsin and elastase-like proteases were also assessed. The panel included four trypsin-like proteases, as well as cathepsin G (CatG), which shares characteristics with chymotrypsin and trypsin-like proteases, and finally, chymotrypsin (ChTryp) and neutrophil elastase (NE).

The IC_{50} values of the alkyne probes were used as a first screening cut-off. All the alkyne probes were initially screened at three concentrations (10, 1, and 0.1 μ M). The probes with an IC_{50} higher than 10 μ M were not analyzed further, whereas the rest were submitted to an exact IC_{50} determination. The results of this first screening are presented in **Table 6.2**. Based on these results, only the most promising alkyne probes (**6.29-6.39**) were clicked to biotin or desthiobiotin (**6.45-6.59**). These were analyzed in the same manner. Since the alkyne probes share the same warhead and selectivity enhancing group (R^1) with the biotin and desthiobiotin probes, inhibitory potencies were similar (**Table 6.3**), as could be expected. Considering that biotin presents a strong interaction with avidin and may present challenges during the ABP profiling, we have based our study primarily on the desthiobiotin probes. The results of the four biotin probes analyzed are shown in the Supplementary Information (**Table S6.1**).

Table 6.2 IC_{50} values of diarylphosphonate alkyne probes against a panel of serine proteases

#	R ¹	R ²	IC_{50} (μ M) ^b						
			Trypsin-3	β -tryptase	Thrombin	uPA ^a	CatG ^a	ChTryp ^a	NE ^a
6.12		H	>10	>10	>10	>10	>10	1.54 \pm 1.34	>10
6.13		H	>10	>10	>10	>10	>10	>10	>10
6.14b		H	>10	>10	>10	>10	>10	>10	>10
6.16b		H	6.85 \pm 0.80	>10	>10	>10	3.74 \pm 0.27	2.67 \pm 0.57	>10
6.17b		NHCOCH ₃	3.71 \pm 0.71	>10	2.97 \pm 0.07	>10	0.37 \pm 0.008	0.49 \pm 0.28	>10
6.18b		Cl	1.72 \pm 0.19	>10	7.88 \pm 0.61	6.38 \pm 0.52	0.36 \pm 0.01	0.19 \pm 0.14	>10
6.19b		H	9.06 \pm 1.10	>10	6.59 \pm 3.90	>10	>10	8.52 \pm 1.81	>10
6.20b		NHCOCH ₃	N.D. ^c	>10	N.D. ^c	>10	>10	N.D. ^c	N.D. ^c
6.21b		Cl	N.D. ^c	>10	N.D. ^c	>10	>10	N.D. ^c	N.D. ^c

Table 6.2 continued

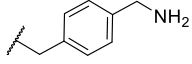
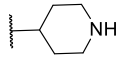
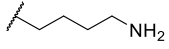
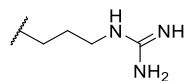
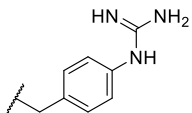
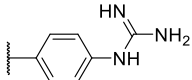
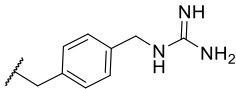
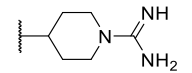
#	R ¹	R ²	Trypsin-3	β -tryptase	Thrombin	uPA ^a	CatG ^a	ChTryp ^a	NE ^a
			IC ₅₀ (μ M) ^b						
6.22b		H	3.82 \pm 0.19	>10	>10	2.30 \pm 0.10	5.26 \pm 0.68	>10	>10
6.23b		H	>10	>10	>10	>10	>10	>10	>10
6.29b		H	0.07 \pm 0.02	3.96 \pm 0.50	7.36 \pm 0.25	5.27 \pm 0.15	>10	5.87 \pm 3.39	>10
6.30b		NHCOCH ₃	0.006 \pm 6x10 ⁻⁴	0.68 \pm 0.05	1.18 \pm 0.07	2.44 \pm 0.35	0.56 \pm 0.002	>10	>10
6.31b	Pro-Lys	H	0.09 \pm 0.03	2.98 \pm 0.05	0.18 \pm 0.003	2.52 \pm 0.29	>10	>10	>10
6.32b		H	0.03 \pm 0.007	3.74 \pm 0.53	0.85 \pm 0.13	4.80 \pm 0.08	7.57 \pm 0.58	>10	>10
6.33b		Cl	0.04 \pm 0.008	0.17 \pm 0.01	0.11 \pm 0.007	0.25 \pm 0.03	2.76 \pm 0.05	>10	N.D. ^c
6.34b		H	0.001 \pm 3x10 ⁻⁴	0.63 \pm 0.03	8.49 \pm 2.25	0.008 \pm 3x10 ⁻⁴	0.45 \pm 0.02	>10	>10
6.35b		NHCOCH ₃	< 0.001	0.05 \pm 0.003	1.11 \pm 0.05	0.005 \pm 0.001	0.06 \pm 0.006	>10	>10
6.36b		Cl	< 0.001	0.07 \pm 0.02	1.77 \pm 0.05	0.005 \pm 3x10 ⁻⁴	0.34 \pm 0.008	3.23 \pm 1.21	>10

Table 6.2 continued

#	R ¹	R ²	IC ₅₀ (μM) ^b						
			Trypsin-3	β-tryptase	Thrombin	uPA ^a	CatG ^a	ChTryp ^a	NE ^a
6.37b		H	0.23 ± 0.01	0.90 ± 0.10	>10	1.79 ± 0.003	0.64 ± 0.03	>10	>10
6.38b		NHCOCH ₃	0.04 ± 0.015	0.12 ± 0.02	>10	1.52 ± 0.4	0.13 ± 0.01	>10	N.D. ^c
6.39b		Cl	0.09 ± 0.009	0.07 ± 0.004	>10	0.22 ± 0.06	0.09 ± 0.022	>10	N.D. ^c
6.40b		H	>10	>10	>10	>10	6.16 ± 0.48	>10	>10
6.41b		H	0.04 ± 0.002	8.37 ± 0.44	0.03 ± 0.001	>10	>10	>10	>10

^a Panel of serine proteases abbreviations: urokinase plasminogen activator (uPA), cathepsin G (catG), chymotrypsin (ChTryp), neutrophil elastase (NE)

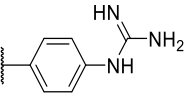
^b Half maximal inhibitory concentration (IC₅₀) value is the concentration of inhibitor required to reduce the enzyme activity to 50% after a 15 min preincubation with the enzyme at 37 °C and activity measurements as mentioned in the Experimental section. IC₅₀ are calculated from two independent experiments; when SD was higher than three times the average value, a third independent experiment was run (mean ± SD)

^c N.D., not determined

Table 6.3 IC_{50} values of diarylphosphonates desthiobiotin probes against a panel of serine proteases

#	R ¹	R ²	IC_{50} (μ M) ^b						
			Trypsin-3	β -tryptase	Thrombin	uPA ^a	CatG ^a	ChTryp ^a	NE ^a
6.42		H	>10	>10	>10	>10	3.23 \pm 0.29	2.07 \pm 0.85	>10
6.44		H	>10	>10	>10	>10	>10	>10	4.70 \pm 0.20
6.45b		H	0.22 \pm 0.02	0.80 \pm 0.05	0.61 \pm 0.17	>10	>10	>10	N.D. ^c
6.46b		Cl	0.07 \pm 0.002	0.04 \pm 0.006	0.04 \pm 0.006	0.42 \pm 0.05	>10	>10	N.D. ^c
6.47b		H	0.52 \pm 0.24	2.49 \pm 0.19	3.55 \pm 0.17	4.62 \pm 0.17	>10	>10	>10
6.49b		NHCOCH ₃	0.09 \pm 0.005	1.11 \pm 0.05	1.18 \pm 0.04	6.75 \pm 0.52	4.47 \pm 0.51	>10	>10
6.50b		H	0.03 \pm 0.01	0.36 \pm 0.07	3.52 \pm 0.39	0.02 \pm 0.0001	0.36 \pm 0.004	1.64 \pm 0.50	>10
6.52b		NHCOCH ₃	0.01 \pm 0.001	0.07 \pm 0.003	0.76 \pm 0.02	0.01 \pm 0.003	0.05 \pm 0.007	>10	>10
6.54b		H	0.008 \pm 0.002	0.11 \pm 0.009	0.20 \pm 0.02	0.006 \pm 0.0001	0.12 \pm 0.01	5.60 \pm 1.06	>10
		Cl							

Table 6.3 continued

#	R ¹	R ²	IC ₅₀ (μM) ^b						
			Trypsin-3	β-tryptase	Thrombin	uPA ^a	CatG ^a	ChTryp ^a	NE ^a
6.55b		H	0.24 ± 0.01	0.37 ± 0.09	>10	2.22 ± 0.07	1.62 ± 0.09	>10	N.D. ^c
6.56b		NHCOCH ₃	0.22 ± 0.004	0.39 ± 0.10	>10	5.19 ± 0.08	0.62 ± 0.009	>10	N.D. ^c
6.57b		Cl	0.18 ± 0.07	0.02 ± 0.0002	>10	0.16 ± 0.04	0.12 ± 0.04	>10	N.D. ^c
6.58b	Pro-Lys	H	0.16 ± 0.004	6.41 ± 0.15	0.16 ± 0.004	6.51 ± 1.15	2.90 ± 0.15	>10	N.D. ^c

^a Panel of serine proteases abbreviations: urokinase plasminogen activator (uPA), cathepsin G (catG), chymotrypsin (ChTryp), neutrophil elastase (NE)

^b Half maximal inhibitory concentration (IC₅₀) value is the concentration of inhibitor required to reduce the enzyme activity to 50% after a 15 min preincubation with the enzyme at 37 °C and activity measurements as mentioned in the Experimental section. IC₅₀ are calculated from two independent experiments; when SD was higher than three times the average value, a third independent experiment was run (mean ± SD)

^c N.D., not determined

Because ABPs are designed to be irreversible serine protease inhibitors, the IC_{50} is exclusively used as a first discriminatory evaluation. When an inhibitor is irreversible, its IC_{50} value not only depends on the substrate and enzyme concentration but also on the time of incubation with the enzyme before the reaction is started by adding the substrate. Kinetic progress curves can show whether an inhibitor displays time-dependent inhibition. The progress curve in the presence of an irreversible inhibitor will show final velocities equal to zero (**Figure 6.2C**). In contrast, for a reversible inhibitor, progress curves have a non-zero final steady-state velocity (**Figure 6.2A**).³¹⁷ To corroborate the inhibitory mechanism of the compounds, jump-dilution assays were performed. These use an inhibitor concentration of 10-fold the IC_{50} for the incubation, and *a posteriori*, the reaction mixture is diluted 10-fold or 100-fold before adding the substrate. In the case of an irreversible inhibitor, enzymatic activity is not regained (**Figure 6.2D**), whereas, in the case of a reversible compound, a slow release of the inhibitor and a gradual increase of the enzymatic activity rate is observed (**Figure 6.2B**).^{316,317} The jump-dilution assays confirmed the behavior described by the progress curves. The results for all probes and proteases are presented in the Supplementary Information (**Table S6.2**).

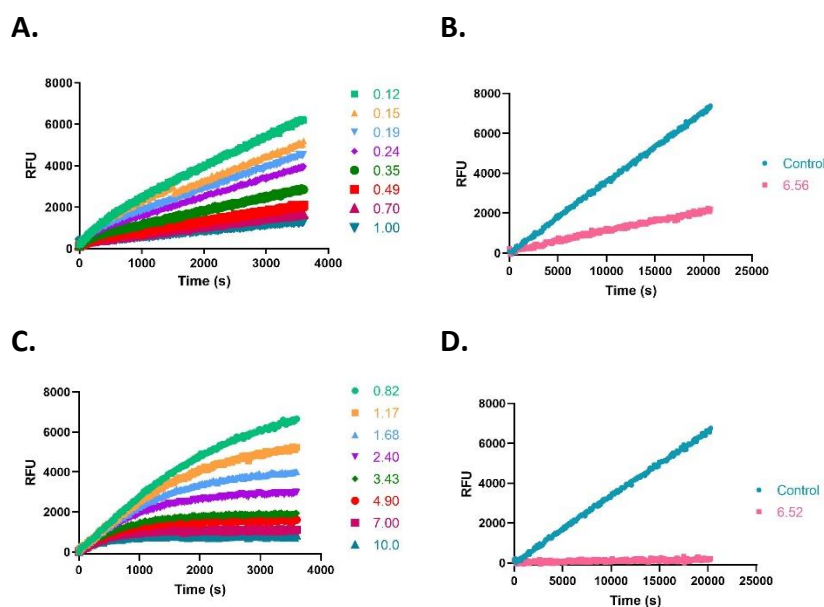


Figure 6.2 Kinetic progress curves; legend concentrations in μ M (**A, C**) and jump dilutions (**B, D**) of β -tryptase; **A & B**. Reversible compound **6.52b**; **C & D**. Irreversible compound **6.56b**.

The apparent second-order rate constants (k_{app}) were derived from the kinetic progress curves. The results of the kinetic assays resemble those expected for a two-step reversible slow-binding or irreversible mechanism. Thus, the rate constant k_{app} accounts for the initial reversible enzyme-inhibitor complex (EI) affinity and the formation rate of the reversible high-affinity complex (E^*I) or the irreversible enzyme-inhibitor complex (E-I). As k_{app} describes the affinity and the reactivity of the inhibitors, it is the best metric to discriminate between the different inhibitors. The k_{app} values are shown in **Table 6.4**.

The equilibrium association constants were derived from the progress curves of trypsin-3, β -tryptase, and thrombin to better describe the affinity of the reversible compounds. The equilibrium constant $K1$ describes the formation of EI, whereas the overall process is defined by $K1^*$.³¹⁶ The equilibrium constants are shown in **Table 6.5**.

Table 6.4 k_{app} values of selected alkyne and desthiobiotin probes against a panel of trypsin-like serine proteases and the description of the mechanism of inhibition defined by the progress curves: slow-binding (Rev.) or irreversible (Irrev.)

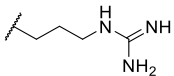
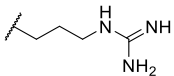
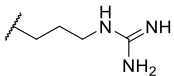
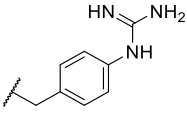
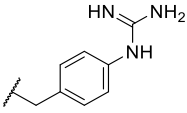
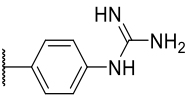
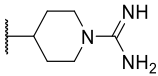
#	R ¹	R ²	Alk / DtB ^a	Trypsin-3	β -trypcase	Thrombin	uPA ^b	CatG ^b
				k_{app} (M ⁻¹ s ⁻¹) ^c				
6.32b		H	Alk	18x10 ² ± 66 Irrev.	41 ± 5 Irrev.	64 ± 8 Rev.	41 ± 4 Irrev.	* ^d Rev.
6.45b			DtB	17x10 ² ± 122 Irrev.	237 ± 42 Irrev.	19 ± 2 Rev.	N.D.	N.D.
6.33b		Cl	Alk	35x10 ² ± 40 Irrev.	28x10 ² ± 82 Irrev.	11x10 ² ± 42 Rev.	15x10 ² ± 12 Irrev.	* ^d Rev.
6.46b			DtB	92x10 ² ± 349 Irrev.	75x10 ² ± 1475 Irrev.	63x10 ² ± 290 Rev.	940 ± 37 Irrev.	N.D.
6.34b		H	Alk	40x10 ³ ± 2642 Rev.	712 ± 41 Rev.	17 ± 1 Rev.	75x10 ² ± 725 Irrev.	* ^d Rev.
6.50b			DtB	49x10 ³ ± 2979 Rev.	32x10 ² ± 613 Rev.	47 ± 5 Rev.	33x10 ³ ± 12x10 ³ Irrev.	* ^d Rev.
6.35b		NHCOCH ₃	Alk	* ^d Rev.	70x10 ² ± 582 Rev.	128 ± 5 Rev.	13x10 ⁴ ± 30x10 ³ Irrev.	477 ± 67 Rev.
6.52b			DtB	86x10 ³ ± 8250 Rev.	18x10 ³ ± 1184 Rev.	49 ± 5 Rev.	38x10 ³ ± 4175 Irrev.	* ^d Rev.
6.36b		Cl	Alk	29x10 ³ ± 6499 Rev.	61x10 ³ ± 6860 Rev.	251 ± 16 Rev.	32x10 ⁴ ± 29x10 ³ Irrev.	* ^d Rev.
6.54b			DtB	* ^d Rev.	* ^d Rev.	* ^d Rev.	23x10 ⁴ ± 36x10 ³ Irrev.	* ^d Rev.

Table 6.4 continued

#	R ¹	R ²	Alk / DtB ^a	Trypsin-3	β-tryptase	k _{app} (M ⁻¹ s ⁻¹) ^c		
						Thrombin	uPA ^b	CatG ^b
6.37b		H	Alk	293 ± 34 Irrev.	375 ± 34 Irrev.	N.D.	124 ± 23 Irrev.	582 ± 2 Irrev.
6.55b			DtB	231 ± 18 Irrev.	347 ± 19 Irrev.	N.D.	77 ± 1 Irrev.	301 ± 85 Irrev.
6.38b		NHCOCH ₃	Alk	358 ± 6 Irrev.	20x10 ² ± 54 Irrev.	N.D.	215 ± 7 Irrev.	14x10 ² ± 52 Irrev.
6.56b			DtB	334 ± 85 Irrev.	321 ± 2 Irrev.	N.D.	62 ± 2 Irrev.	420 ± 37 Irrev.
6.39b		Cl	Alk	11x10 ² ± 164 Irrev.	45x10 ² ± 547 Irrev.	N.D.	25x10 ² ± 86 Irrev.	23x10 ² ± 347 Rev.
6.57b			DtB	13x10 ² ± 340 Irrev.	65x10 ² ± 1203 Irrev.	N.D.	25x10 ² ± 11 Irrev.	11x10 ² ± 117 Rev.
6.41b		H	Alk	17x10 ² ± 142 Irrev.	27 ± 2 Irrev.	41x10 ² ± 38 Irrev.	N.D.	N.D.
6.31b	Pro-Lys	H	Alk	13x10 ² ± 28 Irrev.	136 ± 3 Irrev.	13x10 ² ± 5 Irrev.	188 ± 1 Irrev.	N.D.

^aAlk: alkyne probe; DtB: desthiobiotin probe

^bPanel of serine proteases abbreviations: urokinase plasminogen activator (uPA), cathepsin G (catG)

^ck_{app} are calculated from two independent experiments; when SD was higher than three times the average value, a third independent experiment was run (mean ± SD)

^dk_{app} determination is not possible by curve fitting

N.D.: IC₅₀ is greater than 10 μM, and progress curves were not performed

Table 6.5. Apparent equilibrium constants of the first step of slow-binding (K_1) and the overall process (K_i^*) for the reversible probes

#	Trypsin-3		β -tryptase		Thrombin	
	K_1 (μM) ^b	K_i^* (μM) ^b	K_1 (μM) ^b	K_i^* (μM) ^b	K_1 (μM) ^b	K_i^* (μM) ^b
6.32b	N.D. ^a	N.D. ^a	N.D. ^a	N.D. ^a	22.6 \pm 5	0.45 \pm 0.03
6.45b	N.D. ^a	N.D. ^a	N.D. ^a	N.D. ^a	9.97 \pm 1.0	1.14 \pm 0.11
6.33b	N.D. ^a	N.D. ^a	N.D. ^a	N.D. ^a	4.13 \pm 0.7	0.28 \pm 0.04
6.46b	N.D. ^a	N.D. ^a	N.D. ^a	N.D. ^a	0.95 \pm 0.2	0.07 \pm 0.009
6.34b	0.029 \pm 0.005	0.003 \pm 0.0003	15.8 \pm 5	1.11 \pm 0.09	134 \pm 26	4.93 \pm 0.51
6.50b	0.098 \pm 0.022	0.003 \pm 0.0002	3.28 \pm 0.5	0.41 \pm 0.03	* ^c	1.55 \pm 0.25
6.35b	0.001 \pm 0.0001	1x10 ⁻⁴ \pm 1x10 ⁻⁵	3.20 \pm 1.8	0.12 \pm 0.01	32.7 \pm 4	0.63 \pm 0.04
6.52b	0.017 \pm 0.0005	0.001 \pm 7x10 ⁻⁵	0.68 \pm 0.07	0.06 \pm 0.003	* ^c	0.62 \pm 0.08
6.36b	0.008 \pm 0.0008	0.001 \pm 0.0001	0.34 \pm 0.07	0.09 \pm 0.01	9.03 \pm 0.5	0.03 \pm 0.002
6.54b	0.006 \pm 0.0005	8x10 ⁻⁴ \pm 3x10 ⁻⁵	0.13 \pm 0.03	0.02 \pm 0.001	* ^c	0.06 \pm 0.006

^aN.D.: compounds have an irreversible mechanism of inhibition, K_1 was not calculated

^b K_1 and K_i^* are calculated from two independent experiments; when SD was higher than three times the average value, a third independent experiment was run (mean \pm SD)

^c K_1 determination is not possible by curve fitting

Since the alkyne probes and their corresponding biotin/desthiobiotin analogs behave similarly, we will limit the discussion on the relationship between structure and activity to the alkyne probes. The IC_{50} values (**Table 6.2**) of the benzyl guanidine probes (**6.34b-6.36b**) show their preference for trypsin-3 and uPA (nanomolar range) and, to a lesser extent, for β -tryptase and CatG, whereas the inhibition of thrombin is negligible. Despite the lower potency against β -tryptase and CatG, compound **6.35b** is the most potent probe of the library for β -tryptase ($IC_{50} = 0.05 \pm 0.003 \mu\text{M}$) and CatG ($IC_{50} = 0.06 \pm 0.006 \mu\text{M}$). On the other hand, for thrombin, the benzyl guanidine probes were only in the micromolar range.

Despite being the most potent compounds, the progress curves of the benzyl guanidines show an unexpected reversible inhibition of all trypsin-like proteases tested, except for uPA, where the inhibition is irreversible (**Table 6.4**). The irreversible inhibition of uPA correlates with previous studies on similar diphenyl phosphonates inhibitors.¹²⁹ The unexpected reversible inhibition is not related to the chemical properties of the probes, such as low stability or low reactivity, but is dependent on their interaction with the protease.¹²⁶ Diphenyl phosphonates have been previously described as transition state analogs due to the resemblance with the transition state of peptide hydrolysis. For this type of inhibitor, very high-affinity interactions are expected.¹³² A reason for not being irreversible might be that the warhead proximity and the geometry toward the serine residue on the active site are not ideal for the nucleophilic attack.³³⁴ Alternatively, the compounds could behave as reversible covalent inhibitors where a covalent bond is formed and subsequently hydrolyzed.^{317,335}

The k_{app} values of the benzyl guanidines derived from the progress curves correlate with the trends observed for the IC_{50} values. The benzyl guanidine probes show strong inhibition of trypsin-3, β -tryptase, and uPA, weaker for CatG and much weaker for thrombin. For trypsin-3, these probes are at least 10-fold more potent than any of the other probes. The same occurs for β -tryptase, where the k_{app} of the bis(4-chlorophenyl)phosphonate probe **6.36b** ($k_{app} = 61 \times 10^3 \pm 6860 \text{ M}^{-1} \text{ s}^{-1}$) is 10-fold higher than the second best probes, arginine **6.33b**, and phenyl guanidine **6.39b**. Noteworthy, for uPA, the probe **6.36b** with $k_{app} =$

$32 \times 10^4 \pm 29 \times 10^3 \text{ M}^{-1} \text{ s}^{-1}$ is at least 100-fold more potent than the other probes with different side chains. For all reversible benzyl guanidine probes, the values of K_i^* are at least 10-fold lower than the corresponding K_1 for trypsin-3 and β -tryptase (**Table 6.5**). This is consistent with high-affinity E·I complexes and slow dissociation off-rates. For example, the bis(4-acetamidophenyl)phosphonate alkyne probe (**6.35b**) and the bis(4-chlorophenyl)phosphonate desthiobiotin probes (**6.54b**) presented a sub-nanomolar affinity for trypsin-3 with $K_i^* = 1 \times 10^{-4} \pm 1 \times 10^{-5}$ and $8 \times 10^{-4} \pm 3 \times 10^{-5} \mu\text{M}$, respectively. The rest of the benzyl guanidine probes showed nanomolar affinities for trypsin-3. On β -tryptase, sub-micromolar affinities are achieved with bis(4-chlorophenyl)phosphonate alkyne probe (**6.36b**) and both substituted diphenyl phosphonate desthiobiotin probes (**6.52b**, **6.54b**).

The phenyl guanidine probes (**6.37b-6.39b**) also demonstrated strong sub-micromolar inhibitory potencies (**Table 6.2**). For β -tryptase and CatG, the IC_{50} values are in the same range as for the benzyl guanidine probes (**6.34b-6.36b**). For instance, the IC_{50} for β -tryptase and CatG for the bis(4-chlorophenyl)phosphonate alkyne probe (**6.39b**) are 0.07 ± 0.004 and $0.09 \pm 0.022 \mu\text{M}$, respectively, which is in the same range as for the best-performing benzyl guanidine probe **6.35b**. For trypsin-3 and uPA, the phenyl guanidine probes lost about 100-fold potency compared to the benzyl guanidine analogs. At the concentrations tested, there was no inhibition of thrombin.

However, in contrast to the benzyl guanidine probes that were only irreversible for uPA, the compounds with phenyl guanidine as a side chain demonstrate irreversible inhibition for all proteases evaluated, excluding the bis(4-chlorophenyl)phosphonate probes (**6.39b**, **6.57b**), which, surprisingly, act reversibly on CatG (**Table 6.4**). For this series of compounds, the phosphonate aryl substituents (R^2) have a significant influence on the k_{app} , with the bis(4-chlorophenyl)phosphonate probe **6.39b** as the best-performing for all the proteases. This probe has k_{app} values around $20 \times 10^2 \text{ M}^{-1} \text{ s}^{-1}$ for trypsin-3, β -tryptase, uPA, and CatG.

Whereas the benzyl and phenyl guanidine probes did not show potency towards thrombin, the piperidine-1-carboximidamide **6.41b** is the most potent thrombin inhibitor with an IC_{50}

= $0.03 \pm 0.001 \mu\text{M}$. It is an equipotent inhibitor for trypsin-3 and has weak inhibition for β -trypsinase. There is no inhibition for uPA and CatG. This is also reflected in the k_{app} values obtained from the progress curves with irreversible inhibition of thrombin, trypsin-3, and β -trypsinase (**Table 6.4**).

Among the probes mimicking the natural amino acids, the arginine side chain proved to be the more interesting for most proteases. In particular, the bis(4-chlorophenyl)phosphonate probes **6.33b** showed high potency and irreversibility for trypsin-3, β -trypsinase, and uPA. A similar k_{app} value was obtained for thrombin, although with a reversible inhibition. The lysine mimicking probes (**6.29b**, **6.30b**) had nanomolar inhibition for trypsin-3 but were less potent for β -trypsinase, thrombin, uPA, and CatG. The ornithine probe (**6.14b**) was inactive in all the proteases tested.

In previous studies, the Pro-Lys mimicking probe was reported to be promising for trypsin-3 with higher inhibitory potency than the Lys probe, but it was less active on β -trypsinase.⁹¹ In our study, the proline-lysine diphenyl phosphonate alkyne (**6.31b**) probe was used as a reference compound. This probe showed indeed potent, irreversible inhibition of trypsin-3 and thrombin, whereas the inhibition of β -trypsinase and uPA was also irreversible but less potent. However, compared to this reference compound, it is possible to select a more potent probe from our library for each investigated protease.

In general, our results demonstrate that compounds with a terminal guanidine showed significantly higher potencies than their amine analogs. For example, the less basic aniline probes **6.16b-6.18b** and **6.19b-6.21b** were inactive or presented IC_{50} higher than $1 \mu\text{M}$. The only exceptions are the submicromolar IC_{50} values of **6.17b** and **6.18b** for CatG and chymotrypsin, reflecting the preference of these proteases for aromatic amino acids. In addition, the optimal length of the selectivity enhancing group (R^1) for this panel of trypsin-like proteases lies between 6 and 8 atoms from the α -carbon. Generally, compounds with shorter or longer R^1 groups significantly have reduced inhibitory potency. For instance, the

benzyl methyl guanidine alkyne probe (**6.40b**) only showed an affinity for uPA with an $IC_{50} = 6.16 \pm 0.48 \mu\text{M}$.

The compounds were tested in chymotrypsin and neutrophil elastase to test selectivity over other protease families. All compounds were not potent for neutrophil elastase, including compound **6.13**, designed to target elastase-like proteases. Likewise, most compounds were not potent or only slightly potent for chymotrypsin, except the above-mentioned **6.17b** and **6.18b**.

Concludingly, under these assay conditions, the most potent alkyne probe for trypsin-3 based on the k_{app} values is the benzyl guanidine **6.34b**, with a 5-fold selectivity for uPA, 55-fold over β -tryptase, and over 2000-fold for thrombin. Noteworthy, this probe shows a reversible slow-binding inhibitory mechanism. In case that an irreversible probe would be needed, the arginine **6.32b** combines high potency with at least 30-fold selectivity over the other tested proteases. For β -tryptase, several potent reversible probes, such as **6.36b**, were obtained, but these probes are not selective for trypsin-3 and uPA. In contrast, probes **6.33b** and **6.39b** are also potent for β -tryptase and show an irreversible mechanism of inhibition. The preferred probe for thrombin is the 4-piperidine-1-carboximidamide (**6.41b**), with potent irreversible inhibition and excellent selectivity over β -tryptase, uPA, and CatG. All the probes described in this study are irreversible with uPA. Furthermore, this enzyme has a clear preference for the benzyl guanidine side chain. Last, CatG does not have a clear preference between benzyl guanidine and phenyl guanidine probes. However, benzyl guanidine probes have a reversible mechanism, whereas phenyl guanidine probes are generally irreversible.

6.3.3 Labeling and detection of recombinant proteases

To further characterize the newly synthesized compounds and their potential to be used as ABPs, nine desthiobiotin probes were used to label and detect recombinant proteases. The arginine (**6.45b-6.46b**) and the proline-lysine (**6.58b**) desthiobiotin probes were used as

reference compounds. Whereas the benzyl guanidine (**6.50b**, **6.52b**, **6.54b**) and phenyl guanidine probes (**6.55b-6.57b**) were used to determine whether the mechanism of inhibition (reversible or irreversible) is an obstacle to visualizing the proteases. Samples of human recombinant proteases (trypsin-3, β -tryptase, and CatG) were incubated with the different probes before electrophoresis and detection with NeutrAvidin-HRP on a Western blot. **Figure 6.3A** illustrates the ability of the desthiobiotin probes to indicate the presence of the corresponding trypsin-like enzyme. Surprisingly, the reversible probes with benzyl guanidine as a side-chain (**6.50b**, **6.52b**, **6.54b**) can label trypsin-3, β -tryptase, and CatG under denaturing conditions. This effect can be explained due to the strong interactions between the active site of the protease and the probes. The high affinity and the slow off-rates were described in **Table 6.5** by the equilibrium constants K_i^* . Assuming that there is an excess of inhibitor over enzyme, the free inhibitor concentration must be very low, lower than the K_i^* , in order for the complex to dissociate. Therefore, the high-affinity complex E^*I survives during the whole process of labeling, gel electrophoresis, and visualization.

All the probes tested can label recombinant trypsin-3. However, the phenyl guanidine side chain is the least promising for this enzyme (**6.55b-6.57b**). For β -tryptase, the probes with natural amino acids as a side chain (**6.45b**, **6.46b**, **6.58b**) are not good ABP candidates. Both benzyl guanidine and phenyl guanidine show similar labeling intensity. Nevertheless, the probes with bis(4-chlorophenyl)phosphonate (**6.54b**, **6.57b**) showed a slightly better resolution for the β -tryptase bands. Last, CatG could be labeled by most of the probes, except for the arginine (**6.45b**) and phenylguanidine (**6.55b**) unsubstituted diphenyl phosphonate probes.

In summary, the benzyl guanidine probes are compounds with a high affinity for trypsin-like serine proteases. Although they showed a reversible mechanism of inhibition for trypsin-3, β -tryptase, and CatG, surprisingly, these can label the recombinant proteases in a Western blot assay.

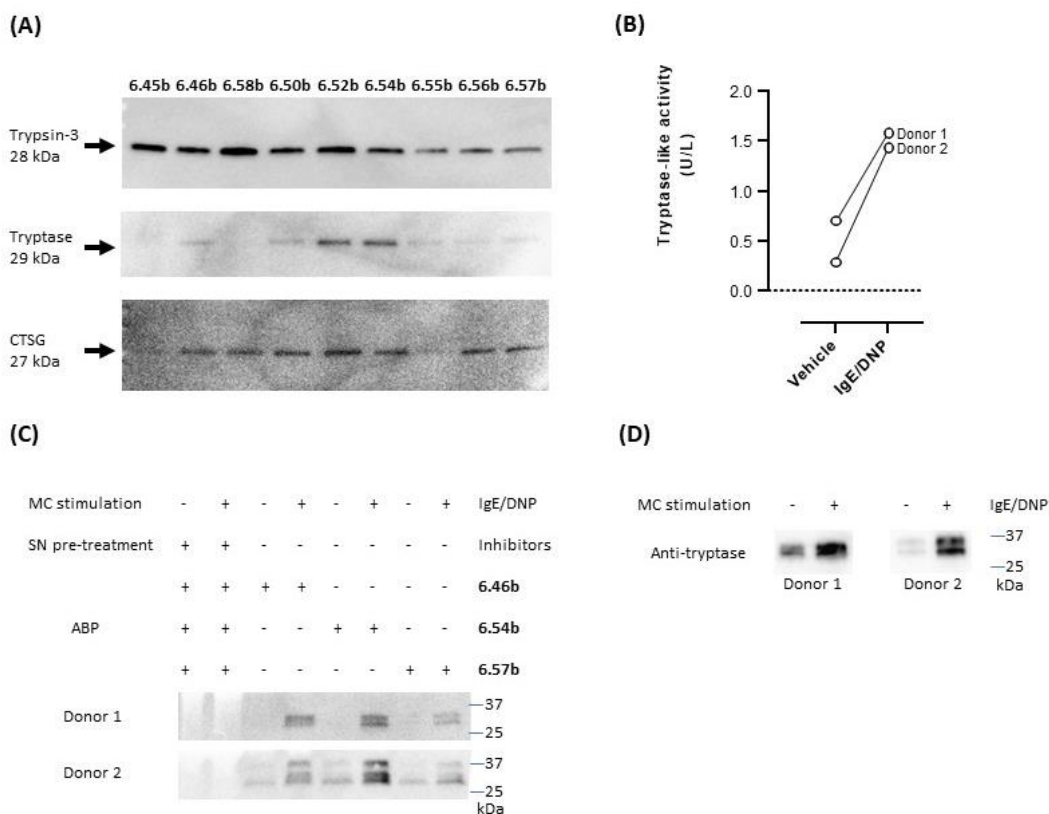


Figure 6.3 Validation of newly synthesized desthiobiotin probes for detection of trypsin-like proteases. **A.** Labeling and detection of recombinant proteases in a SDS-PAGE-Blot. **B.** Tryptase-like activity was measured from the stimulated mast cells of two donors by a spectrophotometric assay with a fluorogenic substrate. IgE/DNP stimulated mast cells were used. The tryptase-like activity is expressed as U/L. **C.** Labeling of mast cell supernatants and identification of proteases. **D.** Detection of tryptase in mast cell supernatants with anti-mast cell tryptase antibody, visualized by Western blot.

6.3.4 Labeling of mast cell supernatants and functional proteomic profiling

The last step to characterize the newly synthesized compounds as potential ABPs was to perform an experiment on biological samples and exemplify the ability of these ABPs to label proteases within a complex proteome. Human mast cells from two donors were stimulated to degranulate with IgE/DNP. Mast cells are immune cells that, upon degranulation, release mediators and play pivotal roles in allergic and inflammatory diseases.^{280,281,336} Mast cell granules predominantly contain histamine and tryptase. Other serine proteases that are associated with mast cell degranulation include soluble and transmembrane chymases and CatG.^{337,338} First, tryptase-like activity was measured from the stimulated mast cells by a spectrophotometric assay with a fluorogenic substrate

(**Figure 6.3B**), which was increased compared to the vehicle. Then, mast cell supernatants were labeled with arginine (**6.46b**), benzyl guanidine (**6.54b**), and phenyl guanidine (**6.57b**) bis(4-chlorophenyl)phosphonate desthiobiotin probes. Probes **6.54b** and **6.57b** were chosen due to the good labeling of recombinant tryptase. Again, arginine probe **6.46b** was used as a reference compound. **Figure 6.3C** shows that the three probes can label proteases in a complex proteome. The absence of bands when the samples are pre-treated with a cocktail of protease inhibitors indicates that the probes only target active proteases. It is worth noticing that samples from non-stimulated mast cells can also be labeled. Thereby, these probes are also successful at highlighting the constitutive release of proteases, which is relevant in a physiological setting.³³⁷ For both donors, there are two overlapping bands around 30 kDa. The second donor shows an extra band at 37 kDa. After staining with an anti-tryptase antibody, only the lower bands are observed (**Figure 6.3D**). These most likely represent α - and β -tryptase.³³⁹ The additional band at 37 kDa might be related to another protease. The benzyl guanidine bis(4-chlorophenyl)phosphonate desthiobiotin (**6.54b**) which is the most potent probe for β -tryptase, displayed the best resolution, even though it shows a reversible slow-binding mechanism.

6.4 Conclusions

ABPP is a powerful proteomic tool which enables researchers to detect and visualize active enzymes within a complex proteome. ABPP uses chemical probes designed to react covalently with the target enzyme. This tool is attractive in target and biomarker identification and drug discovery programs.

This study focuses on the serine protease family, specifically trypsin-like serine proteases. Most ABPs previously reported targeting this family used a diphenyl phosphonate as a warhead. However, there is a lack of chemical diversity as most of the reported probes contain natural amino acid mimetics as selectivity-enhancing moieties. This study aimed to develop an extensive library of ABPs targeting trypsin-like serine proteases with a wide-ranging chemical diversity.

An efficient synthetic route has been implemented for probes bearing a diphenyl phosphonate warhead. A combination of different side chains targeting trypsin-like proteases and the modification of the electrophilicity of the diphenyl phosphonate warhead achieved the desired extensive library of probes. First, the alkyne probes were synthesized, and then the most promising ones were clicked to biotin and desthiobiotin as reporter tags. Furthermore, this synthetic route allows a straightforward approach to couple diverse reporter tags. Thus, alternative tags will enable other applications, such as visualization by fluorescence or PET.

To determine the inhibitory potency of the synthesized probes, their IC_{50} values were determined as a first measurement. However, since the probes were designed to be irreversible inhibitors, the IC_{50} value is not a good parameter to describe their potency. Therefore, kinetic progress curves were measured to determine the mechanism and the kinetic constants of inhibition.

For trypsin-3, β -tryptase, and uPA, the benzyl guanidine probes presented the highest inhibitory potencies. Surprisingly, only for uPA, the interaction was irreversible, whereas a reversible slow-binding mechanism with trypsin-3, β -tryptase, thrombin, and CatG was observed. The phenyl guanidines, on the other hand, are good irreversible probes for trypsin-3, β -tryptase, and CatG. The preferred probe for thrombin is the 4-piperidine-1-carboximidamide, with potent irreversible inhibition and excellent selectivity over β -tryptase, uPA, and CatG.

Last, we demonstrated that our probes can label recombinant proteases and tryptase released from mast cell degranulation. Surprisingly, not only the irreversible ABPs but also the probes that presented a reversible slow-binding mechanism can label proteases under denaturing conditions.

Concludingly, these new probes for trypsin-like proteases offer significant advantages in terms of potency over the traditional probes mimicking the natural amino acids arginine

and lysine. Detailed enzyme kinetic studies learn that, surprisingly, not all diaryl phosphonates show irreversible inhibition and that the inhibitory mechanism of a specific probe can differ from one protease to another. Even more surprising is the observation that irreversible binding is not needed to maintain protease labeling under denaturing conditions, but that reversible slow-tight binding is also sufficient.

6.5 Experimental section

6.5.1 Chemistry

Reagents were obtained from commercial sources and were used without further purification. Characterization of all compounds was done with ^1H and ^{13}C NMR and mass spectrometry. ^1H and ^{13}C NMR spectra were recorded on a 400 MHz Bruker Avance III Nanobay spectrometer with Ultrashield working at 400 and 100 MHz, respectively, and analyzed by use of MestReNova or TopSpin analytical chemistry software. Chemical shifts (δ) are in parts per million (ppm), and coupling constants (J) are in hertz (Hz). The signal splitting patterns were described as s = singlet, d = doublet, t = triplet, q = quartet, p = pentuplet, dd = doublet of doublet, dt = doublet of triplet, td = triplet of doublet, tt = triplet of triplet, ddd = doublet of doublet of doublet, br = broad, and m = multiplet. The LC-MS analysis was performed on a Waters UPLC-MS system equipped with a TUV and QDa detector; the column used is an Acquity UPLC BEH C18 (1.7 μm , 2.1 \times 50 mm), and as eluent, a mixture of 0.1% FA in H_2O , 0.1% FA in CH_3CN , H_2O , and CH_3CN . The wavelengths for UV detection were 254 and 214 nm.

When necessary, flash chromatography separations were carried out using a Biotage Isolera One purification system equipped with an internal variable dual-wavelength diode array detector (200–400 nm). Silica gel columns were used for normal phase purifications, and reverse-phase purifications were done using C18 cartridges, both from Büchi or Biotage. Dry sample loading was done by self-packing sample cartridges using Celite 545. Gradients used varied for each purification.

HRMS involved the following: the dry samples of final compounds were dissolved in CH₃CN to a concentration of 0.1 mM and then diluted 10x in a solution 50:50 of CH₃CN:H₂O.

Every reaction was performed under an N₂ atmosphere if not stated otherwise. Several synthetic procedures used to prepare intermediates and final products are summarized here as “General Procedures”. Target compounds were obtained with a purity >95% and as amorphous solids unless stated otherwise.

6.5.1.1 *General procedures*

GENERAL PROCEDURE A: Boc protection; Di-*tert*-butyl dicarbonate (1.1 eq.) was added to a solution of **selected amine** (1 eq.) in EtOH (1M) at room temperature and was stirred for 3 h. The reaction mixture was concentrated under reduced pressure to yield the desired **protected amine**.

GENERAL PROCEDURE B: Dess Martin periodinane oxidation; Dess-Martin periodinane (1.2 eq.) was added portion-wise to a solution of selected **primary alcohol** (1 eq.) in DCM (0.2 M) at 0 °C. The mixture was stirred at room temperature for 4 h. Then, the solvent was removed under reduced pressure. The crude product was purified by column chromatography on silica gel (SiO₂, EtOAc in heptane, 0/100 to 100/0). The desired fractions were collected and concentrated to yield the corresponding **aldehyde**.

GENERAL PROCEDURE C: Birum-Oleksyzyn reaction; Selected **aldehyde** (1 eq.), pent-4-yn-1-yl carbamate (1 eq.), and triphenyl phosphite (if not stated otherwise) (1.1 eq.) were dissolved in anhydrous solvent (0.3 M). Then the Lewis acid (0.1 eq.) was added, and the mixture was stirred at room temperature for 16 h. Then the solvent was evaporated and the residue dissolved in the minimum amount of CH₃OH. The solution was kept at –20 °C for 48 h and then filtrated. When precipitation did not succeed, the crude was purified by flash column chromatography (SiO₂, EtOAc in heptane, 0/100 to 100/0) and, if still not pure, by reverse phase column chromatography (C18, CH₃CN in H₂O, 20/80 to 100/0). The desired

fractions were collected and concentrated to yield the corresponding **α -amino diarylphosphonate** as a racemic mixture.

GENERAL PROCEDURE D: Boc deprotection with TFA; TFA (100 eq.) was added to a solution of the selected **protected amine** (1 eq.) in DCM (0.02 M) at room temperature and was stirred for 1-5 h. The volatiles were removed under reduced pressure to yield the corresponding **deprotected amine** as a trifluoroacetate salt.

GENERAL PROCEDURE E: Boc deprotection with HCl; The selected **protected amine** was stirred in HCl (4 M in dioxane) (0.03 M) at room temperature for 1-5 h. The volatiles were removed under reduced pressure to yield the corresponding **deprotected amine** as a hydrochloride salt.

GENERAL PROCEDURE F: Azide deprotection; Polymer supported triphenylphosphine (2 eq.) was suspended in anhydride THF (0.1 M) and stirred for 30 min, then the **azide** (1 eq.) was added. The mixture was stirred at rt for 24 h. Then, water (0.05 M) was added, and the mixture was stirred at rt for 3 h. The polymer was removed by filtration and washed with THF and H₂O. The filtrate was concentrated under reduced pressure and then diluted in EtOH. Di-*tert*-butyl dicarbonate (2 eq.) and triethylamine (2 eq.) were added to the solution. The reaction mixture was stirred at rt for 40 min. The solvent was removed under reduced pressure. The crude product was purified by column chromatography on silica gel (SiO₂, EtOAc in Heptane, 0/100 to 20/80) to yield the corresponding **protected amine**.

GENERAL PROCEDURE G: Guanylation; Triethylamine (6 eq.) was added to a solution of N, N'-bis-Boc-1-guanylpyrazole (2 eq.) and **selected amine** (1 eq.) in DCM/CH₃CN (1:1, 0.1 M) at room temperature. The mixture was stirred for 2-48 h, and the solvent was removed under reduced pressure. EtOAc was added, and the mixture was washed with a solution of HCl (1N), saturated NaHCO₃ and brine. The organic layer was dried over Na₂SO₄ and concentrated. The crude product was purified by flash chromatography (SiO₂, EtOAc in heptane, 0/100 to 100/0) to yield the corresponding **protected guanidine**.

GENERAL PROCEDURE H: Click chemistry; L-Ascorbicacidsodium salt (0.6 eq.), BlueCopper (2 eq.) and the selected **alkyl carbamate** (1 eq.) were added to a solution of biotin or desthiobiotin azide (1 eq.) in THF/H₂O (1:1, 0.02 M). The reaction mixture was stirred at room temperature for 16 h. After reaction completion, excess copper was removed by adding Chelex and subsequent filtration. The crude product was purified by reverse phase column chromatography (C18, CH₃CN in H₂O, 20/80 to 100/0). The desired fractions were collected and concentrated to yield the desired **activity-based probe**.

6.5.1.2 Synthesis and chemical characterization

***N, N'*-bis-*tert*-butyloxycarbonyl 5-aminobutan-1-al (6.3)** A solution of DMSO (2.0 mL, 27.6 mmol) in DCM (14 mL) was added over 30 min to a stirred solution of oxalyl chloride (1.2 mL, 13.82 mmol) in DCM (52.5 mL) at -78 °C. Upon completion of the addition, the mixture was stirred at -78 °C for 5 min, followed by adding **S6.7** (2 g, 6.91 mmol) in DCM (14 mL) over 30 min at -78 °C. The solution was stirred for 40 min after addition completion. Then, triethylamine (5.78 mL, 41.5 mmol) was added dropwise over 10 min. The reaction mixture was let warm to 0 °C and stirred for 1 h. Water was added, followed by ether. The organic layer was washed with water (2x) and brine (2x). The organic layer was dried over Na₂SO₄, filtered and concentrated under reduced pressure to yield **6.3** (1.98 g, 6.89 mmol, 100% yield) as a yellow oil. ¹H NMR (400 MHz, CDCl₃) δ (ppm) 9.71 (t, *J* = 1.3 Hz, 1H), 3.54 (t, *J* = 7.1 Hz, 2H), 2.40 (td, *J* = 7.3, 1.3 Hz, 2H), 1.83 (q, *J* = 7.2 Hz, 2H), 1.43 (s, 18H). No ionization was found.

***Tert*-butyl (4-(2-oxoethyl)phenyl)carbamate (6.4)** General procedure **B** with *tert*-butyl (4-(2-hydroxyethyl)phenyl)carbamate (2 g, 8.43 mmol) to yield **6.4** (1.66 g, 7.06 mmol, 84% yield). ¹H NMR (400 MHz, CDCl₃) δ 9.71 (t, *J* = 2.5 Hz, 1H), 7.38 (t, *J* = 12.5 Hz, 2H), 7.17–7.08 (m, 2H), 3.63 (d, *J* = 2.5 Hz, 2H), 1.53 (d, *J* = 7.0 Hz, 9H). No ionization was found.

***Tert*-butyl (4-formylphenyl)carbamate (6.5)** General procedure **B** with *tert*-butyl (4-(hydroxymethyl)phenyl)carbamate (2.7 g, 12.09 mmol) to yield **6.5** (1.67 g, 7.55 mmol, 62%

yield). ^1H NMR (400 MHz, CDCl_3) δ (ppm) 9.88 (s, 1H), 7.81 (d, $J = 8.5$ Hz, 2H), 7.54 (d, $J = 8.5$ Hz, 2H), 7.00 (br s, 1H), 1.51 (s, 9H). MS (ESI) m/z 222.2 $[\text{M}+\text{H}]^+$.

Tert-butyl (4-(2-oxoethyl)benzyl)carbamate (6.6) A solution of diisopropyl aluminium hydride (10 mL, 1M, 9.29 mmol) was added dropwise to a solution of **S6.15** (1.73 g, 6.19 mmol) in anhydrous toluene (30 mL) at -78 °C. The solution was stirred at -78 °C for 1 h and was quenched by adding CH_3OH , followed by adding 10% solution of Rochelle salt. The suspension was diluted in EtOAc, and the layers were separated. The aqueous layer was extracted with EtOAc (2 x 50 mL), and the combined organic layers were dried over MgSO_4 , filtered and concentrated under reduced pressure to yield **6.6** (1.30 g, 5.21 mmol, 84% yield). ^1H NMR (400 MHz, CDCl_3) δ (ppm) 9.73 (t, $J = 2.3$ Hz, 1H), 7.28 (d, $J = 8.0$ Hz, 2H), 7.18 (d, $J = 8.1$ Hz, 2H), 4.93 (br s, 1H), 4.31 (d, $J = 6.0$ Hz, 2H), 3.68 (d, $J = 2.5$ Hz, 2H), 1.46 (s, 9H). MS (ESI) m/z 523.3 $[2x\text{M}+\text{Na}]^+$.

Tert-butyl 4-formylpiperidine-1-carboxylate (6.7) General procedure **B** with **S6.3** (1.0 g, 4.64 mmol) to yield **6.7** (0.99 g, 4.64 mmol, 99% yield). ^1H -NMR (400 MHz, CDCl_3) δ (ppm) 9.65 (s, 1H), 3.97 (br s, 2H), 2.97-2.87 (m, 2H), 2.45-2.35 (m, 1H), 1.89 (d, $J = 13.0$ Hz, 2H), 1.61-1.52 (m, 2H), 1.45 (s, 9H). No ionization was found.

Pent-4-yn-1-yl carbamate (6.8) Trichloroacetylisocyanate (5 mL, 42.0 mmol) was added to a solution of 4-pentyn-1-ol (3.23 mL, 35.0 mmol) in dry DCM (70 mL) at 0 °C. The reaction mixture was allowed to warm up to room temperature and was stirred for 1h. The solvent was removed *under vacuo*, and the mixture was dissolved in CH_3OH (70 mL) and water (10 mL). Potassium carbonate (7.25 g, 52.5 mmol) was added portion-wise, and the mixture was stirred overnight at room temperature. The solvent was removed *under vacuo*, and water (100 mL) was added. The aqueous layer was extracted with EtOAc (3 x 100mL). The combined organic layers were washed with brine solution, dried over MgSO_4 , and removed the solvent *under vacuo*. The crude product was recrystallized from DCM/heptane to yield **6.8** (4.289 g, 33.7 mmol, 96.0% yield). ^1H NMR (400 MHz, CDCl_3) δ (ppm) 4.76 (s, 2H), 4.16

(t, $J = 6.3$ Hz, 2H), 2.29 (td, $J = 7.1, 2.7$ Hz, 1H), 1.97 (t, $J = 2.7$ Hz, 1H), 1.89 – 1.80 (m, 2H). MS (ESI) m/z 150 [M+Na]⁺.

Tris (4-acetamidophenyl) phosphite (6.10) Triethylamine (0.95 mL, 6.86 mmol) was added dropwise to a stirred solution of phosphorus trichloride (0.2 mL, 2.287 mmol) and acetaminophen (1.037 g, 6.86 mmol) in THF (20 mL) at 0 °C. Upon addition completion, the reaction mixture was stirred at 0 °C for 15 min and then was slowly left to reach room temperature and stirred for 2 h. The mixture was filtered through a celite pad, and the filtrate was concentrated under reduced pressure. The crude product **6.10** was obtained as a white foam (1.1 g, 2.28 mmol, 100%) and used for the next synthetic step without further purification. MS (ESI) m/z 482.2 [M+H]⁺.

Tris(4-chlorophenyl) phosphite (6.11) Phosphorustribromide (0.6 mL, 6.32 mmol) was added to a solution of 4-chlorophenol (2.436 g, 18.95 mmol) and triethylamine (3.52 mL, 25.3 mmol) in dry diethyl ether (20 mL) at 0 °C. Following the addition, the mixture was warmed to room temperature and stirred for 1 h. The mixture was filtered through a celite pad. The filtrate was washed with a solution of HCl (1N, 20 mL), a saturated solution of NaHCO₃ (20 mL) and brine. The organic layer was concentrated under reduced pressure. The crude product was purified by flash column chromatography (SiO₂, Heptane 100%) to yield **6.11** (1.76 g, 4.26 mmol, 67% yield). ¹H NMR (400 MHz, CDCl₃) δ 7.04 (dd, $J = 8.9, 1.1$ Hz, 6H), 7.29 (dt, $J = 8.9, 2.0$ Hz, 6H). No ionization was found.

Pent-4-yn-1-yl (1-(diphenoxyphosphoryl)-2-phenylethyl)carbamate (6.12) General procedure **C** with **1** (0.483 mL, 4.16 mmol) and copper (II) trifluoromethanesulfonate in DCM to yield **6.12** (1.21 g, 2.59 mmol, 62% yield). ¹H NMR (400 MHz, CDCl₃) δ (ppm) 7.38-7.09 (m, 15H), 5.08 (d, $J = 10.5$ Hz, 1H), 4.86-4.72 (m, 1H), 4.13-3.99 (m, 2H), 3.48-3.36 (m, 1H), 3.13-2.97 (m, 1H), 2.16 (td, $J = 10.5, 2.3$ Hz, 2H), 1.96 (t, $J = 2.6$ Hz, 1H), 1.75-1.67 (m, 2H). ¹³C NMR (100 MHz, CDCl₃) δ (ppm) 155.7, 155.6, 150.3, 150.2, 150.0, 149.9, 135.8, 135.7, 129.8, 129.7, 129.3, 128.5, 127.0, 125.5, 125.3, 120.6, 120.5, 120.4, 120.3, 83.0, 68.9,

63.9, 50.0, 48.4, 36.0, 35.9, 27.7, 15.0. MS (ESI) m/z 464.2 $[M+H]^+$. HRMS for $C_{26}H_{26}N_1O_5P_1$, mass calculated 464.1621, mass measured 464.1634.

Pent-4-yn-1-yl (1-(diphenoxyphosphoryl)-2-methylpropyl)carbamate (6.13) General procedure **C** with **2** (0.253 mL, 2.77 mmol) and copper (II) trifluoromethanesulfonate in DCM to yield **6.13** (0.63 g, 1.517 mmol, 55% yield). 1H NMR (400 MHz, $CDCl_3$) δ (ppm) 7.39-7.27 (m, 4H), 7.25-7.10 (m, 6H), 5.24 (d, $J = 10.4$ Hz, 1H), 4.44 (ddd, $J = 19.6, 12.9, 4.0$ Hz, 1H), 4.21 (td, $J = 6.4, 3.2$ Hz, 2H), 2.50-2.37 (m, 1H), 2.27 (td, $J = 7.0, 2.8$ Hz, 2H), 2.00 (t, $J = 2.8$ Hz, 1H), 1.84 (p, $J = 6.6$ Hz, 2H), 1.16-1.08 (m, 6H). ^{13}C NMR (100 MHz, $CDCl_3$) δ (ppm) 156.3, 150.3, 150.0, 129.8, 125.4, 120.6, 83.0, 69.2, 64.4, 53.3, 29.2, 27.8, 20.4, 17.7, 15.1. MS (ESI) m/z 416.2 $[M+H]^+$. HRMS for $C_{22}H_{26}N_1O_5P_1$, mass calculated 416.1621, mass measured 416.1611.

Tert-butyl (tert-butoxycarbonyl)(4-(diphenoxyphosphoryl)-4-(((pent-4-yn-1-yloxy)carbonyl)amino) butyl) carbamate (6.14a) General procedure **C** with **6.3** (2.2 g, 7.66 mmol) and copper (II) trifluoromethanesulfonate in DCM to yield **6.14a** (215 mg, 0.34 mmol, 5% yield). 1H NMR (400 MHz, $CDCl_3$) δ (ppm) 7.31 (q, $J = 7.9$ Hz, 4H), 7.20-7.13 (m, 4H), 7.12 (d, $J = 8.5$ Hz, 2H), 5.15 (d, $J = 10.3$ Hz, 1H), 4.56-4.43 (m, 1H), 4.23-4.10 (m, 2H), 3.63 (t, $J = 6.6$ Hz, 2H), 2.25 (td, $J = 7.0, 2.6$ Hz, 2H), 1.97 (t, $J = 2.6$ Hz, 1H), 1.88-1.77 (m, 4H), 1.48 (s, 18H). MS (ESI) m/z 653.3 $[M+Na]^+$.

Pent-4-yn-1-yl (4-amino-1-(diphenoxyphosphoryl)butyl)carbamate trifluoroacetate salt (6.14b) General procedure **D** with **6.14a** (70 mg, 0.13 mmol) to yield **6.14b** (71 mg, 0.13 mmol, 99% yield). 1H NMR (400 MHz, Methanol- d_4) δ (ppm) 7.89 (d, $J = 9.84$ Hz, 1H), 7.39 (t, $J = 7.9$ Hz, 4H), 7.28-7.22 (m, 2H), 7.19 (d, $J = 7.8$ Hz, 4H), 4.51-4.39 (m, 1H), 4.25-4.12 (m, 2H), 3.07-2.97 (m, 2H), 2.32-2.26 (m, 3H), 2.21-2.10 (m, 1H), 2.01-1.89 (m, 2H), 1.89-1.77 (m, 3H). ^{13}C NMR (100 MHz, Methanol- d_4) δ (ppm) 157.3, 157.2, 150.2, 150.1, 150.0, 149.9, 129.6, 129.6, 125.5, 125.4, 120.4, 120.3, 120.2, 120.1, 82.4, 68.9, 63.8, 38.6, 27.7, 26.0, 25.9, 23.8, 23.7, 14.3. MS (ESI) m/z 431.3 $[M+H]^+$. HRMS for $C_{22}H_{27}N_2O_5P_1$, mass calculated 431.1730, mass measured 431.1747.

Tert-butyl (4-(bis(4-chlorophenoxy)phosphoryl)-4-(((pent-4-yn-1-yloxy)carbonyl)amino)butyl) (*tert*-butoxycarbonyl)carbamate (**6.15a**) General procedure **C** with **6.3** (1 g, 3.48 mmol), **6.11**, and bismuth(III) trifluoromethanesulfonate in THF to yield **6.15a** (210 mg, 0.35 mmol, 10% yield). ¹H NMR (400 MHz, CDCl₃) δ (ppm) 7.31-7.26 (m, 4H), 7.10 (dd, *J* = 12.8, 8.5 Hz, 4H), 5.10 (d, *J* = 10.0 Hz, 1H), 4.59 (br s, 1H), 4.52 – 4.38 (m, 1H), 4.19 (t, *J* = 6.2 Hz, 2H), 3.18 (br d, *J* = 5.7 Hz, 2H), 2.26 (td, *J* = 7.0, 2.5 Hz, 2H), 2.10 (m, 1H), 1.98 (t, *J* = 2.6 Hz, 1H), 1.87 – 1.61 (m, 5H), 1.43 (s, 9H). MS (ESI) *m/z* 621.1 [M+Na]⁺.

Pent-4-yn-1-yl (4-amino-1-(bis(4-chlorophenoxy)phosphoryl)butyl)carbamate trifluoroacetate salt (**6.15b**) General procedure **D** with **6.15a** (150 mg, 0.25 mmol) to yield **6.15b** (123 mg, 0.246 mmol, 98% yield). ¹H NMR (400 MHz, Methanol-*d*₄) δ (ppm) 7.88 (d, *J* = 9.8 Hz, 1H), 7.41 (d, *J* = 8.8 Hz, 4H), 7.24 – 7.16 (m, 4H), 4.52 – 4.40 (m, 1H), 4.26 – 4.10 (m, 2H), 3.08 – 2.94 (m, 2H), 2.33 – 2.25 (m, 3H), 2.22 – 2.05 (m, 1H), 2.02 – 1.75 (m, 5H). MS (ESI) *m/z* 499.1 [M+H]⁺.

Pent-4-yn-1-yl (2-(4-(((*tert*-butoxycarbonyl)amino)phenyl)-1-(diphenoxyphosphoryl)ethyl)carbamate (**6.16a**) General procedure **C** with **6.4** (1.40 g, 5.99 mmol) and copper (II) trifluoromethanesulfonate in DCM to yield **6.16a** (1.0 g, 1.72 mmol, 29% yield). ¹H NMR (400 MHz, DMSO-*d*₆) δ 9.28 (s, 1H), 8.00 (d, *J* = 9.5 Hz, 1H), 7.45 – 7.32 (m, 6H), 7.27 – 7.14 (m, 8H), 4.40 (dd, *J* = 26.5, 9.5 Hz, 1H), 3.90 (dtd, *J* = 17.0, 10.8, 6.2 Hz, 2H), 3.17 (d, *J* = 14.6 Hz, 1H), 2.96 – 2.84 (m, 1H), 2.77 (t, *J* = 2.5 Hz, 1H), 2.13 (td, *J* = 7.0, 2.5 Hz, 2H), 1.66 – 1.54 (m, 2H), 1.46 (s, 9H). MS (ESI) *m/z* 601.3 [M+Na]⁺.

Pent-4-yn-1-yl (2-(4-aminophenyl)-1-(diphenoxyphosphoryl)ethyl)carbamate hydrochloride salt (**6.16b**) General procedure **E** with **6.16a** (120 mg, 0.207 mmol) to yield **6.16b** (98 mg, 0.207 mmol, 99% yield). ¹H NMR (400 MHz, Methanol-*d*₄) δ (ppm) 7.89 (d, *J* = 9.9 Hz, 1H), 7.50 (d, *J* = 8.2 Hz, 2H), 7.38 (q, *J* = 8.1 Hz, 6H), 7.26 (d, *J* = 7.2 Hz, 2H), 7.24-7.17 (m, 4H), 4.73-4.61 (m, 1H), 4.08-3.94 (m, 2H), 3.46 (dt, *J* = 14, 4.3 Hz, 1H). 3.17-3.05 (m, 1H), 2.26 (t, *J* = 2.6 Hz, 1H), 2.19 (td, *J* = 7.1, 2.6 Hz, 2H), 1.71 (p, *J* = 6.7 Hz, 2H). ¹³C NMR (100 MHz, Methanol-*d*₄) δ (ppm) 156.9, 150.3, 150.2, 150.0, 149.9, 137.8, 137.6, 130.8,

129.6, 129.6, 125.5, 125.4, 122.5, 120.4, 120.3, 120.2, 120.1, 82.4, 68.8, 63.5, 34.4, 34.3, 27.7, 14.2. MS (ESI) m/z 479.3 $[M+H]^+$. HRMS for $C_{26}H_{27}N_2O_5P_1$, mass calculated 479.1730, mass measured 479.1727.

Pent-4-yn-1-yl (1-(bis(4-acetamidophenoxy)phosphoryl)-2-(4-((tert-butoxycarbonyl)amino)phenyl)ethyl) carbamate (6.17a) General procedure **C** with **6.4** (0.75 g, 3.19 mmol), **6.10** and boron trifluoride etherate in CH_3CN to yield **6.17a** (420 mg, 0.60 mmol, 19% yield). 1H NMR (400 MHz, $CDCl_3$) δ (ppm) 8.35 (s, 2H), 7.33 (t, 4H, $J = 7.54$ Hz), 7.28 (m, 2H), 7.11 (d, 2H, $J = 8.08$), 6.96 (d, 2H, $J = 8.25$ Hz), 6.91 (d, 2H, $J = 8.35$ Hz), 6.76 (br s, 1H), 4.75-4.61 (m, 1H), 4.14-3.97 (m, 2H), 3.35-3.22 (m, 1H), 3.05-2.92 (m, 1H), 2.12 (t, 2H, $J = 6.54$ Hz), 2.04 (s, 6H), 1.97-1.91 (m, 1H), 1.72-1.62 (m, 2H), 1.50 (s, 9H). MS (ESI) m/z 710.0 $[M+NH_4]^+$.

Pent-4-yn-1-yl (2-(4-aminophenyl)-1-(bis(4-acetamidophenoxy)phosphoryl)ethyl)carbamate trifluoroacetate salt (6.17b) General procedure **D** with **6.17a** (120 mg, 0.173 mmol) to yield **6.17b** (100 mg, 0.169 mmol, 97% yield). 1H NMR (400 MHz, Methanol- d_4) δ (ppm) 7.54 (d, $J = 8.8$ Hz, 4H) 7.38 (d, $J = 8.4$ Hz, 2H), 7.18 (d, $J = 8.4$ Hz, 2H), 7.17-7.11 (m, 4H), 4.71-4.59 (m, 1H), 4.08-3.96 (m, 2H), 3.49-3.41 (m, 1H), 3.15-3.04 (m, 1H), 2.25 (t, $J = 2.4$ Hz, 1H), 2.22-2.17 (m, 2H), 2.11 (s, 6H), 1.74-1.66 (m, 2H). ^{13}C NMR (100 MHz, Methanol- d_4) δ (ppm) 170.2, 130.8, 122.6, 121.0, 120.9, 120.6, 120.5, 120.3, 120.2, 82.4, 68.8, 63.5, 27.7, 22.3, 14.2. MS (ESI) m/z 593.2 $[M+H]^+$. HRMS for $C_{30}H_{33}N_4O_7P_1$, mass calculated 593.2160, mass measured 593.2155.

Pent-4-yn-1-yl (1-(bis(4-chlorophenoxy)phosphoryl)-2-(4-((tert-butoxycarbonyl)amino)phenyl)ethyl) carbamate (6.18a) General procedure **C** with **6.4** (0.88g, 3.74 mmol), **6.11** and boron trifluoride etherate in CH_3CN to yield **6.18a** (234 mg, 0.361 mmol, 10%). 1H NMR (400 MHz, $CDCl_3$) δ 7.34-7.2234 (m, 6H), 7.14 (d, $J = 8.6$ Hz, 2H), 7.09 (dd, $J = 8.8, 1.2$ Hz, 2H), 7.02 (dd, $J = 8.7, 1.2$ Hz, 2H), 6.68 (br s, 1H), 4.93 (d, $J = 10.3$ Hz, 1H), 4.77-4.59 (m, 1H), 4.10-3.98 (m, 2H), 3.32 (dd, $J = 14.7, 12.9, 4.6$ Hz, 1H), 2.97 (dt,

$J = 14.3, 10.3$ Hz, 1H), 2.14 (td, $J = 6.9, 2.6$ Hz, 2H), 1.96 (t, $J = 2.7$ Hz, 1H), 1.73 (p, $J = 6.7$ Hz, 2H), 1.68-1.54 (m, 2H), 1.49 (s, 9H). MS (ESI) m/z 669.2 [M+Na]⁺.

Pent-4-yn-1-yl 2-(4-aminophenyl)-1-(bis(4-chlorophenoxy)phosphoryl)ethyl carbamate hydrochloride salt (6.18b) General procedure *E* with **6.18a** (230 mg, 0.355 mmol) to yield **6.18b** (200 mg, 0.343 mmol, 96% yield). ¹H NMR (400 MHz, Methanol-*d*₄) δ (ppm) 7.99 (br d, $J = 9.3$ Hz, 1H), 7.50 (d, $J = 8.0$ Hz, 2H), 7.43-7.34 (m, 6H), 7.20 (td, $J = 8.3, 1.2$ Hz, 4H), 4.75-4.59 (m, 1H), 4.07-3.93 (m, 2H), 3.44 (dt, $J = 14.0, 4.1$ Hz, 1H), 3.10 (ddd, $J = 25.1, 14.4, 9.9$ Hz, 1H), 2.26 (t, $J = 2.4$ Hz, 1H), 2.17 (td, $J = 7.4, 2.6$ Hz, 2H), 1.69 (p, $J = 6.6$ Hz, 2H). ¹³C NMR (100 MHz, Methanol-*d*₄) δ (ppm) 158.3, 150.3, 150.2, 139.4, 132.3, 131.0, 130.9, 124.2, 123.4, 123.1, 83.8, 70.3, 64.9, 51.0, 35.7, 29.1, 15.6. MS (ESI) m/z 547.1 [M+H]⁺.

Pent-4-yn-1-yl ((4-((tert-butoxycarbonyl)amino)phenyl)(diphenoxyphosphoryl)methyl) carbamate (6.19a) General procedure *C* with **6.5** (1.67 g, 7.55 mmol) and copper(II) trifluoromethanesulfonate in DCM to yield **6.19a** (2.12 g, 3.76 mmol, 50% yield). ¹H NMR (400 MHz, CDCl₃) δ 7.48-7.01 (m, 12H), 6.89 (d, $J = 8.3$ Hz, 2H), 6.55 (s, 1H), 5.75 (dd, $J = 9.9, 5.7$ Hz, 1H), 5.50 (dd, $J = 22.4, 10.2$ Hz, 1H), 4.26-4.06 (m, 2H), 2.23 (t, $J = 6.5$ Hz, 2H), 1.95 (t, $J = 2.5$ Hz, 1H), 1.80 (p, $J = 6.5$ Hz, 2H), 1.51 (s, 9H). MS (ESI) m/z 587.2 [M+Na]⁺.

Pent-4-yn-1-yl ((4-aminophenyl)(diphenoxyphosphoryl)methyl)carbamate trifluoroacetate salt (6.19b) General procedure *D* with **6.19a** (57 mg, 0.101 mmol) to yield **6.19b** (57 mg, 0.099 mmol, 98% yield). ¹H NMR (400 MHz, Methanol-*d*₄) δ (ppm) 8.66 (br d, $J = 10.4$ Hz, 1H), 7.70 (d, $J = 7.7$ Hz, 2H), 7.41-7.25 (m, 6H), 7.24-7.14 (m, 2H), 7.08 (d, $J = 7.3$ Hz, 2H), 7.00 (d, $J = 8.1$ Hz, 2H), 5.70 (br d, $J = 23.2$ Hz, 1H), 4.27-4.08 (m, 2H), 2.33-2.20 (m, 3H), 1.83 (br t, $J = 6.1$ Hz, 2H). ¹³C NMR (100 MHz, Methanol-*d*₄) δ (ppm) 158.3, 151.6, 151.3, 135.4, 134.5, 131.3, 131.0, 126.9, 123.7, 121.5, 83.9, 70.3, 65.4, 53.8, 29.2, 15.7. MS (ESI) m/z 465.2 [M+H]⁺. HRMS for C₂₅H₂₅N₂O₅P₁, mass calculated 465.1574, mass measured 465.1583.

Pent-4-yn-1-yl ((bis(4-acetamidophenoxy)phosphoryl)(4-((tert-butoxycarbonyl)amino)phenyl)methyl) carbamate (6.20a) General procedure **C** with **6.5** (1.68 g, 7.59 mmol), **6.10**, and copper (II) trifluoromethanesulfonate in THF to yield **6.20a** (1.73 g, 2.56 mmol, 34% yield). ^1H NMR (400 MHz, DMSO- d_6) δ (ppm) 9.98 (s, 1H), 9.43 (s, 1H), 8.66 (d, $J = 9.51$ Hz, 1H), 7.53-7.42 (m, $J = 8.8$ Hz, 8H), 6.99 (d, $J = 8.8$ Hz, 2H), 6.90 (d, $J = 6.8$ Hz, 2H), 5.40 (dd, $J = 22, 10.3$ Hz, 1H), 4.12-3.96 (m, 2H), 2.80 (s, 1H), 2.23 (td, $J = 7.2, 2.6$ Hz, 2H), 2.01 (s, 6H), 1.72 (p, $J = 6.7$ Hz, 2H), 1.47 (s, 9H). MS (ESI) m/z 701.4 [M+Na] $^+$.

Pent-4-yn-1-yl ((4-aminophenyl)(bis(4-acetamidophenoxy)phosphoryl)methyl) carbamate trifluoroacetate salt (6.20b) General procedure **D** with **6.20a** (0.8 g, 1.179 mmol) to yield **6.20b** (0.68 g, 1.173 mmol, 99% yield). ^1H NMR (400 MHz, Methanol- d_4) δ (ppm) 7.73 (dd, $J = 8.7, 2.3$ Hz, 1H), 7.50 (t, $J = 9.0$ Hz, 2H), 7.42 (d, $J = 8.6$ Hz, 1H), 7.02 (d, $J = 7.7$ Hz, 1H), 6.95 (d, $J = 7.6$ Hz, 1H), 4.26 – 4.08 (m, 0H), 2.29 (d, $J = 9.8$ Hz, 0H), 2.10 (s, 2H), 1.82 (p, $J = 6.4$ Hz, 1H). ^{13}C NMR (100 MHz, Methanol- d_4) δ (ppm) 170.2, 145.8, 145.7, 136.2, 134.9, 131.9, 130.0, 129.9, 122.7, 121.0, 120.9, 120.3, 120.3, 120.2, 82.3, 68.8, 64.0, 53.0, 51.4, 39.0, 27.7, 22.3, 14.3. MS (ESI) m/z 601.2 [M+Na] $^+$. HRMS for C₂₉H₃₁N₄O₇P₁, mass calculated 579.2003, mass measured 579.2013.

Pent-4-yn-1-yl ((bis(4-chlorophenoxy)phosphoryl)(4-((tert-butoxycarbonyl)amino)phenyl)methyl)carbamate (6.21a) General procedure **C** with **6.5** (1.69 g, 7.64 mmol), **6.11**, and copper (II) trifluoromethanesulfonate in THF to yield **6.21a** (2 g, 3.16 mmol, 41% yield). ^1H NMR (400 MHz, CDCl₃) δ (ppm) 7.48 – 7.32 (t, $J = 9.7$ Hz, 4H), 7.29 (d, $J = 8.2$ Hz, 2H), 7.18 (d, $J = 9.0$ Hz, 2H), 7.08 (d, $J = 9.0$ Hz, 2H), 6.81 (d, $J = 8.4$ Hz, 2H), 6.61 (s, 1H), 5.52 (dd, $J = 21.9, 10.2$ Hz, 1H), 4.22-4.10 (m, 2H), 2.27-2.18 (m, 2H), 1.95 (t, $J = 2.7$ Hz, 1H), 1.79 (p, $J = 6.7$ Hz, 2H), 1.54 (s, 9H). MS (ESI) m/z 655.2 [M+Na] $^+$.

Pent-4-yn-1-yl ((4-aminophenyl)(bis(4-chlorophenoxy)phosphoryl)methyl)carbamate trifluoroacetate salt (6.21b) General procedure **D** with **6.21a** (0.8 g, 1.263 mmol) to yield **6.21b** (0.65 g, 1.216 mmol, 96% yield). ^1H NMR (400 MHz, Methanol- d_4) δ 7.72 (dd, $J = 8.7, 2.3$ Hz, 2H), 7.40 (d, $J = 8.4$ Hz, 2H), 7.34 (t, $J = 9.5$ Hz, 4H), 7.10 (d, $J = 8.8$ Hz, 2H), 7.01 (d, J

= 10.4 Hz, 2H), 5.73 (d, J = 21.8 Hz, 1H), 4.26 – 4.09 (m, 2H), 2.34 – 2.17 (m, 3H), 1.87 – 1.76 (m, 2H). ^{13}C NMR (100 MHz, Methanol- d_4) δ (ppm) 156.7, 148.6, 148.5, 133.6, 133.1, 130.9, 130.8, 129.9, 129.8, 129.6, 129.5, 122.2, 121.7, 121.6, 121.6, 121.6, 82.4, 68.9, 64.0, 53.0, 51.4, 29.5, 29.4, 27.7, 22.3, 14.3. MS (ESI) m/z 555.1 $[\text{M}+\text{Na}]^+$. HRMS for $\text{C}_{25}\text{H}_{23}\text{N}_2\text{O}_5\text{Cl}_2\text{P}_1$, mass calculated 533.0794, mass measured 533.0775.

Pent-4-yn-1-yl (2-(4-(((tert-butoxycarbonyl)amino)methyl)phenyl)-1-(diphenoxyphosphoryl)ethyl) carbamate (6.22a) General procedure **C** with **6.6** (1.30 g, 5.21 mmol) and copper(II) trifluoromethanesulfonate in DCM to yield **6.22a** (1.4 g, 2.362 mmol, 45% yield) ^1H NMR (400 MHz, CDCl_3) δ (ppm) 7.37-7.27 (m, 4H), 7.24-7.08 (m, 10H), 5.23-5.06 (m, 1H), 4.96-4.67 (m, 2H), 4.29 (d, J = 5.6 Hz, 2H), 4.14-3.98 (m, 2H), 3.45-3.31 (m, 1H), 3.02 (dt, J = 14.5, 10.0 Hz, 1H), 2.13 (t, J = 6.7 Hz, 2H), 1.97 (t, J = 2.7 Hz, 1H), 1.70 (p, J = 6.7 Hz, 2H), 1.46 (s, 9H). MS (ESI) m/z 615.2 $[\text{M}+\text{Na}]^+$.

Pent-4-yn-1-yl (2-(4-(aminomethyl)phenyl)-1-(diphenoxyphosphoryl)ethyl)carbamate hydrochloride salt (6.22b) General procedure **E** with **6.22a** (42 mg, 0.071 mmol) to yield **6.22b** (37 mg, 0.070 mmol, 99% yield). ^1H NMR (400 MHz, Methanol- d_4) δ (ppm) 7.95 (d, J = 10.1 Hz, 1H), 7.49-7.32 (m, 8H), 7.28-7.14 (m, 6H), 4.71-4.57 (m, 1H), 4.10 (s, 2H), 4.06-3.91 (m, 2H), 3.78-3.60 (m, 1H), 3.42 (dt, J = 14.0, 4.3 Hz, 1H), 3.07 (ddd, J = 25.6, 13.3, 8.4 Hz, 1H), 2.26 (t, J = 2.2 Hz, 1H), 2.16 (td, J = 7.3, 2.4 Hz, 2H), 1.69 (p, J = 6.7 Hz, 2H). ^{13}C NMR (100 MHz, Methanol- d_4) δ (ppm) 158.3, 151.7, 151.6, 151.4, 151.3, 139.4, 139.3, 133.1, 131.1, 131.0, 130.2, 126.8, 126.7, 121.8, 121.5, 83.9, 70.2, 64.8, 51.3, 44.0, 35.9, 29.2, 15.6. MS (ESI) m/z 493.2 $[\text{M}+\text{H}]^+$. HRMS for $\text{C}_{27}\text{H}_{29}\text{N}_2\text{O}_5\text{P}_1$, mass calculated 493.1887, mass measured 493.1881.

Tert-butyl 4-((diphenoxyphosphoryl)(((pent-4-yn-1-yloxy)carbonyl)amino)methyl) piperidine-1-carboxylate (6.23a) General procedure **C** with **6.7** (0.99 g, 4.69 mmol) and copper(II) trifluoromethanesulfonate in DCM to yield **6.23a** (1.2 g, 2.15 mmol, 46% yield). ^1H -NMR (400 MHz, CDCl_3) δ (ppm) 7.35 – 7.27 (m, 4H), 7.21 – 7.14 (m, 4H), 7.14 – 7.10 (m, 2H), 5.24-5.15 (m, 1H), 4.52-4.39 (m, 1H), 4.26-4.09 (m, 4H), 2.79-2.61 (br s, 2H), 2.30-2.12

(m, 3H), 2.01-1.91 (m, 2H), 1.87-1.73 (m, 3H), 1.44 (s, 9H), 1.40-1.32 (m, 1H). MS (ESI) m/z 579.2 $[M+Na]^+$.

Pent-4-yn-1-yl ((diphenoxyphosphoryl)(piperidin-4-yl)methyl)carbamate trifluoroacetate salt (6.23b) General procedure **D** with **6.23a** (32 mg, 0.057 mmol) to yield **6.23b** (26 mg, 0.057 mmol, 99%). ^1H NMR (400 MHz, Methanol- d_4) δ (ppm) 7.40 (t, $J=7.88$ Hz, 4 H), 7.28-7.22 (m, 2H), 7.22-7.16 (m, 4H), 4.47 (dd, $J = 19.2, 6.3$ Hz, 1H), 4.25 - 4.13 (m, 2H), 3.47 (t, $J = 11.3$ Hz, 2H), 3.13 - 3.01 (m, 2H), 2.46 - 2.34 (m, 1H), 2.32 - 2.26 (m, 3H), 2.26 - 2.17 (m, 2H), 1.88 - 1.79 (m, 2H), 1.79 - 1.66 (m, 2H). ^{13}C NMR (100 MHz, Methanol- d_4) δ (ppm) 157.4, 157.3, 150.1, 150.0, 149.9, 149.8, 129.7, 129.6, 125.5, 125.4, 120.4, 120.4, 120.2, 120.1, 82.3, 68.9, 63.9, 52.7, 51.1, 43.4, 43.3, 34.8, 34.7, 27.8, 26.3, 26.2, 24.8, 24.7, 14.3. MS (ESI) m/z 457.3 $[M+H]^+$. HRMS for $\text{C}_{24}\text{H}_{29}\text{N}_2\text{O}_5\text{P}_1$, mass calculated 457.1887, mass measured 457.1903.

5-azidopentan-1-ol (6.25) Sodiumazide (1.074 g, 16.52 mmol) was added to a solution of pentamethylenebromohydrin (1 mL, 8.26 mmol) in H_2O (15 mL). The reaction mixture was stirred at 80 °C for 18 h. After cooling down to room temperature, the aqueous solution was extracted with DCM (3 x 20 mL). The combined organic layers were dried over anhydrous MgSO_4 , filtered and concentrated under reduced pressure to yield **6.25** (1.00 g, 7.80 mmol, 94% yield) as a colourless oil used for the next step without any further purification. ^1H NMR (400 MHz, CDCl_3) δ (ppm) 1.36-1.47 (m, 2H), 1.50-1.65 (m, 4H), 2.06 (br t, $J = 4.2$ Hz, 1H), 3.26 (t, $J = 6.7$ Hz, 2H), 3.63 (dd, $J = 6.2, 4.0$ Hz, 2H). No ionization was found.

5-azidopentanal (6.26) General procedure **B** with **6.25** (1 g, 7.74 mmol) to yield **6.26** (0.48 g, 3.81 mmol, 49% yield). ^1H NMR (400 MHz, CDCl_3) δ (ppm) 1.64-1.55 (m, 2H), 1.75-1.64 (m, 2H), 2.47 (td, $J = 6.8, 1.4$ Hz, 2H), 3.28 (t, $J = 7.0$ Hz, 2H), 9.74 (t, $J = 1.5$ Hz, 1H). No ionization was found.

Pent-4-yn-1-yl (5-azido-1-(diphenoxyphosphoryl)pentyl)carbamate (6.27) General procedure **C** with **6.26** (0.99 g, 7.81 mmol) and copper (II) trifluoromethanesulfonate in DCM to yield **6.27** (2.62 g, 5.57 mmol, 71% yield). ^1H NMR (400 MHz, CDCl_3) δ (ppm) 7.38-7.27 (m, 4H), 7.22-7.07 (m, 6H), 5.22 (br d, $J = 10.4$ Hz, 1H), 4.74 (br s, 1H), 4.53-4.39 (m, 1H), 4.25-4.11 (m, 2H), 3.28 (t, $J = 6.4$ Hz, 2H), 2.34-2.18 (m, 2H), 2.13-1.99 (m, 1H), 1.97 (q, $J = 2.6$ Hz, 1H), 1.89-1.43 (m, 6H). MS (ESI) m/z 471.3 $[\text{M}+\text{H}]^+$.

Pent-4-yn-1-yl (5-azido-1-(bis(4-acetamidophenoxy)phosphoryl)pentyl)carbamate (6.28) General procedure **C** with **6.26** (0.481 g, 3.78 mmol), tris(4-acetamidophenyl) phosphite and Boron trifluoride etherate in CH_3CN to yield **6.28** (1.3 g, 2.22 mmol, 59% yield). ^1H NMR (400 MHz, CDCl_3) δ (ppm) 8.78 (d, $J = 9.7$ Hz, 2H), 7.30 (dd, $J = 8.7, 5.5$ Hz, 4H), 6.89 (t, $J = 8.3$ Hz, 4H), 5.98 (d, $J = 10.1$ Hz, 1H), 4.51-4.35 (m, 1H), 4.23-4.14 (m, 2H), 3.27 (t, $J = 6.0$ Hz, 2H), 2.22 (td, $J = 6.7, 2.7$ Hz, 2H), 2.05-1.94 (m, 9H), 1.79 (p, $J = 6.5$ Hz, 2H), 1.72-1.44 (m, 4H). MS (ESI) m/z 585.3 $[\text{M}+\text{H}]^+$.

Tert-butyl pent-4-yn-1-yl (1-(diphenoxyphosphoryl)pentane-1,5-diyl)dicarbamate (6.29a) General procedure **F** with **6.27** (0.765 g, 1.627 mmol) to yield **6.29a** (0.49 g, 0.91 mmol, 64% yield). ^1H NMR (400 MHz, Methanol- d_4) δ (ppm) 7.36 (t, $J = 7.7$ Hz, 4H), 7.22 (td, $J = 7.4, 3.1$ Hz, 2H), 7.13-7.19 (m, 4H), 4.38 (ddd, $J = 15.7, 13.4, 3.5$ Hz, 1H), 4.12 (m, 2H), 4.09 (t, $J = 6.3$ Hz, 2H), 3.06 (t, $J = 6.0$ Hz, 2H), 2.22-2.32 (m, 4H), 1.97-2.10 (m, 1H), 1.72-1.92 (m, 4H), 1.45-1.52 (m, 2H), 1.43 (s, 9H). MS (ESI) m/z 445.3 $[(\text{M}-\text{Boc})+\text{H}]^+$.

Pent-4-yn-1-yl (5-amino-1-(diphenoxyphosphoryl)pentyl)carbamate trifluoroacetate salt (6.29b) General procedure **D** with **6.29a** (57 mg, 0.105 mmol) to yield **6.29b** (52 mg, 0.093 mmol, 89% yield). ^1H NMR (400 MHz, Methanol- d_4) δ (ppm) 7.81 (d, $J = 9.8$ Hz, 1H), 7.37 (t, $J = 7.5$ Hz, 4H), 7.22 (t, $J = 7.4$ Hz, 2H), 7.16 (d, $J = 8.6$ Hz, 4H), 4.48-4.34 (m, 1H), 4.24-4.08 (m, 2H), 2.93 (t, $J = 6.9$ Hz, 2H), 2.31-2.23 (m, 3H), 2.14-1.99 (m, 1H), 1.98-1.45 (m, 7H). ^{13}C NMR (100 MHz, Methanol- d_4) δ (ppm) 158.7, 151.6, 151.4, 131.0, 126.7, 121.8, 121.6, 83.9, 70.3, 65.1, 40.5, 29.8, 29.2, 27.9, 23.9, 23.7, 15.7. MS (ESI) m/z 445.3 $[\text{M}+\text{H}]^+$. HRMS for $\text{C}_{23}\text{H}_{29}\text{N}_2\text{O}_5\text{P}_1$, mass calculated 445.1887, mass measured 445.1899.

Tert-butyl pent-4-yn-1-yl (1-(bis(4-acetamidophenoxy)phosphoryl)pentane-1,5-diyl)dicarbamate (6.30a) General procedure *F* with **6.28** (0.20 g, 0.342 mmol) to yield **6.30a** (0.078 g, 0.119 mmol, 35% yield). ^1H NMR (400 MHz, CDCl_3) δ (ppm) 8.73 (d, $J = 14.8$ Hz, 2H), 7.93 (d, $J = 8.1$ Hz, 4H), 6.90 (dd, $J = 13.7, 8.7$ Hz, 4H), 5.99 (d, $J = 9.5$ Hz, 1H), 4.83 (t, $J = 5.8$ Hz, 1H), 4.48-4.32 (m, 1H), 4.17 (t, $J = 5.9$ Hz, 2H), 3.13-2.97 (m, 2H), 2.27-2.12 (m, 3H), 2.03 (s, 9H), 1.97 (t, $J = 2.8$ Hz, 2H), 1.79 (p, $J = 6.7$ Hz, 2H), 1.36-1.60 (m, 13H). MS (ESI) m/z 559.2 [(M-Boc)+H] $^+$.

Pent-4-yn-1-yl (5-amino-1-(bis(4-acetamidophenoxy)phosphoryl)pentyl)carbamate hydrochloride salt (6.30b) General procedure *E* with **6.30a** (42 mg, 0.064 mmol) to yield **6.30b** (25.3 mg, 0.043 mmol, 67% yield). ^1H NMR (400 MHz, Methanol- d_4) δ (ppm) 7.55 (d, $J = 8.5$ Hz, 4H), 7.11 (d, $J = 8.7$ Hz, 4H), 4.38 (ddd, $J = 16.8, 13.4, 3.6$ Hz, 1H), 4.24-4.08 (m, 2H), 3.77-3.70 (m, 1H), 3.69-3.67 (m, 2H), 3.60-3.55 (m, 1H), 2.93 (t, $J = 7.2$ Hz, 2H), 2.31-2.24 (m, 3H), 2.11 (s, 6H), 2.06-1.45 (m, 8H). ^{13}C NMR (100 MHz, Methanol- d_4) δ (ppm): 171.6, 158.7, 137.7, 122.4, 122.0, 121.7, 83.9, 73.6, 72.5, 70.3, 68.2, 65.2, 62.2, 40.5, 29.8, 29.2, 27.8, 23.8, 15.7. MS (ESI) m/z 559.2 [M+H] $^+$.

Tert-butyl (5-(diphenoxyphosphoryl)-5-(1-(hex-5-ynoyl)pyrrolidine-2-carboxamido)pentyl) carbamate (6.31a) General procedure *F* with **S6.11** (1.0 g, 1.810 mmol) to yield **6.31a** (112 mg, 0.179 mmol, 10% yield). ^1H NMR (400 MHz, CDCl_3) δ (ppm): 7.70 (br d, $J = 10.1$ Hz, 1H), 7.38-7.25 (m, 4H), 7.25-7.18 (m, 2H), 7.18-7.11 (m, 4H), 7.09 (d, $J = 8.2$ Hz, 1H), 5.05 (br t, $J = 5.4$ Hz, 1H), 4.82-4.65 (m, 2H), 4.44 (d, $J = 8.0$ Hz, 1H), 3.67-3.57 (m, 1H), 3.50-3.31 (m, 2H), 3.14-2.98 (m, 2H), 2.48 (td, $J = 7.2, 3.3$ Hz, 1H), 2.44-2.30 (m, 1H), 2.27 (td, $J = 6.8, 2.6$ Hz, 1H), 2.24-1.45 (m, 13H), 1.41 (s, 9H). MS m/z 648.3 [M+Na] $^+$.

(5-(diphenoxyphosphoryl)-5-(1-(hex-5-ynoyl)pyrrolidine-2-carboxamido)pentyl) carbamate trifluoroacetate salt (6.31b) General procedure *D* with **6.31a** (42.6 mg, 0.07 mmol) to yield **6.31b** (41 mg, 0.06 mmol, 94% yield). ^1H NMR (400 MHz, Methanol- d_4) δ (ppm) 7.44-7.30 (m, 4H), 7.30-7.05 (m, 6H), 4.79-4.68 (m, 2H), 4.47 (dd, $J = 8.7, 5.3$ Hz, 1H),

3.79-3.54 (m, 4H), 3.32 (t, $J = 1.7$ Hz, 1H), 3.06-2.87 (m, 2H), 2.53 (t, $J = 7.3$ Hz, 1H), 2.34-1.38 (m, 15H). ^{13}C NMR (100 MHz, Methanol- d_4) δ (ppm) 175.1, 173.8, 151.6, 151.4, 131.0, 126.9, 121.9, 121.7, 121.6, 84.3, 70.4, 61.2, 47.5, 45.9, 40.7, 34.1, 30.9, 29.2, 27.4, 25.9, 25.8, 25.0, 23.5, 18.6. MS m/z 526.3 $[\text{M}+\text{H}]^+$. HRMS for $\text{C}_{29}\text{H}_{36}\text{N}_3\text{O}_5\text{P}_1$, mass calculated 526.2465, mass measured 526.2457.

N, N'-bis-tert-butoxycarbonyl pent-4-yn-1-yl (1-(diphenoxyphosphoryl)-4-guanidinobutyl) carbamate (6.32a) General procedure **G** with **6.14b** (173 mg, 0.32 mmol) to yield **6.32a** (128 mg, 0.19 mmol, 60% yield). ^1H NMR (400 MHz, CDCl_3) δ (ppm) 11.49 (s, 1H), 8.37 (t, $J = 5.27$ Hz, 1H), 7.31 (q, $J = 8.0$ Hz, 4H), 7.18 (t, $J = 6.7$ Hz, 4H), 7.13 (d, $J = 8.5$ Hz, 2H), 5.42 (d, $J = 10.3$ Hz, 1H), 4.56-4.43 (m, 1H), 4.25-4.13 (m, 2H), 3.59-3.36 (m, 2H), 2.26 (dt, $J = 7.0, 2.6$ Hz, 2H), 2.16 -2.04 (m, 1H), 1.97 (t, $J = 2.6$ Hz, 1H), 1.88-1.78 (m, 4H), 1.48 (s, 9H), 1.47 (s, 9H). MS (ESI) m/z 673.1 $[\text{M}+\text{H}]^+$.

Pent-4-yn-1-yl (1-(diphenoxyphosphoryl)-4-guanidinobutyl)carbamate trifluoroacetate salt (6.32b) General procedure **D** with **6.32a** (34 mg, 0.05 mmol) to yield **6.32b** (29 mg, 0.05 mmol, 98% yield). ^1H NMR (400 MHz, Methanol- d_4) δ (ppm) 7.85 (d, $J = 9.8$ Hz, 1H), 7.57 (t, $J = 5.4$ Hz, 1H), 7.37 (t, $J = 7.9$ Hz, 4H), 7.26-7.19 (m, 2H), 7.16 (d, $J = 8.2$ Hz, 4H), 4.5-4.36 (m, 1H), 4.23-4.10 (m, 2H), 3.28-3.19 (m, 2H), 2.30-2.23 (m, 3H), 2.16-2.05 (m, 1H), 1.97-1.65 (m, 5H). ^{13}C NMR (100 MHz, Methanol- d_4) δ (ppm) 157.4, 157.2, 150.2, 150.1, 150.0, 149.9, 129.6, 129.6, 125.5, 125.4, 120.4, 120.4, 120.2, 120.1, 82.4, 68.9, 63.8, 40.3, 27.8, 26.0, 25.0, 25.0, 14.3. MS (ESI) m/z 473.1 $[\text{M}+\text{H}]^+$. HRMS for $\text{C}_{23}\text{H}_{29}\text{N}_4\text{O}_5\text{P}_1$, mass calculated 473.1948, mass measured 473.1940.

N, N'-bis-tert-butoxycarbonyl pent-4-yn-1-yl (1-(bis(4-chlorophenoxy)phosphoryl)-4-guanidinobutyl) carbamate (6.33a) General procedure **G** with **6.15b** (150 mg, 0.245 mmol) to yield **6.33a** (137 mg, 0.185 mmol, 75% yield). ^1H NMR (400 MHz, CDCl_3) δ 11.48 (s, 1H), 8.37 (t, $J = 5.5$ Hz, 1H), 7.28 (t, $J = 7.1$ Hz, 4H), 7.11 (dd, $J = 19.9, 8.0$ Hz, 4H), 5.63 (d, $J = 10.2$ Hz, 1H), 4.56-4.42 (m, 1H), 4.19 (t, $J = 6.2$ Hz, 2H), 3.63-3.50 (m, 1H), 3.45-3.33 (m, 1H), 2.27

(td, $J = 7.0, 2.6$ Hz, 2H), 2.13 – 2.01 (m, 1H), 1.98 (t, $J = 2.6$ Hz, 1H), 1.89 – 1.71 (m, 5H), 1.48 (s, 9H), 1.46 (s, 9H). MS (ESI) m/z 763.3 $[M+Na]^+$.

Pent-4-yn-1-yl (1-(bis(4-chlorophenoxy)phosphoryl)-4-guanidinobutyl)carbamate trifluoroacetate salt (6.33b) General procedure **D** with **6.33a** (30 mg, 0.04 mmol) to yield **6.33b** (21 mg, 0.039 mmol, 96% yield). ^1H NMR (400 MHz, Methanol- d_4) δ 7.84 (d, $J = 9.8$ Hz, 1H), 7.39 (d, $J = 8.9$ Hz, 4H), 7.24 – 7.13 (m, 4H), 4.51 – 4.33 (m, 1H), 4.16 (q, $J = 6.3$ Hz, 2H), 3.31 – 3.17 (m, 2H), 2.30 – 2.24 (m, 3H), 2.16 – 2.02 (m, 1H), 1.97 – 1.65 (m, 5H). ^{13}C NMR (100 MHz, Methanol- d_4) δ (ppm) 158.6, 150.3, 150.1, 150.0, 149.9, 132.3, 132.1, 131.0, 131.0, 123.4, 123.3, 123.1, 123.0, 83.8, 70.2, 65.2, 41.6, 30.9, 30.8, 29.2, 27.4, 26.3, 26.2, 15.7. MS (ESI) m/z 541.1 $[M+H]^+$. HRMS for $\text{C}_{23}\text{H}_{27}\text{N}_4\text{O}_5\text{Cl}_2\text{P}_1$, mass calculated 541.1169, mass measured 541.1142.

N, N'-bis-tert-butoxycarbonyl pent-4-yn-1-yl (1-(diphenoxyphosphoryl)-2-(4-guanidinophenyl)ethyl) carbamate (6.34a) General procedure **G** with **6.16b** (1.21 g, 2.350 mmol) to yield **6.34a** (910 mg, 1.26 mmol, 54% yield). ^1H NMR (400 MHz, DMSO- d_6) δ 11.43 (s, 1H), 9.98 (s, 1H), 8.04 (d, $J = 9.6$ Hz, 1H), 7.49 (d, $J = 8.5$ Hz, 2H), 7.45 – 7.37 (m, 4H), 7.29 (d, $J = 8.5$ Hz, 2H), 7.27 – 7.16 (m, 6H), 4.53 – 4.40 (m, 1H), 3.98 – 3.85 (m, 2H), 3.24 (d, $J = 14.1$ Hz, 1H), 3.03 – 2.91 (m, 1H), 2.77 (t, $J = 2.6$ Hz, 1H), 2.13 (td, $J = 7.1, 2.3$ Hz, 2H), 1.64 – 1.55 (m, 2H), 1.51 (s, 9H), 1.41 (s, 9H). MS (ESI) m/z 601.3 $[M+Na]^+$.

Pent-4-yn-1-yl (1-(diphenoxyphosphoryl)-2-(4-guanidinophenyl)ethyl)carbamate trifluoroacetate salt (6.34b) General procedure **D** with **6.34a** (70 mg, 0.097 mmol) to yield **6.34b** (50 mg, 0.096 mmol, 99% yield). ^1H NMR (400 MHz, CDCl_3) δ (ppm) 9.80 (s, 1H), 7.36 – 7.24 (m, 7H), 7.23 – 7.12 (m, 6H), 7.08 (t, $J = 6.9$ Hz, 5H), 5.71 (d, $J = 10.2$ Hz, 1H), 4.77 – 4.62 (m, 1H), 4.12 – 3.93 (m, 2H), 3.41 – 3.27 (m, 1H), 3.06 (dd, $J = 24.5, 10.4$ Hz, 1H), 2.15 (td, $J = 6.9, 2.4$ Hz, 2H), 1.95 (t, $J = 2.5$ Hz, 1H), 1.71 (p, $J = 6.6$ Hz, 2H). ^{13}C NMR (101 MHz, CDCl_3) δ (ppm) 156.62, 156.07, 156.00, 149.96, 149.86, 149.73, 149.63, 136.18, 133.01, 131.07, 130.04, 129.92, 125.89, 125.76, 125.67, 120.52, 120.48, 120.31, 120.27, 82.88,

77.24, 69.22, 64.22, 27.61, 14.89. MS (ESI) m/z 521.3 [M+H]⁺. HRMS for C₂₇H₂₉N₄O₅P₁, mass calculated 521.1948, mass measured 521.1936.

***N,N'*-bis-*tert*-butyloxycarbonyl pent-4-yn-1-yl (1-(bis(4-acetamidophenoxy)phosphoryl)-2-(4-guanidinophenyl)ethyl) carbamate (6.35a)** General procedure **G** with **6.17b** (68.5 mg, 0.097 mmol) to yield **6.35a** (80 mg, 0.096 mmol, 99% yield). ¹H NMR (400 MHz, DMSO-*d*₆) δ (ppm) 11.43 (s, 1H), 9.98 (s, 1H), 8.04 (d, J = 9.6 Hz, 1H), 7.49 (d, J = 8.5 Hz, 2H), 7.45 – 7.37 (m, 4H), 7.29 (d, J = 8.5 Hz, 2H), 7.27 – 7.16 (m, 6H), 4.53 – 4.40 (m, 1H), 3.98 – 3.85 (m, 2H), 3.24 (d, J = 14.1 Hz, 1H), 3.03 – 2.91 (m, 1H), 2.77 (t, J = 2.6 Hz, 1H), 2.13 (td, J = 7.1, 2.3 Hz, 2H), 1.64 – 1.55 (m, 2H), 1.51 (s, 9H), 1.41 (s, 9H). MS (ESI) m/z 835.0 [M+H]⁺.

Pent-4-yn-1-yl (1-(bis(4-acetamidophenoxy)phosphoryl)-2-(4-guanidinophenyl)ethyl) carbamate trifluoroacetate salt (6.35b) General procedure **D** with **6.35a** (70 mg, 0.084 mmol) to yield **6.35b** (51 mg, 0.080 mmol, 96% yield). ¹H NMR (400 MHz, Methanol-*d*₄) δ (ppm) 7.55 (m, 4H), 7.40 (d, J = 8.4 Hz, 2H), 7.22 (d, J = 8.4 Hz, 2H), 7.13 (m, 4H), 4.68-4.54 (m, 1H), 4.02 (m, 1H), 3.40 (m, 1H), 3.12 (m, 1H), 2.23 (t, J = 2.8 Hz, 1H), 2.18 (m, 2H), 2.11 (s, 6H), 1.71 (m, 2H). ¹³C NMR (100 MHz, Methanol-*d*₄) δ (ppm) 170.3, 157.1, 157.0, 156.6, 146.1, 146.0, 145.8, 145.7, 136.4, 136.3, 136.2, 133.6, 130.5, 125.2, 121.0, 120.9, 120.7, 120.6, 120.4, 120.3, 82.4, 68.8, 63.6, 34.5, 27.8, 22.4, 14.2. MS (ESI) m/z 635.3 [M+H]⁺. HRMS for C₃₁H₃₅N₆O₅P₁, mass calculated 635.2378, mass measured 635.2382.

***N,N'*-bis-*tert*-butyloxycarbonyl pent-4-yn-1-yl (1-(bis(4-chlorophenoxy)phosphoryl)-2-(4-guanidinophenyl) ethyl) carbamate (6.36a)** General procedure **G** with **6.18b** (0.170 g, 0.291 mmol) to yield **6.36a** (165.4 mg, 0.209 mmol, 81% yield). ¹H NMR (400 MHz, CDCl₃) δ (ppm) 11.63 (br s, 1H), 10.31 (br s, 1H), 7.54 (d, J = 8.5 Hz, 2H), 7.29 (d, J = 9.3 Hz, 2H), 7.23 (d, J = 7.3 Hz, 2H), 7.17 (d, J = 7.3 Hz, 2H), 7.11 (d, J = 8.1 Hz, 2H), 7.03 (d, J = 8.0 Hz, 2H), 5.71-5.38 (m, 1H), 4.83-4.63 (m, 1H), 4.14-3.94 (m, 2H), 3.35-3.21 (m, 1H), 2.99 (dd, J = 12.3, 10.2 Hz, 1H), 2.15 (br s, 2H), 1.98 (t, J = 2.6 Hz, 1H), 1.70 (p, J = 6.0 Hz, 2H), 1.52 (s, 9H), 1.49 (s, 9H). MS (ESI) m/z 791.2 [M+H]⁺.

Pent-4-yn-1-yl (1-(bis(4-chlorophenoxy)phosphoryl)-2-(4-guanidinophenyl)ethyl) carbamate trifluoroacetate salt (6.36b) General procedure **D** with **6.36a** (52.7 mg, 0.067 mmol) to yield **6.36b** (47 mg, 0.067 mmol, 100% yield). ^1H NMR (400 MHz, Methanol- d_4) δ (ppm) 7.44-7.34 (m, 6H), 7.28-7.15 (m, 6H), 4.64 (ddd, $J = 15.8, 13.5, 3.8$ Hz, 1H), 4.02 (t, $J = 6.2$ Hz, 2H), 3.40 (dt, $J = 14.2, 4.3$ Hz, 1H), 3.13-3.00 (m, 1H), 2.25 (t, $J = 2.8$ Hz, 1H), 2.19 (td, $J = 7.1, 2.4$ Hz, 2H), 1.70 (p, $J = 6.4$ Hz, 2H). ^{13}C NMR (100 MHz, Methanol- d_4) δ (ppm) 161.3, 158.1, 150.2, 149.9, 137.5, 135.1, 132.3, 131.9, 131.1, 126.6, 123.4, 123.1, 83.8, 70.3, 65.0, 51.3, 35.8, 29.2, 27.8, 15.7. MS (ESI) m/z 589.1 $[\text{M}+\text{H}]^+$. HRMS for $\text{C}_{27}\text{H}_{27}\text{N}_4\text{O}_5\text{Cl}_2\text{P}_1$, mass calculated 589.1169, mass measured 589.1188.

***N,N'*-bis-*tert*-butyloxycarbonyl pent-4-yn-1-yl ((diphenoxyphosphoryl)(4-guanidinophenyl)methyl)carbamate (6.37a)** General procedure **G** with **6.19b** (1.75 g, 3.49 mmol) to yield **6.37a** (1.38 g, 1.953 mmol, 56% yield). ^1H NMR (400 MHz, CDCl_3) δ (ppm) 11.62 (s, 1H), 10.38 (s, 1H), 7.64 (d, $J = 8.0$ Hz, 2H), 7.46 (d, $J = 8.3$ Hz, 2H), 7.31 (t, $J = 8.0$ Hz, 2H), 7.24 (t, $J = 7.9$ Hz, 2H), 7.21-7.04 (m, 4H), 6.91 (d, $J = 8.3$ Hz, 2H), 5.70 (dd, $J = 9.9, 3.0$ Hz, 1H), 5.52 (dd, $J = 22.8, 5.5$ Hz, 1H), 4.26-4.08 (m, 2H), 2.25 (t, $J = 6.2$ Hz, 2H), 1.96 (t, $J = 2.5$ Hz, 1H), 1.81 (p, $J = 6.8$ Hz, 2H), 1.53 (s, 9H), 1.50 (s, 9H). MS (ESI) m/z 729.3 $[\text{M}+\text{Na}]^+$.

Pent-4-yn-1-yl ((diphenoxyphosphoryl)(4-guanidinophenyl)methyl)carbamate trifluoroacetate salt (6.37b) General procedure **D** with **6.37a** (57 mg, 0.081 mmol) to yield **6.37b** (50.6 mg, 0.081 mmol, 100% yield). ^1H NMR (400 MHz, Methanol- d_4) δ (ppm) 8.65 (br d, $J = 9.6$ Hz, 1H), 7.69 (dd, $J = 8.2, 2.0$ Hz, 2H), 7.29-7.38 (m, 6H), 7.21 (t, $J = 7.6$ Hz, 2H), 7.10 (d, $J = 8.2$ Hz, 2H), 7.05 (d, $J = 7.8$ Hz, 2H), 5.74-5.59 (m, 1H), 4.25-4.08 (m, 2H), 2.32-2.22 (m, 3H), 1.82 (p, $J = 6.5$ Hz, 2H). ^{13}C NMR (100 MHz, Methanol- d_4) δ (ppm) 158.0, 151.4, 136.7, 134.9, 131.0, 126.9, 126.5, 121.6, 83.8, 70.3, 65.3, 29.2, 15.7. MS (ESI) m/z 507.2 $[\text{M}+\text{H}]^+$. HRMS for $\text{C}_{26}\text{H}_{27}\text{N}_4\text{O}_5\text{P}_1$, mass calculated 507.1792, mass measured 507.1796.

***N,N'*-bis-*tert*-butyloxycarbonyl pent-4-yn-1-yl ((bis(4-acetamidophenoxy)phosphoryl)(4-guanidinophenyl) methyl) carbamate (6.38a)** General procedure **G** with **6.20b** (680 mg, 1.173 mmol) to yield **6.38a** (765 mg, 0.932 mmol, 79% yield). ^1H NMR (400 MHz, Methanol-

d_4) δ (ppm) 7.53 (d, J = 8.4 Hz, 2H), 7.57-7.46 (m, 6H), 7.04 (d, J = 9.1 Hz, 2H), 6.94 (d, J = 8.7 Hz, 2H), 5.59 (d, J = 22.3 Hz, 1H), 4.24-4.09 (m, 2H), 2.30 – 2.22 (m, 3H), 2.09 (d, J = 3.4 Hz, 6H), 1.81 (p, J = 6.6 Hz, 2H), 1.57 (s, 9H), 1.45 (s, 9H). MS (ESI) m/z 821.5 [M+H]⁺.

Pent-4-yn-1-yl ((bis(4-acetamidophenoxy)phosphoryl)(4-guanidinophenyl) methyl) carbamate (6.38b) General procedure **D** with **6.38a** (100 mg, 0.122 mmol) to yield **6.38b** (76 mg, 0.122 mmol, 99% yield). ¹H NMR (400 MHz, Methanol- d_4) δ (ppm) 7.67 (d, J = 6.9 Hz, 2H), 7.51 (dd, J = 8.8, 5.2 Hz, 4H), 7.33 (d, J = 8.3 Hz, 2H), 7.02 (dd, J = 22.3, 8.7 Hz, 4H), 5.64 (d, J = 22.8 Hz, 1H), 4.24 – 4.06 (m, 2H), 2.31-2.23 (m, 3H) 2.10 (s, 6H), 1.86 – 1.73 (m, 2H). ¹³C NMR (100 MHz, Methanol- d_4) δ (ppm) 170.2, 156.9, 156.8, 156.5, 146.1, 146.0, 145.8, 145.7, 136.3, 136.2, 135.3, 135.3, 133.4, 129.8, 129.7, 125.1, 121.0, 120.9, 120.4, 120.4, 120.3, 120.3, 82.4, 68.9, 53.0, 51.4, 27.8, 22.3, 14.3. MS (ESI) m/z 621.3 [M+H]⁺. HRMS for C₃₀H₃₃N₆O₇P₁, mass calculated 621.2221, mass measured 621.2243.

***N,N'*-bis-*tert*-butyloxycarbonyl pent-4-yn-1-yl ((bis(4-chlorophenoxy)phosphoryl)(4-guanidinophenyl)methyl) carbamate (6.39a)** General procedure **G** with **6.21b** (670 mg, 1.25 mmol) to yield **6.39a** (970 mg, 1.251 mmol, 100% yield). ¹H NMR (400 MHz, CDCl₃) δ (ppm) 11.62 (s, 1H), 10.39 (s, 1H), 7.64 (d, J = 8.4 Hz, 2H), 7.43 (d, J = 7.1 Hz, 2H), 7.27 (d, J = 8.8 Hz, 2H), 7.20 (d, J = 8.4 Hz, 2H), 7.05 (d, J = 8.4 Hz, 2H), 6.82 (d, J = 8.3 Hz, 2H), 5.68 (dd, J = 10.2, 3.0 Hz, 1H), 5.51 (dd, J = 21.8, 9.9 Hz, 1H), 4.26 – 4.08 (m, 2H), 2.29-2.20 (m, 2H), 1.97 (t, J = 2.6 Hz, 1H), 1.87-1.76 (m, 2H), 1.53 (s, 9H), 1.50 (s, 9H). MS (ESI) m/z 777.2 [M+H]⁺.

Pent-4-yn-1-yl ((bis(4-chlorophenoxy)phosphoryl)(4-guanidinophenyl)methyl)carbamate (6.39b) General procedure **D** with **6.39a** (100 mg, 0.129 mmol) to yield **6.39b** (70 mg, 0.121 mmol, 94% yield). ¹H NMR (400 MHz, Methanol- d_4) δ (ppm) 7.67 (d, J = 6.8 Hz, 2H), 7.42 – 7.29 (m, 6H), 7.13 (d, J = 8.6 Hz, 2H), 7.06 (d, J = 8.7 Hz, 2H), 5.69 (d, J = 22.8 Hz, 1H), 4.24 – 4.07 (m, 2H), 2.31-2.24 (m, 3H), 1.87 – 1.71 (m, 1H, CH₂), 1.18 (t, J = 7.0 Hz, 2H). ¹³C NMR (100 MHz, Methanol- d_4) δ (ppm) 158.4, 156.8, 156.5, 135.4, 133.07, 129.8, 129.7, 129.6, 129.6, 125.1, 121.8, 121.7, 121.7, 121.6, 68.9, 64.0, 53.0, 51.5, 29.5, 27.7, 14.3. MS (ESI)

m/z 575.1 $[M+H]^+$. HRMS for $C_{26}H_{25}N_4O_5Cl_2P_1$, mass calculated 575.1012, mass measured 575.1030.

***N,N'*-bis-*tert*-butyloxycarbonyl pent-4-yn-1-yl (1-(diphenoxyphosphoryl)-2-(4-(guanidinomethyl)phenyl) ethyl) carbamate (6.40a)** General procedure **G** with **6.22b** (0.995 g, 1.640 mmol) to yield **6.40a** (0.65 g, 0.885 mmol, 54% yield). 1H NMR (400 MHz, $CDCl_3$) δ (ppm) 11.50 (s, 1H), 8.57 (t, $J = 5.0$ Hz, 1H), 7.38-7.07 (m, 14H), 5.02 (d, $J = 10.5$ Hz, 1H), 4.84-4.69 (m, 1H), 4.61 (d, $J = 5.1$ Hz, 1H), 4.14-4.00 (m, 2H), 3.39 (ddd, $J = 14.4, 9.9, 4.5$ Hz, 1H), 3.03 (dt, $J = 14.5, 10.0$ Hz, 1H), 2.15 (t, $J = 6.7$ Hz, 2H), 1.97 (t, $J = 2.5$ Hz, 1H), 1.71 (p, $J = 6.5$ Hz, 2H), 1.51 (s, 9H), 1.48 (s, 9H). MS (ESI) m/z 535.1 $[(M-2Boc)+H]^+$.

Pent-4-yn-1-yl (1-(diphenoxyphosphoryl)-2-(4-(guanidinomethyl)phenyl)ethyl)carbamate trifluoroacetate salt (6.40b) General procedure **D** with **6.40a** (50 mg, 0.068 mmol) to yield **6.40b** (41 mg, 0.063 mmol, 93% yield). 1H NMR (400 MHz, Methanol- d_4) δ (ppm) 7.93 (d, $J = 9.8$ Hz, 1H), 7.36 (dd, $J = 16.7, 7.7$ Hz, 6H), 7.29 (d, $J = 8.3$ Hz, 2H), 7.23 (t, $J = 7.1$ Hz, 2H), 7.18 (d, $J = 7.9$ Hz, 4H), 4.69-4.51 (m, 1H), 4.38 (br s, 2H), 4.00 (oct, $J = 6.0$ Hz, 2H), 3.39 (dt, $J = 13.8, 3.8$ Hz, 1H), 3.04 (ddd, $J = 26.2, 13.5, 8.9$ Hz, 1H), 2.25 (t, $J = 2.7$ Hz, 1H), 2.17 (td, $J = 7.2, 2.7$ Hz, 2H), 1.69 (p, $J = 6.8$ Hz, 2H). ^{13}C NMR (100 MHz, Methanol- d_4) δ (ppm) 158.7, 158.4, 151.7, 151.4, 138.1, 137.9, 136.4, 131.0, 130.9, 128.6, 126.9, 126.8, 124.3, 121.9, 121.6, 83.9, 70.2, 64.9, 51.3, 45.7, 35.9, 29.2, 15.7. MS (ESI) m/z 535.2 $[M+H]^+$. HRMS for $C_{28}H_{31}N_4O_5P_1$, mass calculated 535.2105, mass measured 535.2081.

***N,N'*-bis-*tert*-butyloxycarbonyl pent-4-yn-1-yl ((1-carbamimidoylpiperidin-4-yl)(diphenoxyphosphoryl) methyl) carbamate (6.41a)** General procedure **G** with **6.23b** (1.2 g, 2.10 mmol) to yield **6.41a** (0.95 g, 1.36 mmol, 65% yield). 1H -NMR (400 MHz, $CDCl_3$) δ (ppm) 10.15 (br s, 1H), 7.39-7.30 (m, 4H), 7.24-7.10 (m, 6H), 5.23 (d, $J = 10.5$ Hz, 1H), 4.50 (ddd, $J = 20.1, 10.6, 4.4$ Hz, 1H), 4.22 (dt, $J = 6.5, 2.2$ Hz, 2H), 3.71 (q, $J = 7.0$ Hz, 1H), 3.02 – 2.86 (m, 2H), 2.28 (dt, $J = 7.0, 2.6$ Hz, 2H), 2.01 (t, $J = 2.6$ Hz, 1H), 1.89 – 1.77 (m, 3H), 1.71 – 1.54 (m, 2H), 1.50 (s, 18H), 1.24 (t, $J = 7.0$ Hz, 2H). MS (ESI) m/z 699.4 $[M+H]^+$.

Pent-4-yn-1-yl ((1-carbamimidoylpiperidin-4-yl)(diphenoxyphosphoryl)methyl)carbamate trifluoroacetate salt (6.41b) General procedure **D** with **6.41a** (75 mg, 0.107 mmol) to yield **6.41b** (52 mg, 0.104 mmol, 97% yield). ^1H NMR (400 MHz, Methanol- d_4) δ (ppm) 7.37 (t, $J = 7.94$ Hz, 4H), 7.26 – 7.20 (m, 2H), 7.19 – 7.14 (m, 4H), 4.43 (dd, $J = 18.6, 6.6$ Hz, 1H), 4.23 – 4.09 (m, 2H), 3.99 – 3.88 (m, 2H), 3.20 – 3.06 (m, 2H), 2.43 – 2.31 (m, 1H), 2.31 - 2.24 (m, 3H), 2.07 (d, $J = 13.8$ Hz), 1.86 – 1.76 (m, 2H), 1.65 -1.46 (m, 2H). ^{13}C NMR (100 MHz, Methanol- d_4) δ (ppm) 157.5, 157.4, 156.2, 150.2, 150.1, 149.9, 149.8, 129.7, 129.6, 125.5, 125.4, 120.4, 120.4, 120.1, 120.1, 82.4, 68.8, 63.8, 52.9, 51.4, 45.3, 45.1, 36.3, 36.2, 28.7, 28.6, 27.8, 27.3, 27.2, 14.3. MS (ESI) m/z 499.3 $[\text{M}+\text{H}]^+$. HRMS for $\text{C}_{25}\text{H}_{31}\text{N}_4\text{O}_5\text{P}_1$, mass calculated 499.2105, mass measured 499.2098.

3-(1-(18-((4R,5S)-5-methyl-2-oxoimidazolidin-4-yl)-13-oxo-3,6,9-trioxa-12-azaoctadecyl)-1H-1,2,3-triazol-4-yl)propyl (1-(diphenoxyphosphoryl)-2-phenylethyl)carbamate (6.42) General procedure **H** with **6.12** (112 mg, 0.241 mmol) and **S6.16** to yield **6.42** (68 mg, 0.077 mmol, 32% yield). ^1H NMR (400 MHz, Methanol- d_4) δ (ppm) 7.61 (s, 1H), 7.42-7.14 (m, 15H), 4.71-4.60 (m, 1H), 4.52 (t, $J = 5.1$ Hz, 2H), 4.01-3.91 (m, 2H) 3.86 (t, $J = 5.0$ Hz, 2H), 3.84-3.75 (m, 1H), 3.71-3.63 (m, 1H), 3.62-3.53 (m, 8H), 3.49 (t, $J = 5.5$ Hz, 2H), 3.39 (dt, $J = 14.3, 4.3$ Hz, 1H), 3.33 (t, $J = 5.6$ Hz, 2H), 3.05 (ddd, $J = 14.3, 13.1, 9$ Hz, 1H), 2.65 (t, $J = 7.6$ Hz, 2H), 2.18 (t, $J = 7.6$ Hz, 2H), 1.85 (p, $J = 6.9$ Hz, 2H), 1.61 (p, $J = 6.9$ Hz, 2H), 1.52-1.24 (m, 6H), 1.08 (d, $J = 6.6$ Hz, 3H). ^{13}C NMR (100 MHz, Methanol- d_4) δ (ppm) 176.1, 166.1, 158.3, 151.6, 151.4, 147.8, 138.1, 131.0, 130.3, 129.5, 127.9, 126.8, 124.1, 121.8, 121.6, 121.5, 71.5, 71.4, 71.2, 70.5, 70.4, 69.4, 65.1, 57.3, 51.4, 51.3, 40.3, 36.9, 36.2, 31.1, 30.7, 30.2, 29.7, 27.1, 26.8, 22.6, 15.7. MS (ESI) m/z 878.5 $[\text{M}+\text{H}]^+$. HRMS for $\text{C}_{44}\text{H}_{60}\text{N}_7\text{O}_{10}\text{P}_1$, mass calculated 878.4212, mass measured 878.4178.

3-(1-(13-oxo-17-((3aS,4S,6aR)-2-oxohexahydro-1H-thieno[3,4-d]imidazol-4-yl)-3,6,9-trioxa-12-zaheptadecyl)-1H-1,2,3-triazol-4-yl)propyl (1-(diphenoxyphosphoryl)-2-phenylethyl)carbamate (6.43) General procedure **H** with **6.12** (52.1 mg, 0.112 mmol) and **S6.18** to yield **6.43** (35 mg, 0.039 mmol, 34% yield). ^1H NMR (400 MHz, Methanol- d_4) δ (ppm) 7.68 (s, 1H), 7.41-7.16 (m, 15H), 4.66 (ddd, $J = 15.5, 12.0, 3.5$ Hz, 1H), 4.52 (t, $J = 5.0$

Hz, 2H), 4.46 (dd, $J = 8.0, 4.5$ Hz, 1H), 4.26 (dd, $J = 8.0, 4.5$ Hz, 1H), 4.01 – 3.91 (m, 2H), 3.89 – 3.83 (m, 2H), 3.57 (d, $J = 12.0$ Hz, 8H), 3.50 (t, $J = 5.5$ Hz, 2H), 3.39 (ddd, $J = 12.0, 8.0, 4.0$ Hz, 1H), 3.34 (d, $J = 5.5$ Hz, 2H), 3.21-3.12 (m, 1H), 3.05 (ddd, $J = 14.0, 12.0, 9.0$ Hz, 1H), 2.89 (dd, $J = 12.5, 5.0$ Hz, 1H), 2.72-2.61 (m, 3H), 2.18 (t, $J = 7.5$ Hz, 2H), 1.91-1.80 (m, 2H), 1.76-1.50 (m, 4H), 1.46-1.34 (m, 2H). ^{13}C NMR (100 MHz, Methanol- d_4) δ (ppm) 176.1, 166.1, 158.4, 151.7, 151.5, 147.9, 138.1, 131.0, 130.9, 130.3, 129.6, 128.0, 126.8, 126.7, 124.1, 121.9, 121.8, 121.6, 121.5, 71.5, 71.5, 71.4, 71.2, 70.6, 70.4, 65.2, 63.3, 61.6, 57.0, 51.4, 51.3, 41.0, 40.3, 36.7, 36.3, 29.8, 29.8, 29.5, 26.8, 22.6. MS (ESI) m/z 908.5 $[\text{M}+\text{H}]^+$. HRMS for $\text{C}_{44}\text{H}_{58}\text{N}_7\text{O}_{10}\text{S}_1\text{P}_1$, mass calculated 908.3776, mass measured 908.3735.

3-(1-(18-((4R,5S)-5-methyl-2-oxoimidazolidin-4-yl)-13-oxo-3,6,9-trioxa-12-azaoctadecyl)-1H-1,2,3-triazol-4-yl)propyl (1-(diphenoxyphosphoryl)-2-methylpropyl)carbamate (6.44b) General procedure *H* with **6.13** (90 mg, 0.217 mmol) and **S6.16** to yield **6.44b** (29.8 mg, 0.036 mmol, 17% yield). ^1H NMR (400 MHz, Methanol- d_4) δ (ppm) 7.74 (s, 1H), 7.40-7.30 (m, 4H), 7.25-7.11 (m, 6H), 4.52 (t, $J = 5.1$ Hz, 2H), 4.32 (dd, $J = 18.4, 5.8$ Hz, 1H), 4.12 (qd, $J = 6.1$ Hz, 2H), 3.87 (t, $J = 5.0$ Hz, 2H), 3.84-3.76 (m, 1H), 3.72-3.63 (m, 1H), 3.61-3.54 (m, 8H), 3.50 (t, $J = 5.4$ Hz, 2H), 3.33 (t, $J = 5.5$ Hz, 2H), 2.78 (t, $J = 7.8$ Hz, 2H), 2.38 (septet, $J = 6.6$ Hz, 1H), 2.20 (t, $J = 7.2$ Hz, 2H), 1.99 (p, $J = 7.2$ Hz, 2H), 1.61 (p, $J = 7.2$ Hz, 2H), 1.52-1.25 (m, 8H), 1.15 (d, $J = 6.6$ Hz, 6H), 1.08 (d, $J = 6.5$ Hz, 3H). ^{13}C NMR (100 MHz, Methanol- d_4) δ (ppm) 176.2, 166.2, 159.1, 151.1, 130.9, 126.4, 124.3, 121.8, 121.6, 71.6, 71.5, 71.4, 71.2, 70.6, 70.3, 65.5, 57.1, 55.4, 52.8, 51.3, 40.3, 36.9, 30.8, 30.3, 30.2, 29.9, 26.9, 22.8, 19.1, 21.0, 15.8. MS (ESI) m/z 830.5 $[\text{M}+\text{H}]^+$. HRMS for $\text{C}_{40}\text{H}_{60}\text{N}_7\text{O}_{10}\text{P}_1$, mass calculated 830.4212, mass measured 830.4188.

3-(1-(18-((4R,5S)-5-methyl-2-oxoimidazolidin-4-yl)-13-oxo-3,6,9-trioxa-12-azaoctadecyl)-1H-1,2,3-triazol-4-yl)propyl (1-(diphenoxyphosphoryl)-4-guanidinobutyl)carbamate trifluoroacetate salt (6.45b) General procedure *H* with **6.32a** (16.23 mg, 0.024 mmol) and **S6.16**, followed by general procedure *D* to yield **6.45b** (18 mg, 0.018 mmol, 75% yield). ^1H NMR (400 MHz, DMSO- d_6) 7.97 (d, $J = 10.1$ Hz, 1H), 7.81 (s, 1H), 7.74-7.60 (m, 2H), 7.38 (q, $J = 7.8$ Hz, 4H), 7.21 (q, $J = 8.1$ Hz, 2H), 7.15 (t, $J = 8.9$ Hz, 4H), 4.46 (t, $J = 5.2$ Hz, 2H), 4.33-

4.21 (m, 3H), 4.11-3.96 (m, 3H), 3.78 (t, $J = 5.2$ Hz, 2H), 3.59 (t, $J = 6.8$ Hz, 1H), 3.52-3.42 (m, 8H), 3.36 (t, $J = 5.8$ Hz, 2H), 3.16 (t, $J = 5.4$ Hz, 3H), 2.66 (t, $J = 7.6$ Hz, 2H), 2.04 (t, $J = 7.3$ Hz, 2H), 1.99-1.92 (m, 1H), 1.88 (t, $J = 7.3$ Hz, 2H), 1.83-1.28 (m, 9H), 1.28-1.12 (m, 9H), 1.11-1.05 (m, 1H), 1.02 (d, $J = 6.4$ Hz, 1H), 0.94 (d, $J = 6.4$ Hz, 2H). ^{13}C NMR (100 MHz, DMSO- d_6) δ (ppm) 172.7, 163.4, 157.0, 150.6, 150.2, 146.4, 130.4, 130.3, 130.3, 125.9, 125.7, 122.7, 121.1, 121.1, 120.8, 120.8, 70.2, 70.1, 70.1, 70.0, 69.6, 69.2, 64.4, 55.4, 50.6, 49.7, 49.3, 47.7, 38.9, 38.7, 35.7, 35.6, 30.0, 29.5, 29.1, 29.0, 26.2, 26.0, 25.6, 21.9, 15.9. MS (ESI) m/z 887.6 $[\text{M}+\text{H}]^+$. HRMS for $\text{C}_{41}\text{H}_{63}\text{N}_{10}\text{O}_{10}\text{P}_1$, mass calculated 887.4539, mass measured 887.4531.

3-(1-(18-((4R,5S)-5-methyl-2-oxoimidazolidin-4-yl)-13-oxo-3,6,9-trioxa-12-azaoctadecyl)-1H-1,2,3-triazol-4-yl)propyl (1-(bis(4-chlorophenoxy)phosphoryl)-4-guanidinobutyl)carbamate trifluoroacetate salt (6.46b) General procedure *H* with **6.33a** (42 mg, 0.101 mmol) and **S6.16**, followed by general procedure *D* to yield **6.46b** (57.2 mg, 0.060 mmol, 60% yield). ^1H NMR (400 MHz, Methanol- d_4) δ (ppm) 7.85 (d, $J = 9.8$ Hz, 1H), 7.81 (s, 1H), 7.38 (d, $J = 8.9$ Hz, 4H), 7.18 (t, $J = 7.4$ Hz, 4H), 4.55 (t, $J = 5.1$ Hz, 2H), 4.50 – 4.38 (m, 1H), 4.12 (t, $J = 6.3$ Hz, 2H), 3.88 (t, $J = 5.1$ Hz, 2H), 3.85 – 3.77 (m, 1H), 3.68 (q, $J = 7.5$ Hz, 1H), 3.60 (s, 4H), 3.57 (s, 4H), 3.51 (t, $J = 5.6$ Hz, 2H), 3.34 (t, $J = 5.6$ Hz, 2H), 3.30 – 3.21 (m, 2H), 2.78 (t, $J = 7.6$ Hz, 2H), 2.18 (t, $J = 7.5$ Hz, 2H), 2.15 – 2.04 (m, 1H), 1.99 (p, $J = 6.5$ Hz, 2H), 1.95 – 1.80 (m, 2H), 1.80 – 1.67 (m, 1H), 1.61 (p, $J = 7.2$ Hz, 2H), 1.53 – 1.42 (m, 2H), 1.42 – 1.26 (m, 4H), 1.09 (d, $J = 6.5$ Hz, 3H). ^{13}C NMR (100 MHz, Methanol- d_4) δ (ppm) 174.9, 157.2, 148.5, 129.7, 122.0, 121.7, 121.7, 70.1, 70.1, 70.0, 69.9, 69.2, 69.0, 64.3, 56.0, 51.3, 50.0, 40.3, 39.0, 35.5, 29.5, 29.3, 28.8, 28.5, 26.0, 25.8, 25.4, 25.0, 24.8, 21.3, 14.2. MS (ESI) m/z 955.5 $[\text{M}+\text{H}]^+$. HRMS for $\text{C}_{41}\text{H}_{61}\text{N}_{10}\text{O}_{10}\text{Cl}_2\text{P}_1$, mass calculated 955.3760, mass measured 955.3773.

3-(1-(18-((4R,5S)-5-methyl-2-oxoimidazolidin-4-yl)-13-oxo-3,6,9-trioxa-12-azaoctadecyl)-1H-1,2,3-triazol-4-yl)propyl (5-amino-1-(diphenoxyphosphoryl)pentyl)carbamate trifluoroacetate salt (6.47b) General procedure *H* with **6.29a** (162 mg, 0.297 mmol) and **S6.16**, followed by general procedure *D* to yield **6.47b** (242 mg, 0.246 mmol, 83% yield). ^1H

NMR (400 MHz, Methanol- d_4) δ (ppm) 7.89 (s, 1H), 7.38 (t, J = 7.6 Hz, 4H), 7.27-7.21 (m, 2H), 7.21-7.13 (m, 4H), 4.56 (t, J = 4.9 Hz, 2H), 4.50-4.37 (m, 1H), 4.21-4.07 (m, 2H), 3.90 (t, J = 4.4 Hz, 2H), 3.87-3.78 (m, 1H), 3.75-3.65 (m, 1H), 3.65-3.56 (m, 8H), 3.53 (t, J = 5.7 Hz, 2H), 3.36 (t, J = 5.8 Hz, 2H), 2.97 (t, J = 7.3 Hz, 2H), 2.87-2.73 (m, 2H), 2.20 (t, J = 7.7 Hz, 2H), 2.16-1.85 (m, 4H), 1.84-1.25 (m, 12H), 1.11 (d, J = 6.6 Hz, 3H). ^{13}C NMR (100 MHz, Methanol- d_4) δ (ppm) 131.0, 126.8, 126.7, 121.8, 121.6, 71.5, 71.4, 71.2, 70.6, 70.3, 65.5, 57.4, 49.4, 49.2, 40.5, 40.3, 36.9, 30.7, 30.2, 29.8, 27.8, 27.2, 26.8, 23.7, 15.6. MS (ESI) m/z 859.5 $[\text{M}+\text{H}]^+$. HRMS for $\text{C}_{41}\text{H}_{63}\text{N}_8\text{O}_{10}\text{P}_1$, mass calculated 859.4477, mass measured 859.4462.

3-(1-(13-oxo-17-((3a*S*,4*S*,6a*R*)-2-oxohexahydro-1*H*-thieno[3,4-*d*]imidazol-4-yl)-3,6,9-trioxa-12-azaheptadecyl)-1*H*-1,2,3-triazol-4-yl)propyl (5-amino-1-(diphenoxyphosphoryl)pentyl) carbamate trifluoroacetate salt (6.48b) General procedure *H* with **6.29a** (0.163 g, 0.367 mmol) and **S6.18**, followed by general procedure *D* to yield **6.48b** (121.1 mg, 0.121 mmol, 33% yield) ^1H NMR (400 MHz, Methanol- d_4) δ (ppm) 7.98-7.80 (m, 1H), 7.38 (t, J = 7.7 Hz, 4H), 7.28-7.12 (m, 6H), 4.56 (t, J = 4.8 Hz, 2H), 4.53-4.37 (m, 2H), 4.31 (dd, J = 7.8, 4.4 Hz, 1H), 4.20-4.07 (m, 2H), 3.90 (t, J = 5.0 Hz, 2H), 3.64-3.57 (m, 8H), 3.53 (t, J = 5.6 Hz, 2H), 3.36 (t, J = 5.6 Hz, 2H), 3.24-3.17 (m, 1H), 3.02-2.89 (m, 4H), 2.87-2.75 (m, 2H), 2.21 (t, J = 7.4 Hz, 2H), 2.16-1.84 (m, 4H), 1.84-1.37 (m, 10H). ^{13}C NMR (100 MHz, Methanol- d_4) δ (ppm) 176.0, 158.7, 151.5, 151.4, 131.0, 126.8, 121.6, 121.5, 71.5, 71.4, 71.2, 70.5, 70.3, 65.5, 63.4, 61.6, 57.0, 51.7, 41.1, 40.5, 40.3, 36.7, 29.7, 29.5, 27.8, 26.8, 23.7, 22.7. MS (ESI) m/z 889.5 $[\text{M}+\text{H}]^+$. HRMS for $\text{C}_{41}\text{H}_{61}\text{N}_8\text{O}_{10}\text{S}_1\text{P}_1$, mass calculated 889.4042, mass measured 889.4017.

3-(1-(18-((4*R*,5*S*)-5-methyl-2-oxoimidazolidin-4-yl)-13-oxo-3,6,9-trioxa-12-azaoctadecyl)-1*H*-1,2,3-triazol-4-yl)propyl (5-amino-1-(bis(4-acetamidophenoxy)phosphoryl)pentyl)carbamate trifluoroacetate salt (6.49b) General procedure *H* with **6.30a** (40 mg, 0.061 mmol) and **S6.16**, followed by general procedure *D* to yield **6.49b** (34.5 mg, 0.032 mmol, 53% yield). ^1H NMR (400 MHz, Methanol- d_4) δ (ppm) 7.81 (s, 1H), 7.54 (d, J = 8.7 Hz, 4H), 7.15-7.08 (m, 4H), 4.53 (t, J = 4.9 Hz, 2H), 4.40 (ddd, J = 16.5, 13.4, 3.5 Hz, 1H), 4.20-4.04 (m, 2H), 3.87 (t, J = 4.9 Hz, 2H), 3.80 (p, J = 7.1 Hz, 1H),

3.73-3.45 (m, 11H), 3.33 (t, $J = 5.4$ Hz, 2H), 2.95 (t, $J = 6.9$ Hz, 2H), 2.78 (br s, 2H), 2.24-2.13 (m, 2H), 2.11 (s, 6H), 2.08-1.84 (m, 4H), 2.07-1.16 (m, 15H). ^{13}C NMR (100 MHz, Methanol- d_4) δ (ppm) 176.2, 171.6, 137.7, 122.3, 122.0, 121.8, 71.5, 71.4, 71.2, 70.6, 70.4, 65.6, 57.4, 52.7, 51.3, 40.5, 40.3, 33.9, 30.7, 30.2, 29.9, 27.1, 26.8, 23.8, 15.6. MS (ESI) m/z 973.7 [M+H] $^+$. HRMS for $\text{C}_{45}\text{H}_{69}\text{N}_{10}\text{O}_{12}\text{P}_1$, mass calculated 973.4907, mass measured 973.4898.

3-(1-(18-((4R,5S)-5-methyl-2-oxoimidazolidin-4-yl)-13-oxo-3,6,9-trioxa-12-azaoctadecyl)-1H-1,2,3-triazol-4-yl)propyl (1-(diphenoxyphosphoryl)-2-(4-guanidinophenyl)ethyl)carbamate trifluoroacetate salt (6.50b) General procedure *H* with **6.34a** (50 mg, 0.069 mmol) and **S6.16**, followed by general procedure *D* to yield **6.50b** (49.3 mg, 0.052 mmol, 76% yield). ^1H NMR (400 MHz, Methanol- d_4) δ (ppm) 8.01 (d, $J = 9.9$ Hz, 1H), 7.75 (s, 1H), 7.43 (d, $J = 8.3$ Hz, 2H), 7.37 (t, $J = 7.3$ Hz, 4H), 7.21 (m, 8H), 4.71 – 4.57 (m, 1H), 4.53 (t, $J = 5.0$ Hz, 2H), 3.99 (td, $J = 6.1, 2.4$ Hz, 2H), 3.87 (t, $J = 5.0$ Hz, 2H), 3.84 – 3.76 (m, 1H), 3.71 – 3.66 (m, 2H), 3.59 (s, 4H), 3.56 (s, 4H), 3.50 (t, $J = 5.5$ Hz, 2H), 3.42 (dt, $J = 14.3, 4.4$ Hz, 1H), 3.34 (d, $J = 6.5$ Hz, 2H), 3.09 (ddd, $J = 14.0, 11.6, 9.1$ Hz, 1H), 2.68 (t, $J = 7.6$ Hz, 2H), 2.18 (t, $J = 7.4$ Hz, 2H), 1.88 (p, $J = 6.7$ Hz, 2H), 1.61 (p, $J = 6.9$ Hz, 2H), 1.51 – 1.42 (m, 2H), 1.09 (d, $J = 6.5$ Hz, 3H). ^{13}C NMR (100 MHz, Methanol- d_4) δ (ppm) 176.2, 166.2, 158.5, 158.5, 158.0, 151.6, 151.5, 151.4, 151.3, 137.9, 137.7, 134.9, 131.9, 131.0, 126.9, 126.8, 126.6, 124.1, 121.8, 121.8, 121.6, 121.6, 71.5, 71.4, 71.4, 71.2, 70.5, 70.4, 65.4, 57.4, 52.7, 52.0, 51.3, 50.5, 49.8, 40.3, 36.9, 30.7, 30.2, 29.8, 27.1, 26.8, 22.6, 15.6. MS (ESI) m/z 935.6 [M+H] $^+$.

3-(1-(13-oxo-17-((3aS,4S,6aR)-2-oxohexahydro-1H-thieno[3,4-d]imidazol-4-yl)-3,6,9-trioxa-12-azaheptadecyl)-1H-1,2,3-triazol-4-yl)propyl(1-(diphenoxyphosphoryl)-2-(4-guanidinophenyl)ethyl) carbamate trifluoroacetate salt (6.51b) General procedure *H* with **6.34a** (50 mg, 0.069 mmol) and **S6.18**, followed by general procedure *D* to yield **6.51b** (41 mg, 0.042 mmol, 61% yield). ^1H NMR (400 MHz, Methanol- d_4) δ (ppm) 8.00 (d, $J = 9.8$ Hz, 1H), 7.75 (s, 1H), 7.43 (d, $J = 8.3$ Hz, 2H), 7.38 (t, $J = 7.3$ Hz, 4H), 7.26-7.16 (m, 8H), 4.70-4.57 (m, 1H), 4.53 (t, $J = 5.0$ Hz, 2H), 4.47 (dd, $J = 7.8, 4.9$ Hz, 1H), 4.28 (dd, $J = 7.8, 4.4$ Hz, 1H), 4.03-3.95 (m, 2H), 3.88 (t, $J = 5.0$ Hz, 2H), 3.60 (s, 4H), 3.57 (s, 4H), 3.51 (t, $J = 5.5$ Hz, 2H),

3.42 (td, $J = 13.59, 4.21$ Hz, 1H), 3.34-3.33 (m, 2H), 3.21-3.14 (m, 1H), 3.14-3.04 (m, 1H), 2.92 (dd, $J = 13.0, 4.9$ Hz, 1H), 2.70 (s, 1H), 2.68-2.65 (m, 2H), 2.19 (t, $J = 7.4$ Hz, 2H), 1.92-1.82 (m, 2H), 1.79-1.50 (m, 4H), 1.46-1.39 (m, 2H). ^{13}C NMR (100 MHz, Methanol- d_4) δ (ppm) 176.1, 166.1, 158.5, 158.0, 151.7, 151.6, 151.4, 151.3, 138.0, 137.8, 134.9, 131.9, 131.0, 126.9, 126.8, 126.6, 121.8, 121.8, 121.6, 121.6, 71.5, 71.4, 71.4, 71.2, 70.5, 70.3, 65.4, 63.4, 61.6, 57.0, 51.4, 41.0, 40.3, 36.7, 29.8, 29.5, 26.8, 22.6, 15.4. MS (ESI) m/z 965.5 [M+H] $^+$. HRMS for $\text{C}_{45}\text{H}_{61}\text{N}_{10}\text{O}_{10}\text{S}_1\text{P}_1$, mass calculated 965.4103, mass measured 965.4106.

3-(1-(18-((4R,5S)-5-methyl-2-oxoimidazolidin-4-yl)-13-oxo-3,6,9-trioxa-12-azaoctadecyl)-1H-1,2,3-triazol-4-yl)propyl (1-(bis(4-acetamidophenoxy)phosphoryl)-2-(4-guanidinophenyl)ethyl)carbamate trifluoroacetate salt (6.52b) General procedure *H* with **6.35a** (59.6 mg, 0.144 mmol) and **S6.16**, followed by general procedure *D* to yield **6.52b** (37 mg, 0.036 mmol, 25% yield). ^1H NMR (400 MHz, Methanol- d_4) δ (ppm) 7.98 (br d, $J = 9.3$ Hz, 1H), 7.75 (br s, 1H), 7.55 (dd, $J = 9.1, 3.1$ Hz, 4H), 7.44 (d, $J = 8.4$ Hz, 2H), 7.24 (d, $J = 8.3$ Hz, 2H), 7.16 (t, $J = 9.5$ Hz, 4H), 4.69-4.56 (m, 1H), 4.53 (t, $J = 5.1$ Hz, 2H), 4.01 (t, $J = 6.2$ Hz, 2H), 3.89 (t, $J = 5.0$ Hz, 2H), 3.80 (p, $J = 7.3$ Hz, 1H), 3.73-3.64 (m, 1H), 3.62-3.52 (m, 8H), 3.50 (t, $J = 5.6$ Hz, 2H), 3.40 (dt, $J = 14.2, 4.5$ Hz, 1H), 3.33 (t, $J = 5.6$ Hz, 2H), 3.07 (q, $J = 11.9$ Hz, 1H), 2.68 (t, $J = 7.6$ Hz, 2H), 2.19 (t, $J = 7.6$ Hz, 2H), 2.11 (s, 6H), 1.88 (p, $J = 6.8$ Hz, 2H), 1.60 (p, $J = 7.3$ Hz, 2H), 1.53-1.19 (m, 7H), 1.08 (d, $J = 6.3$ Hz, 3H). ^{13}C NMR (101 MHz, Methanol- d_4) δ 176.2, 171.6, 158.0, 134.9, 132.0, 126.7, 122.3, 122.1, 121.8, 71.5, 71.4, 71.3, 70.6, 70.4, 65.4, 57.4, 52.7, 51.4, 40.3, 36.9, 30.8, 30.2, 29.9, 27.2, 26.9, 23.8, 22.7, 15.7. MS (ESI) m/z 1049.5 [M+H] $^+$. HRMS for $\text{C}_{49}\text{H}_{69}\text{N}_{12}\text{O}_{12}\text{P}_1$, mass calculated 1049.4968, mass measured 1049.4980.

3-(1-(13-oxo-17-((3aS,4S,6aR)-2-oxohexahydro-1H-thieno[3,4-d]imidazol-4-yl)-3,6,9-trioxa-12-azaheptadecyl)-1H-1,2,3-triazol-4-yl)propyl(1-(bis(4-acetamidophenoxy)phosphoryl)-2-(4-guanidinophenyl)ethyl)carbamate trifluoroacetate salt (6.53b) General procedure *H* with **6.35a** (150 mg, 0.180 mmol) and **S6.18**, followed by general procedure *D* to yield **6.53b** (143.8 mg, 0.120 mmol, 67% yield). ^1H NMR (400 MHz, Methanol- d_4) δ (ppm) 7.98 (d, $J = 9.8$ Hz, 1H), 7.78 (s, 1H), 7.55 (dd, $J = 2.3, 8.9$ Hz, 4H), 7.41 (d, $J = 8.2$ Hz, 2H),

7.21 (d, $J = 8.2$ Hz, 2H), 7.14 (t, $J = 8.5$ Hz, 4H), 4.66-4.58 (m, 1H), 4.53 (t, $J = 4.8$ Hz, 2H), 4.47 (dd, $J = 4.7, 7.6$ Hz, 1H), 4.27 (dd, $J = 4.4, 7.7$ Hz, 1H), 3.98 (t, $J = 5.5$ Hz, 2H), 3.86 (t, $J = 4.8$ Hz, 2H), 3.72-3.48 (s, 8H), 3.49 (t, $J = 5.3$ Hz, 2H), 3.42-3.38 (m, 1H), 3.31-3.28 (m, 2H), 3.17-3.11 (m, 1H), 3.10-3.06 (m, 1H), 2.90 (dd, $J = 4.9, 12.7$ Hz, 1H), 2.71-2.65 (m, 3H), 2.18 (t, $J = 7.3$ Hz, 2H), 2.11 (s, 6H), 1.89-1.85 (m, 2H), 1.62-1.59 (m, 4H), 1.42-1.39 (m, 2H). ^{13}C NMR (101 MHz, Methanol- d_4) δ (ppm) 176.1, 171.6, 166.1, 158.5, 157.9, 147.4, 147.2, 137.7, 137.6, 134.9, 131.9, 126.6, 124.1, 122.4, 122.0, 121.8, 71.5, 71.4, 71.3, 71.2, 70.5, 70.3, 65.4, 63.3, 61.6, 57.0, 51.5, 51.1, 41.0, 40.2, 36.7, 35.9, 29.7, 29.4, 26.8, 23.7, 22.6. MS (ESI) m/z 1079.5 $[\text{M}+\text{H}]^+$. HRMS for $\text{C}_{49}\text{H}_{67}\text{N}_{12}\text{O}_{12}\text{S}_1\text{P}_1$, mass calculated 1079.4532, mass measured 1079.4541.

3-(1-(18-((4R,5S)-5-methyl-2-oxoimidazolidin-4-yl)-13-oxo-3,6,9-trioxa-12-azaoctadecyl)-1H-1,2,3-triazol-4-yl)propyl (1-(bis(4-chlorophenoxy)phosphoryl)-2-(4-guanidinophenyl)ethyl)carbamate trifluoroacetate salt (6.54b) General procedure **H** with **6.36a** (156 mg, 0.198 mmol) and **S6.16**, followed by general procedure **D** to yield **6.54b** (86.8 mg, 0.077 mmol, 39% yield). ^1H NMR (400 MHz, Methanol- d_4) δ (ppm) 8.03 (d, $J = 9.8$ Hz, 1H), 7.81 (br s, 1H), 7.48-7.35 (m, 6H), 7.25-7.15 (m, 6H), 4.65 (ddd, $J = 15.2, 13.6, 3.6$ Hz, 1H), 4.54 (t, $J = 5.0$ Hz, 2H), 3.98 (t, $J = 5.7$ Hz, 1H), 3.88 (t, $J = 4.8$ Hz, 2H), 3.81 (p, $J = 6.8$ Hz, 1H), 3.68 (q, $J = 7.1$ Hz, 1H), 3.64-3.53 (m, 8H), 3.50 (t, $J = 5.7$ Hz, 2H), 3.41 (dt, $J = 14.3, 4.7$ Hz, 1H), 3.33 (t, $J = 5.7$ Hz, 1H), 3.21 (q, $J = 7.2$ Hz, 1H), 3.14-3.02 (m, 1H), 2.68 (br t, $J = 7.2$ Hz, 2H), 2.18 (t, $J = 7.7$ Hz, 2H), 1.87 (br t, $J = 5.6$ Hz, 1H), 1.55-1.21 (m, 2H), 1.51-1.24 (m, 8H), 1.09 (d, $J = 6.3$ Hz, 3H). ^{13}C NMR (100 MHz, Methanol- d_4) δ (ppm) 176.3, 158.4, 158.0, 150.1, 150.0, 135.1, 132.3, 132.0, 131.1, 126.6, 123.4, 123.2, 71.5, 71.4, 71.3, 70.6, 70.4, 65.5, 57.4, 52.8, 51.5, 51.3, 47.9, 40.3, 36.9, 30.8, 30.2, 29.8, 27.2, 26.9, 22.7, 15.7. MS (ESI) m/z 1005.5 $[\text{M}+\text{H}]^+$. HRMS for $\text{C}_{45}\text{H}_{61}\text{N}_{10}\text{O}_{10}\text{Cl}_2\text{P}_1$, mass calculated 1003.3760, mass measured 1003.3767.

3-(1-(18-((4R,5S)-5-methyl-2-oxoimidazolidin-4-yl)-13-oxo-3,6,9-trioxa-12-azaoctadecyl)-1H-1,2,3-triazol-4-yl)propyl (1-(diphenoxyphosphoryl) (4-guanidinophenyl)carbamate trifluoroacetate salt (6.55b) General procedure **H** with **6.37a** (150 mg, 0.212 mmol) and

S6.16, followed by general procedure **D** to yield **6.55b** (82 mg, 0.089 mmol, 42% yield). ^1H NMR (400 MHz, Methanol- d_4) δ (ppm) 7.80 (s, 1H), 7.70 (d, $J = 7.6$ Hz, 2H), 7.34 (t, $J = 8.1$ Hz, 6H), 7.20 (t, $J = 7.6$ Hz, 2H), 7.10 (d, $J = 7.7$ Hz, 2H), 7.05 (d, $J = 7.7$ Hz, 2H), 5.68 (d, $J = 22.5$ Hz, 1H), 4.53 (t, $J = 4.9$ Hz, 2H), 4.20-4.05 (m, 2H), 3.87 (t, $J = 4.9$ Hz, 2H), 3.80 (t, $J = 7.5$ Hz, 1H), 3.71-3.61 (m, 2H), 3.58 (d, $J = 12.4$ Hz, 8H), 3.50 (t, $J = 5.5$ Hz, 2H), 3.36-3.32 (m, 2H), 2.75 (t, $J = 7.5$ Hz, 2H), 2.18 (t, $J = 6.9$ Hz, 2H), 2.05-1.93 (m, 2H, CH_2), 1.65-1.54 (m, 2H, CH_2), 1.52-1.42 (m, 2H), 1.37-1.31 (m, 4H), 1.08 (d, $J = 6.2$ Hz, 3H). ^{13}C NMR (100 MHz, Methanol- d_4) δ (ppm) 176.3, 134.9, 131.2, 131.1, 131.0, 131.0, 126.9, 126.8, 126.5, 121.6, 121.6, 121.5, 121.5, 71.5, 71.4, 71.4, 71.2, 70.6, 70.4, 65.8, 57.4, 53.0, 52.7, 51.4, 40.3, 36.9, 30.9, 30.7, 30.2, 29.9, 27.1, 26.9, 22.7, 15.6. MS (ESI) m/z 921.5 $[\text{M}+\text{H}]^+$. HRMS for $\text{C}_{44}\text{H}_{61}\text{N}_{10}\text{O}_{10}\text{P}_1$, mass calculated 921.4382, mass measured 921.4416.

3-(1-(18-((4R,5S)-5-methyl-2-oxoimidazolidin-4-yl)-13-oxo-3,6,9-trioxa-12-azaoctadecyl)-1H-1,2,3-triazol-4-yl)propyl (1-(bis(4-acetamido-phenoxy)phosphoryl) (4-guanidinophenyl)carbamate trifluoroacetate salt (6.56b) General procedure **H** with **6.38a** (150 mg, 0.183 mmol) and **S6.16**, followed by general procedure **D** to yield **6.56b** (41.6 mg, 0.040 mmol, 22% yield). ^1H NMR (400 MHz, Methanol- d_4) δ (ppm) 7.81 (br s, 1H), 7.68 (d, $J = 6.9$ Hz, 2H), 7.51 (dd, $J = 8,9$ Hz, 5 Hz, 4H), 7.34 (d, $J = 8.3$ Hz, 2H), 7.05 (d, $J = 8.4$ Hz, 2H), 6.99 (d, $J = 8.4$ Hz, 2H), 5.65 (d, $J = 22.8$ Hz, 1H), 4.53 (t, $J = 4.9$ Hz, 2H), 4.19-4.02 (m, 2H), 3.87 (t, $J = 4.9$ Hz, 2H), 3.84-3.77 (m, 1H), 3.71-3.65 (m, 2H), 3.57 (d, $J = 11.4$ Hz, 8H), 3.49 (t, $J = 5.89$, 2H), 3.35-3.31 (m, 2H), 2.77 (br s, 2H), 2.18 (t, $J = 7.1$ Hz, 2H), 2.10 (s, 6H), 2.04-1.96 (m, 2H, CH_2), 1.64-1.54 (m, 2H), 1.51-1.42 (m, 2H), 1.37-1.30 (m, 4H), 1.08 (d, $J = 6.4$ Hz, 3H). ^{13}C NMR (100 MHz, Methanol- d_4) δ (ppm) 170.2, 129.8, 129.7, 125.1, 120.9, 120.9, 120.5, 120.4, 120.4, 120.3, 70.1, 70.1, 70.0, 69.8, 69.2, 69.0, 56.0, 51.3, 39.0, 35.5, 29.3, 29.0, 25.8, 25.4, 22.3, 14.2. MS (ESI) m/z 1057.6 $[\text{M}+\text{Na}]^+$.

3-(1-(18-((4R,5S)-5-methyl-2-oxoimidazolidin-4-yl)-13-oxo-3,6,9-trioxa-12-azaoctadecyl)-1H-1,2,3-triazol-4-yl)propyl (1-(bis(4-chlorophenoxy)phosphoryl) (4-guanidinophenyl)carbamate trifluoroacetate salt (6.57b) General procedure **H** with **6.39a** (105 mg, 0.252 mmol) and **S6.16**, followed by general procedure to yield **6.57b** (50.4 mg,

0.050 mmol, 20% yield). ^1H NMR (400 MHz, Methanol- d_4) δ (ppm) 7.78 (s, 1H), 7.69 (d, J = 8.0 Hz, 2H), 7.35-7.30 (m, 6H), 7.12 (d, J = 9.1 Hz, 2H), 7.05 (d, J = 9.1 Hz, 2H), 5.66 (d, J = 23.2 Hz, 1H), 4.50 (t, J = 4.7 Hz, 2H), 4.16-4.01 (m, 2H), 3.83 (t, J = 4.8 Hz, 2H), 3.84-3.77 (m, 1H), 3.71-3.62 (m, 3H), 3.59 (s, 4H), 3.54 (s, 4H), 3.47 (t, J = 6.08 Hz, 2H), 3.30 (d, J = 5.8 Hz, 2H), 2.75 (t, J = 8.2 Hz, 2H), 2.15 (t, J = 6.7 Hz, 2H), 2.04-1.93 (m, 2H), 1.65-1.41 (m, 6H), 1.04 (d, J = 6.2 Hz, 3H). ^{13}C NMR (100 MHz, Methanol- d_4) δ (ppm) 176.2, 136.8, 136.8, 134.5, 132.3, 132.2, 131.2, 131.1, 131.0, 131.0, 126.5, 123.2, 123.2, 123.1, 123.0, 71.5, 71.5, 71.4, 71.2, 70.6, 70.4, 65.8, 57.4, 53.0, 52.7, 51.3, 40.3, 36.9, 30.9, 30.7, 30.2, 29.9, 27.5, 27.1, 26.8, 22.7, 15.6. MS (ESI) m/z 989.4 $[\text{M}+\text{H}]^+$. HRMS for $\text{C}_{44}\text{H}_{59}\text{N}_{10}\text{O}_{10}\text{Cl}_2\text{P}_1$, mass calculated 989.3603, mass measured 989.3636.

Diphenyl (5-amino-1-(1-(4-(1-(18-((4S,5R)-5-methyl-2-oxoimidazolidin-4-yl)-13-oxo-3,6,9-trioxa-12-azaoctadecyl)-1H-1,2,3-triazol-4-yl)butanoyl)pyrrolidine-2-carboxamido)pentyl)phosphonate trifluoroacetate salt (6.58b) General procedure **H** with **6.31a** (52,5 mg, 0,127 mmol) and **S6.16**, followed by general procedure **D** to yield **6.58b** (5.6 mg, 5.31 μmol , 6% yield). ^1H NMR (400 MHz, Methanol- d_4) δ (ppm) 7.86-7.75 (m, 2H), 7.36 (t, J = 7.7 Hz, 4H), 7.27-7.19 (m, 2H), 7.19-7.11 (m, 4H), 4.54 (t, J = 5.1 Hz, 2H), 4.48 (dd, J = 7.7, 4.6 Hz, 1H), 4.45-4.35 (m, 1H), 4.29 (dd, J = 7.7, 4.6 Hz, 1H), 4.19-4.04 (m, 2H), 3.88 (t, J = 5.1 Hz, 2H), 3.63-3.55 (m, 8H), 3.51 (t, J = 5.4 Hz, 2H), 3.34 (t, J = 5.7 Hz, 4H), 3.23-3.15 (m, 1H), 3.02-2.87 (m, 4H), 2.79 (t, J = 7.4 Hz, 2H), 2.72-2.65 (m, 1H), 2.19 (t, J = 7.4 Hz, 2H), 2.15-1.34 (m, 19H). ^{13}C NMR (100 MHz, Methanol- d_4) δ (ppm) 131.1, 121.5, 71.5, 70.6, 52.7, 40.4, 36.9, 30.8, 30.2, 26.9, 15.7. MS m/z 940.6 $[\text{M}+\text{H}]^+$. HRMS for $\text{C}_{46}\text{H}_{70}\text{N}_9\text{O}_{10}\text{P}_1$, mass calculated 940.5056, mass measured 940.5059.

6.5.2 Determination of IC_{50} values

The IC_{50} value is defined as the concentration of inhibitor required to reduce the enzyme activity to 50% after a 15 min preincubation with the enzyme at 37 °C before the addition of the substrate. The IC_{50} values were determined using a spectrophotometric assay. All the experiments were conducted in duplicate. The readout consisted of evaluating the

protease-mediated release of the chromophore *para*-nitroaniline (pNA) or fluorophore 7-amino-4-methyl coumarin (AMC) moieties from the respective substrates. Enzymatic activity was measured for 30 min at 37 °C. All compounds were initially screened at three concentrations (10, 1, and 0.1 μM) to estimate the range of the IC₅₀ value. Those which were able to reduce protease activity by at least 50% at a concentration of 10 μM were submitted to an exact IC₅₀ determination. The final IC₅₀ values of the most potent inhibitors were the average of two independent experimental results. A third independent experiment was performed when the standard deviation of the two independent experiments was higher than three times the IC₅₀ value. IC₅₀ values were obtained by fitting the data with the four-parameter logistics equation using GraphPad Prism 9.

The conditions for each protease are described as follows, the concentration of substrate used was at the corresponding K_m.

Trypsin-3 (recombinant trypsin-3, R&D) and fluorogenic substrate tosyl-Gly-Pro-Arg-AMC (K_m = 22.5 μM) were used in Tris buffer (100 mM Tris, 1 mM CaCl₂) at pH 8.0 (25°C). Trypsase (recombinant trypsinase β-2, EnzoLife Sciences) and fluorogenic substrate Boc-Gln-Ala-Arg-AMC (K_m = 250 μM) were used in Tris buffer (50 mM Tris, 120 mM NaCl, 0.1 mg/mL BSA, 0.1 mg/mL heparin) at pH 8.0 (25°C). Thrombin (recombinant thrombin, R&D) and fluorogenic substrate Boc-Val-Pro-Arg-AMC (K_m = 15 μM) were used in TRIS buffer (50 mM Tris HCl, 50 mM Tris base, 10 mM CaCl₂, 150 mM NaCl) at pH 8.3 (25°C). uPA (recombinant urokinase plasminogen activator, HYPHEN BioMed) and chromogenic substrate *pyro*-Glu-Gly-Arg-pNA (K_m = 80 μM) were used in HEPES buffer (50 mM HEPES) at pH 8.1 (25°C). Cathepsin G (cathepsin G human neutrophil, Sigma-Aldrich) and fluorogenic substrate Suc-Ala-Ala-Pro-Phe-AMC (K_m = 130 μM) were used in Tris buffer (50 mM Tris, 120 mM NaCl) at pH 8.0 (25°C). TLCK-treated pancreatic bovine chymotrypsin (Sigma-Aldrich) and fluorescent substrate Suc-Ala-Ala-Pro-Phe-AMC (K_m = 58 μM) were used in Tris buffer (50 mM Tris, 20 mM CaCl₂) at pH 8.3 (25°C). Neutrophil Elastase (recombinant neutrophil elastase, Enzo LifeSciences) and fluorogenic substrate Suc-Ala-Ala-Pro-Val-AMC (K_m = 500 μM) were used in Tris buffer (50 mM Tris, 120 mM NaCl) at pH 8.0 (25°C).

6.5.3 Kinetic experiments and determination of k_{app} , K_1 , and K_i^*

Because the compounds described in this paper were previously described as irreversible inhibitors, the IC_{50} value is inversely correlated with the second-order rate constant of inactivation. For a simple pseudo-first-order inactivation process, the activity after incubation with inhibitor (v_i) varies with the inhibitor concentration (i), as described in the following equation: $v_i = v_0 \cdot e^{-kit}$, where v_0 is the activity in the absence of an inhibitor, k is the second-order rate constant of inactivation, and t is the time. The inactivation rate constant was determined from the time course of inhibition.

Kinetic assays were performed in the following manner. The inhibitor was mixed with the substrate, and the buffer solution with the enzyme was added at the time zero. The progress curves show the release of pNA or AMC as a function of time. Initially, no inhibitor is bound to the enzyme, and the tangent to the progress curve (dA/dt) is proportional to the free enzyme concentration. The free enzyme concentration decreases over time due to inhibitor binding kinetics, as described above. Progress curves were recorded in pseudo-first-order conditions ($[I]_0 \gg [E]_0$) and with less than 10% conversion of the substrate during the entire time course. In these conditions, dA/dt decreases exponentially with time. The progress curves were fitted with the integrated rate equation with GraFit7 to yield a value for k_{obs} , a pseudo-first-order rate constant.

$A_t = A_0 + v_s \cdot t + (v_i - v_s) \cdot (1 - e^{-k_{obs} \cdot t}) / k_{obs}$, where A_t is the absorbance at time t , A_0 is the absorbance at time zero, v_i is the initial rate, and v_s is the velocity at the steady-state.

The apparent second-order rate constant (k_{app}) was calculated from the slope of the linear part of the plot of k_{obs} vs. the inhibitor concentration ($[I]_0$). In the case of competition between the inhibitor and the substrate, k_{app} is smaller than the “real” second-order rate constant k discussed above because a certain fraction of the enzyme is present as an enzyme-substrate complex. k_{app} depends on the substrate concentration used in the experiment, as described by Lambeir *et al.* 1996.¹²⁵

The apparent equilibrium constants were obtained from the following equations,

$v_i/v_0 = 1 / (1 + ([I]/K_1))$ and $v_s/v_0 = 1 / (1 + ([I]/K_i^*))$, where v_i is the initial rate, v_s is the steady-state velocity and v_0 is the uninhibited initial rate.

6.5.4 Determination of inhibition type

To monitor the dissociation of the inhibitor-enzyme, aliquots of the enzyme were incubated at 37°C without and with the inhibitor at a concentration 10 times higher than its IC₅₀. The enzyme concentration was 2.5 times higher than the concentration used for the IC₅₀ determinations. After 15 min, the aliquots were diluted 10-fold or 100-fold into the substrate concentration and assay buffer used for the IC₅₀ determination. The dissociation of the enzyme-inhibitor complex was monitored by substrate hydrolysis over time.¹²⁹

6.5.5 Labeling and detection of recombinant proteases

Recombinant proteases (100 ng) were labeled with 1 μM ABP in reaction buffer in a final volume of 40 μL for 30 min at 37 °C. After the addition of 4X Laemmli buffer (Bio-Rad, GmbH) supplemented with Bond-Breaker Tris(2-CarboxyEthyl)Phosphine (TCEP) Solution (Thermo Scientific, USA), the samples were heated at 95 °C for 5 min and loaded into 4–20% Mini-Protean TGX precast gels (Bio-Rad, GmbH). After electrophoresis, the proteins were blotted onto nitrocellulose membranes using the Trans-Blot Transfer Turbo System (Bio-Rad). Membranes were incubated with NeutrAvidin-HRP (1:50,000), and bands were visualized with ECL Select Western Blot Detection Reagent (GE Healthcare Life Sciences) by chemiluminescence (Chemidoc XRS; Bio-Rad). The molecular weight of each band was determined with the Image Lab Software v5 (Bio-Rad).

6.5.6 Primary human mast cells culture

Peripheral blood mononuclear cells (PBMCs) were obtained from buffy coats (Etablissement Français du Sang). CD34+ precursors cells were isolated from PBMCs (EasySep™ Human CD34 Positive Selection Kit, STEMCELL Technologies) and grown under

serum-free conditions using StemSpan™ medium (STEMCELL Technologies) supplemented with recombinant human IL-6 (50 ng/mL; Peprotech), human IL-3 (10 ng/mL; Peprotech) and 3% supernatant of CHO transfectants secreting murine SCF (a gift from Dr. P. Dubreuil, Marseille, France, 3% correspond to ~50 ng/mL SCF) for one week. Cells were next grown in IMDM Glutamax I, sodium pyruvate, 2-mercaptoethanol, 0.5% BSA, Insulin-transferrin selenium (all from Invitrogen), penicillin (100 U/mL), streptomycin (100 µg/mL) and 3% supernatant of CHO transfectants secreting murine SCF for 8 weeks then tested phenotypically (CD117+, FcεRI+) and functionally (β-hexosaminidase release in response to FcεRI crosslinking) before use for experiments. Only primary cell lines showing more than 95% CD117+ /FcεRI+ cells were used for experiments.

6.5.7 Mast cell degranulation assay

1x10⁵ mast cells were distributed in 50 µL Tyrode's Buffer and adapted to 37°C for 30 minutes. Mast cells were next stimulated with DNP-BSA (200 ng/mL) after sensitization with 1 µg/mL of IgE anti DNP (Sigma-Aldrich) overnight. Supernatants were harvested and stored at -80°C. (β-hexosaminidase was assayed by measuring the release of p-nitrophenol from the substrate p-nitrophenyl N-acetyl-β-D-glucosaminide).

6.5.8 Measurement of protein concentration

The concentration of protein in supernatants was determined using the Pierce Protein BCA Assay Kit, according to instructions (Thermo Scientific).

6.5.9 Measurement of proteolytic activity

Tryptase-like activity in mast cell supernatants was measured with 0.075 mM Boc-Gln-Ala-Arg-AMC hydrochloride as substrate in 50 mM Tris 120 mM NaCl + 0.1 mg/mL BSA + 50 µg/mL heparin pH = 8 at 25°C (Sigma-Aldrich). Substrate cleavage was calculated by the change in fluorescence (excitation: 355 nm, emission: 460 nm), measured over 30 min at 37 °C on a FLUOstar Omega microplate reader (BMG Labtech). Sample values were

interpolated into a linear regression generated with a standard curve of AMC (Sigma-Aldrich). Data were expressed as U of tryptase-like activity per L (U defined as 1 $\mu\text{mol}/\text{min}$).

6.5.10 Functional proteomic profiling of mast cell supernatants

Mast cell supernatants (10 μg of total protein) were labeled with 1 μM individual ABPs (**6.46b**, **6.52b**, or **6.57b**) in 50 mM Tris, 120 mM NaCl, 0.1 mg/mL BSA, 50 $\mu\text{g}/\text{mL}$ heparin, pH 8 at 25 °C (Sigma-Aldrich) in a final volume of 500 μL . As a control, supernatants were pre-incubated for 60 min at 37 °C under stirring (1000 rpm) in 4 mM AEBSF (Sigma), and 1X complete EDTA-free inhibitor cocktail (Roche) before incubation with a mixture containing the 3 ABPs mentioned above. The pre-incubation with protease inhibitors allows the identification of active proteases since enzyme inhibition abrogates their interaction with the ABP. The reaction product was then precipitated in 15% trichloroacetic acid at 4 °C overnight. The pellet was washed twice in cold acetone (−20 °C) and solubilized in 45 μL of Laemmli buffer (Bio-Rad) supplemented with Bond-Breaker TCEP Solution (Thermo Scientific). Samples were then heated at 95 °C for 5 min, clarified by centrifugation at 12000 $\times g$ for 5 min, and the solubilized sample was loaded into 4–20% Mini-Protean TGX precast gels (Bio-Rad, GmbH). After electrophoresis, the proteins were blotted onto nitrocellulose membranes using the Trans-Blot Transfer Turbo System (Bio-Rad). Membranes were incubated with NeutrAvidin-HRP, and bands were visualized with ECL Select Western Blot Detection Reagent (GE Healthcare Life Sciences) by chemiluminescence (Chemidoc XRS; Bio-Rad). The molecular weight of each band was determined with the Image Lab Software v5 (Bio-Rad) with Dual Color Protein Precision Plus Standard (10-250 kDa; Bio-Rad) as a reference. The bands corresponding to active proteases were identified by their sensitivity to the pre-incubation with protease inhibitors.

6.5.11 Detection of tryptase in mast cell supernatants

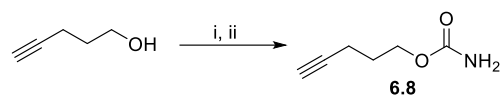
Protein in the mast cell supernatants (75 μg of total protein) was precipitated in 15% trichloroacetic acid at 4 °C overnight. The pellet was washed twice in cold acetone (−20 °C) and solubilized in 75 μL of Laemmli buffer protein supplemented with TCEP (Bio-Rad).

Samples were then heated at 95 °C for 5 min, clarified by centrifugation at 12000 × *g* for 5 min, and 5µg of the solubilized sample was loaded into 4–20% Mini-Protean TGX precast gels (Bio-Rad, GmbH). After electrophoresis, the proteins were blotted onto a nitrocellulose membrane using the Trans-Blot Transfer Turbo System (Bio-Rad). The membrane was incubated with a primary anti-mast cell tryptase antibody (sc-32889, Santa Cruz Biotechnology) at 1:1000 dilution overnight at 4°C. Subsequently, the membrane was labeled with the secondary HRP-conjugated antibody (1:10.000; P0448, Dako) for 1 h at room temperature. Bands were visualized with ECL Select Western Blot Detection Reagent (GE Healthcare Life Sciences) by chemiluminescence (Chemidoc XRS; Bio-Rad). The molecular weight of each band was determined with the Image Lab Software v5 (Bio-Rad).

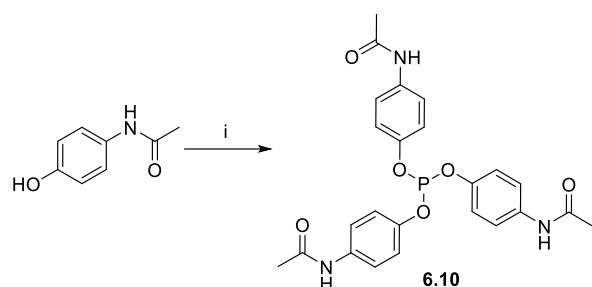
6.6 Supplementary information

6.6.1 Chemical synthesis

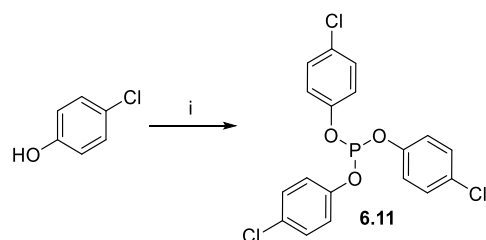
6.6.1.1 Chemical schemes



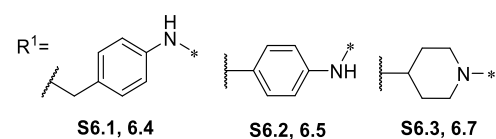
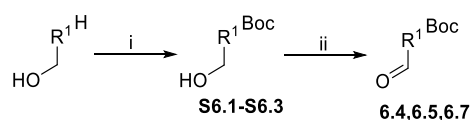
Scheme S6.1 Synthesis alkyne carbamate **6.8**; (i) CCl_3CONCO , DCM, $0\text{ }^\circ\text{C}$, 1 h; (ii) , K_2CO_3 , $\text{CH}_3\text{OH}/\text{H}_2\text{O}$ (10:1), rt, 16 h.



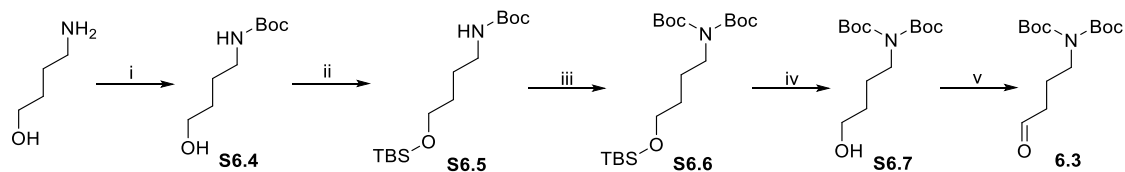
Scheme S6.2 Synthesis tris(4-acetamidophenyl)phosphite; (i) PCl_3 , Et_3N , THF, $0\text{ }^\circ\text{C}$ to rt, 1 h.



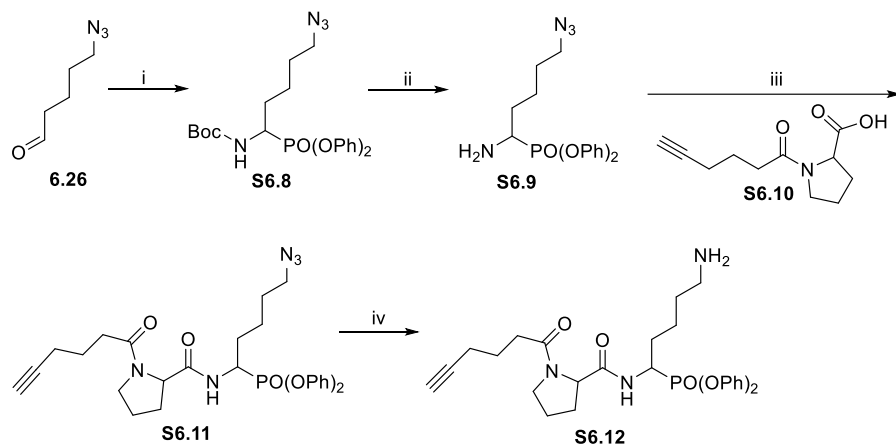
Scheme S6.3 Synthesis tris(4-chlorophenyl)phosphite; (i) PBr_3 , Et_3N , Et_2O , $0\text{ }^\circ\text{C}$ to rt, 1 h.



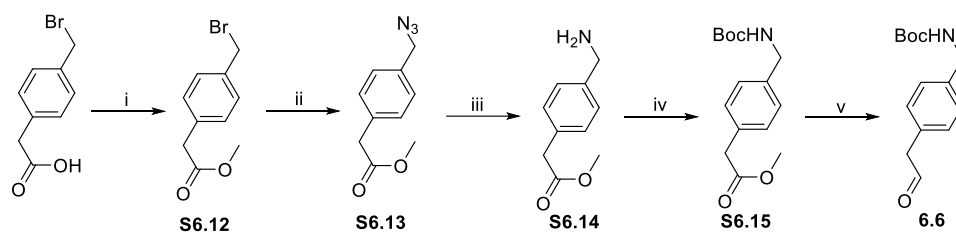
Scheme S6.4 Synthesis protected aldehydes (i) Boc_2O , Et_3N , EtOH, rt, 3 h; (ii) DMP, DCM, $0\text{ }^\circ\text{C}$ to rt, 4 h.



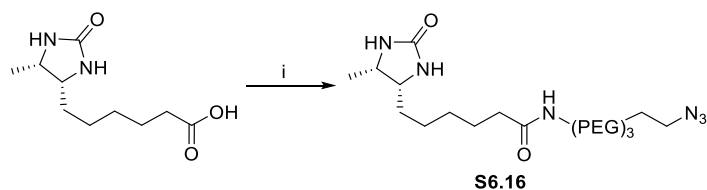
Scheme S6.5 Synthesis of protected aldehyde to synthesize arginine analog; (i) Boc_2O , Et_3N , EtOH , rt , 4 h; (ii) Imidazole , TBSCl , DCM , 0°C , 2 h; (iii) $n\text{-BuLi}$, Boc_2O , THF , 0°C to rt , 1 h; (iv) TBAF , THF , rt , 5 h; (v) $(\text{COCl})_2$, DMSO , Et_3N , DCM , -78°C to 0°C , 2 h



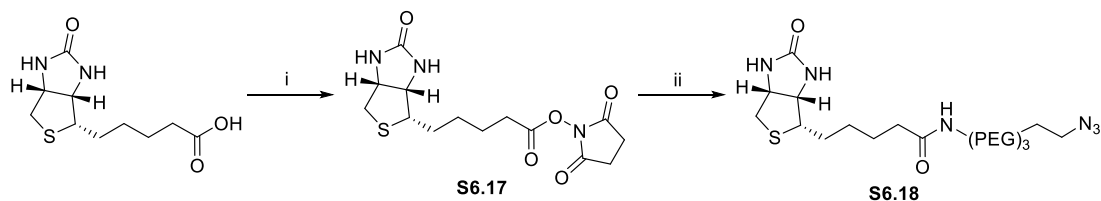
Scheme S6.6 Synthesis Pro-Lys ABP precursor; (i) NH_2Boc , $\text{Cu}(\text{OTf})_2$, DCM , rt , 16 h; (ii) TFA , DCM , rt , 2 h; (iii) **S6.10**, HOBT , DIPEA , EDC , DMP , rt , 16 h; (iv) Polymer supported triphenylphosphine, THF , rt , 24 h



Scheme S6.7 Synthesis of protected aldehyde used to synthesize methyl benzyl analogs; (i) SOCl_2 , CH_3OH , rt , 2 h; (ii) NaN_3 , H_2O , 80°C , 18 h; (iii) Polymer supported triphenylphosphine, THF , rt , 24 h (iv) Boc_2O , Et_3N , EtOH , rt , 16 h; (v) DIBAL-H , toluene , -78°C , 1 h



Scheme S6.8 Synthesis desthiobiotin azide; (i) 11-Azido-3,6,9-trioxaundecan-1-amine, HOBT , EDC , DIPEA , DMF , rt , 16 h



Scheme S6.9 Synthesis biotin azide; (i) NHS, DCC, DMF, 70 °C, 16 h; (ii) 11-Azido-3,6,9-trioxaundecan-1-amine, Et₃N, DMF, rt, 16 h

6.6.1.2 Synthesis and chemical characterization

Tert-butyl (4-(2-hydroxyethyl)phenyl)carbamate (S6.1) General procedure **A** with *p*-aminophenylethanol (4 g, 29.2 mmol) to yield **S6.1** (6.91 g, 29.1 mmol, 100% yield). ¹H NMR (400 MHz, CDCl₃) δ (ppm) 7.30 (d, *J* = 8.3 Hz, 1H), 7.18 – 7.12 (m, 1H), 3.82 (t, *J* = 6.5 Hz, 1H), 2.82 (t, *J* = 6.5 Hz, 1H), 1.51 (s, 9H). No ionization was found.

Tert-butyl (4-(hydroxymethyl)phenyl)carbamate (S6.2) General procedure **A** with *p*-aminobenzylalcohol (1.5 g, 12.18 mmol) to yield **S6.2** (2.7 g, 12.09 mmol, 99% yield). ¹H NMR (400 MHz, CDCl₃) δ (ppm) 7.32 (d, *J* = 8.3 Hz, 2H), 7.27-7.22 (m, 2H), 6.58 (br s, 1H), 4.59 (d, *J* = 5.6 Hz, 2H), 1.50 (s, 9H). No ionization was found.

Tert-butyl 4-(hydroxymethyl)piperidine-1-carboxylate (S6.3) General procedure **A** with piperidin-4-ylmethanol (2 g, 17.36 mmol) to yield **S6.3** (3.7 g, 17.19 mmol, 99% yield). ¹H-NMR (400 MHz, CDCl₃) δ (ppm) 4.08 (br s, 2H), 3.45 (t, *J* = 5.80, 2H), 2.76-2.58 (m, 2H), 2.12 (br s, 1H), 1.68 (d, 2H, *J* = 14.04), 1.64-1.55 (m, 1H), 1.4 (s, 9H), 1.10 (ddd, *J* = 4.1, 12.3, 24.4 Hz, 2H). MS (ESI) *m/z* 238.2 [M+Na]⁺.

tert-butyl (4-hydroxybutyl)carbamate (S6.4) General procedure **A** with 4-aminobutan-1-ol (5.17 mL, 56.1 mmol), the residue was purified through a silica plug (50/50 EtOAc in heptane to 100/0 EtOAc). The desired fractions were combined and concentrated *under vacuo* to yield **S6.4**, which was used without further purification for the next step. ¹H NMR (400 MHz, CDCl₃) δ (ppm) 4.69 (br s, 1H), 3.64 (d, *J* = 4.2 Hz, 2H), 3.13 (d, *J* = 5.6 Hz, 2H), 1.66-1.51 (m, 4H), 1.42 (s, 9H). MS (ESI) *m/z* 212.2 [M+Na]⁺.

***tert*-butyl (4-((*tert*-butyldimethylsilyloxy)butyl)carbamate (S6.5)** Imidazole (8.62 g, 127 mmol) and *tert*-butyldimethylsilylchloride (9.16 g, 60.8 mmol) were added to a solution of **S6.4** in DCM (100 mL) at 0 °C. The reaction mixture was stirred at 0 °C for 2 h. Then Et₂O was added to dilute the reaction mixture and further washed with water and brine. The organic solution was dried over Na₂SO₄, filtered and concentrated to give **S6.5**, which was used for the next operation directly without further purification. ¹H NMR (400 MHz, CDCl₃) δ (ppm) 4.69 (s, 1H), 3.68 – 3.58 (m, 2H), 3.14 (d, *J* = 6.0 Hz, 2H), 1.55 (dt, *J* = 6.5, 3.5 Hz, 4H), 1.45 (s, 9H), 0.90 (s, 9H), 0.06 (s, 6H). MS (ESI) *m/z* 304.2 [M+H]⁺.

***tert*-butyl (*tert*-butoxycarbonyl)(4-((*tert*-butyldimethylsilyloxy)butyl)carbamate (S6.6)** *n*-Butyllithium (38.0 mL, 60.8 mmol) was added to a stirred solution of **S6.5** in THF (250 mL) at 0 °C. The reaction mixture was stirred for 15 min at 0 °C before adding di-*t*-butyl dicarbonate (13.27 g, 60.8 mmol). The resulting reaction mixture was warmed to room temperature and stirred for 1 h. Then Et₂O was added to dilute the reaction mixture and washed with water and brine. The organic solution was dried over Na₂SO₄, filtered, and concentrated, giving **S6.6** used for the next step without further purification. ¹H NMR (400 MHz, CDCl₃) δ (ppm) 3.62 - 3.49 (m, 4H), 1.64 - 1.52 (m, 2H), 1.51 - 1.41 (m, 20H), 0.85 (s, 9H), 0.00 (s, 6H). No ionization was found.

***N, N'*-bis-*tert*-butyloxycarbonyl 5-aminobutan-1-ol (S6.7)** Tetrabutylammoniumfluoride (70.0 mL, 70.0 mmol) was added slowly to a stirred solution of **S6.6** in THF (112 mL) at room temperature. The resulting solution was stirred at room temperature for 5 h. Then Et₂O (100 mL) was added to dilute the reaction mixture and washed with water (100 mL). The aqueous layer was extracted with Et₂O (3 x 80 mL). The combined organic layers were washed with brine, dried over Na₂SO₄, filtered and concentrated under reduced pressure. The crude product was purified by flash chromatography (SiO₂, EtOAc in heptane, 0/100 to 100/0) to yield **S7** (12 g, 41.5 mmol, 74% yield). ¹H NMR (400 MHz, CDCl₃) δ (ppm) 3.61 (t, *J* = 6.0 Hz, 2H), 3.56 (t, *J* = 7.6 Hz, 2H), 1.97 (br s, 1H), 1.66-1.48 (m, 4H), 1.46 (s, 18H). No ionization was found.

Tert-butyl (5-azido-1-(diphenoxyphosphoryl)pentyl)carbamate (S6.8) Copper (II) trifluoromethanesulfonate (0.65 g, 1.81 mmol) was added to a solution of **6.26** (2.3 g, 18.09 mmol), *tert*-butyl carbamate (2.12 g, 18.09 mmol) and **6.9** (5.2 mL, 19.90 mmol) in DCM (40 mL) at room temperature and the mixture was stirred for 16 h. The solvent was removed under reduced pressure. The crude product was purified by flash chromatography (SiO₂, EtOAc in Heptane, 0/100 to 20/80) to yield **S6.8** (5.7 g, 12.46 mmol, 69% yield). ¹H NMR (400 MHz, Methanol-*d*₄) δ (ppm) 7.38-7.29 (m, 4H) 7.25-7.10 (m, 6H), 4.36 (ddd, *J* = 15.5, 13.8, 3.9 Hz, 1H), 3.33-3.26 (m, 2H), 2.07-1.95 (m, 1H), 1.91-1.76 (m, 1H), 1.73-1.46 (m, 4H), 1.44 (s, 9H). MS (ESI) *m/z* 483.2 [M+Na]⁺.

Diphenyl (1-amino-5-azidopentyl)phosphonate hydrochloric salt (S6.9) General procedure **E** with **S6.8** (3.65 g, 7.93 mmol) to yield **S6.9** (3.15 g, 7.94 mmol, 99% yield). ¹H NMR (400 MHz, CDCl₃) δ (ppm) 10.05 (br s, 2H), 7.34-7.26 (m, 4H), 7.20-7.16 (m, 2H), 7.12-6.99 (m, 4H), 4.06-3.90 (m, 1H), 3.37-3.16 (m, 2H), 2.37-1.95 (m, 2H), 1.82-1.47 (m, 4H). MS (ESI) *m/z* 361.8 [M+H]⁺.

Hex-5-ynoylproline (S6.10) DIPEA (12.6 mL, 72.5 mmol) was added to a solution of H-Pro-OtBu·HCl (8.28 g, 39.9 mmol), hex-5-ynoic acid (4 mL, 36.2 mmol) EDC (8.34 g, 43.5 mmol) and HOBT (6.66 g, 43.5 mmol) in DMF (50 mL). The reaction mixture is stirred for 2 h at room temperature. Upon completion, it is diluted with EtOAc (100 mL) and washed with 1M HCl (50 mL). The aqueous layer is extracted with EtOAc (3x50 mL) and the combined organic layers were washed with saturated NaHCO₃ (60 mL) and brine (60 mL). The organic layer is dried over anhydrous magnesium sulfate, filtered and the solvent evaporated under *vacuo*. The crude was purified by flash chromatography (SiO₂, EtOAc in heptane, 0/100 to 100/0) to yield *tert*-butyl hex-5-ynoylprolinate (6.97 g, 26.3 mmol, 72% yield). ¹H NMR (400 MHz, CDCl₃) δ (ppm) 4.34 (dd, *J* = 8.6, 3.4 Hz, 2H), 3.65-3.42 (m, 2H), 2.42 (td, *J* = 7.39, 2.4 Hz, 2H), 2.28-2.21 (m, 2H), 1.97-1.80 (m, 6H), 1.42 (s, 9H). MS (ESI) *m/z* 288.2 [M+Na]⁺. General procedure **D** with *tert*-butyl hex-5-ynoylprolinate (6.97 g, 26.3 mmol) to yield **S6.10** (5.5 g, 26.3 mmol, 99% yield). ¹H NMR (400 MHz, CDCl₃) δ (ppm) 1.89-1.78 (m, 2H), 2.34-

1.93 (m, 7H), 2.53 (t, $J = 6.9$ Hz, 2H), 3.63-3.51 (m, 1H), 3.77-3.63 (m, 1H), 4.52 (dd, $J = 7.9$, 4.7 Hz, 1H). MS (ESI) m/z 210.2 $[M+H]^+$.

Diphenyl (5-azido-1-(1-(hex-5-ynoyl)pyrrolidine-2-carboxamido)pentyl)phosphonate (S6.11) N,N-Di-iso-propylethylamine (5.5 mL, 31.8 mmol) was added to a solution of **S6.9** (3.15 g, 7.94 mmol), **S6.10** (2.66 g, 12.70 mmol), 1-hydroxybenzotriazolehydrate (1.46 g, 9.53 mmol), EDC (1.83 g, 9.53 mmol) in DMF (50 mL). The mixture was stirred at room temperature for 16 h. The solvent was coevaporated with toluene and the resulting mixture was diluted in EtOAc (100 mL), washed with a solution of HCl (1N, 50 mL), saturated aqueous solution of NaHCO_3 (60 mL) and brine. The organic layer was dried over anhydrous magnesium sulfate, filtered, and concentrated under reduced pressure. The crude product was purified by column chromatography on silica gel (SiO_2 , EtOAc in Heptane, 0/100 to 70/30) to yield **S6.11** (2.15 g, 3.90 mmol, 49% yield). ^1H NMR (400 MHz, CDCl_3) δ (ppm): 7.81 (br d, $J = 10.2$ Hz, 1H), 7.53 (br d, $J = 10.2$ Hz, 1H), 7.27-7.35 (m, 4H), 7.20-7.26 (m, 2H), 7.12-7.20 (m, 4H), 7.07-7.12 (m, 1H), 4.66-4.83 (m, 2H), 4.50 (dd, $J = 8.3$, 1.5 Hz, 1H), 3.55-3.65 (m, 1H), 3.34-3.51 (m, 2H), 3.26 (dd, $J = 12.8$, 6.3 Hz, 2H), 2.48 (td, $J = 7.4$, 1.7 Hz, 2H), 2.32-2.42 (m, 1H), 2.29 (td, $J = 7.2$, 2.6 Hz, 2H), 2.20 (td, $J = 6.8$, 2.6 Hz, 1H), 1.34-2.17 (m, 9H). MS m/z 552.3 $[M+H]^+$.

Methyl 2-(4-(bromomethyl)phenyl)acetate (S6.12) Sulfurchlorideoxide (0.068 mL, 0.873 mmol) was added to a solution of 2-(4-(bromomethyl)phenyl)acetic acid (2 g, 8.73 mmol) in CH_3OH (30 mL) at room temperature and the mixture was stirred for 1 h. The reaction mixture was concentrated under reduced pressure and neutralized with a saturated solution of NaHCO_3 . The product was extracted with EtOAc (100 mL). The organic layer was washed with a saturated solution of NaHCO_3 (20mL) and brine (20mL), dried, filtered and concentrated under reduced pressure to yield **S6.12** (2.07 g, 8.52 mmol, 98% yield). ^1H NMR (400 MHz, CDCl_3) δ (ppm) 7.35 (d, $J = 8.0$ Hz, 2H), 7.26 (d, $J = 8.0$ Hz, 2H), 4.48 (s, 2H), 3.69 (s, 3H), 3.62 (s, 2H). MS (ESI) m/z 260.0 $[M+H_2O]$.

Methyl 2-(4-(azidomethyl)phenyl)acetate (S6.13) Sodiumazide (1.498 g, 23.04 mmol) was added to a solution of **S6.12** (2.8 g, 11.52 mmol) in H₂O (40 mL) at room temperature. Following the addition, the solution was heated to 80 °C and stirred for 18 h. The reaction mixture was cooled down to room temperature, and the product was extracted with DCM (3 x 50 mL). The combined organic layers were dried over anhydrous MgSO₄, filtered and concentrated under reduced pressure to yield **S6.13** (2.21 g, 10.77 mmol, 93% yield). ¹H NMR (400 MHz, CDCl₃) δ (ppm) 7.32-7.24 (m, 4H), 4.31 (s, 2H), 3.69 (s, 3H), 3.63 (s, 2H). MS (ESI) *m/z* 178.1 [M-N₂].

Methyl 2-(4-(aminomethyl)phenyl)acetate (S6.14) Polymer supported triphenylphosphine (5.63 g, 21.54 mmol) was suspended in anhydride THF (100 mL) and stirred for 30 min, then **S6.13** (2.21 g, 10.77 mmol) was added. The mixture was stirred at room temperature for 21 h. H₂O (20 mL) was added, and the mixture was stirred for an additional 5 h. The polymer was removed by filtration and washed with THF (2 x 20 mL) and H₂O (20 mL). The filtrate was concentrated under reduced pressure and freeze-dried. The crude product was diluted in DCM (30 mL) and washed with brine (30 mL). The aqueous layer was extracted with DCM (2 x 30 mL), and the combined organic layers were dried over sodium sulfate, filtered and concentrated under reduced pressure to yield **S6.14** (1.66 g, 9.26 mmol, 86% yield). ¹H NMR (400 MHz, CDCl₃) δ (ppm) 7.30-7.22 (m, 4H), 3.85 (s, 2H), 3.68 (s, 3H), 3.62 (s, 2H). MS (ESI) *m/z* 357.2 [2xM].

Methyl 2-(4-(((tert-butoxycarbonyl)amino)methyl)phenyl)acetate (S6.15) General procedure **A** with **S6.14** (1.66 g, 9.26 mmol). The mixture was diluted in EtOAc (100 mL) and washed with a solution of HCl (2N, 100 mL), saturated solution of NaHCO₃ (100 mL) and brine. The organic layer was dried over Na₂SO₄, filtered and concentrated under reduced pressure. The crude product was purified by chromatography on silica gel (SiO₂, EtOAc in Heptane, 0/100 to 20/80) to yield **S6.15** (1.83 g, 6.55 mmol, 71% yield). ¹H NMR (400 MHz, CDCl₃) δ (ppm) 7.23 (s, 4H), 5.03 (br s, 1H), 4.27 (d, *J* = 5.9 Hz, 2H), 3.67 (s, 3H), 3.59 (s, 2H), 1.45 (s, 9H). MS (ESI) 302.1 [M+Na]⁺.

N-(2-(2-(2-(2-azidoethoxy)ethoxy)ethoxy)ethyl)-6-((4R,5S)-5-methyl-2-oxoimidazolidin-4-yl)hexanamide (S6.16) DIPEA (0.777 mL, 4.46 mmol) was added to a solution of 2-(2-(2-(2-azidoethoxy)ethoxy)ethoxy)ethan-1-amine (0.8 mL, 4.09 mmol), 6-((4R,5S)-5-methyl-2-oxoimidazolidin-4-yl)hexanoic acid (0.79 g, 3.72 mmol), EDC (0.85 g, 4.46 mmol), and HOBT (0.68 g, 4.46 mmol) in DMF (30 mL). The mixture was stirred at room temperature for 16h. The solvent was removed under reduced pressure by co-evaporation with toluene. The mixture was diluted with EtOAc (40 mL) and washed with 1 M HCl (30 mL). The aqueous layer was extracted with EtOAc (3 x 50 mL) and the combined organic layer was washed with saturated solution of NaHCO₃ and brine, dried over MgSO₄ and concentrated under reduced pressure. The crude product was purified by reverse phase chromatography (C18, CH₃CN in H₂O, 0/100 to 60/40) to yield **S6.16** (1.09 g, 2.63 mmol, 71% yield). ¹H NMR (400 MHz, CDCl₃) δ (ppm) 6.72 (br s, 1H), 6.00 (br s, 1H), 5.17 (br s, 1H), 3.79 (p, *J* = 6.9 Hz, 1H), 3.73-3.56 (m, 11H), 3.53 (t, *J* = 5.0 Hz, 2H), 3.41 (t, *J* = 5.0 Hz, 2H), 3.36 (t, *J* = 5.0 Hz, 2H), 2.16 (t, *J* = 7.3 Hz, 2H), 1.63 (p, *J* = 7.0 Hz, 2H), 1.51-1.15 (m, 6H), 1.08 (d, *J* = 6.4 Hz, 3H). MS (ESI) *m/z* 415.4 [M+H]⁺.

2,5-dioxopyrrolidin-1-yl 5-((3aS,4S,6aR)-2-oxohexahydro-1H-thieno[3,4-d]imidazol-4-yl)pentanoate (S6.17) D-Biotin (100 mg, 0.41 mmol) and N-hydroxysuccinimide (56.5 mg, 0.49 mmol) were dissolved in anhydrous DMF (10 mL) at 70 °C. 1,3-Dicyclohexylcarbodiimide (101 mg, 0.49 mmol) was added, and the solution was stirred at room temperature for 16 h. The formed DCU was filtered off, and the solution was evaporated to dryness. The residue was taken up into boiling isopropanol, and the solution was allowed to cool down to room temperature. The target compound was precipitated out, and the product was filtered off to yield **S6.17** (72 mg, 0.21 mmol, 52% yield). ¹H NMR (400 MHz, DMSO-*d*₆) δ (ppm) 6.40 (d, *J* = 24.3 Hz, 2H), 4.34 – 4.26 (m, 1H), 4.20 – 4.10 (m, 1H), 3.14 – 3.07 (m, 1H), 2.87 – 2.77 (m, 5H), 2.67 (t, *J* = 7.4 Hz, 2H), 2.58 (d, *J* = 12.4 Hz, 1H), 1.71 – 1.58 (m, 3H), 1.56 – 1.35 (m, 3H). MS (ESI) *m/z* 342.2 [M+H]⁺.

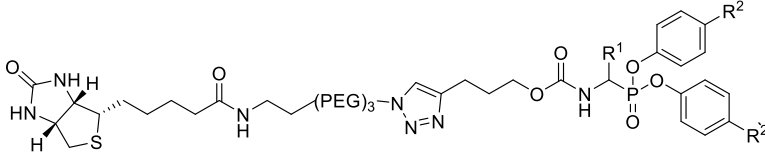
N-(2-(2-(2-(2-azidoethoxy)ethoxy)ethoxy)ethyl)-5-((3aS,4S,6aR)-2-oxohexahydro-1H-thieno[3,4-d]imidazol-4-yl)pentanamide (S6.18) Triethylamine (0.059 mL, 0.422 mmol)

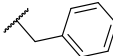
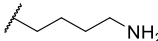
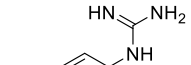
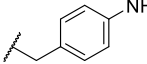
was added to a solution of 1-Amino-11-azido-3,6,9-trioxaundecane (0.042 mL, 0.211 mmol) in DMF (35 mL), followed by the addition of **S6.17** (72 mg, 0.211 mmol). The resulting solution was stirred at room temperature for 16 h. The solvent was evaporated. The crude product was purified by reverse phase chromatography (C18, CH₃OH in H₂O, 0/100 to 100/0). The desired fractions were collected to yield **S6.18** (25 mg, 0.056 mmol, 14% yield). ¹H NMR (400 MHz, DMSO-*d*₆) δ (ppm) 4.42-4.31 (m, 1H), 4.19-4.12 (m, 1H), 3.62 (m, 2H), 3.53 (m, 8H), 3.38 (m, 4H), 3.18 (m, 2H), 3.09 (m, 1H), 2.82 (dd, *J* = 12.4, 5.2 Hz, 1H), 2.59 (d, *J* = 12.8 Hz, 1H), 2.07 (t, *J* = 7.2 Hz, 2H), 1.29-1.64 (m, 6H). MS (ESI) *m/z* 445.3 [M+H]⁺.

6.6.2 Biochemistry evaluation

6.6.2.1 Additional IC_{50} values

Table S6.1 IC_{50} values of biotin probes against a panel of serine proteases



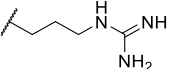
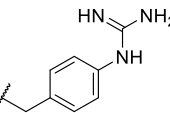
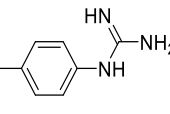
#	R ¹	R ²	IC_{50} (μ M) ^b						
			Trypsin-3	β -tryptase	Thrombin	uPA ^a	CatG ^a	ChTryp ^a	NE ^a
6.43		H	>10	>10	>10	>10	2.77 ± 0.07	2.64 ± 0.27	>10
6.48		H	0.21 ± 0.005	2.11 ± 0.10	2.73 ± 0.17	3.54 ± 0.23	>10	>10	>10
6.51		H	0.02 ± 0.003	0.91 ± 0.09	6.04 ± 0.40	0.04 ± 0.001	0.17 ± 0.01	>10	>10
6.53		NHCOCH ₃	0.01 ± 0.001	0.08 ± 0.003	0.49 ± 0.02	0.01 ± 0.002	0.05 ± 0.001	>10	>10

^aPanel of serine proteases abbreviations: urokinase plasminogen activator (uPA), cathepsin G (catG), chymotrypsin (ChTryp), neutrophil elastase (NE)

^bHalf maximal inhibitory concentration (IC_{50}) value is the concentration of inhibitor required to reduce the enzyme activity to 50% after a 15 min preincubation with the enzyme at 37 °C. IC_{50} are calculated from two independent experiments; when SD was higher than three times the average value, a third independent experiment was run (mean ± SD)

6.6.2.2 Jump dilution results

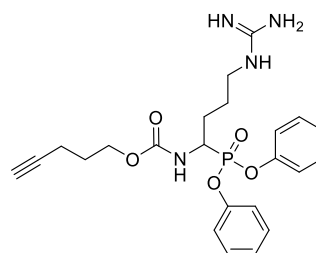
Table S6.2 Jump dilution of selected probes against a panel of trypsin-like serine proteases.

#	R ¹	R ²	Alk DtB ^a	Trypsin- 3	β- trypt. ^a	Thromb. ^a	uPA ^a	CatG ^a
6.32b		H	Alk	Irrev.	Irrev.	Rev.	Irrev.	Rev.
6.45b			DtB	Irrev.	Irrev.	Rev.	N.D.	N.D.
6.33b		Cl	Alk	Irrev.	Irrev.	Rev.	Irrev.	Rev.
6.46b			DtB	Irrev.	Irrev.	Rev.	N.D.	N.D.
6.34b		H	Alk	Rev.	Rev.	Rev.	Irrev.	Rev.
6.50b			DtB	Rev.	Rev.	Rev.	Irrev.	Rev.
6.34b		NHCOCH ₃	Alk	Rev.	Rev.	Rev.	Irrev.	Rev.
6.51b			DtB	Rev.	Rev.	Rev.	Irrev.	Rev.
6.35b		Cl	Alk	Rev.	Rev.	Rev.	Irrev.	Rev.
6.52b			DtB	Rev.	Rev.	Rev.	Irrev.	Rev.
6.37b		H	Alk	Irrev.	Irrev.	N.D.	Irrev.	Irrev.
6.55b			DtB	Irrev.	Irrev.	N.D.	Irrev.	Irrev.
6.38b		NHCOCH ₃	Alk	Irrev.	Irrev.	N.D.	Irrev.	Irrev.
6.56b			DtB	Irrev.	Irrev.	N.D.	Irrev.	Irrev.
6.39b		Cl	Alk	Irrev.	Irrev.	N.D.	Irrev.	Rev.
6.57b			DtB	Irrev.	Irrev.	N.D.	Irrev.	Rev.
6.41b		H	Alk	Irrev.	Irrev.	Irrev.	N.D.	N.D.
6.31b	Pro-Lys	H	Alk	Irrev.	Irrev.	Irrev.	Irrev.	N.D.

^a Alk: ABP precursor bearing an alkyne; DtB: desthiobiotin probe; Panel of serine proteases abbreviations: trypsin (trypt.), thrombin (throm.), urokinase plasminogen activator (uPA), cathepsin G (catG)
N.D.: IC₅₀ is greater than 10 μM, and jump dilution was not performed

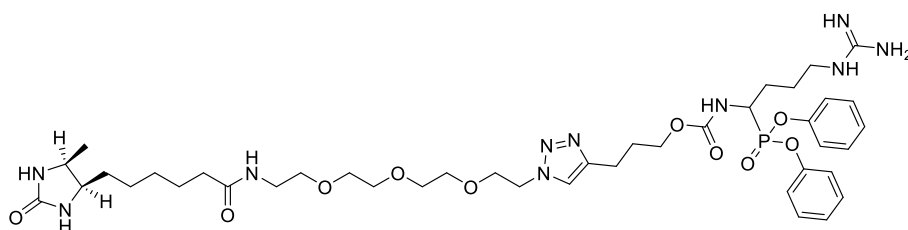
6.6.2.3 Progress curves and jump dilution experiments

Compound 6.32b



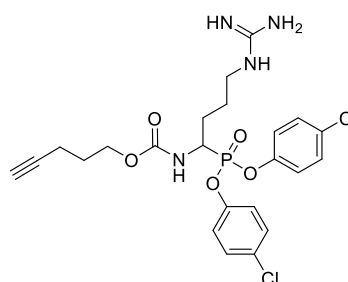
	Progress curve	k_{app} calculation	Jump dilution
Trypsin-3 IRREV.			
β-trypase IRREV.			
Thrombin REV.			
uPA IRREV.			
CatG REV.		N.D.	v_i/v_0 original – 0,37 v_i/v_0 diuted – 0,91 Activity increases when diluted

Compound 6.45b



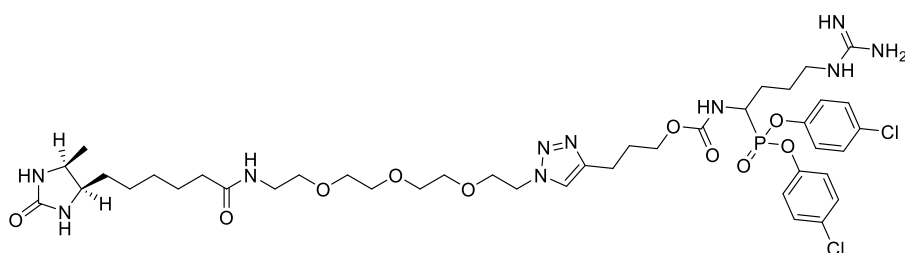
	Progress curve	k_{app} calculation	Jump dilution
Trypsin-3 IRREV.			
β-tryptase IRREV.			
Thrombin REV.			

Compound 6.33b



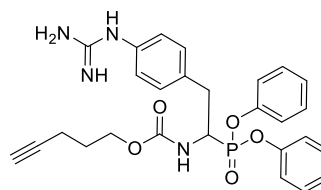
	Progress curve	k_{app} calculation	Jump dilution
Trypsin-3 IRREV.			
β-tryptase IRREV.			
Thrombin REV.			
uPA IRREV.			
CatG REV.		N.D.	

**Compound
6.46b**



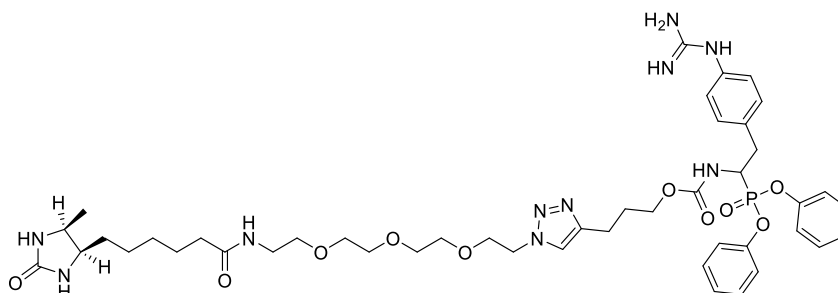
	Progress curve	k_{app} calculation	Jump dilution
Trypsin-3 IRREV.			
β-tryptase IRREV.			
Thrombin REV.			
uPA IRREV.			

Compound 6.34b



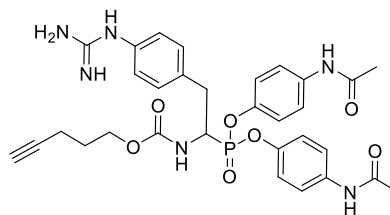
	Progress curve	k_{app} calculation	Jump dilution
Trypsin-3 REV.			
β-tryptase REV.			
Thrombin REV.			
uPA IRREV.			
CatG REV.		N.D.	

**Compound
6.50b**

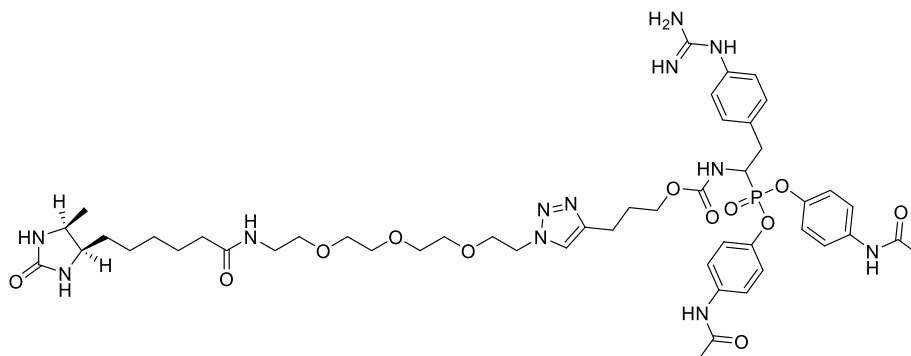


	Progress curve	k_{app} calculation	Jump dilution
Trypsin-3 REV.			
β-tryptase REV.			
Thrombin REV.			
uPA IRREV.			
CatG REV.		N.D.	<p>v_i/v_0 original – 0,19 v_i/v_0 diuted – 0,39 Activity increases when diluted</p>

Compound 6.35b

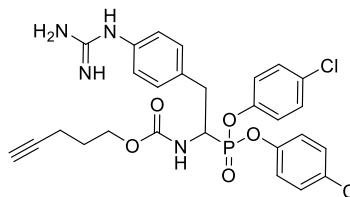


	Progress curve	k_{app} calculation	Jump dilution
Trypsin-3 REV.		N.D.	
β-trypase REV.			
Thrombin REV.			
uPA IRREV.			
CatG REV.			

Compound
6.52b

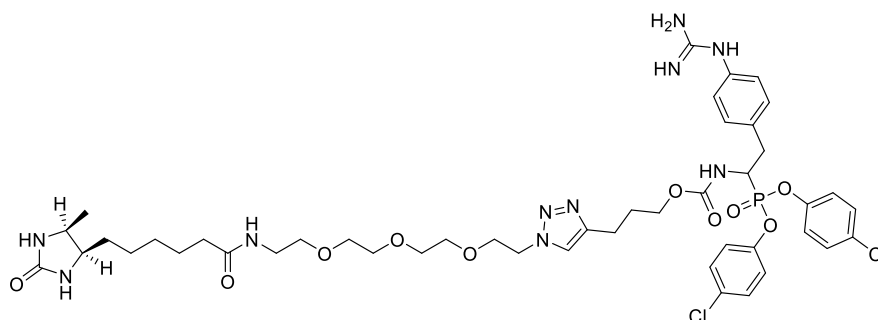
	Progress curve	k_{app} calculation	Jump dilution
Trypsin-3 REV.			
β-tryptase REV.			
Thrombin REV.			
uPA IRREV.			
CatG REV.		N.D.	v_i/v_0 original – 0,11 v_i/v_0 diuted – 0,31 Activity increases when diluted

Compound 6.36b



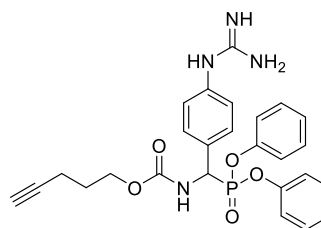
	Progress curve	k_{app} calculation	Jump dilution
Trypsin-3 REV.			
β- trypsin REV.			
Thrombin REV.			
uPA IRREV.			
CatG REV.		N.D.	

**Compound
6.54b**



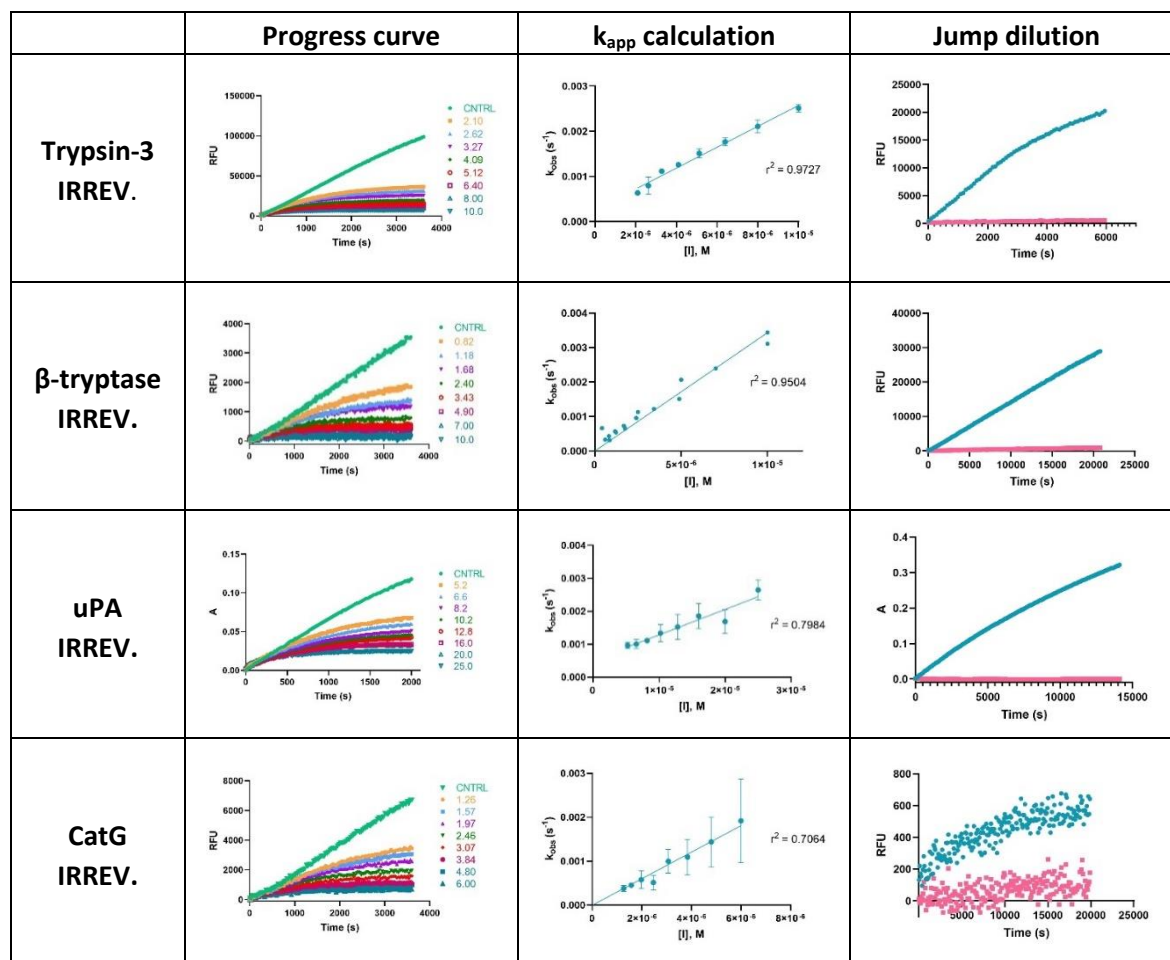
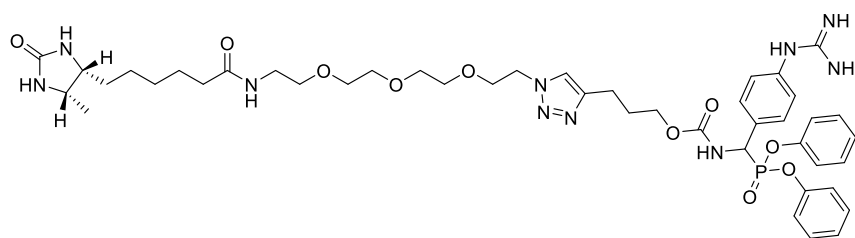
	Progress curve	k_{app} calculation	Jump dilution
Trypsin-3 REV.		N.D.	
β-tryptase REV.		N.D.	
Thrombin REV.		N.D.	
uPA IRREV.			
CatG REV.		N.D.	v_i/v_0 original – 0,13 v_i/v_0 diuted – 0,38 Activity increases when diluted

Compound 6.37b

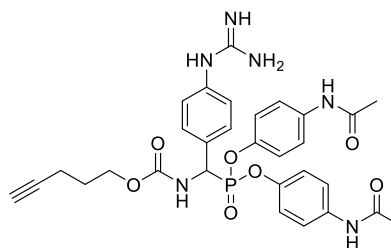


	Progress curve	k_{app} calculation	Jump dilution
Trypsin-3 IRREV.			
β-tryptase IRREV.			
uPA IRREV.			
CatG IRREV.			<p>v_i/v_0 original – 0,16 v_i/v_0 diuted– 0,20 Activity does not increase when diluted</p>

**Compound
6.55b**

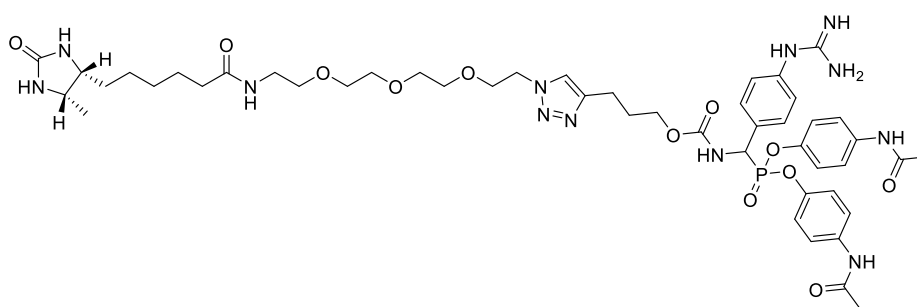


Compound 6.38b



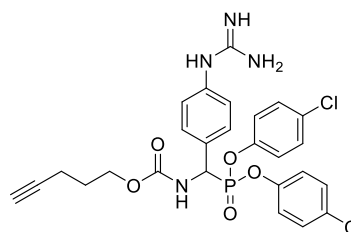
	Progress curve	k_{app} calculation	Jump dilution
Trypsin-3 IRREV.			
β-tryptase IRREV.			
uPA IRREV.			
CatG IRREV.			

**Compound
6.56b**



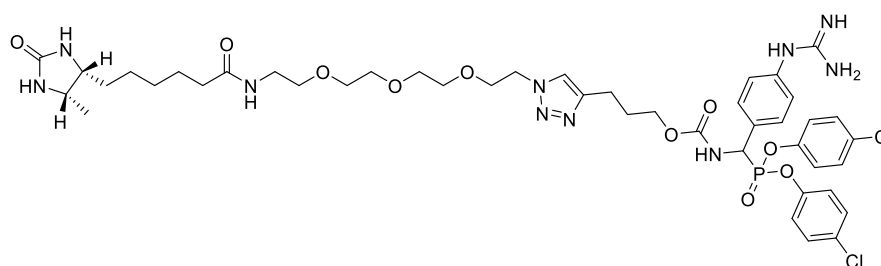
	Progress curve	k_{app} calculation	Jump dilution
Trypsin-3 IRREV.			
β-tryptase IRREV.			
uPA IRREV.			
CatG IRREV.			

Compound 6.39b



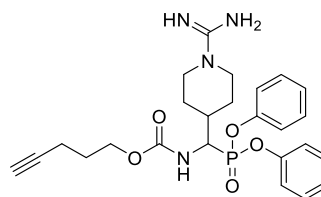
	Progress curve	k_{app} calculation	Jump dilution
Trypsin-3 IRREV.			
β-tryptase IRREV.			
uPA IRREV.			
CatG REV.			

**Compound
6.57b**



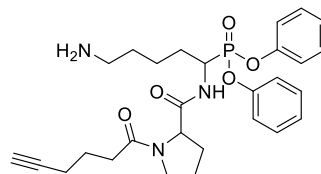
	Progress curve	k_{app} calculation	Jump dilution
Trypsin-3 IRREV.			
β-tryptase IRREV.			
uPA IRREV.			
CatG REV.			

Compound 6.41b



	Progress curve	k_{app} calculation	Jump dilution
Trypsin-3 IRREV.			
β-tryptase IRREV.			
Thrombin IRREV.			

Compound 6.31b



	Progress curve	k_{app} calculation	Jump dilution
Trypsin-3 IRREV.			
β-tryptase IRREV.			
Thrombin IRREV.			
uPA IRREV.			

CHAPTER 7

FROM ABPs TO SMALL MOLECULES:
NOVEL INHIBITORS UAMC-0004206 &
UAMC-0004207

Responsible for design and biochemical characterization of the molecules.

Chapter 7 From ABPs to small molecules: novel inhibitors

UAMC-0004206 & UAMC-00042067

7.1 Introduction

Activity-based protein profiling (ABPP) is a powerful proteomic tool with target identification and visualization applications.^{76,77} Moreover, activity-based probes (ABPs) have been previously used to develop new inhibitors for different enzyme families, including serine proteases.³⁴⁰ Niphakis *et al.* described two different approaches for their design. The first is a target-centric approach, where a selective probe is developed for a specific target. For this route, it is necessary to know the desired target before designing and developing a selective ABP. The second one is called chemocentric and focuses the priority on a small molecule that targets a complex proteome. Through ABPP, the desired target is identified, and *a posteriori*, there is a phase of inhibitor optimization to develop the desired inhibitor (Figure 7.1).⁷⁸

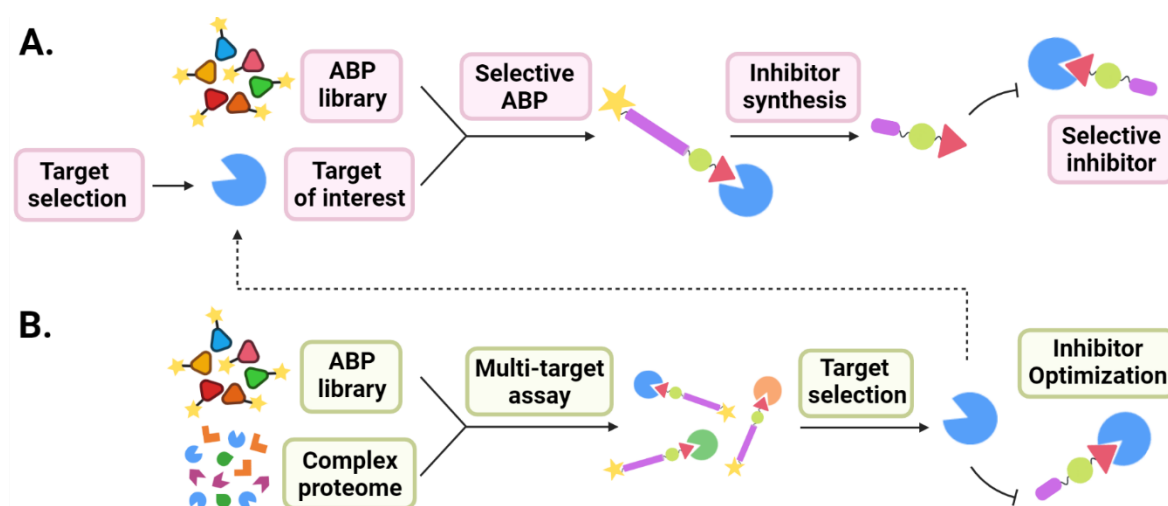


Figure 7.1 From ABPs to inhibitor discovery. **A.** The target-centric approach starts with a target of choice. A selective ABP is designed, leading to selective inhibitors' development. **B.** The chemocentric method screens the ABPs in a complex biological proteome to identify promising compound-target pairs. Later, the target is identified, and the inhibitors can be optimized (e.g., enhancing selectivity).

In **Chapter 6**, we reported ABPs that target trypsin-like serine proteases. These probes were designed with a diaryl phosphonate warhead, and the small molecules had a terminal alkyne that could be coupled to different reporter tags by click chemistry. We described high-affinity probes with an irreversible mechanism of inhibition for a panel of trypsin-like serine proteases. A set of probes with phenyl guanidine as a side chain emerged as a good starting point for inhibitor development. We also demonstrated by proteomics that these compounds target specifically active trypsin-like serine proteases.

In this chapter, we report the synthesis and detailed biochemical characterization of novel inhibitors designed based on the promising phenyl guanidine probes presented earlier (**UAMC-0003970** and **UAMC-0003971**). For the design of the new inhibitors, the probe terminal alkyne was substituted by a benzyl carbamate as previously described for the design of **UAMC-00050** by Joossens *et al.*¹²⁸ to yield **UAMC-0004206** and **UAMC-0004207** (**Figure 7.2**).

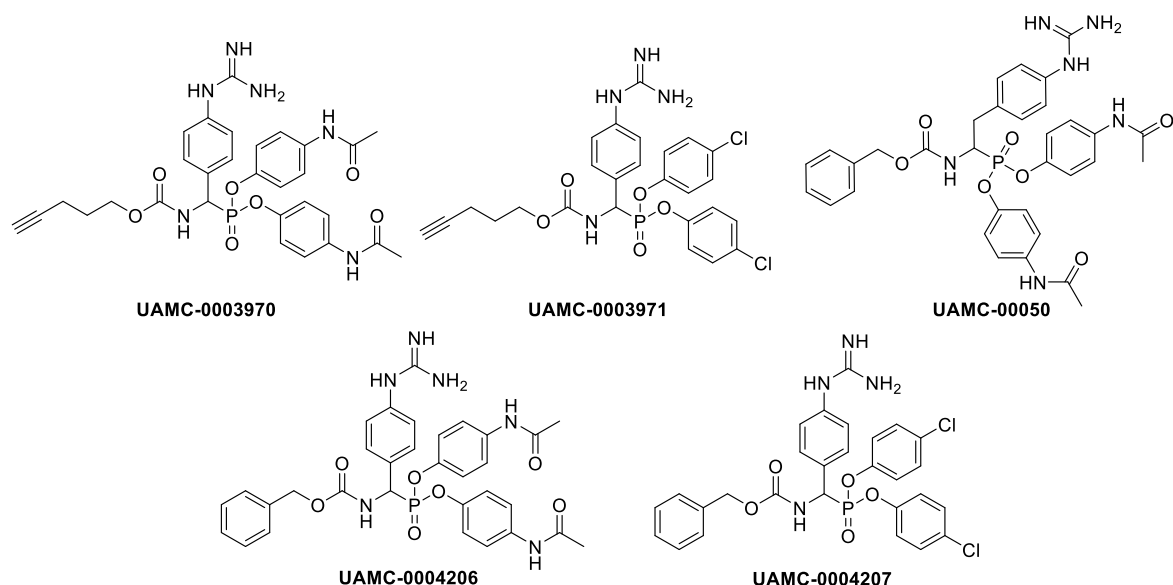
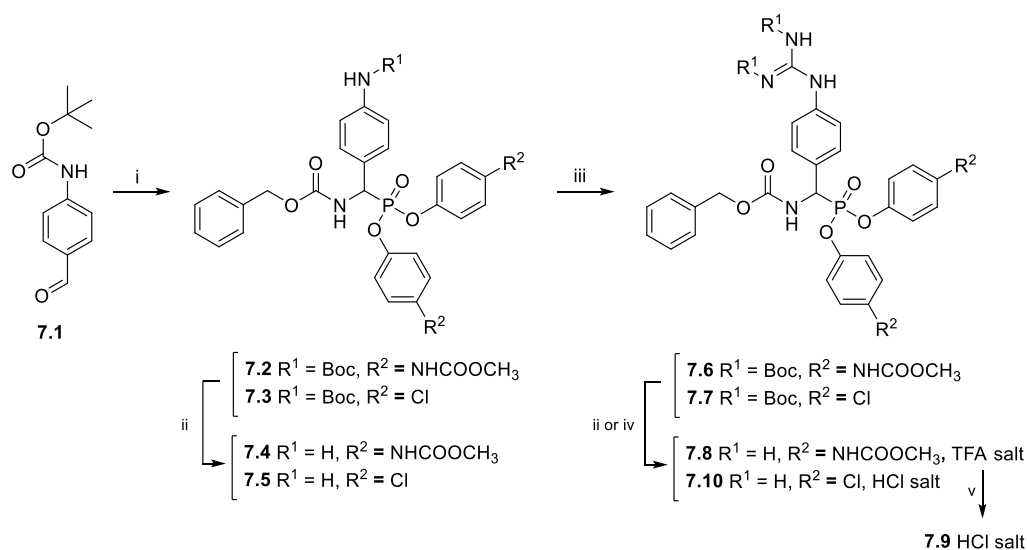


Figure 7.2 Structures of previously reported related analogs; ABPs: UAMC-0003970 and UAMC-0003971; inhibitor: UAMC-00050.

7.2 Results and discussion

7.2.1 Chemistry

The chemical synthesis of compounds UAMC-0004206 and UAMC-0004207 was performed by PhD student Davide Ceradini at the Latvian Institute of Organic Synthesis (LIOS) in Riga, Latvia, within the IT-DED³ consortium. The synthetic route is depicted in **Scheme 7.1** and follows the same steps as the initial synthesis of UAMC-00050 explained in **Chapter 5**.



Scheme 7.1 Synthesis of inhibitors UAMC-0004206 and UAMC-0004207. (i) Benzyl carbamate, triaryl phosphite, 0.1 eq. $\text{Y}(\text{OTf})_3$, $\text{THF}/\text{CH}_3\text{CN}$ (1:1), 0.2 eq. TFAA, rt, 2-4 h; (ii) TFA/DCM (1:1), rt, 30 min to 3 h; (iii) *N, N'*-Bis-Boc-1-Guanylpyrazole, Et_3N or DIPEA, $\text{DCM}/\text{CH}_3\text{CN}$, rt, 96-144 h; (iv) HCl 4 N dioxane, rt, 30 h; (v) DOWEX 1X8 Cl, $\text{EtOH}/\text{H}_2\text{O}$ (2:1), rt, 32 h

For the first step, the Birum-Oleksyszyn reaction, the aldehyde used was the Boc-protected 4-aminobenzaldehyde (**7.1**) with benzyl carbamate and the corresponding triaryl phosphite. Through the optimization and scale-up of UAMC-00050, the Lewis acid $\text{Y}(\text{OTf})_3$ and the addition of TFAA were found to give the best yields and fewer impurities. Thus, these conditions were used to synthesize phosphonates **7.2** and **7.3**. After deprotection of the Boc group, the guanylation was done with *N, N'*-Bis-Boc-1-guanylpyrazole. Acetate or HCl salts in the final compound are desirable when using the compounds *in vivo* or cell-

based assays to avoid abnormal responses.³⁴¹ Hence, deprotection was attempted with HCl 4 N in dioxane to achieve the final compounds (**7.10**) as HCl salts. Unfortunately, for the bis(4-(acetaminophenyl)phosphonate analog, the complete conversion required a long time of reaction (20-24 h), and throughout the reaction time, the formation of the hydrolyzed monoaryl side product was noted. The substitution of HCl 4 N for TFA/DCM (1:1) avoided the formation of the hydrolyzed byproduct and provided a complete conversion after 3 h. Then, the last step involved the salt exchange between the TFA and the chloride. This was done with DOWEX 1x8 Cl resin for 32 h to give the final products UAMC-0004206 (**7.9**).

7.2.2 Biochemical characterization

The newly synthesized compounds were submitted to a detailed biochemical characterization. IC₅₀ values of compounds **7.9** and **7.10** were determined for a panel of four trypsin-like serine proteases, including trypsin-3, tryptase, thrombin, urokinase plasminogen activator (uPA), and cathepsin G (CatG) which presents characteristics from trypsin-like and chymotrypsin-like serine proteases. The values are compared to the previously reported inhibitor **UAMC-00050** and the corresponding alkyne probe analogs **UAMC-0003970** and **UAMC-0003971** (Table 7.1).

Because the diaryl phosphonate compounds, with phenyl guanidine as a side chain, were previously described with an irreversible mechanism for the chosen panel of trypsin-like serine proteases, the IC₅₀ value is not a good description of their inhibitory potency. Therefore, kinetic progress curves were measured to calculate the apparent second-order rate constants (k_{app}) and determine the mechanism of inhibition. The latter was confirmed by jump-dilution assays (Table 7.2).

Table 7.1 IC_{50} values against a panel of trypsin-like serine proteases

#	Trypsin-3	β -tryptase	Thrombin	uPA ^a	CatG ^a
	IC_{50} (μ M)				
UAMC-0004206 (7.9)	0.03 \pm	0.14 \pm	>10	1.13 \pm	0.06 \pm
	0.001	0.006		0.11	0.007
UAMC-0004207 (7.10)	0.003 \pm	0.03 \pm	>10	0.09 \pm	0.03 \pm
	3×10^{-5}	0.002		0.004	0.001
UAMC-0003970	0.04 \pm	0.12 \pm	>10	1.52 \pm	0.13 \pm
	0.015	0.02		0.4	0.01
UAMC-0003971	0.09 \pm	0.07 \pm	>10	0.22 \pm	0.09 \pm
	0.009	0.004		0.06	0.022
UAMC-00050	0.0005 \pm	0.02 \pm	0.39 \pm	0.004 \pm	0.04 \pm
	7×10^{-5}	0.004	0.03 ^{ref.128}	5×10^{-4}	0.003

^a Panel of serine proteases abbreviations: urokinase plasminogen activator (uPA), cathepsin G (CatG)

^b Half maximal inhibitory concentration (IC_{50}) value is the concentration of inhibitor required to reduce the enzyme activity to 50% after a 15 min preincubation with the enzyme at 37 °C and activity measurements as mentioned in the Experimental section. IC_{50} values are calculated from two independent experiments; when SD was higher than three times the average value, a third independent experiment was run (mean \pm SD).

Table 7.2 k_{app} values and the description of the mechanism of inhibition defined by the jump-dilution against a panel of trypsin-like serine proteases: slow-binding (Rev.) or irreversible (Irrev.)

#	Trypsin-3	β -tryptase	Thrombin	uPA ^a	CatG ^a
	k_{app} ($M^{-1} s^{-1}$) ^b				
UAMC-0004206 (7.9)	10x10 ² \pm	35x10 ² \pm	N.D.	286 \pm	33x10 ² \pm
	93	88		7	265
	Irrev.	Irrev.		Irrev.	Irrev.
UAMC-0004207 (7.10)	13x10 ² \pm	71x10 ² \pm	N.D.	30x10 ² \pm	*c
	182	370		202	Rev.
	Irrev.	Irrev.		Irrev.	
UAMC-0003970	358 \pm	20x10 ² \pm	N.D.	215 \pm	14x10 ² \pm
	6	54		7	52
	Irrev.	Irrev.		Irrev.	Irrev.
UAMC-0003971	11x10 ² \pm	45x10 ² \pm	N.D.	25x10 ² \pm	23x10 ² \pm
	164	547		86	347
	Irrev.	Irrev.		Irrev.	Rev.
UAMC-00050	19x10 ⁴ \pm	21x10 ³ \pm	868 \pm	80x10 ³ \pm	*c
	32x10 ³	661	51	5×10^3 ^{ref.128}	
	Rev.	Rev.	Rev.	Irrev.	

^a Panel of serine proteases abbreviations: urokinase plasminogen activator (uPA), cathepsin G (CatG)

^b k_{app} values are calculated from two independent experiments; when SD was higher than three times the average value, a third independent experiment was run (mean \pm SD)

^d k_{app} determination is not possible by curve fitting

N.D.: IC_{50} is greater than 10 μ M, and progress curves were not performed

The IC_{50} values of **7.9** and **7.10** are comparable to the alkyne probe analogs **UAMC-0003970** and **UAMC-0003971** for most proteases (**Table 7.1**). Thus, replacing the terminal alkyne with a benzyl carbamate does not influence the inhibitory potency of the compounds. Only, for trypsin, bis(4-chlorophenyl)phosphonate inhibitor **7.10** ($IC_{50} = 0.003 \pm 3 \times 10^{-5} \mu\text{M}$) is 30-fold more potent than the alkyne probe analog (**UAMC-0003971**). Moreover, the bis(4-chlorophenyl)phosphonate substitution is preferred by all proteases.

Comparing the novel phenyl guanidine inhibitors (**7.9-7.10**) to **UAMC-00050** demonstrates that trypsin-3 and uPA prefer the benzyl guanidine side chain. Noteworthy, inhibitor **7.9** lost about 60 and 280-fold potency for trypsin-3 and uPA compared with **UAMC-00050**, which shares the same aryl phosphonate substitution. In contrast, the IC_{50} values for **7.9** and **7.10** against β -tryptase and CatG remain in the same range. **UAMC-00050** inhibits thrombin with a sub-micromolar potency, whereas the new inhibitors do not inhibit thrombin at any concentration tested.

The k_{app} values confirm the preferences. Trypsin-3 and uPA prefer **UAMC-00050** with over a 100- and 10-fold potency increase. Whereas β -tryptase slightly favors the new phenyl guanidine compounds **7.9** and **7.10**.

The progress curves and jump dilution assays confirmed that the phenyl guanidine compounds present an irreversible mechanism for this panel of trypsin-like serine proteases, except for **7.10**, which, as the alkyne probe **UAMC-0003971**, behaves reversibly with CatG. Contrary, **UAMC-00050** showed a reversible slow-binding mechanism for all proteases tested, except for uPA.

In summary, the new diaryl phosphonate inhibitors **7.9** and **7.10** would be good irreversible inhibitor candidates for trypsin-3, β -tryptase, and CatG. On the other hand, **UAMC-00050** is the most potent compound for trypsin-3 but behaves reversibly. Moreover, it would be the chosen irreversible inhibitor for uPA.

Furthermore, compounds **7.9** and **7.10** were evaluated for their physicochemical properties to elucidate the feasibility of using them in future *in vivo* studies (**Table 7.3**).

Table 7.3 Physicochemical properties of novel inhibitors compared to UAMC-00050.

#	LogD (pH 7.5)	Solubility (μ M)
UAMC-00050	0.2	> 200
UAMC-0004206 (7.9)	0.65	> 200
UAMC-0004207 (7.10)	2.8	< 50

7.3 Conclusion and future perspectives

ABPs have been used previously for the design of new inhibitors.⁷⁸ In this chapter, we report two newly synthesized inhibitors with a diaryl phosphonate warhead and phenyl guanidine as a side chain designed from previously reported irreversible ABPs. The synthetic route used was performed at LIOS in Riga, and the biochemical evaluation was performed at UAMC.

To determine the inhibitory potency of the new inhibitors, the IC_{50} values were determined. However, phenyl guanidine diaryl phosphonates were described in **Chapter 6** with an irreversible mechanism. Therefore, the IC_{50} values are not suitable for measuring their potency. Kinetic progress curves were measured to calculate their k_{app} . The inhibitory potency was compared to the alkyne probes **UAMC-0003970** and **UAMC-0003971** and the inhibitor **UAMC-00050**.

Replacing the terminal alkyne with a benzyl carbamate did not significantly influence the inhibitory potency on a panel of trypsin-like serine proteases. Therefore, this approach is a convenient pathway to design new inhibitors from promising ABPs. The progress curves confirmed that **UAMC-0004206 (7.9)** and **UAMC-0004207 (7.10)** have an irreversible mechanism with all proteases tested besides thrombin which is not inhibited at the concentrations tested. In contrast, **UAMC-00050** is only irreversible with uPA. Despite the

mechanism of inhibition, trypsin-3, thrombin, and uPA prefer the benzyl guanidine side chain. Contrary, β -tryptase, and CatG do not display any preference.

The physicochemical properties of the compounds showed moderate LogD_{7.5} values. However, the solubility of **7.10** was lower than **7.9** and **UAMC-00050**. Therefore, inhibitor **7.9**, with better solubility and acceptable LogD values, would be the choice for future experiments. However, to use these compounds in *in vivo* studies, their stability in different media should be assessed.

7.4 Experimental section

7.4.1 Chemistry

General information: All commercially available reagents were used as received unless otherwise specified. All reactions were carried out under an argon atmosphere in oven-dried glassware with magnetic stirring. Dry solvents were dispensed by a solvent purification system using dry neutral alumina cartridges. ^1H and proton decoupled ^{13}C NMR spectra were obtained on a 400 MHz Bruker Avance 400 spectrometer at room temperature at 400 and 101 MHz, respectively. Chemical shifts (δ) are reported in parts per million (ppm). Multiplicities are given as s (singlet), d (doublet), t (triplet), q (quartet), and m (multiplet). Complex splittings are described by a combination of these abbreviations, i.e., dd (doublet of doublets). Reaction conversion was estimated by thin-layer chromatography (TLC) on aluminium sheets coated with silica gel 60 F₂₅₄ and visualized by ultraviolet light or by LC-MS on Waters Acquity UPLC H-class instrument, column Waters Acquity UPLC BEH-C18, 2.1 × 50 mm, 1.7 μm , eluent 5–95% MeCN in 0.1% aq. HCOOH; flow rate: 0.8 ml/min; detection Waters PDA Detector (200–300 nm). GC-MS analysis was performed on Agilent 5975C Series GC/MSD spectrometer, column HP-5MS 5% Phenyl Methyl Silox, 30 m × 250 μm × 0.25 μm , temperature 50–275 °C, carrier gas helium, flow rate 1 ml/min. High-resolution mass spectra were recorded on a Waters Synapt GII Q-ToF UPLC/MS system, positive ESI mode.

Benzyl ((bis(4-acetamidophenoxy)phosphoryl)(4-((tert-butoxycarbonyl)amino)phenyl)methyl) carbamate (7.2) In a dry 100 ml flask equipped with a magnetic stirrer bar were added **7.1** (5.00 g, 0.023 mol, 1.0 eq.), the $\text{Y}(\text{OTf})_3$ (1.23 g, 2.3 mmol, 0.1 eq.) dissolved in 17 ml of dry CH_3CN , benzyl carbamate (3.48 g, 0.023 mol, 1.0 eq.), tris(4-acetamidophenyl) phosphite (11.07 g, 0.023 mol, 1.0 eq.) followed by 17 ml of dry THF. The solution was stirred for 4 h. The solvent was removed. The residue was suspended in 200 ml of EtOH 96%, and the solution was poured into 500 ml of EtOAc and stirred for 2 h at 0 °C, filtered, and dried in the vacuum to yield **7.2** (11.78 g, 0.016 mol, 63% yield) as yellow solid. ^1H NMR

(400 MHz, DMSO- d^6) δ (ppm) 9.97 (2H, s), 9.41 (1H, s), 8.78 (1H, d, $J = 8$ Hz), 7.49 (8H, m), 7.35 (5H, m), 6.98 (2H, d, $J = 8$ Hz), 6.90 (2H, d, $J = 8$ Hz), 5.45 (1H, dd, $J = 24.8$ Hz), 5.09 (2H, dd, $J = 32.1$ Hz), 2.03 (6H, d, $J = 4$ Hz), 1.47 (9H, s). ^{13}C NMR (100 MHz, DMSO- d^6) δ (ppm) 168.7, 156.5, 153.2, 145.5, 140.0, 137.1, 136.9, 128.8, 128.4, 128.2, 121.0, 120.6, 118.4, 79.6, 66.6, 53.5, 28.6, 24.4. ^{31}P NMR (162 MHz, DMSO- d^6) δ (ppm) 15.23. HPLC purity 87%. HRMS (ESI+) m/z calculated for $\text{C}_{36}\text{H}_{39}\text{N}_4\text{O}_9\text{P}$ $[\text{M}+\text{Na}]^+$ was 725.2336, mass measured 725.2352.

Benzyl ((bis(4-chlorophenoxy)phosphoryl)(4-((tert butoxycarbonyl)amino)phenyl)methyl) carbamate (7.3) In a dry 50 ml flask equipped with a magnetic stirrer bar were added **7.1** (1.00 g, 4.5 mmol, 1.0 eq.), $\text{Y}(\text{OTf})_3$ (241 mg, 4.5 mmol, 0.1 eq.) dissolved in 1.1 ml of dry CH_3CN , benzyl carbamate (680 mg, 4.5 mmol, 1.0 eq.), and tris(4-chlorophenyl) phosphite (2.08 g, 4.5 mmol, 1.0 eq.) followed by 1.1 ml of dry THF. The solution was stirred for 2 h. The solvent was removed, and the residue was purified by chromatography (petroleum ether/EtOAc gradient) to yield **7.3** (2.60 g, 3.15 mmol, 70% yield). ^1H NMR (400 MHz, DMSO- d^6) δ (ppm) 9.41 (1H, s), 8.83 (1H, d, $J = 8$ Hz), 7.47 (4H, q, $J = 8$ Hz), 7.37 (8H, m), 7.11 (2H, d, $J = 8$ Hz), 7.02 (2H, d, $J = 8$ Hz), 1.47 (9H, s). ^{13}C NMR (100 MHz, DMSO- d^6) δ (ppm) 156.3, 153.2, 149.4, 140.2, 137.1, 130.3, 129.8, 129.3, 128.5, 127.6, 122.6, 122.5, 118.4, 117.4, 79.7, 66.7, 53.6, 28.5. ^{31}P NMR (162 MHz, DMSO- d^6) δ (ppm) 15.40. HPLC purity 81%. HRMS (ESI+) m/z calculated for $\text{C}_{32}\text{H}_{31}\text{Cl}_2\text{N}_2\text{O}_7\text{P}$ $[\text{M}+\text{Na}]^+$ 679.1147, mass measured 679.1144.

4-(((benzyloxy)carbonyl)amino)(bis(4-acetamidophenoxy)phosphoryl)methyl) benzenaminium trifluoroacetate salt (7.4) In a 250 ml flask were added **7.2** (6.60 g, 8.2 mmol, 1.0 eq.), TFA/DCM 1:1 (66 ml), and the mixture was stirred for 45 min. The solvent was removed, and the residue was dissolved in 66 ml of dry EtOH. The mixture was poured into 660 ml of MTBE at 0°C and stirred at 0°C for 2 h, filtered under vacuum, washed with 330 ml of MTBE, and dry overnight to yield **7.4** (7.57 g, 8.11 mmol, 99% yield). ^1H NMR (400 MHz, DMSO- d^6) δ (ppm) 10.13 (2H, s), 8.94 (1H, d, $J = 12$ Hz), 7.74 (2H, d, $J = 8$ Hz), 7.56 (4H, m), 7.37 (6H, m), 6.98 (2H, d, $J = 8$ Hz), 6.91 (2H, d, $J = 8$ Hz), 5.61 (1H, dd, $J = 24.8$ Hz), 5.10

(2H, dd, $J = 32.1$ Hz), 2.04 (6H, s). ^{13}C NMR (100 MHz, DMSO- d^6) δ (ppm) 168.7, 156.5, 145.2, 137.0, 134.8, 132.7, 130.2, 128.8, 128.4, 123.6, 121.0, 120.7, 66.8, 53.5, 51.9, 24.4. ^{31}P NMR (162 MHz, DMSO- d^6) δ (ppm) 14.69. HPLC purity 97%. HRMS (ESI+) m/z calculated for $\text{C}_{31}\text{H}_{31}\text{N}_4\text{O}_7\text{P}$ [M+Na] $^+$ 625.1828, mass measured 625.1841.

4-(((benzyloxy)carbonyl)amino)(bis(4-chlorophenoxy)phosphoryl)methyl

benzenaminium trifluoroacetate salt (7.5) In a 50 ml flask were added **7.3** (840 mg, 1.0 mmol, 1.0 eq.) and TFA/DCM 1:1 (8.5 ml), and the mixture was stirred for 3 h. The solvent was removed to get **7.5** (804 mg, 0.99 mmol, 99% yield). ^1H NMR (400 MHz, DMSO- d^6) δ (ppm) 8.97 (1H, d, $J = 12$ Hz), 7.72 (2H, d, $J = 8$ Hz), 7.38 (11H, m), 7.11 (2H, d, $J = 8$ Hz), 7.02 (2H, d, $J = 8$ Hz), 5.70 (1H, dd, $J = 24.8$ Hz), 5.09 (2H, dd, $J = 32.1$ Hz). ^{13}C NMR (100 MHz, DMSO- d^6) δ (ppm) 156.4, 149.0, 137.0, 133.7, 137.5, 130.3, 130.2, 129.9, 128.9, 128.9, 128.5, 123.3, 122.6, 122.5, 66.8, 53.6. ^{31}P NMR (162 MHz, DMSO) δ (ppm- d^6) 15.33. HPLC purity 87%. HRMS (ESI+) m/z calculated for $\text{C}_{27}\text{H}_{23}\text{Cl}_2\text{N}_2\text{O}_5\text{P}$ [M+Na] $^+$ 579.0619, mass measured 579.0624.

Benzyl(E)-((bis(4-acetamidophenoxy)phosphoryl)(4-(N,N'-bis(tert-butyloxycarbonyl)

guanidino)phenyl)methyl)carbamate (7.6) A mixture of **7.4** (5.50 g, 7.1 mmol, 1.0 eq.), N, N'-Bis-Boc-1-Guanylpirazole (2.66 g, 8.52 mmol, 1.2 eq.) was dissolved in 16 ml of dry DCM/MeCN 1:1 (final concentration 1M), TEA (1.49 ml, 0.011 mol, 1.5 eq.) was added and the mixture stirred at rt for 96 h. The solvent was removed with rotavapor. The solid was first purified with a slurry residue in 110 ml (20 ml for 1g of S.M.) of Petroleum Ether/EtOAc 2:1 for 2 h at rt, filtered, washed with 55 ml of Petroleum Ether/EtOAc 2:1, and dried under vacuum. The product was purified by silica column (1600 ml DCM/CH₃OH 19:1 and 800 ml DCM/CH₃OH 9:1) to yield **7.6** (4.02 g, 4.61 mmol, 65% yield). ^1H NMR (400 MHz, DMSO- d^6) δ (ppm) 11.41 (1H, s), 10.03 (1H, s), 9.96 (2H, s), 8.84 (1H, d, $J = 8$ Hz), 7.58 (4H, s), 7.51 (4H, m), 7.35 (5H, m), 6.98 (2H, d, $J = 8$ Hz), 6.91 (2H, d, $J = 12$ Hz), 5.54 (1H, dd, $J = 20.8$ Hz), 5.10 (2H, dd, $J = 32.1$ Hz), 2.02 (6H, s), 1.51 (9H, s), 1.40 (9H, s). ^{13}C NMR (100 MHz, DMSO- d^6) δ (ppm) 168.7, 163.1, 156.5, 153.2, 152.5, 145.3, 137.1, 137.0, 131.3, 129.3, 128.8, 128.4, 123.1, 121.1, 120.9, 120.6, 83.9, 79.4, 60.7, 53.5, 28.1, 24.4. ^{31}P NMR (162 MHz, DMSO- d^6)

δ (ppm) 14.93. HPLC purity 97%. HRMS (ESI+) m/z calculated for $C_{42}H_{50}N_6O_{11}P$ $[M+H]^+$ 845.3290, mass measured 845.3275.

Benzyl(E)-((bis(4-chlorophenoxy)phosphoryl)(4-(N,N'-bis(tert-butyloxycarbonyl)guanidino)phenyl)methyl)carbamate (7.7) A mixture of **7.5** (794 mg, 1.0 mmol, 1.0 eq.), N, N'-Bis-Boc-1-Guanylpurazole (378 mg, 1.2 mmol, 1.2 eq.) was dissolved in 2.2 ml DCM/MeCN 1:1, DIPEA (0.261 ml, 1.5 mmol, 1.5 eq.) was added, and the mixture was stirred at rt for 96 hours. The solvent was removed, and the solid was purified by silica chromatography (1000 ml Petroleum Ether/EtOAc 5:1 and 500 ml Petroleum Ether/EtOAc 2:1) to yield **7.7** (383 mg, 0.45 mmol, 45% yield). 1H NMR (400 MHz, DMSO- d^6) δ (ppm) 11.42 (1H, s), 10.03 (1H, s), 8.89 (1H, d, $J = 8$ Hz), 7.58 (4H, q, $J = 8$ Hz), 7.38 (9H, m), 7.11 (2H, d, $J = 8$ Hz), 7.01 (2H, d, $J = 8$ Hz), 5.63 (1H, dd, $J = 20.8$ Hz), 5.10 (2H, dd, $J = 32.12$ Hz), 1.51 (9H, s), 1.40 (9H, s). ^{13}C NMR (100 MHz, DMSO- d^6) δ (ppm) 163.1, 156.4, 153.3, 152.5, 149.0, 137.3, 137.0, 130.7, 130.2, 129.6, 129.3, 128.8, 128.5, 123.3, 122.7, 122.5, 117.4, 83.9, 79.4, 66.8, 53.6, 28.1. ^{31}P NMR (162 MHz, DMSO- d^6) δ (ppm) 15.16. HPLC purity 95%. HRMS (ESI+) m/z calculated for $C_{38}H_{42}Cl_2N_4O_9P$ $[M+H]^+$ 799.2066, mass measured 799.2090.

Amino((4-(((benzyloxy)carbonyl)amino)(bis(4-acetamidophenoxy)phosphoryl)methyl)phenyl)amino)methaniminium trifluoroacetate salt (7.8) In a 50 ml flask was added **7.6** (1.24 g, 1.4 mmol, 1.0 eq.) and 12 ml of TFA/DCM 1:1, and the solution was stirred for 3 h. The solvent was removed, and the residue was dissolved in 12 ml of dry EtOH. The solution was poured into cold MTBE (120 ml) and stirred for 1 h at 0°C. The solid was filtered in vacuum and dried overnight to yield **7.8** (1.07 g, 1.35 mmol, 97% yield). 1H NMR (400 MHz, DMSO- d^6) δ (ppm) 9.99 (2H, s), 9.91 (1H, s), 8.92 (2H, d, $J = 8$ Hz), 7.68 (2H, d, $J = 8$ Hz), 7.57 (3H, s), 7.53 (4H, m), 7.37 (5H, m), 7.27 (2H, d, $J = 8$ Hz), 7.00 (2H, d, $J = 12$ Hz), 6.95 (2H, d, $J = 12$ Hz), 5.58 (1H, dd, $J = 24.8$ Hz), 5.09 (2H, dd, $J = 36.1$ Hz), 2.02 (6H, s). HPLC purity 96%. HRMS (ESI+) m/z calculated for $C_{32}H_{34}N_6O_7P$ $[M+H]^+$ 645.2258, mass measured 645.2227.

Amino((4-(((benzyloxy)carbonyl)amino)(bis(4-acetamidophenoxy)phosphoryl)methyl)phenyl) amino)methaniminium chloride salt (7.9) In a 5 ml flask were added **7.8** (104 mg, 1.35 mmol, 1.0 eq.), 3 ml of EtOH/H₂O (2:1) and 1.01 g of DOWEX 1X8 Cl, and the mixture was stirred for 32 h. Then, the resin was removed by filtration through a glass filter, and the solvent was removed with rotavapor. The residue was dissolved in 1 ml of EtOH and precipitated in MTBE at rt. The mixture was stirred for 1 h and filtered on a glass filter to yield **7.10** (65 mg, 0.96 mmol, 71% yield) as a white-off solid. ¹H NMR (400 MHz, DMSO-*d*⁶) δ (ppm) 9.99 (2H, s), 9.91 (1H, s), 8.92 (2H, d, *J* = 8 Hz), 7.68 (2H, d, *J* = 8 Hz), 7.57 (3H, s), 7.53 (4H, m), 7.37 (5H, m), 7.27 (2H, d, *J* = 8 Hz), 7.00 (2H, d, *J* = 12 Hz), 6.95 (2H, d, *J* = 12 Hz), 5.58 (1H, dd, *J* = 24.8 Hz), 5.09 (2H, dd, *J* = 36.1 Hz), 2.02 (6H, s). HPLC purity 95%. HRMS (ESI+) *m/z* calculated for C₃₂H₃₄N₆O₇P [M+H]⁺ 645.2258, mass measured 645.2227.

Amino((4-(((benzyloxy)carbonyl)amino)(bis(4-chlorophenoxy)phosphoryl)methyl)phenyl)amino) methaniminium chloride salt (7.10)

In a 25 mL flask were added **7.7** (500 mg, 0.63 mmol) and HCl 4N dioxane (6 mL), then the mixture was stirred for 30 h at rt. The solvent was removed, and the residue was dissolved in absolute EtOH (5 mL), then dropped in cold MTBE (200 mL), stirred for 1 h at 0°C, filtered, and dried in a vacuum to yield **7.10** (335 mg, 0.50 mmol, 80% yield). ¹H NMR (400 MHz, DMSO-*d*⁶) δ (ppm) 10.18 (1H, s), 8.97 (1H, d, *J* = 8 Hz), 7.69 (2H, m), 7.63 (3H, s), 7.38 (9H, m), 7.26 (2H, d, *J* = 8 Hz), 7.13 (2H, d, *J* = 8 Hz), 7.07 (2H, d, *J* = 8 Hz), 5.67 (1H, dd, *J* = 24.8 Hz), 5.08 (2H, dd, *J* = 32.1 Hz). ¹³C NMR (101 MHz, DMSO-*d*⁶) δ (ppm) 155.9, 148.8, 148.4, 136.5, 135.5, 131.8, 129.8, 129.6, 129.4, 128.4, 123.9, 122.2, 122.0, 66.3. ³¹P NMR (162 MHz, DMSO) δ (ppm) 14.86. HPLC purity 95.2%.

7.4.2 Biochemical characterization

7.4.2.1 Determination of IC₅₀ values

The IC₅₀ value is defined as the concentration of inhibitor required to reduce the enzyme activity to 50% after a 15 min preincubation with the enzyme at 37 °C before adding the

substrate. The IC_{50} values were determined using a spectrophotometric assay. All the experiments were conducted in duplicate in buffer. The readout consisted of evaluating the protease-mediated release of the chromophore *para*-nitroaniline (pNA) or fluorophore 7-amino-4-methyl coumarin (AMC) moieties from the respective substrates. Enzymatic activity was measured for 30 min at 37 °C. All compounds were initially screened at three concentrations (10, 1, and 0.1 μ M) to estimate the range of the IC_{50} value. Those able to reduce protease activity by at least 50% at a concentration of 10 μ M were submitted to an exact IC_{50} determination. The final IC_{50} values of the most potent inhibitors were the average of two independent experimental results. A third independent experiment was performed when the standard deviation of the two independent experiments was higher than three times the IC_{50} value. IC_{50} values were obtained by fitting the data with the four-parameter logistics equation using GraphPad Prism 9.

The conditions for each protease are described as follows, the concentration of substrate used was at the corresponding K_m .

Trypsin-3 (recombinant trypsin-3, R&D) and fluorogenic substrate tosyl-GPR-AMC (K_m = 22.5 μ M) were used in Tris buffer (100 mM Tris HCl, 100 mM Tris base, 1 mM $CaCl_2$) at pH 8.0 (25°C). Tryptase (recombinant tryptase β -2, EnzoLife Sciences) and fluorogenic substrate Boc-Gln-Ala-Arg-AMC (K_m = 250 μ M) were used in Tris buffer (50 mM Tris, 120 mM NaCl, 0.1 mg/mL BSA, 0.1 mg/mL heparin) at pH 8.0 (25°C). Thrombin (recombinant thrombin, R&D) and fluorogenic substrate Boc-VPR-AMC (K_m = 15 μ M) were used in TRIS buffer (50 mM Tris HCl, 50 mM Tris base, 10 mM $CaCl_2$, 150 mM NaCl) at pH 8.3 (25°C). uPa (recombinant urokinase plasminogen activator, HYPHEN BioMed) and chromogenic substrate *pyro*-Glu-Gly-Arg-pNA (K_m = 80 μ M) were used in HEPES buffer (50 mM HEPES) at pH 8.1 (25°C). Cathepsin G (cathepsin G human neutrophil, Sigma-Aldrich) and fluorogenic substrate Suc-AAPF-AMC (K_m = 130 μ M) were used in Tris buffer (50 mM Tris, 120 mM NaCl) at pH 8.0 (25°C).

7.4.2.2 Kinetic experiments and determination of k_{app}

For a simple pseudo-first-order inactivation process, the activity after incubation with inhibitor (v_i) varies with the inhibitor concentration (i), as described in the following equation: $v_i = v_0 \cdot e^{-kit}$, where v_0 is the activity in the absence of an inhibitor, k is the second-order rate constant of inactivation, and t is the time. The inactivation rate constant was determined from the time course of inhibition.

Kinetic assays were performed in the following manner. The inhibitor was mixed with the substrate, and the buffer solution with the enzyme was added at the time zero. The progress curves show the release of pNA or AMC as a function of time. Initially, no inhibitor is bound to the enzyme, and the tangent to the progress curve (dA/dt) is proportional to the free enzyme concentration. The free enzyme concentration decreases over time due to inhibitor binding kinetics, as described above. Progress curves were recorded in pseudo-first-order conditions ($[I]_0 \gg [E]_0$) and with less than 10% conversion of the substrate during the entire time course. In these conditions, dA/dt decreases exponentially with time. The progress curves were fitted with the integrated rate equation with GraFit7 to yield a value for k_{obs} , a pseudo-first-order rate constant. $A_t = A_0 + v_s \cdot t + (v_i - v_s) \cdot (1 - e^{-k_{obs} \cdot t}) / k_{obs}$, where A_t is the absorbance at time t , A_0 is the absorbance at time zero, v_i is the initial rate, and v_s is the velocity at the steady-state.

The apparent second-order rate constant (k_{app}) was calculated from the slope of the linear part of the plot of k_{obs} vs. the inhibitor concentration ($[I]_0$). In the case of competition between the inhibitor and the substrate, k_{app} is smaller than the “real” second-order rate constant k discussed above because a certain fraction of the enzyme is present as an enzyme-substrate complex. k_{app} depends on the substrate concentration used in the experiment, as described by Lambeir *et al.* 1996.¹²⁵

7.4.2.3 Determination of inhibition type

To monitor the dissociation of the inhibitor-enzyme, aliquots of the enzyme were incubated at 37°C without and with the inhibitor at a concentration 10 times higher than

its IC₅₀. The enzyme concentration was 2.5 times higher than the concentration used for the IC₅₀ determinations. After 15 min, the aliquots were diluted 10-fold or 100-fold into the substrate concentration and assay buffer used for the IC₅₀ determination. The dissociation of the enzyme-inhibitor complex was monitored by substrate hydrolysis over time.¹²⁹

7.4.3 Physicochemical properties

7.4.3.1 Determination of Log D

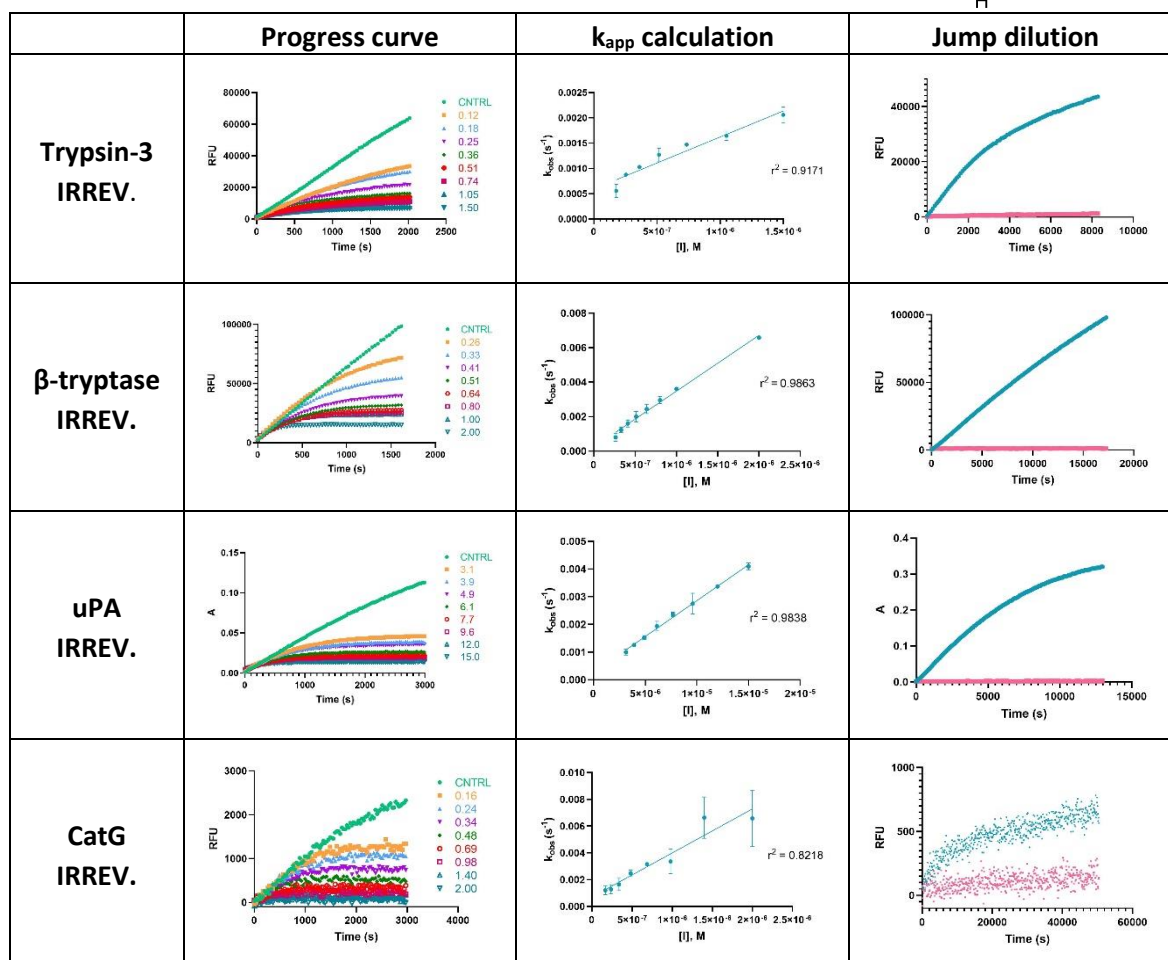
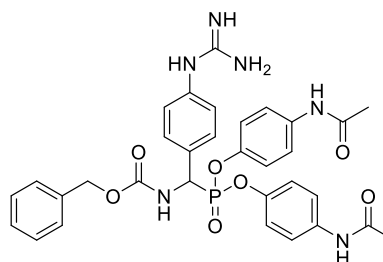
A total of 40 µL of a 10 mM stock solution in DMSO was added to 1.960 mL of a mixture of octanol and phosphate buffer saline (PBS), pH 7.4 (1/1). Octanol was first saturated with PBS, and PBS was first saturated with octanol before the two solvents were mixed. After two hours of shaking at room temperature, the two layers were separated. A total of 10 µL of each layer was added to 390 µL of CH₃OH before the sample was analyzed with LC/MS/MS. The logD is calculated from the formula: $\text{LogD} = \log(\text{AUC}_{\text{Octanol}}/\text{AUC}_{\text{PBS}})$. The experiment was done in duplicate.

7.4.3.2 Solubility

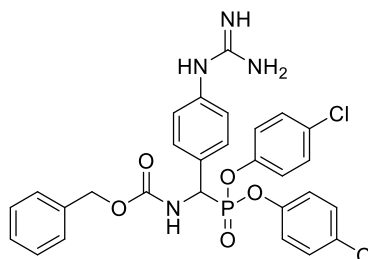
A total of seven different dilutions of an initial 10 mM test compound solution were prepared in DMSO. Each dilution was further diluted in PBS pH 7.4 to give a final DMSO concentration of 2% and a final test compound concentration range of between 3.1 µM and 200 µM (4 µL DMSO solution in 196 µL buffer solution). Two replicates were prepared per concentration in a 96-well microtiter plate. The plates were incubated for 2 h at 37 °C. Absorbance was measured at 620 nm, and solubility was determined by an increase in absorbance (turbidimetry).

7.5 Supplementary data

UAMC-0004206 (7.9)



UAMC-0004207 (7.10)



	Progress curve	k_{app} calculation	Jump dilution
Trypsin-3 IRREV.			
β-tryptase IRREV.			
uPA IRREV.			
CatG REV.		N.D.	

CHAPTER 8

CONCLUSIONS AND FUTURE PERSPECTIVES

Chapter 8 **Conclusions and future perspectives**

The first goal of this doctoral thesis was the evaluation of the potential role of serine proteases in the pathophysiology of Dry eye disease (DED) and Irritable bowel syndrome (IBS). The role of other protease families in DED has been previously widely described. In particular, the role of metalloprotease MMP-9 is well defined and considered a DED biomarker among clinicians.³⁴² However, the role of serine proteases is not yet fully understood, and research considering them as therapeutic targets has just emerged. For instance, the treatment with α -amino diaryl phosphonate serine protease inhibitor UAMC-00050 in a DED experimental model could reduce tissue damage parameters and pro-inflammatory markers.¹⁸⁵ On the other hand, for IBS, the study of serine proteases in abdominal pain and visceral hypersensitivity is somewhat more extensively studied.¹⁵¹ However, the use of serine protease inhibitors as therapeutic agents has been little explored.¹⁸⁶ Interestingly, the local or intraperitoneal administration of inhibitor UAMC-00050 in a rat model with TNBS-induced colitis in the post-inflammatory phase and an acetic acid neonatal mice model could reduce visceral hypersensitivity.^{295,296,298}

The results of these experiments gave a proof of concept of the involvement of serine proteases in DED and IBS. Nevertheless, UAMC-00050 is a multi-target trypsin-like serine protease inhibitor, thus, it has a high affinity for different proteases within the family. Therefore, it is not possible to identify the specific proteases which are upregulated and inhibited in these experimental settings. Hence, the primary goal of this doctoral thesis was to develop a tool to unequivocally determine the activity of upregulated proteases in biological samples. For this, activity-based protein profiling (ABPP) was chosen as a promising proteomic tool.

8.1 Activity-based probes for biomarker identification

ABPP is a powerful proteomic tool that enables the detection and visualization of active enzymes within a complex proteome.³¹⁹ During this doctoral thesis, we have developed an extensive library of activity-based probes (ABPs) targeting the trypsin-like serine protease family. The α -amino diaryl phosphonate warhead is widely used for this enzymatic family due to its high selectivity over other enzymes and protease families.⁹⁰ Moreover, UAMC-00050, the lead compound, belongs to this class.¹²⁹ Therefore, α -amino diaryl phosphonate was the warhead of choice for our ABP library. Even though there are probes previously described in literature targeting trypsin-like serine proteases, there is a lack of chemical diversity as most of the reported probes contain natural amino acids as a selectivity-enhancing group. Thus, the newly synthesized library includes different basic polar residues to achieve a wide-ranging chemical diversity.

The establishment of an efficient synthetic route with the potential of combining a variety of reporter tags in the last step by “click chemistry” was implemented. A combination of different side chains and the modification of the electrophilicity of the diphenyl phosphonate achieved the desired chemical diversity (**Figure 8.1**). An extensive library of 24 alkyne probes and 17 desthiobiotin and biotin probes was synthesized. Alternatively, the alkyne probes could be conjugated to other reporter tags, which would enable other applications, such as visualization by fluorescence or positron emission tomography (PET).

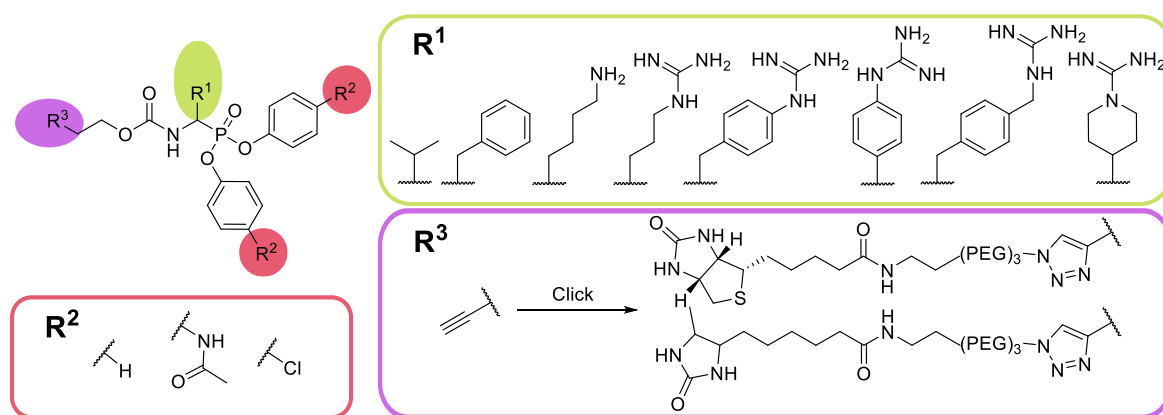


Figure 8.1 Design of the activity-based probe (ABPs) library with the different modifications.

To fully characterize the biochemical activity of the newly synthesized probes, a panel of different serine proteases was chosen by their implication in different immune and inflammatory responses. The biochemical protocol to determine the IC₅₀ values for β -tryptase was introduced in the laboratory of Medicinal Chemistry (UAMC), and the existing protocols for urokinase plasminogen activator (uPA) were optimized and validated. For trypsin-3, thrombin, cathepsin G, chymotrypsin, and neutrophil elastase, the collaboration with the Laboratory for Intestinal Neuroimmune Interactions at KU Leuven and the Laboratory of Medical Biochemistry at the University of Antwerp was of utmost help. Further, the protocols to determine the kinetic curves and the mechanism of inhibition for trypsin-3, β -tryptase, thrombin, and uPA were developed at UAMC. The protocols for cathepsin G were developed at the Laboratory of Medical Biochemistry and used and validated at UAMC. Jump dilution assays corroborated the mechanism of inhibition. The protocols were developed at UAMC.

The detailed biochemical characterization of the new probes led to identifying some high-affinity compounds. More in detail, the benzyl guanidine probes presented the highest inhibitory potencies for trypsin-3, β -tryptase, and uPA. Even though these compounds are designed to inhibit serine proteases irreversibly, these only showed an irreversible mechanism for uPA, whereas for trypsin-3, β -tryptase, thrombin, and cathepsin G these presented a reversible slow-binding mechanism. On the other hand, the phenyl guanidine probes inhibit irreversibly with high-affinity trypsin-3, β -tryptase, and cathepsin G. Thrombin does not present a high affinity for these families of compounds. Instead, the preferred probe for thrombin is the 4-piperidine-1-carboximidamide side chain, which shows an irreversible inhibition and selectivity over β -tryptase, uPA, and CatG.

The reason for the difference in the mechanism of inhibition between the benzyl guanidine and the phenyl guanidine probes is not yet understood. Two hypotheses could explain this (**Figure 8.2**). The first one is the formation of a covalent bond between the phosphonate and the serine on the active site, which is rapidly hydrolyzed. In the second, the covalent bond is not formed due to the geometry and proximity of the probe to the serine in the

active site. Nevertheless, the probe is well positioned to create a high-affinity complex. To corroborate these hypotheses, one could first run molecular modeling to computationally recreate the probe allocation within the active site and the possible formation of a covalent bond. Alternatively, a crystal structure of the protease with the desired probe could elucidate whether one of the phenolates of the phosphonate acts as a leaving group to form the covalent bond. Even though this experimental technique could help explain the mechanism of inhibition, it would not be undoubtedly proof as the phenolate could be hydrolyzed without forming the covalent bond by the process of aging.

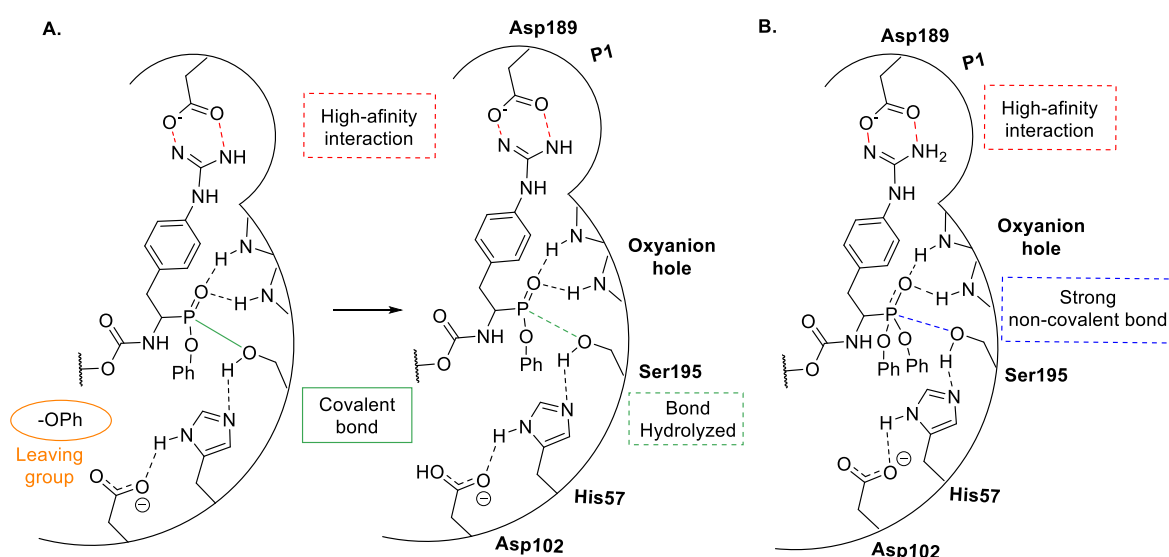


Figure 8.2 Hypothesis for a reversible slow-binding mechanism. A) The covalent bond is formed but rapidly hydrolyzed, forming high-affinity interactions. B) The position of the warhead is not ideal for the formation of a covalent bond, but high-affinity interactions are possible.

Last, we aimed to label proteases in complex biological samples to identify active trypsin-like serine proteases participating in physiological processes. We demonstrated that both irreversible and slow-binding probes could label recombinant proteases and trypsin released from mast cell degranulation in SDS-PAGE. Interestingly, this indicates that irreversible binding is not needed to label proteases under denaturing conditions. As a next step, it would be interesting to label proteases from biological samples of DED and IBS patients and identify upregulated proteases. Moreover, exploring other analytical techniques, such as mass spectrometry, would be of utmost interest.

Recently, the Laboratory for Intestinal Neuroimmune Interactions at KU Leuven has proven that the novel alkyne probes can inhibit trypsin-like serine protease activity against rectal biopsy supernatants from IBS patients. This experiment was performed with bis(4-chlorophenyl)phosphonate alkyne probes with arginine (**6.33b**), benzyl guanidine (**6.36b**), and phenyl guanidine (**6.39b**) as a side chain, the diphenyl phosphonate alkyne probe with 4-piperidine-1-carboximidamide (**6.41b**) as a side chain and the proline-lysine alkyne probe (**6.31b**). The results show that **6.36b** and **6.39b** present greater inhibitory potencies for these samples correlating with their inhibitory potencies against recombinant proteases (**Figure 8.3**).

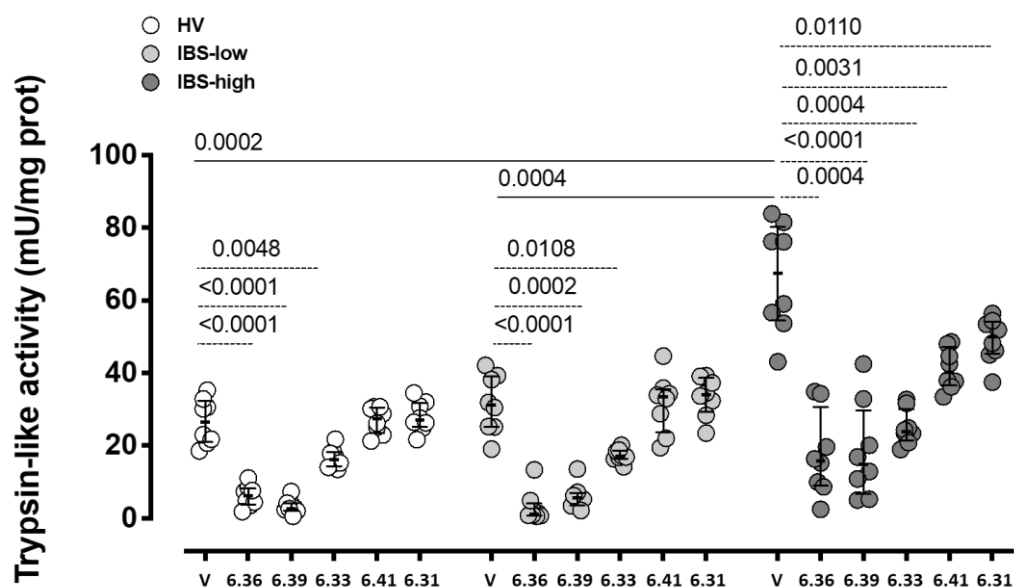


Figure 8.3 Translational potential of novel alkyne probes, inhibiting the trypsin-like serine protease activity against rectal biopsy supernatant. The experiments were conducted in supernatants from 8 representative subjects from each group (healthy volunteers, IBS-low, and IBS-high). The compounds at a concentration of 1 μ M were pre-incubated with the supernatants for 15 min at 37°C. The trypsin-like activity is expressed as mU/mg protein. The P values represented as continuous lines refer to the comparison between groups treated with vehicle (HV vs. IBS-high and IBS-low vs. IBS-high). The P values represented as dotted lines refer to the comparison between each compound with the vehicle. When not indicated, P value > 0.05.

Subsequently, the Laboratory for Intestinal Neuroimmune Interactions at KU Leuven has planned to test the bis(4-chlorophenyl)phosphonate desthiobiotin probes with arginine (**6.46b**), benzyl guanidine (**4.54b**), and phenyl guanidine (**4.57b**) as a side chain with biopsy supernatants of IBS patients. These assays will have two main objectives. First, we want to confirm that trypsin released from mast cells is upregulated in IBS. And second, it would

be interesting to investigate the pathway linking the trypsin upregulation and the TRP channel sensitization, which is hypothesized to be correlated with the protease-activated receptor (PAR) activation.

8.2 Novel trypsin-like serine protease inhibitors

Driven by the surprising finding that UAMC-00050 presents a reversible slow-binding mechanism of inhibition for all the trypsin-like serine proteases tested, except for uPA, together with the promising results of the phenyl guanidine probes offering a high affinity for β -trypsin and cathepsin G and an irreversible mechanism for the proteases tested, we designed novel inhibitors targeting trypsin-like serine proteases. These maintained the phenyl guanidine as a selectivity-enhancing group and the α -amino diaryl phosphonate warhead. The terminal alkyne of the probes UAMC-0003970 and UAMC-0003971 was modified to a benzyl carbamate to convert them to an inhibitor-like structure and mimic the structure of UAMC-00050.

The new inhibitors were fully biochemically characterized in the same panel of trypsin-like serine proteases as the ABPs. Modifying the terminal alkyne for benzyl guanidine did not significantly influence their inhibitory potency. The kinetic progress curves and jump dilutions confirmed that the phenyl guanidine compounds present an irreversible mechanism of inhibition. Despite the different inhibition mechanisms, trypsin-3, thrombin, and uPA have a higher affinity for UAMC-00050, whereas β -trypsin and CatG do not display any preference.

Following the synthesis and biochemical characterization of UAMC-0004206 and UAMC-0004207, we started to characterize their physicochemical properties. This showed that UAMC-0004206 offers comparable physicochemical properties to UAMC-00050. On the other hand, UAMC-0004207 presents a lower solubility than UAMC-00050 and UAMC-0004206.

Following the promising *in vitro* results of UAMC-0004206, in the near future, we have planned to test it in the IBS rat model with TNBS-induced colitis in the post-inflammatory phase in the Laboratory of Experimental Medicine and Pediatrics at the University of Antwerp. The results of this experiment will be compared to the ones of UAMC-00050 for further conclusions and planning of experiments.

For DED, it would be of interest to use UAMC-0004206 in the same experimental model as UAMC-00050 with the same purpose as above. This could be done in collaboration with the Laboratory for Microbiology, Parasitology and Hygiene at the University of Antwerp.

Consequently, to the future perspective with the ABPs, it would be of interest to describe the specific trypsin-like serine proteases involved in the pathophysiology of DED and IBS. Then, it would be of relevance to design and synthesize novel inhibitors focusing on selectivity for those proteases over other trypsin-like serine proteases. For this, first, the active site could be studied by its crystal structure and, together with molecular docking, help to design novel selective inhibitors. The design and synthesis of more potent and selective inhibitors will be helpful to describe their potential as therapeutic agents.

CHAPTER 9

SUMMARY

Chapter 9 Summary

Proteases catalyze the hydrolysis of peptides or proteins by cleaving peptide bonds. These enzymes are of great interest in biomedical research due to their involvement in many physiological processes.^{2,3} In this PhD thesis, special attention is given to serine proteases which can be divided into trypsin-, chymotrypsin-, and elastase-like serine proteases, depending on their substrate specificity.¹⁴ In **Chapter 1**, an introduction to trypsin-like serine proteases was given with attention to proteases involved in immune and inflammatory responses. Serine proteases have been previously proposed as biomarkers for diverse diseases such as cancer, lung, cardiovascular or intestinal disorders. Moreover, serine protease inhibitors are of interest as therapeutic agents. However, it is important to identify and characterize the specific proteases involved in the pathophysiology of the disease under study to design selective inhibitors.³⁴³ In recent decades, protease activity has been studied by activity-based protein profiling (ABPP).⁷³

ABPP uses chemical probes, known as activity-based probes (ABP), which react covalently with the active form of the target enzyme. These allow detection, visualization, or affinity purification of the labeled enzymes.⁷⁵ **Chapter 1** aims to describe the characteristics of ABPs and summarize the previously developed ABPs relevant to this PhD thesis. Special attention is given to ABPs with an α -amino diphenyl phosphonate as a warhead. This reactive group has proven to specifically and irreversibly inhibit the serine protease family. Thus, it is an excellent option for the design of ABPs and the warhead of choice for this work.

The focus of this PhD thesis starts with the description of the potential role of serine proteases in the pathophysiology of Dry eye disease (DED) and Irritable bowel syndrome (IBS) and the proof of concept that serine proteases play a role in these diseases by the results obtained with inhibitor UAMC-00050 and followed by the design and synthesis of novel α -amino diaryl phosphonates activity-based probes with potential applications in

target and biomarker identification. Last, it focuses on developing novel trypsin-like serine protease inhibitors as potential therapeutic agents. The objectives of this work are explained in detail in **Chapter 2 (Figure 9.1)**.

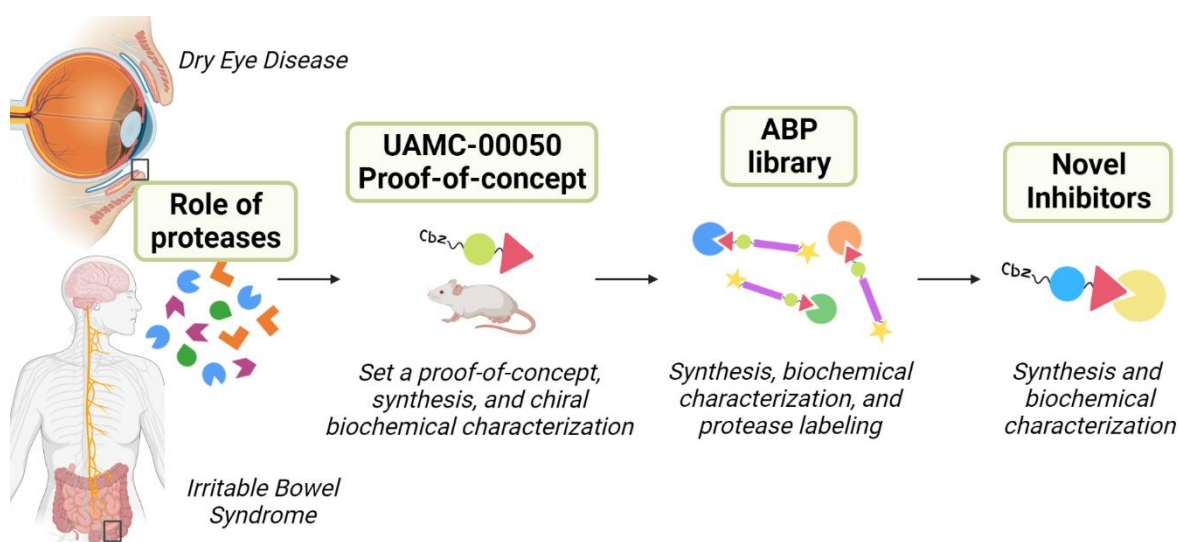


Figure 9.1 Overview of the work carried out in this PhD thesis.

DED is a multifactorial disorder that leads to ocular discomfort, visual disturbance, and tear film instability and is accompanied by ocular surface inflammation. The pathophysiology of DED is very complex and not yet fully understood. Thus, the diagnosis and treatment of DED still present significant challenges for clinicians, and novel biomarkers and treatments are of great interest. Proteases are abundant in different ocular surface tissues, and their activity is upregulated in various pathologies, including DED. In **Chapter 3**, we assessed the implications of different families of proteases in the development of DED. Previous studies focus their attention on the role of metalloproteases (MMPs). However, there is a lack of research on the role of other protease families, such as serine or cysteine proteases. With this literature research, we aimed to give suggestions for potential novel biomarkers and therapeutic targets to treat DED.

Likewise, in **Chapter 4**, we assessed the potential role of serine proteases in the development of IBS and visceral hypersensitivity. IBS is a gut-brain interaction disorder characterized by abdominal pain. The mechanism characterizing abdominal pain is visceral

hypersensitivity, an increased perception of stimuli in the gastrointestinal tract. The role of serine proteases in the intestinal tract and their potential role in IBS and visceral hypersensitivity have been previously studied.¹⁵¹ However, their role is not yet fully understood. This chapter focus on the involvement of serine proteases in the pathophysiology of visceral hypersensitivity in IBS and the therapeutic potential of serine protease inhibitors.

Prior to this PhD research, the Laboratory of Medicinal Chemistry at the University of Antwerp (UAMC) developed a multi-target trypsin-like serine protease α -amino diaryl phosphonate inhibitor known as UAMC-00050. Joossen *et al.* reported *in vivo* studies carried out in a rat animal model, where DED was induced by the surgical removal of the exorbital lacrimal gland. The treatment with a topical administration of UAMC-00050 could reduce tissue damage parameters and pro-inflammatory markers in these experimental settings.¹⁸⁵ For IBS, Ceuleers *et al.* reported that the local or intraperitoneal administration of inhibitor UAMC-00050 in a rat model with TNBS-induced colitis in the post-inflammatory phase and an acetic acid neonatal mice model could reduce visceral hypersensitivity.^{295,296,298} These studies are summarized in **Chapter 5**.

UAMC-00050 is synthesized as a mixture of enantiomers. Noteworthy, it has been used as a racemic mixture in previous studies, as the enantioselective synthesis of this compound is not available. Recently, the two enantiomers of UAMC-00050 were available for biochemical evaluation. These results and the development and validation of all the biochemical protocols used in this PhD are also described in **Chapter 5**.

Chapter 6 focuses on the synthesis and biochemical characterization of novel ABPs targeting trypsin-like serine proteases to identify and characterize the exact proteases involved in DED and IBS. We developed an extensive library of ABPs with “clickable” affinity tags and a diaryl phosphonate warhead. The ABP library has a wide chemical diversity achieved by combining different basic polar residues as a side chain and substituents in the warhead to modify its electrophilicity. A detailed enzymatic characterization was

performed in a panel of trypsin-like serine proteases with important roles in inflammatory and immune responses. Their inhibitory potencies, kinetic rate constants, and mechanism of inhibition were examined and determined. We described high-affinity probes for the selected protease panel. Surprisingly, some of these high-affinity probes with benzyl guanidine as a side chain presented a reversible slow-binding inhibitory mechanism. Contrary, probes with different side chains exhibited the expected irreversible mechanism. To demonstrate their ability and translational potential to label proteases in complex proteomes, we used probes with both inhibitory mechanisms to label recombinant proteases and proteases released from human mast cells in SDS-PAGE gels. Unexpectedly, probes with a reversible slow-binding mechanism could also label proteases even under denaturing SDS-PAGE conditions due to the formation of high-affinity complexes and slow dissociation rates (**Figure 9.2**). In further studies, we aim to identify upregulated proteases in DED and IBS biological samples. This research can lead to the identification of novel biomarkers and therapeutic targets for these diseases.

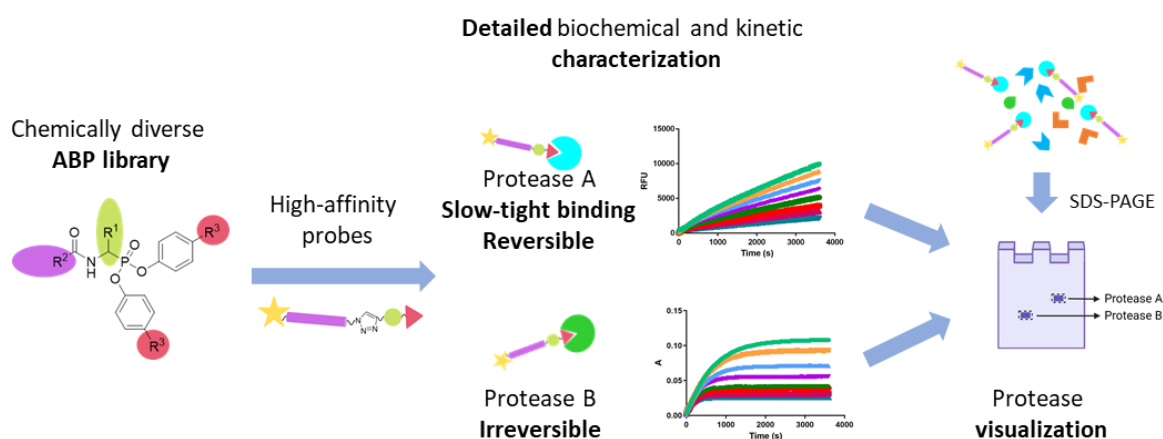


Figure 9.2 Development of diverse ABPLibrary with unexpected inhibition mechanism able to label proteases under SDS-PAGE assay conditions

Given the promising *in vitro* results with recombinant enzymes and the phenyl guanidine probes (**6.38b-6.39b**), together with the surprising finding that the benzyl guanidine probes (**6.35b-6.36b**) and UAMC-00050 only present an irreversible mechanism for uPA, we developed two new inhibitors targeting trypsin-like serine proteases. **Chapter 7** reports the synthesis and biochemical characterization of the new inhibitors UAMC-0004206 and

UAMC-0004207. Their physicochemical properties, such as logD and solubility, were determined. The results of their inhibitory potencies for a panel of trypsin-like serine proteases and the first study of their physicochemical properties showed that UAMC-0004206 is a promising backup compound with the potential to be a therapeutic agent for DED and IBS. In future research, this inhibitor will be administered to post-inflammatory colitis rats to compare its activity in this IBS animal model with UAMC-00050.

CHAPTER 10

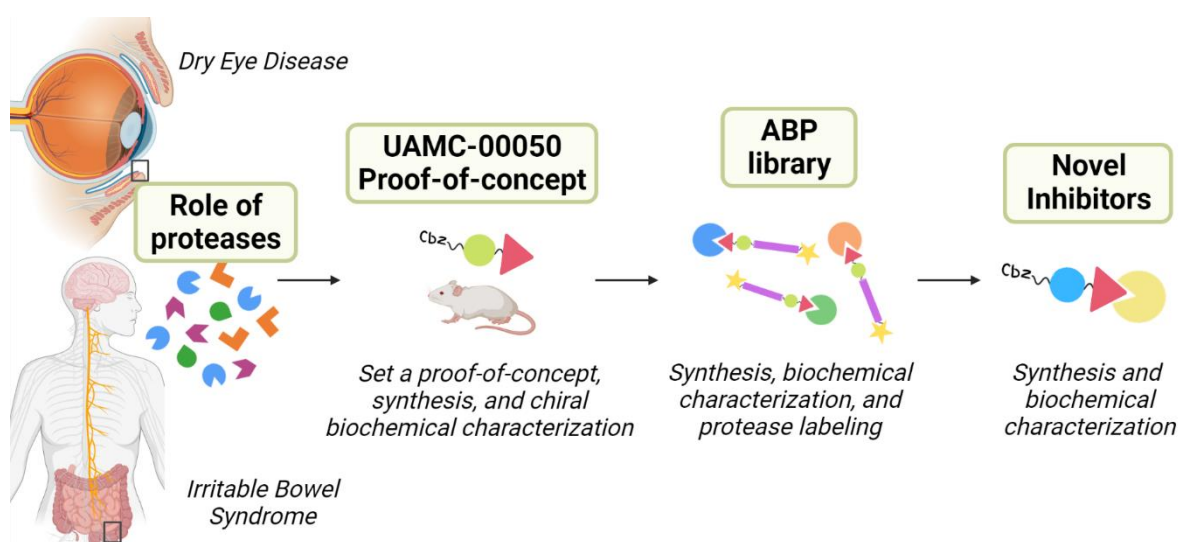
SAMENVATTING

Chapter 10 Samenvatting

Proteasen katalyseren de hydrolyse van peptiden of eiwitten door peptidebindingen te splitsen. Deze enzymen zijn van groot belang in het biomedisch onderzoek vanwege hun betrokkenheid bij vele fysiologische processen.^{2,3} In dit proefschrift wordt speciale aandacht besteed aan serine proteasen die, afhankelijk van hun substraatspecificiteit, kunnen worden onderverdeeld in trypsine-, chymotrypsine-, en elastase-achtige serine proteasen.¹⁴ In **Hoofdstuk 1** werd een inleiding gegeven over trypsine-achtige serine proteasen met aandacht voor proteasen die betrokken zijn bij immuun- en ontstekingsreacties. Serine proteasen zijn kunnen dienen als biomarkers voor diverse ziekten zoals kanker, long-, cardiovasculaire of darmaandoeningen. Bovendien zijn hun remmers interessant als therapeutische middelen. Het is echter belangrijk de specifieke proteasen die betrokken zijn bij de pathofysiologie van de bestudeerde ziekte te identificeren en te karakteriseren om selectieve remmers te ontwerpen.³⁴³ In de afgelopen decennia is de proteaseactiviteit bestudeerd door middel van activity-based protein profiling (ABPP).⁷³

ABPP gebruikt chemische probes, bekend als 'activity-based probes' in de vakliteratuur (ABP), die covalent reageren met de actieve vorm van het doelenzym. Deze maken detectie, visualisatie of affiniteitszuivering van de gelabelde enzymen mogelijk.⁷⁵ In **Hoofdstuk 1** worden de kenmerken van ABP's beschreven en worden de eerder ontwikkelde en voor dit proefschrift relevante ABP's samengevat. Speciale aandacht wordt besteed aan ABP's met een α -amino difenylfosfonaat als kern. Deze reactieve groep blijkt de serine protease familie specifiek en onomkeerbaar te remmen. Het is dus een uitstekende optie voor het ontwerp van ABP's en de uitgelezen reactieve groep voor dit werk.

De focus van dit proefschrift begint met de beschrijving van de potentiële rol van serine proteasen in de pathofysiologie van droge ogen (DED) en prikkelbare darm syndroom (IBS) en het bewijs dat serine proteasen een mogelijke rol spelen in deze ziekten door de resultaten verkregen met remmer UAMC-00050. Vervolgens wordt het ontwerp en de synthese van nieuwe α -amino diaryl fosfonaten ABPs met potentiële toepassingen in target en biomarker identificatie beschreven. Ten slotte richt het zich op de ontwikkeling van nieuwe trypsineachtige serineproteaseremmers als potentiële therapeutische middelen. De doelstellingen van dit werk worden in detail toegelicht in **Hoofdstuk 2 (Figuur 10.1)**.



Figuur 10.1 Overzicht van het werk uitgevoerd in deze thesis.

DED is een multifactoriële aandoening die leidt tot oculair ongemak, visuele verstoring en traanfilminstabiliteit en gepaard gaat met oculaire oppervlakteontsteking. De pathofysiologie van DED is zeer complex en wordt nog niet volledig begrepen. Daarom vormen de diagnose en behandeling van DED nog steeds een grote uitdaging voor klinici, en zijn nieuwe biomarkers en behandelingen van groot belang. Proteasen zijn overvloedig aanwezig in verschillende oculaire oppervlakteweefsels, en hun activiteit is verhoogd bij verschillende pathologieën, waaronder DED. In **Hoofdstuk 3** onderzochten wij de implicaties van verschillende families van proteasen bij de ontwikkeling van DED. Eerdere studies richten hun aandacht op de rol van metalloproteasen. Er is echter weinig bekend over de rol van andere protease families, zoals serine of cysteine proteasen. Met dit

literatuuronderzoek beoogden wij suggesties te geven voor potentiële nieuwe biomarkers en therapeutische doelwitten voor de behandeling van DED.

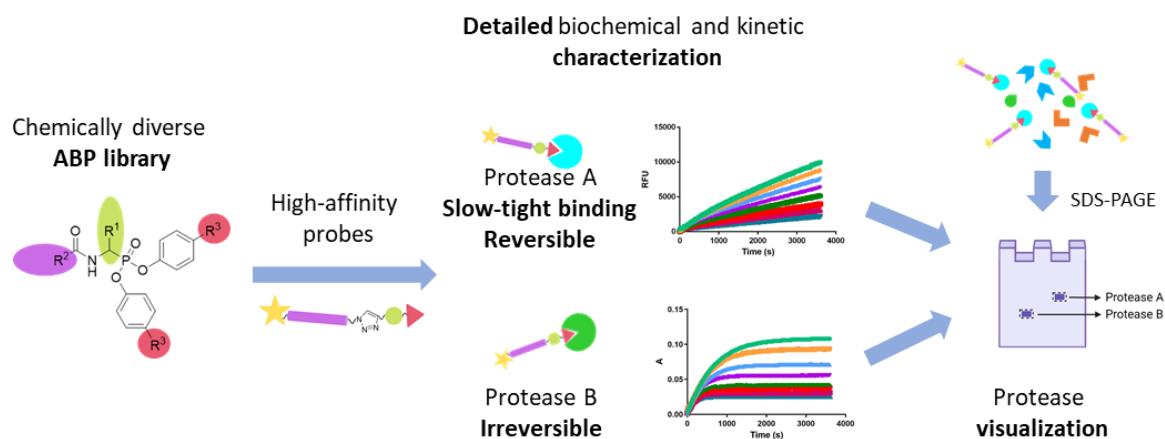
Evenzo onderzochten wij in **Hoofdstuk 4** de mogelijke rol van serine proteasen bij de ontwikkeling van IBS en viscerale overgevoeligheid. IBS is een interactie stoornis tussen de darmen en de hersenen gekenmerkt door buikpijn. Het mechanisme dat buikpijn kenmerkt is viscerale overgevoeligheid, een verhoogde waarneming van prikkels in het maagdarmkanaal. De rol van serine proteasen in het darmkanaal en hun mogelijke rol bij IBS en viscerale overgevoeligheid zijn eerder bestudeerd.¹⁵¹ Echter, hun rol is echter nog niet volledig begrepen. Dit hoofdstuk richt zich op de betrokkenheid van serine proteasen in de pathofysiologie van viscerale overgevoeligheid bij IBS en het therapeutisch potentieel van serine protease remmers.

Voorafgaand aan dit doctoraatsonderzoek ontwikkelde het Laboratorium voor Medicinale Chemie van de Universiteit Antwerpen (UAMC) een multi-target trypsine-achtige serine protease α -amino diaryl fosfonaat remmer bekend als UAMC-00050. Joossen *et al.* rapporteerden in vivo studies uitgevoerd in een diermodel voor ratten, waarbij DED werd geïnduceerd door de chirurgische verwijdering van de exorbitale traanklier. De behandeling met een topische toediening van UAMC-00050 kon de parameters voor weefselschade en pro-inflammatoire markers in deze experimentele settings verminderen.¹⁸⁵ Voor IBS rapporteerden Ceuleers *et al.* dat de lokale of intraperitoneale toediening van remmer UAMC-00050 in een rattenmodel met TNBS-geïnduceerde colitis in de post-inflammatoire fase en in een model van neonatale muizen behandeld met azijnzuur de viscerale overgevoeligheid kon verminderen.^{295,296,298} Deze studies zijn samengevat in **Hoofdstuk 5**.

UAMC-00050 wordt gesynthetiseerd als een mengsel van enantiomeren. Opmerkelijk is dat het in eerdere studies is gebruikt als een racemisch mengsel, aangezien de enantioselectieve synthese van deze verbinding niet beschikbaar is. Onlangs waren de twee enantiomeren van UAMC-00050 beschikbaar voor biochemische evaluatie. Deze resultaten

en de ontwikkeling en validering van alle in dit proefschrift gebruikte biochemische protocollen worden eveneens beschreven in **Hoofdstuk 5**.

Hoofdstuk 6 richt zich op de synthese en biochemische karakterisering van nieuwe ABP's gericht op trypsine-achtige serine proteasen om de exacte proteasen die betrokken zijn bij DED en IBS te identificeren en te karakteriseren. Wij ontwikkelden een uitgebreide bibliotheek van ABP's met "klikbare" affiniteitstags en een diaryl fosfonaatkop. De ABP-bibliotheek heeft een grote chemische diversiteit, bereikt door het combineren van verschillende polaire basisresiduen als zijketen en substituenten in de kop om de elektrofiliciteit ervan te wijzigen. Een gedetailleerde enzymatische karakterisering werd uitgevoerd in een panel van trypsine-achtige serine proteasen met een belangrijke rol in ontstekings- en immuunreacties. Hun remmend vermogen, kinetische snelheidsconstanten en remmingsmechanisme werden onderzocht en bepaald. We beschreven hoge-affiniteitssondes voor het geselecteerde protease-panel. Verrassend genoeg vertoonden sommige van deze probes met hoge affiniteit en benzylguanidine als zijketen een omkeerbaar langzaam-bindend remmingsmechanisme. Sondes met andere zijketens vertoonden daarentegen het verwachte onomkeerbare mechanisme. Om hun vermogen om proteasen in complexe proteomen te labelen aan te tonen, gebruikten wij probes met beide remmende mechanismen om recombinante proteasen en proteasen vrijgemaakt uit menselijke mestcellen in SDS-PAGE gels te labelen. Onverwacht konden probes met een omkeerbaar langzaam-bindend mechanisme ook proteasen labelen, zelfs onder denaturende SDS-PAGE-condities, als gevolg van de vorming van complexen met hoge affiniteit en langzame dissociatiesnelheden (Figuur 10.2). In verdere studies trachten wij de verhoogde niveaus van proteasen in biologische monsters van DED en IBS te identificeren. Dit onderzoek kan leiden tot de identificatie van nieuwe biomarkers en therapeutische doelwitten voor deze ziekten.



Figuur 10.2 Ontwikkeling van diverse ABP-bibliotheken met onverwachte remmingsmechanismen die proteasen kunnen labelen onder SDS-PAGE-testomstandigheden

Gezien de veelbelovende in vitro resultaten met recombinante enzymen en de fenylguanidinesondes (**6.38b-6.39b**), samen met de verrassende bevinding dat de benzylguanidinesondes (**6.35b-6.36b**) en UAMC-00050 alleen een irreversibel mechanisme voor uPA vertonen, hebben wij twee nieuwe remmers ontwikkeld die gericht zijn op trypsine-achtige serineproteasen. **Hoofdstuk 7** beschrijft de synthese en biochemische karakterisering van de nieuwe remmers UAMC-0004206 en UAMC-0004207. Hun fysisch-chemische eigenschappen, zoals logD en oplosbaarheid, werden bepaald. De resultaten van hun remmende activiteiten voor een panel van trypsine-achtige serineproteasen en de eerste studie van hun fysisch-chemische eigenschappen toonden aan dat UAMC-0004206 een veelbelovende reserveverbinding is met het potentieel om een therapeutisch middel te zijn voor DED en IBS. In toekomstig onderzoek zal deze remmer worden toegediend aan post-inflammatoire colitis ratten om zijn activiteit in dit IBS diermodel te vergelijken met **UAMC-00050**.

REFERENCES

References

1. Gurumallesh, P.; Alagu, K.; Ramakrishnan, B.; Muthusamy, S. A Systematic Reconsideration on Proteases. *Int J Biol Macromol* **2019**, *128*, 254–267.
2. Rawlings, N. D.; Barrett, A. J.; Bateman, A. MEROPS: The Database of Proteolytic Enzymes, Their Substrates and Inhibitors. *Nucleic Acids Res* **2012**, *40* (D1), D343–D350.
3. Turk, B.; Turk, D.; Turk, V. Protease Signalling: The Cutting Edge. *EMBO J* **2012**, *31* (7), 1630–1643.
4. Silverman, G. A.; Bird, P. I.; Carrell, R. W.; Church, F. C.; Coughlin, P. B.; Gettins, P. G. W.; Irving, J. A.; Lomas, D. A.; Luke, C. J.; Moyer, R. W.; et al. The Serpins Are an Expanding Superfamily of Structurally Similar but Functionally Diverse Proteins. Evolution, Mechanism of Inhibition, Novel Functions, and a Revised Nomenclature. *Journal of Biological Chemistry* **2001**, *276* (36), 33293–33296.
5. Hooper, N. M. *Proteases in Biology and Medicine.*, Portland P.; London, 2002.
6. Raksakulthai, R.; Haard, N. F. Exopeptidases and Their Application to Reduce Bitterness in Food: A Review. *Crit Rev Food Sci Nutr* **2003**, *43* (4), 401–445.
7. Barrett, A. J.; Rawlings, N. D. Types and Families of Endopeptidases. *Biochem Soc Trans* **1991**, *19* (3), 707–715.
8. Puente, X. S.; Sánchez, L. M.; Overall, C. M.; López-Otín, C. Human and Mouse Proteases: A Comparative Genomic Approach. *Nat Rev Genet* **2003**, *4* (7), 544–558.
9. di Cera, E. Serine Proteases. *IUBMB Life* **2009**, *61* (5), 510–515.
10. Rawlings, N. D.; Barrett, A. J. Evolutionary Families of Peptidases. *Biochemical Journal* **1993**, *290* (1), 205–218.
11. Matthews, B. W.; Sigler, P. B.; Henderson, R.; Blow, D. M. Three-Dimensional Structure of Tosyl- α -Chymotrypsin. *Nature* **1967**, *214* (5089), 652–656.
12. Goettig, P.; Brandstetter, H.; Magdolen, V. Surface Loops of Trypsin-like Serine Proteases as Determinants of Function. *Biochimie* **2019**, *166*, 52–76.

13. Náray-Szabó, G.; Oláh, J.; Krámos, B. Quantum Mechanical Modeling: A Tool for the Understanding of Enzyme Reactions. *Biomolecules* **2013**, *3* (3), 662–702.
14. Hedstrom, L. Serine Protease Mechanism and Specificity. *Chem Rev* **2002**, *102* (12), 4501–4523.
15. Perona, J. J.; Craik, C. S. Structural Basis of Substrate Specificity in the Serine Proteases. *Protein Science* **2008**, *4* (3), 337–360.
16. Heutinck, K. M.; ten Berge, I. J. M.; Hack, C. E.; Hamann, J.; Rowshani, A. T. Serine Proteases of the Human Immune System in Health and Disease. *Mol Immunol* **2010**, *47* (11–12), 1943–1955.
17. Hedstrom, L.; Lin, T.-Y.; Fast, W. Hydrophobic Interactions Control Zymogen Activation in the Trypsin Family of Serine Proteases. *Biochemistry* **1996**, *35* (14), 4515–4523.
18. van Gent, D.; Sharp, P.; Morgan, K.; Kalsheker, N. Serpins: Structure, Function and Molecular Evolution. *Int J Biochem Cell Biol* **2003**, *35* (11), 1536–1547.
19. Zamolodchikova, T. S. Serine Proteases of Small Intestine Mucosa — Localization, Functional Properties, and Physiological Role. *Biochemistry (Moscow)* **2012**, *77* (8), 820–829.
20. Jerke, U.; Hernandez, D. P.; Beaudette, P.; Korkmaz, B.; Dittmar, G.; Kettritz, R. Neutrophil Serine Proteases Exert Proteolytic Activity on Endothelial Cells. *Kidney Int* **2015**, *88* (4), 764–775.
21. Pham, C. T. N. Neutrophil Serine Proteases: Specific Regulators of Inflammation. *Nat Rev Immunol* **2006**, *6* (7), 541–550.
22. Kettritz, R. Neutral Serine Proteases of Neutrophils. *Immunol Rev* **2016**, *273* (1), 232–248.
23. Meyer-Hoffert, U.; Wiedow, O. Neutrophil Serine Proteases: Mediators of Innate Immune Responses. *Curr Opin Hematol* **2011**, *18* (1), 19–24.
24. Wiedow, O.; Meyer-Hoffert, U. Neutrophil Serine Proteases: Potential Key Regulators of Cell Signalling during Inflammation. *J Intern Med* **2005**, *257* (4), 319–328.

25. Polanowska, J.; Krokoszynska, I.; Czapinska, H.; Watorek, W.; Dadlez, M.; Otlewski, J. Specificity of Human Cathepsin G. *Biochimica et Biophysica Acta (BBA) - Protein Structure and Molecular Enzymology* **1998**, *1386* (1), 189–198.
26. Gao, S. Cathepsin G and Its Role in Inflammation and Autoimmune Diseases. *Arch Rheumatol* **2018**, *33* (4), 498–504.
27. Stone, K. D.; Prussin, C.; Metcalfe, D. D. IgE, Mast Cells, Basophils, and Eosinophils. *Journal of Allergy and Clinical Immunology* **2010**, *125* (2), S73–S80.
28. Theoharides, T. C.; Alysandratos, K. D.; Angelidou, A.; Delivanis, D. A.; Sismanopoulos, N.; Zhang, B.; Asadi, S.; Vasiadi, M.; Weng, Z.; Miniati, A.; et al. Mast Cells and Inflammation. *Biochimica et Biophysica Acta (BBA) - Molecular Basis of Disease* **2012**, *1822* (1), 21–33.
29. Schwartz, L. B.; Irani, A. M.; Roller, K.; Castells, M. C.; Schechter, N. M. Quantitation of Histamine, Tryptase, and Chymase in Dispersed Human T and TC Mast Cells. *The Journal of Immunology* **1987**, *138* (8).
30. Schechter, N. M.; Irani, A. M.; Sprows, J. L.; Abernethy, J.; Wintroub, B.; Schwartz, L. B. Identification of a Cathepsin G-like Proteinase in the MCTC Type of Human Mast Cell. *The Journal of Immunology* **1990**, *145* (8).
31. Kahler, J. P.; Vanhoutte, R.; Verhelst, S. H. L. Activity-Based Protein Profiling of Serine Proteases in Immune Cells. *Arch Immunol Ther Exp (Warsz)* **2020**, *68* (4).
32. Sommerhoff, C. P.; Bode, W.; Matschiner, G.; Bergner, A.; Fritz, H. The Human Mast Cell Tryptase Tetramer: A Fascinating Riddle Solved by Structure. *Biochimica et Biophysica Acta - Protein Structure and Molecular Enzymology* **2000**, *1477* (1–2), 75–89.
33. Jogie-Brahim, S.; Min, H.-K.; Fukuoka, Y.; Xia, H.-Z.; Schwartz, L. B. Expression of α -Tryptase and β -Tryptase by Human Basophils. *Journal of Allergy and Clinical Immunology* **2004**, *113* (6), 1086–1092.
34. Theoharides, T. C.; Kalogeromitros, D. The Critical Role of Mast Cells in Allergy and Inflammation. *Ann N Y Acad Sci* **2006**, *1088* (1), 78–99.

35. Payne, V.; Kam, P. C. A. Mast Cell Tryptase: A Review of Its Physiology and Clinical Significance. *Anaesthesia* **2004**, *59* (7), 695–703.
36. Maun, H. R.; Jackman, J. K.; Choy, D. F.; Loyet, K. M.; Staton, T. L.; Jia, G.; Dressen, A.; Hackney, J. A.; Bremer, M.; Walters, B. T.; et al. An Allosteric Anti-Tryptase Antibody for the Treatment of Mast Cell-Mediated Severe Asthma. *Cell* **2019**, *179* (2), 417–431.e19.
37. Mohajeri, M.; Kovanen, P. T.; Bianconi, V.; Pirro, M.; Cicero, A. F. G.; Sahebkar, A. Mast Cell Tryptase – Marker and Maker of Cardiovascular Diseases. *Pharmacol Ther* **2019**, *199*, 91–110.
38. Jesky, M. D.; Stringer, S. J.; Fenton, A.; Ng, K. P.; Yadav, P.; Ndumbo, M.; McCann, K.; Plant, T.; Dasgupta, I.; Harding, S. J.; et al. Serum Tryptase Concentration and Progression to End-Stage Renal Disease. *Eur J Clin Invest* **2016**, *46* (5), 460–474.
39. DeBruin, E. J.; Gold, M.; Lo, B. C.; Snyder, K.; Cait, A.; Lasic, N.; Lopez, M.; McNagny, K. M.; Hughes, M. R. Mast Cells in Human Health and Disease. In *Methods in Molecular Biology*; Humana Press Inc., 2015; Vol. 1220, pp 93–119.
40. Liang, W. J.; Zhang, G.; Luo, H. S.; Liang, L. X.; Huang, D.; Zhang, F. C. Tryptase and Protease-Activated Receptor 2 Expression Levels in Irritable Bowel Syndrome. *Gut Liver* **2016**, *10* (3), 382–390.
41. Chávez-Galán, L.; Arenas-Del Angel, M. C.; Zenteno, E.; Chávez, R.; Lascurain, R. Cell Death Mechanisms Induced by Cytotoxic Lymphocytes. *Cell Mol Immunol* **2009**, *6* (1), 15–25.
42. Voskoboinik, I.; Whisstock, J. C.; Trapani, J. A. Perforin and Granzymes: Function, Dysfunction and Human Pathology. *Nat Rev Immunol* **2015**, *15* (6), 388–400.
43. Buzza, M. S.; Bird, P. I. Extracellular Granzymes: Current Perspectives. *Biol Chem* **2006**, *387* (7), 827–837.
44. Wensink, A. C.; Hack, C. E.; Bovenschen, N. Granzymes Regulate Proinflammatory Cytokine Responses. *The Journal of Immunology* **2015**, *194* (2), 491–497.
45. van Daalen, K. R.; Reijneveld, J. F.; Bovenschen, N. Modulation of Inflammation by Extracellular Granzyme A. *Front Immunol* **2020**, *11*, 931.

46. Thakur, A.; Mikkelsen, H.; Jungersen, G. Intracellular Pathogens: Host Immunity and Microbial Persistence Strategies. *J Immunol Res* **2019**, *2019*, 1–24.
47. Guggino, G.; Orlando, V.; Cutrera, S.; la Manna, M. P.; di Liberto, D.; Vanini, V.; Petruccioli, E.; Dieli, F.; Goletti, D.; Caccamo, N. Granzyme A as a Potential Biomarker of Mycobacterium Tuberculosis Infection and Disease. *Immunol Lett* **2015**, *166* (2), 87–91.
48. Santiago, L.; Menea, C.; Arias, M.; Martin, P.; Jaime-Sánchez, P.; Metkar, S.; Comas, L.; Erill, N.; Gonzalez-Rumayor, V.; Esser, E.; et al. Granzyme A Contributes to Inflammatory Arthritis in Mice Through Stimulation of Osteoclastogenesis. *Arthritis & Rheumatology* **2017**, *69* (2), 320–334.
49. Tremblay, G. M.; Wolbink, A. M.; Cormier, Y.; Hack, C. E. Granzyme Activity in the Inflamed Lung Is Not Controlled by Endogenous Serine Proteinase Inhibitors. *The Journal of Immunology* **2000**, *165* (7), 3966–3969.
50. Augustin, M. T.; Kokkonen, J.; Karttunen, R.; Karttunen, T. J. Serum Granzymes and CD30 Are Increased in Children’s Milk Protein Sensitive Enteropathy and Celiac Disease. *Journal of Allergy and Clinical Immunology* **2005**, *115* (1), 157–162.
51. Paju, A.; Stenman, U.-H. Biochemistry and Clinical Role of Trypsinogens and Pancreatic Secretory Trypsin Inhibitor. *Crit Rev Clin Lab Sci* **2006**, *43* (2), 103–142.
52. Kaur, J.; Singh, P. K. Trypsin Detection Strategies: A Review. *Crit Rev Anal Chem* **2022**, *52* (5), 949–967.
53. Huber, R.; Bode, W. Structural Basis of the Activation and Action of Trypsin. *Acc Chem Res* **1978**, *11* (3), 114–122.
54. Hirota, M.; Ohmuraya, M.; Baba, H. The Role of Trypsin, Trypsin Inhibitor, and Trypsin Receptor in the Onset and Aggravation of Pancreatitis. *J Gastroenterol* **2006**, *41* (9), 832–836.
55. Dandona, P.; Hodson, M.; Bell, J.; Ramdial, L.; Beldon, I.; Batten, J. C. Serum Immunoreactive Trypsin in Cystic Fibrosis. *Thorax* **1981**, *36* (1), 60–62.

56. Fonseca, V.; Epstein, O.; Katrak, A.; Junglee, D.; Mikhailidis, D. P.; McIntyre, N.; Dandona, P. Serum Immunoreactive Trypsin and Pancreatic Lipase in Primary Biliary Cirrhosis. *J Clin Pathol* **1986**, *39* (6), 638–640.
57. Davie, E.; Kulman, J. An Overview of the Structure and Function of Thrombin. *Semin Thromb Hemost* **2006**, *32* (S 1), 003–015.
58. di Cera, E. Thrombin. *Mol Aspects Med* **2008**, *29* (4), 203–254.
59. Krenzlin, H.; Lorenz, V.; Danckwardt, S.; Kempfski, O.; Alessandri, B. The Importance of Thrombin in Cerebral Injury and Disease. *Int J Mol Sci* **2016**, *17* (1), 84.
60. Shlobin, N. A.; Har-Even, M.; Itsekson-Hayosh, Z.; Harnof, S.; Pick, C. G. Role of Thrombin in Central Nervous System Injury and Disease. *Biomolecules* **2021**, *11* (4), 562.
61. Arsenault, K. A.; Hirsh, J.; Whitlock, R. P.; Eikelboom, J. W. Direct Thrombin Inhibitors in Cardiovascular Disease. *Nat Rev Cardiol* **2012**, *9* (7), 402–414.
62. Hayat, M.; Ariëns, R. A. S.; Moayyedi, P.; Grant, P. J.; O'Mahony, S. Coagulation Factor XIII and Markers of Thrombin Generation and Fibrinolysis in Patients with Inflammatory Bowel Disease. *Eur J Gastroenterol Hepatol* **2002**, *14* (3).
63. Mahmood, N.; Mihalcioiu, C.; Rabbani, S. A. Multifaceted Role of the Urokinase-Type Plasminogen Activator (UPA) and Its Receptor (UPAR): Diagnostic, Prognostic, and Therapeutic Applications. *Front Oncol* **2018**, *8*, 24.
64. Crippa, M. P. Urokinase-Type Plasminogen Activator. *Int J Biochem Cell Biol* **2007**, *39* (4), 690–694.
65. Schmidt, M.; Grünfelder, P. Urokinase-Type Plasminogen Activator Expression and Proliferation Stimulation in Head and Neck Squamous Cell Carcinoma In Vitro and In Situ. *Arch Otolaryngol Head Neck Surg* **2001**, *127* (6), 679.
66. Dinesh, P.; Rasool, M. UPA/UPAR Signaling in Rheumatoid Arthritis: Shedding Light on Its Mechanism of Action. *Pharmacol Res* **2018**, *134*, 31–39.
67. Lotti, T.; Benci, M. Plasminogen Activators, Venous Leg Ulcers and Reepithealization. *Int J Dermatol* **1995**, *34* (10), 696–699.

68. Graves, P. R.; Haystead, T. A. J. Molecular Biologist's Guide to Proteomics. *Microbiology and Molecular Biology Reviews* **2002**, *66* (1), 39–63.
69. Dupree, E. J.; Jayathirtha, M.; Yorkey, H.; Mihasan, M.; Petre, B. A.; Darie, C. C. A Critical Review of Bottom-up Proteomics: The Good, the Bad, and the Future of This Field. *Proteomes* **2020**, *8* (3), 1–26.
70. Sutandy, F. X. R.; Qian, J.; Chen, C. S.; Zhu, H. Overview of Protein Microarrays. *Curr Protoc Protein Sci* **2013**, *72* (1), 27.1.1-27.1.16.
71. Aslam, B.; Basit, M.; Nisar, M. A.; Khurshid, M.; Rasool, M. H. Proteomics: Technologies and Their Applications. *J Chromatogr Sci* **2017**, *55* (2), 182–196.
72. Zhou, H.; Yu, Z.; Ye, Z.; Su, M. Multiplex Analyses of the Changes of Aromatic Compounds during the Development of Peach Fruit Using GC–MS and ITRAQ Proteomic Techniques. *Sci Horti* **2018**, *236*, 96–105.
73. Serim, S.; Haedke, U.; Verhelst, S. H. L. Activity-Based Probes for the Study of Proteases: Recent Advances and Developments. *ChemMedChem* **2012**, *7* (7), 1146–1159.
74. Sanman, L. E.; Bogyo, M. Activity-Based Profiling of Proteases. *Annu Rev Biochem* **2014**, *83* (1), 249–273.
75. Cravatt, B. F.; Wright, A. T.; Kozarich, J. W. Activity-Based Protein Profiling: From Enzyme Chemistry to Proteomic Chemistry. *Annu Rev Biochem* **2008**, *77* (1), 383–414.
76. Li, J.; Fang, B.; Kinose, F.; Bai, Y.; Kim, J. Y.; Chen, Y. A.; Rix, U.; Koomen, J. M.; Haura, E. B. Target Identification in Small Cell Lung Cancer via Integrated Phenotypic Screening and Activity-Based Protein Profiling. *Mol Cancer Ther* **2016**, *15* (2), 334–342.
77. Herrera Moro Chao, D.; Kallemeijn, W. W.; Marques, A. R. A.; Orre, M.; Ottenhoff, R.; van Roomen, C.; Foppen, E.; Renner, M. C.; Moeton, M.; van Eijk, M.; et al. Visualization of Active Glucocerebrosidase in Rodent Brain with High Spatial Resolution Following In Situ Labeling with Fluorescent Activity Based Probes. *PLoS One* **2015**, *10* (9), e0138107.

78. Niphakis, M. J.; Cravatt, B. F. Enzyme Inhibitor Discovery by Activity-Based Protein Profiling. *Annu Rev Biochem* **2014**, *83*, 341–377.
79. Jessani, N.; Cravatt, B. F. The Development and Application of Methods for Activity-Based Protein Profiling. *Curr Opin Chem Biol* **2004**, *8* (1), 54–59.
80. Berger, A. B.; Vitorino, P. M.; Bogoy, M. Activity-Based Protein Profiling. *American Journal of Pharmacogenomics* **2012**, *4* (6), 371–381.
81. Fonović, M.; Bogoy, M. Activity-Based Probes as a Tool for Functional Proteomic Analysis of Proteases. *Expert Rev Proteomics* **2008**, *5* (5), 721–730.
82. Kasperkiewicz, P. Peptidyl Activity-Based Probes for Imaging Serine Proteases. *Front Chem* **2021**, *9*, 315.
83. Chakrabarty, S.; Kahler, J. P.; van de Plassche, M. A. T.; Vanhoutte, R.; Verhelst, S. H. L. Recent Advances in Activity-Based Protein Profiling of Proteases. In *Current topics in Microbiology and Immunology*; 2018; Vol. 37, pp 253–281.
84. Schechter, I.; Berger, A. On the Size of the Active Site in Proteases. I. Papain. *Biochem Biophys Res Commun* **1967**, *27* (2), 157–162.
85. Greenbaum, D. C.; Arnold, W. D.; Lu, F.; Hayrapetian, L.; Baruch, A.; Krumrine, J.; Toba, S.; Chehade, K.; Brömme, D.; Kuntz, I. D.; et al. Small Molecule Affinity Fingerprinting: A Tool for Enzyme Family Subclassification, Target Identification, and Inhibitor Design. *Chem Biol* **2002**, *9* (10), 1085–1094.
86. Haedke, U.; Götz, M.; Baer, P.; Verhelst, S. H. L. Alkyne Derivatives of Isocoumarins as Clickable Activity-Based Probes for Serine Proteases. *Bioorg Med Chem* **2012**, *20* (2), 633–640.
87. Liu, Y.; Patricelli, M. P.; Cravatt, B. F. Activity-Based Protein Profiling: The Serine Hydrolases. *PNAS* **1999**, *96* (26), 14694–14699.
88. Patricelli, M. P.; Giang, D. K.; Stamp, L. M.; Burbaum, J. J. Direct Visualization of Serine Hydrolase Activities in Complex Proteomes Using Fluorescent Active Site-Directed Probes. *Proteomics* **2001**, *1* (8), 1067–1071.
89. Kidd, D.; Liu, Y.; Cravatt, B. F. Profiling Serine Hydrolase Activities in Complex Proteomes. *Biochemistry* **2001**, *40* (13), 4005–4015.

-
90. Hawthorne, S.; Hamilton, R.; Walker, B. J.; Walker, B. Utilization of Biotinylated Diphenyl Phosphonates for Disclosure of Serine Proteases. *Anal Biochem* **2004**, *326* (2), 273–275.
91. Pan, Z.; Jeffery, D. A.; Chehade, K.; Beltman, J.; Clark, J. M.; Grothaus, P.; Bogoyo, M.; Baruch, A. Development of Activity-Based Probes for Trypsin-Family Serine Proteases. *Bioorg Med Chem Lett* **2006**, *16* (11), 2882–2885.
92. Haedke, U. R.; Frommel, S. C.; Hansen, F.; Hahne, H.; Kuster, B.; Bogoyo, M.; Verhelst, S. H. L. Phosphoramidates as Novel Activity-Based Probes for Serine Proteases. *ChemBioChem* **2014**, *15* (8), 1106–1110.
93. Ferguson, T. E. G.; Reihill, J. A.; Martin, S. L.; Walker, B. Novel Inhibitors and Activity-Based Probes Targeting Trypsin-Like Serine Proteases. *Front Chem* **2022**, *10*, 433.
94. Ides, J.; Thomae, D.; Wyffels, L.; Vangestel, C.; Messagie, J.; Joossens, J.; Lardon, F.; Van der Veken, P.; Augustyns, K.; Stroobants, S.; et al. Synthesis and in Vivo Preclinical Evaluation of an ¹⁸F Labeled UPA Inhibitor as a Potential PET Imaging Agent. *Nucl Med Biol* **2014**, *41* (6), 477–487.
95. Grzywa, R.; Burchacka, E.; Łęcka, M.; Winiarski, Ł.; Walczak, M.; Łupicka-Słowik, A.; Wysocka, M.; Burster, T.; Bobrek, K.; Csencsits-Smith, K.; et al. Synthesis of Novel Phosphonic-Type Activity-Based Probes for Neutrophil Serine Proteases and Their Application in Spleen Lysates of Different Organisms. *ChemBioChem* **2014**, *15* (17), 2605–2612.
96. Lovell, S.; Zhang, L.; Kryza, T.; Neodo, A.; Bock, N.; de Vita, E.; Williams, E. D.; Engelsberger, E.; Xu, C.; Bakker, A. T.; et al. A Suite of Activity-Based Probes To Dissect the KLK Activome in Drug-Resistant Prostate Cancer. *Cite This: J. Am. Chem. Soc* **2021**, *143*, 8911–8924.
97. Edgington, L. E.; Verdoes, M.; Bogoyo, M. Functional Imaging of Proteases: Recent Advances in the Design and Application of Substrate-Based and Activity-Based Probes. *Curr Opin Chem Biol* **2011**, *15* (6), 798–805.

98. Harris, J. L.; Backes, B. J.; Leonetti, F.; Mahrus, S.; Ellman, J. A.; Craik, C. S. Rapid and General Profiling of Protease Specificity by Using Combinatorial Fluorogenic Substrate Libraries. *Proc Natl Acad Sci U S A* **2000**, *97* (14), 7754–7759.
99. Kasperkiewicz, P.; Poreba, M.; Snipas, S. J.; Parker, H.; Winterbourn, C. C.; Salvesen, G. S.; Drag, M. Design of Ultrasensitive Probes for Human Neutrophil Elastase through Hybrid Combinatorial Substrate Library Profiling. *Proc Natl Acad Sci U S A* **2014**, *111* (7), 2518–2523.
100. Kasperkiewicz, P.; Altman, Y.; D’Angelo, M.; Salvesen, G. S.; Drag, M. Toolbox of Fluorescent Probes for Parallel Imaging Reveals Uneven Location of Serine Proteases in Neutrophils. *J Am Chem Soc* **2017**, *139* (29), 10115–10125.
101. Kořt, S.; Janiszewski, T.; Kaiserman, D.; Modrzycka, S.; Snipas, S. J.; Salvesen, G.; Drą, M.; Bird, P. I.; Kasperkiewicz, P. Detection of Active Granzyme A in NK92 Cells with Fluorescent Activity-Based Probe. *Cite This: J. Med. Chem* **2020**, *63*, 3359–3369.
102. Mahrus, S.; Craik, C. S. Selective Chemical Functional Probes of Granzymes A and B Reveal Granzyme B Is a Major Effector of Natural Killer Cell-Mediated Lysis of Target Cells. *Chem Biol* **2005**, *12* (5), 567–577.
103. Kahler, J. P.; Verhelst, S. H. L. Phosphinate Esters as Novel Warheads for Activity-Based Probes Targeting Serine Proteases. *RSC Chem Biol* **2021**, *2* (4), 1285–1290.
104. Sadaghiani, A. M.; Verhelst, S. H.; Bogoyo, M. Tagging and Detection Strategies for Activity-Based Proteomics. *Curr Opin Chem Biol* **2007**, *11* (1), 20–28.
105. Jeffery, D. A.; Bogoyo, M. Chemical Proteomics and Its Application to Drug Discovery. *Curr Opin Biotechnol* **2003**, *14* (1), 87–95.
106. Li, N.; Kuo, C.-L.; Paniagua, G.; van den Elst, H.; Verdoes, M.; Willems, L. I.; van der Linden, W. A.; Ruben, M.; van Genderen, E.; Gubbens, J.; et al. Relative Quantification of Proteasome Activity by Activity-Based Protein Profiling and LC-MS/MS. *Nat Protoc* **2013**, *8* (6), 1155–1168.
107. Ngo, C.; Mehta, R.; Aggarwal, K.; Fikes, A. G.; Santos, I. C.; Greer, S. M.; Que, E. L. Pull-Down of Metalloproteins in Their Native States by Using Desthiobiotin-Based Probes. *ChemBioChem* **2019**, *20* (8), 1003–1007.

108. Hirsch, J. D.; Eslamizar, L.; Filanoski, B. J.; Malekzadeh, N.; Haugland, R. P.; Beechem, J. M.; Haugland, R. P. Easily Reversible Desthiobiotin Binding to Streptavidin, Avidin, and Other Biotin-Binding Proteins: Uses for Protein Labeling, Detection, and Isolation. *Anal Biochem* **2002**, *308* (2), 343–357.
109. Vangestel, C.; Thomae, D.; van Soom, J.; Ides, J.; wyffels, L.; Pauwels, P.; Stroobants, S.; van der Veken, P.; Magdolen, V.; Joossens, J.; et al. Preclinical Evaluation of [¹¹¹In]MICA-401, an Activity-Based Probe for SPECT Imaging of in Vivo UPA Activity. *Contrast Media Mol Imaging* **2016**, *11* (6), 448–458.
110. Poreba, M.; Groborz, K. M.; Rut, W.; Pore, M.; Snipas, S. J.; Vizovisek, M.; Turk, B.; Kuhn, P.; Drag, M.; Salvesen, G. S. Multiplexed Probing of Proteolytic Enzymes Using Mass Cytometry-Compatible Activity-Based Probes. *J Am Chem Soc* **2020**, *142* (39), 16704–16715.
111. Ong, S. E. The Expanding Field of SILAC. *Anal Bioanal Chem* **2012**, *404* (4), 967–976.
112. Edgington-Mitchell, L. E.; Barlow, N.; Aurelio, L.; Samha, A.; Szabo, M.; Graham, B.; Bunnett, N. Fluorescent Diphenylphosphonate-Based Probes for Detection of Serine Protease Activity during Inflammation. *Bioorg Med Chem Lett* **2017**, *27* (2), 254–260.
113. Schulz-Fincke, A.-C.; Blaut, M.; Braune, A.; Gütschow, M. A BODIPY-Tagged Phosphono Peptide as Activity-Based Probe for Human Leukocyte Elastase. *ACS Med Chem Lett* **2018**, *9* (4), 345–350.
114. Shannon, D. A.; Gu, C.; McLaughlin, C. J.; Kaiser, M.; van der Hoorn, R. A. L.; Weerapana, E. Sulfonyl Fluoride Analogues as Activity-Based Probes for Serine Proteases. *ChemBioChem* **2012**, *13* (16), 2327–2330.
115. Sabidó, E.; Tarragó, T.; Niessen, S.; Cravatt, B. F.; Giral, E. Activity-Based Probes for Monitoring Postproline Protease Activity. *ChemBioChem* **2009**, *10* (14), 2361–2366.
116. Speers, A. E.; Adam, G. C.; Cravatt, B. F. Activity-Based Protein Profiling in Vivo Using a Copper(I)-Catalyzed Azide-Alkyne [3 + 2] Cycloaddition. *J Am Chem Soc* **2003**, *125* (16), 4686–4687.
117. Speers, A. E.; Cravatt, B. F. Profiling Enzyme Activities in Vivo Using Click Chemistry Methods. *Chem Biol* **2004**, *11* (4), 535–546.

118. Powers, J. C.; Asgian, J. L.; Ekici, Ö. D.; James, K. E. Irreversible Inhibitors of Serine, Cysteine, and Threonine Proteases. *Chem Rev* **2002**, *102* (12), 4639–4750.
119. Guo, L.; Suarez, A. I.; Braden, M. R.; Gerdes, J. M.; Thompson, C. M. Inhibition of Acetylcholinesterase by Chromophore-Linked Fluorophosphonates. *Bioorg Med Chem Lett* **2010**, *20* (3), 1194–1197.
120. Serim, S.; Baer, P.; Verhelst, S. H. L. Mixed Alkyl Aryl Phosphonate Esters as Quenched Fluorescent Activity-Based Probes for Serine Proteases. *Org Biomol Chem* **2015**, *13* (8), 2293–2299.
121. Kam, C. M.; Abuelyaman, A. S.; Li, Z.; Hudig, D.; Powers, J. C. Biotinylated Isocoumarins, New Inhibitors and Reagents for Detection, Localization, and Isolation of Serine Proteases. *Bioconjug Chem* **1993**, *4* (6), 560–567.
122. Ruivo, E. F. P.; Gonçalves, L. M.; Carvalho, L. A. R.; Guedes, R. C.; Hofbauer, S.; Brito, J. A.; Archer, M.; Moreira, R.; Lucas, S. D. Clickable 4-Oxo- β -Lactam-Based Selective Probing for Human Neutrophil Elastase Related Proteomes. *ChemMedChem* **2016**, *11* (18), 2037–2042.
123. Schulz-Fincke, A.-C.; Tikhomirov, A. S.; Braune, A.; Girbl, T.; Gilberg, E.; Bajorath, J.; Blaut, M.; Nourshargh, S.; Gütschow, M. Design of an Activity-Based Probe for Human Neutrophil Elastase: Implementation of the Lossen Rearrangement To Induce Förster Resonance Energy Transfers. *Biochemistry* **2018**, *57* (5), 742–752.
124. Mangold, M.; Gütschow, M.; Stirnberg, M. A Short Peptide Inhibitor as an Activity-Based Probe for Matriptase-2. *Pharmaceuticals* **2018**, *11* (2).
125. Lambeir, A. Dipeptide-Derived Diphenyl Phosphonate Esters: Mechanism-Based Inhibitors of Dipeptidyl Peptidase IV. *Biochimica et Biophysica Acta (BBA) - General Subjects* **1996**, *1290* (1), 76–82.
126. van Soom, J.; Cuzzucoli Crucitti, G.; Gladysz, R.; van der Veken, P.; di Santo, R.; Stuyver, I.; Buck, V.; Lambeir, A.-M. M.; Magdolen, V.; Joossens, J.; et al. The First Potent Diphenyl Phosphonate KLK4 Inhibitors with Unexpected Binding Kinetics. *Medchemcomm* **2015**, *6* (11), 1954–1958.

127. Moreno-Cinos, C.; Sassetti, E.; Salado, I. G.; Witt, G.; Benramdane, S.; Reinhardt, L.; Cruz, C. D.; Joossens, J.; van der Veken, P.; Brötz-Oesterhelt, H.; et al. α -Amino Diphenyl Phosphonates as Novel Inhibitors of *Escherichia Coli* ClpP Protease. *J Med Chem* **2019**, *62* (2), 774–797.
128. Joossens, J.; Ali, O. M.; El-Sayed, I.; Surpateanu, G.; Van der Veken, P.; Lambeir, A.-M.; Setyono-Han, B.; Foekens, J. A.; Schneider, A.; Schmalix, W.; et al. Small, Potent, and Selective Diaryl Phosphonate Inhibitors for Urokinase-Type Plasminogen Activator with In Vivo Antimetastatic Properties. *J Med Chem* **2007**, *50* (26), 6638–6646.
129. Joossens, J.; van der Veken, P.; Surpateanu, G.; Lambeir, A.-M.; El-Sayed, I.; Ali, O. M.; Augustyns, K.; Haemers, A. Diphenyl Phosphonate Inhibitors for the Urokinase-Type Plasminogen Activator: Optimization of the P4 Position. *J Med Chem* **2006**, *49* (19), 5785–5793.
130. Augustyns, K.; van der Veken, P.; Messagie, J.; Joossens, J.; Lambeir, A.-M. Activity-Based Probes for the Urokinase Plasminogen Activator. WO2012152807 A1, 2012.
131. Oleksyszyn, J.; Subotkowska, L.; Mastalerz, P. Diphenyl 1-Aminoalkanephosphonates. *Synthesis (Stuttg)* **1979**, *1979* (12), 985–986.
132. Oleksyszyn, J.; Powers, J. C. Irreversible Inhibition of Serine Proteases by Peptide Derivatives of (Alpha-Aminoalkyl)Phosphonate Diphenyl Esters. *Biochemistry* **1991**, *30* (2), 485–493.
133. Bertrand, J. A.; Oleksyszyn, J.; Kam, C. M.; Boduszek, B.; Presnell, S.; Plaskon, R. R.; Suddath, F. L.; Powers, J. C.; Williams, L. D. Inhibition of Trypsin and Thrombin by Amino(4-Amidinophenyl)Methanephosphonate Diphenyl Ester Derivatives: X-Ray Structures and Molecular Models. *Biochemistry* **1996**, *35* (10), 3147–3155.
134. Hof, P.; Mayr, I.; Huber, R.; Korzus, E.; Potempa, J.; Travis, J.; Powers, J. C.; Bode, W. The 1.8 Å Crystal Structure of Human Cathepsin G in Complex with Suc-Val-Pro-PheP-(OPh)₂: A Janus-Faced Proteinase with Two Opposite Specificities. *EMBO J* **1996**, *15* (20), 5481–5491.

135. Oleksyszyn, J.; Powers, J. C. Amino Acid and Peptide Phosphonate Derivatives as Specific Inhibitors of Serine Peptidases. In *Methods in Enzymology*; Academic Press, 1994; Vol. 244, pp 423–441.
136. Boduszek, B.; Brown, A. D.; Powers, J. C. α -Aminoalkylphosphonate Di(Chlorophenyl) Esters as Inhibitors of Serine Proteases. *J Enzyme Inhib Med Chem* **1994**, *8* (3), 147–158.
137. Augustyns, K.; Joossens, J.; van der Veken, P.; Lambeir, A.-M.; Scharpe, S.; Haemers, A. Novel Urokinase Inhibitors. WO 2007/045496 A1, 2007.
138. Jackson, D. S.; Fraser, S. A.; Ni, L.-M.; Kam, C.-M.; Winkler, U.; Johnson, D. A.; Froelich, C. J.; Hudig, D.; Powers, J. C. Synthesis and Evaluation of Diphenyl Phosphonate Esters as Inhibitors of the Trypsin-like Granzymes A and K and Mast Cell Trypsase. *J Med Chem* **1998**, *41* (13), 2289–2301.
139. Deng, S.-L.; Baglin, I.; Nour, M.; Cavé, C. Synthesis of Phosphonodipeptide Conjugates of Ursolic Acid and Their Homologs. *Heteroatom Chemistry* **2008**, *19* (1), 55–65.
140. van der Veken, P.; el Sayed, I.; Joossens, J.; Stevens, C.; Augustyns, K.; Haemers, A. Lewis Acid Catalyzed Synthesis of N-Protected Diphenyl 1-Aminoalkylphosphonates. *Synthesis (Stuttg)* **2004**, *2005* (04), 634–638.
141. Abuelyaman, A. S.; Jackson, D. S.; Hudig, D.; Woodard, S. L.; Powers, J. C. Synthesis and Kinetic Studies of Diphenyl 1-(N- Peptidylamino)Alkanephosphonate Esters and Their Biotinylated Derivatives as Inhibitors of Serine Proteases and Probes for Lymphocyte Granzymes. *Arch Biochem Biophys* **1997**, *344* (2), 271–280.
142. Zou, F.; Schmon, M.; Sienczyk, M.; Grzywa, R.; Palesch, D.; Boehm, B. O.; Sun, Z. L.; Watts, C.; Schirmbeck, R.; Burster, T. Application of a Novel Highly Sensitive Activity-Based Probe for Detection of Cathepsin G. *Anal Biochem* **2012**, *421* (2), 667–672.
143. Guarino, C.; Legowska, M.; Epinette, C.; Kellenberger, C.; Dallet-Choisy, S.; Sienczyk, M.; Gabant, G.; Cadene, M.; Zoidakis, J.; Vlahou, A.; et al. New Selective Peptidyl Di(Chlorophenyl) Phosphonate Esters for Visualizing and Blocking Neutrophil

- Proteinase 3 in Human Diseases. *Journal of Biological Chemistry* **2014**, *289* (46), 31777–31791.
144. Kasperkiewicz, P.; Poreba, M.; Snipas, S. J.; Lin, S. J.; Kirchhofer, D.; Salvesen, G. S.; Drag, M. Design of a Selective Substrate and Activity Based Probe for Human Neutrophil Serine Protease 4. *PLoS One* **2015**, *10* (7), e0132818.
145. Craig, J. P.; Nichols, K. K.; Akpek, E. K.; Caffery, B.; Dua, H. S.; Joo, C.-K.; Liu, Z.; Nelson, J. D.; Nichols, J. J.; Tsubota, K.; et al. TFOS DEWS II Definition and Classification Report. *Ocul Surf* **2017**, *15* (3), 276–283.
146. Stern, M. E.; Pflugfelder, S. C. Inflammation in Dry Eye. *Ocul Surf* **2004**, *2* (2), 124–130.
147. Luo, L.; Li, D.-Q. Q.; Doshi, A.; Farley, W.; Corrales, R. M.; Pflugfelder, S. C. Experimental Dry Eye Stimulates Production of Inflammatory Cytokines and MMP-9 and Activates MAPK Signaling Pathways on the Ocular Surface. *Invest Ophthalmol Vis Sci* **2004**, *45* (12), 4293–4301.
148. *IT-DED³ Integrated Training in Dry Eye Disease Drug Development | Integrated Training in Dry Eye Disease Drug Development | University of Antwerp*. <http://itded3.eu/> (accessed 2022-09-14).
149. Drossman, D. A. Functional Gastrointestinal Disorders: History, Pathophysiology, Clinical Features, and Rome IV. *Gastroenterology* **2016**, *150* (6), 1262-1279.e2.
150. Vermeulen, W. Neuroanatomy of Lower Gastrointestinal Pain Disorders. *World J Gastroenterol* **2014**, *20* (4), 1005.
151. Ceuleers, H.; van Spaendonk, H.; Hanning, N.; Heirbaut, J.; Lambeir, A.-M.; Joossens, J.; Augustyns, K.; de Man, J. G.; de Meester, I.; de Winter, B. Y. Visceral Hypersensitivity in Inflammatory Bowel Diseases and Irritable Bowel Syndrome: The Role of Proteases. *World J Gastroenterol* **2016**, *22* (47), 10275.
152. *TRP sensation*. <https://www.trpsensation.com/> (accessed 2022-09-14).
153. Gomes, J. A. P.; Santo, R. M. The Impact of Dry Eye Disease Treatment on Patient Satisfaction and Quality of Life: A Review. *Ocul Surf* **2019**, *17* (1), 9–19.

154. Barabino, S.; Labetoulle, M.; Rolando, M.; Messmer, E. M. Understanding Symptoms and Quality of Life in Patients With Dry Eye Syndrome. *Ocul Surf* **2016**, *14* (3), 365–376.
155. Rouen, P. A.; White, M. L. Dry Eye Disease. *Home Healthc Now* **2018**, *36* (2), 74–83.
156. Stapleton, F.; Alves, M.; Bunya, V. Y.; Jalbert, I.; Lekhanont, K.; Malet, F.; Na, K.-S.; Schaumberg, D.; Uchino, M.; Vehof, J.; et al. TFOS DEWS II Epidemiology Report. *Ocul Surf* **2017**, *15* (3), 334–365.
157. Ahn, J. H.; Choi, Y.-H.; Paik, H. J.; Kim, M. K.; Wee, W. R.; Kim, D. H. Sex Differences in the Effect of Aging on Dry Eye Disease. *Clin Interv Aging* **2017**, *12*, 1331–1338.
158. Verjee, M. A.; Brissette, A. R.; Starr, C. E. Dry Eye Disease: Early Recognition with Guidance on Management and Treatment for Primary Care Family Physicians. *Ophthalmol Ther* **2020**, *9* (4), 877–888.
159. Krolo, I.; Blazeka, M.; Merdzo, I.; Vrtar, I.; Sabol, I.; Vickovic, I. Mask-Associated Dry Eye During COVID-19 Pandemic-How Face Masks Contribute to Dry Eye Disease Symptoms. *Medical Archives* **2021**, *75* (2), 144.
160. Boccardo, L. Self-Reported Symptoms of Mask-Associated Dry Eye: A Survey Study of 3,605 People. *Contact Lens and Anterior Eye* **2022**, *45* (2), 101408.
161. Reyes, J. L.; Vannan, D. T.; Eksteen, B.; Avelar, I. J.; Rodríguez, T.; González, M. I.; Mendoza, A. V. Innate and Adaptive Cell Populations Driving Inflammation in Dry Eye Disease. *Mediators Inflamm* **2018**, *2018*, 2532314.
162. Sullivan, D. A.; Sullivan, B. D.; Evans, J. E.; Schirra, F.; Yamagami, H.; Liu, M.; Richards, S. M.; Suzuki, T.; Schaumberg, D. A.; Sullivan, R. M.; et al. Androgen Deficiency, Meibomian Gland Dysfunction, and Evaporative Dry Eye. *Ann N Y Acad Sci* **2002**, *966* (1), 211–222.
163. Bai, Y.; Ngo, W.; Khanal, S.; Nichols, K. K.; Nichols, J. J. Human Precorneal Tear Film and Lipid Layer Dynamics in Meibomian Gland Dysfunction. *Ocul Surf* **2021**, *21*, 250–256.
164. Messmer, E. M. The Pathophysiology, Diagnosis, and Treatment of Dry Eye Disease. *Dtsch Arztebl Int* **2015**, *112*, 71–82.

165. Brito-Zerón, P.; Baldini, C.; Bootsma, H.; Bowman, S. J.; Jonsson, R.; Mariette, X.; Sivils, K.; Theander, E.; Tzioufas, A.; Ramos-Casals, M. Sjögren Syndrome. *Nat Rev Dis Primers* **2016**, *2* (1), 16047.
166. Baudouin, C.; Messmer, E. M.; Aragona, P.; Geerling, G.; Akova, Y. A.; Benítez-del-Castillo, J.; Boboridis, K. G.; Merayo-Llodes, J.; Rolando, M.; Labetoulle, M. Revisiting the Vicious Circle of Dry Eye Disease: A Focus on the Pathophysiology of Meibomian Gland Dysfunction. *British Journal of Ophthalmology* **2016**, *100* (3), 300–306.
167. Bron, A. J.; de Paiva, C. S.; Chauhan, S. K.; Bonini, S.; Gabison, E. E.; Jain, S.; Knop, E.; Markoulli, M.; Ogawa, Y.; Perez, V.; et al. TFOS DEWS II Pathophysiology Report. *Ocul Surf* **2017**, *15* (3), 438–510.
168. Wolffsohn, J. S.; Arita, R.; Chalmers, R.; Djalilian, A.; Dogru, M.; Dumbleton, K.; Gupta, P. K.; Karpecki, P.; Lazreg, S.; Pult, H.; et al. TFOS DEWS II Diagnostic Methodology Report. *Ocul Surf* **2017**, *15* (3), 539–574.
169. Stevenson, W. Dry Eye Disease. *Archives of Ophthalmology* **2012**, *130* (1), 90.
170. Fong, P.; Shih, K.; Lam, P.; Chan, T. Y.; Jhanji, V.; Tong, L. Role of Tear Film Biomarkers in the Diagnosis and Management of Dry Eye Disease. *Taiwan J Ophthalmol* **2019**, *9* (3), 150.
171. Jones, L.; Downie, L. E.; Korb, D.; Benitez-del-Castillo, J. M.; Dana, R.; Deng, S. X.; Dong, P. N.; Geerling, G.; Hida, R. Y.; Liu, Y.; et al. TFOS DEWS II Management and Therapy Report. *Ocul Surf* **2017**, *15* (3), 575–628.
172. Pflugfelder, S. C. Antiinflammatory Therapy for Dry Eye. *Am J Ophthalmol* **2004**, *137* (2), 337–342.
173. Kunert, K. S.; Tisdale, A. S.; Stern, M. E.; Smith, J. A.; Gipson, I. K. Analysis of Topical Cyclosporine Treatment of Patients With Dry Eye Syndrome<subtitle>Effect on Conjunctival Lymphocytes</Subtitle>. *Archives of Ophthalmology* **2000**, *118* (11), 1489.
174. Semba, C.; Gadek, T. Development of Lifitegrast: A Novel T-Cell Inhibitor for the Treatment of Dry Eye Disease. *Clinical Ophthalmology* **2016**, *10*, 1083.

175. Paton, D. M. Loteprednol Etabonate: A Formulation for Short-Term Use in Inflammatory Flares in Dry Eye Disease. *Drugs of Today* **2022**, *58* (2), 77.
176. de Souza, G. A.; Godoy, L. M. F.; Mann, M. Identification of 491 Proteins in the Tear Fluid Proteome Reveals a Large Number of Proteases and Protease Inhibitors. *Genome Biol* **2006**, *7* (8), R72.
177. Ehrmann, M.; Clausen, T. Proteolysis as a Regulatory Mechanism. *Annu Rev Genet* **2004**, *38* (1), 709–724.
178. Bond, J. S. Proteases: History, Discovery, and Roles in Health and Disease. *Journal of Biological Chemistry* **2019**, *294* (5), 1643–1651.
179. López-Otín, C.; Overall, C. M. Protease Degradomics: A New Challenge for Proteomics. *Nat Rev Mol Cell Biol* **2002**, *3* (7), 509–519.
180. López-Otín, C.; Bond, J. S. Proteases: Multifunctional Enzymes in Life and Disease. *Journal of Biological Chemistry* **2008**, *283* (45), 30433–30437.
181. Turk, B. Targeting Proteases: Successes, Failures and Future Prospects. *Nat Rev Drug Discov* **2006**, *5* (9), 785–799.
182. Heuberger, D. M.; Schuepbach, R. A. Protease-Activated Receptors (PARs): Mechanisms of Action and Potential Therapeutic Modulators in PAR-Driven Inflammatory Diseases. *Thromb J* **2019**, *17* (1), 4.
183. Fu, R.; Klinngam, W.; Heur, M.; Edman, M. C.; Hamm-Alvarez, S. F. Tear Proteases and Protease Inhibitors: Potential Biomarkers and Disease Drivers in Ocular Surface Disease. *Eye & Contact Lens: Science & Clinical Practice* **2020**, *46* (2), S70–S83.
184. Yu, Z.; Li, J.; Govindarajan, G.; Hamm-Alvarez, S. F.; Alam, J.; Li, D.-Q.; de Paiva, C. S. Cathepsin S Is a Novel Target for Age-Related Dry Eye. *Exp Eye Res* **2022**, *214*, 108895.
185. Joossen, C.; Baán, A.; Moreno-Cinos, C.; Joossens, J.; Cools, N.; Lanckacker, E.; Moons, L.; Lemmens, K.; Lambeir, A.-M. M.; Franssen, E.; et al. A Novel Serine Protease Inhibitor as Potential Treatment for Dry Eye Syndrome and Ocular Inflammation. *Sci Rep* **2020**, *10* (1), 17268.

186. Decraecker, L.; Boeckxstaens, G.; Denadai-Souza, A. Inhibition of Serine Proteases as a Novel Therapeutic Strategy for Abdominal Pain in IBS. *Front Physiol* **2022**, *13*, 948.
187. Bleuez, C.; Koch, W. F.; Urbach, C.; Hollfelder, F.; Jermutus, L. Exploiting Protease Activation for Therapy. *Drug Discov Today* **2022**, *27* (6), 1743–1754.
188. Verma, R. P.; Hansch, C. Matrix Metalloproteinases (MMPs): Chemical–Biological Functions and (Q)SARs. *Bioorg Med Chem* **2007**, *15* (6), 2223–2268.
189. Page-McCaw, A.; Ewald, A. J.; Werb, Z. Matrix Metalloproteinases and the Regulation of Tissue Remodelling. *Nat Rev Mol Cell Biol* **2007**, *8* (3), 221–233.
190. van Wart, H. E.; Birkedal-Hansen, H. The Cysteine Switch: A Principle of Regulation of Metalloproteinase Activity with Potential Applicability to the Entire Matrix Metalloproteinase Gene Family (Collagenase/Gelatinase/Stromelysin/Zinc Enzyme). *Proc. Natl. Acad. Sci. USA* **1990**, *87*, 5578–5582.
191. Xu, I.; Thériault, M.; Brunette, I.; Rochette, P. J.; Proulx, S. Matrix Metalloproteinases and Their Inhibitors in Fuchs Endothelial Corneal Dystrophy. *Exp Eye Res* **2021**, *205*, 108500.
192. Corrales, R. M.; Stern, M. E.; de Paiva, C. S.; Welch, J.; Li, D.-Q.; Pflugfelder, S. C. Desiccating Stress Stimulates Expression of Matrix Metalloproteinases by the Corneal Epithelium. *Investigative Ophthalmology & Visual Science* **2006**, *47* (8), 3293.
193. de Paiva, C. S.; Corrales, R. M.; Villarreal, A. L.; Farley, W. J.; Li, D.-Q.; Stern, M. E.; Pflugfelder, S. C. Corticosteroid and Doxycycline Suppress MMP-9 and Inflammatory Cytokine Expression, MAPK Activation in the Corneal Epithelium in Experimental Dry Eye. *Exp Eye Res* **2006**, *83* (3), 526–535.
194. Qu, M.; Qi, X.; Wang, Q.; Wan, L.; Li, J.; Li, W.; Li, Y.; Zhou, Q. Therapeutic Effects of STAT3 Inhibition on Experimental Murine Dry Eye. *Investigative Ophthalmology & Visual Science* **2019**, *60* (12), 3776.
195. Seo, M. J.; Kim, J. M.; Lee, M. J.; Sohn, Y. S.; Kang, K. K.; Yoo, M. The Therapeutic Effect of DA-6034 on Ocular Inflammation via Suppression of MMP-9 and Inflammatory Cytokines and Activation of the MAPK Signaling Pathway in an Experimental Dry Eye Model. *Curr Eye Res* **2010**, *35* (2), 165–175.

196. Pflugfelder, S. C.; Farley, W.; Luo, L.; Chen, L. Z.; de Paiva, C. S.; Olmos, L. C.; Li, D.-Q.; Fini, M. E. Matrix Metalloproteinase-9 Knockout Confers Resistance to Corneal Epithelial Barrier Disruption in Experimental Dry Eye. *Am J Pathol* **2005**, *166* (1), 61–71.
197. Lee, Y. H.; Bang, S.-P.; Shim, K.-Y.; Son, M.-J.; Kim, H.; Jun, J. H. Association of Tear Matrix Metalloproteinase 9 Immunoassay with Signs and Symptoms of Dry Eye Disease: A Cross-Sectional Study Using Qualitative, Semiquantitative, and Quantitative Strategies. *PLoS One* **2021**, *16* (10), e0258203.
198. Schargus, M.; Ivanova, S.; Kakkassery, V.; Dick, H. B.; Joachim, S. Correlation of Tear Film Osmolarity and 2 Different MMP-9 Tests With Common Dry Eye Tests in a Cohort of Non-Dry Eye Patients. *Cornea* **2015**, *34* (7), 739–744.
199. Kang, M.-J.; Kim, H. S.; Kim, M. S.; Kim, E. C. The Correlation between Matrix Metalloproteinase-9 Point-of-Care Immunoassay, Tear Film Osmolarity, and Ocular Surface Parameters. *J Ophthalmol* **2022**, *2022*, 6132016.
200. Kook, K. Y.; Jin, R.; Li, L.; Yoon, H. J.; Yoon, K. C. Tear Osmolarity and Matrix Metalloproteinase-9 in Dry Eye Associated with Sjögren’s Syndrome. *Korean Journal of Ophthalmology* **2020**, *34* (3), 179–186.
201. Lanza, N. L.; Valenzuela, F.; Perez, V. L.; Galor, A. The Matrix Metalloproteinase 9 Point-of-Care Test in Dry Eye. *Ocul Surf* **2016**, *14* (2), 189–195.
202. Drag, M.; Salvesen, G. S. Emerging Principles in Protease-Based Drug Discovery. *Nat Rev Drug Discov* **2010**, *9* (9), 690–701.
203. Vergnolle, N. Protease Inhibition as New Therapeutic Strategy for GI Diseases. *Gut* **2016**, *65* (7), 1215–1224.
204. Safavi, F.; Rostami, A. Role of Serine Proteases in Inflammation: Bowman–Birk Protease Inhibitor (BBI) as a Potential Therapy for Autoimmune Diseases. *Exp Mol Pathol* **2012**, *93* (3), 428–433.
205. Denadai-Souza, A.; Bonnart, C.; Tapias, N. S.; Marcellin, M.; Gilmore, B.; Alric, L.; Bonnet, D.; Burlet-Schiltz, O.; Hollenberg, M. D.; Vergnolle, N.; et al. Functional

- Proteomic Profiling of Secreted Serine Proteases in Health and Inflammatory Bowel Disease. *Sci Rep* **2018**, *8* (1), 7834.
206. Sathe, S.; Sakata, M.; Beaton, A. R.; Sack, R. A. Identification, Origins and the Diurnal Role of the Principal Serine Protease Inhibitors in Human Tear Fluid. *Curr Eye Res* **1998**, *17* (4), 348–362.
207. Mun, Y.; Hwang, J. S.; Shin, Y. J. Role of Neutrophils on the Ocular Surface. *Int J Mol Sci* **2021**, *22* (19), 10386.
208. Döring, G. The Role of Neutrophil Elastase in Chronic Inflammation. *Am J Respir Crit Care Med* **1994**, *150* (6_pt_2), S114–S117.
209. Pham, C. T. N. Neutrophil Serine Proteases Fine-Tune the Inflammatory Response. *Int J Biochem Cell Biol* **2008**, *40* (6–7), 1317–1333.
210. Sonawane, S.; Khanolkar, V.; Namavari, A.; Chaudhary, S.; Gandhi, S.; Tibrewal, S.; Jassim, S. H.; Shaheen, B.; Hallak, J.; Horner, J. H.; et al. Ocular Surface Extracellular DNA and Nuclease Activity Imbalance: A New Paradigm for Inflammation in Dry Eye Disease. *Investigative Ophthalmology & Visual Science* **2012**, *53* (13), 8253.
211. Nair, A. P.; D'Souza, S.; Shetty, R.; Ahuja, P.; Kundu, G.; Khamar, P.; Dadachanji, Z.; Paritekar, P.; Patel, P.; Dickman, M. M.; et al. Altered Ocular Surface Immune Cell Profile in Patients with Dry Eye Disease. *Ocul Surf* **2021**, *21*, 96–106.
212. Postnikoff, C. K.; Held, K.; Viswanath, V.; Nichols, K. K. Enhanced Closed Eye Neutrophil Degranulation in Dry Eye Disease. *Ocul Surf* **2020**, *18* (4), 841–851.
213. Tibrewal, S.; Ivanir, Y.; Sarkar, J.; Nayeb-Hashemi, N.; Bouchard, C. S.; Kim, E.; Jain, S. Hyperosmolar Stress Induces Neutrophil Extracellular Trap Formation: Implications for Dry Eye Disease. *Invest Ophthalmol Vis Sci* **2014**, *55* (12), 7961–7969.
214. Mahajan, A.; Hasíková, L.; Hampel, U.; Grüneboom, A.; Shan, X.; Herrmann, I.; Garreis, F.; Bock, F.; Knopf, J.; Singh, J.; et al. Aggregated Neutrophil Extracellular Traps Occlude Meibomian Glands during Ocular Surface Inflammation. *Ocul Surf* **2021**, *20*, 1–12.
215. Magrini, L.; Bonini, S.; Centofanti, M.; Schiavone, M.; Bonini, S. Tear Tryptase Levels and Allergic Conjunctivitis. *Allergy* **1996**, *51* (8), 577–581.

216. Caughey, G. H. Mast Cell Tryptases and Chymases in Inflammation and Host Defense. *Immunol Rev* **2007**, *217* (1), 141–154.
217. Butrus, S. I.; Ochsner, K. I.; Abelson, M. B.; Schwartz, L. B. The Level of Tryptase in Human Tears. *Ophthalmology* **1990**, *97* (12), 1678–1683.
218. Li, Q.; Jie, Y.; Wang, C.; Zhang, Y.; Guo, H.; Pan, Z. Tryptase Compromises Corneal Epithelial Barrier Function. *Cell Biochem Funct* **2014**, *32* (2), 183–187.
219. Ebihara, N.; Funaki, T.; Murakami, A.; Takai, S.; Miyazaki, M. Mast Cell Chymase Decreases the Barrier Function and Inhibits the Migration of Corneal Epithelial Cells. *Curr Eye Res* **2005**, *30* (12), 1061–1069.
220. Villani, E.; Rabbio, G.; Nucci, P. Ocular Allergy as a Risk Factor for Dry Eye in Adults and Children. *Curr Opin Allergy Clin Immunol* **2018**, *18* (5), 398–403.
221. Turk, B.; Turk, D.; Salvesen, G. Regulating Cysteine Protease Activity: Essential Role of Protease Inhibitors As Guardians and Regulators. *Curr Pharm Des* **2002**, *8* (18), 1623–1637.
222. Rawlings, N. D.; Barrett, A. J.; Thomas, P. D.; Huang, X.; Bateman, A.; Finn, R. D. The MEROPS Database of Proteolytic Enzymes, Their Substrates and Inhibitors in 2017 and a Comparison with Peptidases in the PANTHER Database. *Nucleic Acids Res* **2018**, *46* (D1), D624–D632.
223. Tušar, L.; Usenik, A.; Turk, B.; Turk, D. Mechanisms Applied by Protein Inhibitors to Inhibit Cysteine Proteases. *Int J Mol Sci* **2021**, *22* (3), 997.
224. Roush, W. R.; Gwaltney, S. L.; Cheng, J.; Scheidt, K. A.; McKerrow, J. H.; Hansell, E. Vinyl Sulfonate Esters and Vinyl Sulfonamides: Potent, Irreversible Inhibitors of Cysteine Proteases. *J Am Chem Soc* **1998**, *120* (42), 10994–10995.
225. Im, E.; Kazlauskas, A. The Role of Cathepsins in Ocular Physiology and Pathology. *Exp Eye Res* **2007**, *84* (3), 383–388.
226. Lin, H.-H.; Chen, S.-J.; Shen, M.-R.; Huang, Y.-T.; Hsieh, H.-P.; Lin, S.-Y.; Lin, C.-C.; Chang, W.-S. W.; Chang, J.-Y. Lysosomal Cysteine Protease Cathepsin S Is Involved in Cancer Cell Motility by Regulating Store-Operated Ca²⁺ Entry. *Biochimica et Biophysica Acta (BBA) - Molecular Cell Research* **2019**, *1866* (12), 118517.

-
227. Wolters, P. J.; Chapman, H. A. Importance of Lysosomal Cysteine Proteases in Lung Disease. *Respir Res* **2000**, *1* (3), 170–177.
228. Li, X.; Wu, K.; Edman, M.; Schenke-Layland, K.; MacVeigh-Aloni, M.; Janga, S. R.; Schulz, B.; Hamm-Alvarez, S. F. Increased Expression of Cathepsins and Obesity-Induced Proinflammatory Cytokines in Lacrimal Glands of Male NOD Mouse. *Investigative Ophthalmology & Visual Science* **2010**, *51* (10), 5019.
229. Hamm-Alvarez, S. F.; Janga, S. R.; Edman, M. C.; Madrigal, S.; Shah, M.; Frousiakis, S. E.; Renduchintala, K.; Zhu, J.; Bricel, S.; Silka, K.; et al. Tear Cathepsin S as a Candidate Biomarker for Sjögren’s Syndrome. *Arthritis & Rheumatology* **2014**, *66* (7), 1872–1881.
230. Edman, M. C.; Janga, S. R.; Meng, Z.; Bechtold, M.; Chen, A. F.; Kim, C.; Naman, L.; Sarma, A.; Teekappanavar, N.; Kim, A. Y.; et al. Increased Cathepsin S Activity Associated with Decreased Protease Inhibitory Capacity Contributes to Altered Tear Proteins in Sjögren’s Syndrome Patients. *Sci Rep* **2018**, *8* (1), 11044.
231. Ossovskaya, V. S.; Bunnett, N. W. Protease-Activated Receptors: Contribution to Physiology and Disease. *Physiol Rev* **2004**, *84* (2), 579–621.
232. Adams, M. N.; Ramachandran, R.; Yau, M.-K.; Suen, J. Y.; Fairlie, D. P.; Hollenberg, M. D.; Hooper, J. D. Structure, Function and Pathophysiology of Protease Activated Receptors. *Pharmacol Ther* **2011**, *130* (3), 248–282.
233. Sébert, M.; Sola-Tapias, N.; Mas, E.; Barreau, F.; Ferrand, A. Protease-Activated Receptors in the Intestine: Focus on Inflammation and Cancer. *Front Endocrinol (Lausanne)* **2019**, *10*, 717.
234. Cumashi, A.; Ansuini, H.; Celli, N.; Blasi, A. de; O’Brien, P.; Brass, L.; Molino, M. Neutrophil Proteases Can Inactivate Human PAR3 and Abolish the Co-Receptor Function of PAR3 on Murine Platelets. *Thromb Haemost* **2001**, *85* (03), 533–538.
235. Price, R.; Mercuri, N. B.; Ledonne, A. Emerging Roles of Protease-Activated Receptors (PARs) in the Modulation of Synaptic Transmission and Plasticity. *Int J Mol Sci* **2021**, *22* (2), 869.

236. Rothmeier, A. S.; Ruf, W. Protease-Activated Receptor 2 Signaling in Inflammation. *Semin Immunopathol* **2012**, *34* (1), 133–149.
237. Macfarlane, S. R.; Sloss, C. M.; Cameron, P.; Kanke, T.; McKenzie, R. C.; Plevin, R. The Role of Intracellular Ca²⁺ in the Regulation of Proteinase-Activated Receptor-2 Mediated Nuclear Factor Kappa B Signalling in Keratinocytes. *Br J Pharmacol* **2005**, *145* (4), 535–544.
238. Chandrabalan, A.; Ramachandran, R. Molecular Mechanisms Regulating Proteinase-Activated Receptors (PARs). *FEBS J* **2021**, *288* (8), 2697–2726.
239. Ramachandran, R.; Mihara, K.; Chung, H.; Renaux, B.; Lau, C. S.; Muruve, D. A.; DeFea, K. A.; Bouvier, M.; Hollenberg, M. D. Neutrophil Elastase Acts as a Biased Agonist for Proteinase-Activated Receptor-2 (PAR2). *Journal of Biological Chemistry* **2011**, *286* (28), 24638–24648.
240. Stern, M. E.; Schaumburg, C. S.; Pflugfelder, S. C. Dry Eye as a Mucosal Autoimmune Disease. *Int Rev Immunol* **2013**, *32* (1), 19–41.
241. Valdez-Morales, E. E.; Overington, J.; Guerrero-Alba, R.; Ochoa-Cortes, F.; Ibeakanma, C. O.; Spreadbury, I.; Bunnett, N. W.; Beyak, M.; Vanner, S. J. Sensitization of Peripheral Sensory Nerves by Mediators From Colonic Biopsies of Diarrhea-Predominant Irritable Bowel Syndrome Patients: A Role for PAR2. *American Journal of Gastroenterology* **2013**, *108* (10), 1634–1643.
242. Bucci, M.; Roviezzo, F.; Cirino, G. Protease-Activated Receptor-2 (PAR2) in Cardiovascular System. *Vascul Pharmacol* **2005**, *43* (4), 247–253.
243. Sokolova, E.; Reiser, G. A Novel Therapeutic Target in Various Lung Diseases: Airway Proteases and Protease-Activated Receptors. *Pharmacol Ther* **2007**, *115* (1), 70–83.
244. Lang, R.; Song, P. I.; Legat, F. J.; Lavker, R. M.; Harten, B.; Kalden, H.; Grady, E. F.; Bunnett, N. W.; Armstrong, C. A.; Ansel, J. C. Human Corneal Epithelial Cells Express Functional PAR-1 and PAR-2. *Investigative Ophthalmology & Visual Science* **2003**, *44* (1), 99–105.
245. Tripathi, T.; Alizadeh, H. Role of Protease-Activated Receptors 2 (PAR2) in Ocular Infections and Inflammation. *Receptors Clin Investig* **2014**, *2*, 1–12.

-
246. Zhao, P.; Lieu, T.; Barlow, N.; Metcalf, M.; Veldhuis, N. A.; Jensen, D. D.; Kocan, M.; Sostegni, S.; Haerteis, S.; Baraznenok, V.; et al. Cathepsin S Causes Inflammatory Pain via Biased Agonism of PAR2 and TRPV4. *Journal of Biological Chemistry* **2014**, *289* (39), 27215–27234.
247. Klinggam, W.; Fu, R.; Janga, S.; Edman, M.; Hamm-Alvarez, S. Cathepsin S Alters the Expression of Pro-Inflammatory Cytokines and MMP-9, Partially through Protease—Activated Receptor-2, in Human Corneal Epithelial Cells. *Int J Mol Sci* **2018**, *19* (11), 3530.
248. Mori, M.; de Lorenzo, E.; Torre, E.; Fragai, M.; Nativi, C.; Luchinat, C.; Arcangeli, A. A Highly Soluble Matrix Metalloproteinase-9 Inhibitor for Potential Treatment of Dry Eye Syndrome. *Basic Clin Pharmacol Toxicol* **2012**, *111* (5), 289–295.
249. Richichi, B.; Baldoneschi, V.; Buralassi, S.; Fragai, M.; Vullo, D.; Akdemir, A.; Dragoni, E.; Louka, A.; Mamusa, M.; Monti, D.; et al. A Divalent PAMAM-Based Matrix Metalloproteinase/Carbonic Anhydrase Inhibitor for the Treatment of Dry Eye Syndrome. *Chemistry - A European Journal* **2016**, *22* (5), 1714–1721.
250. Shoari, A.; Rasaee, M. J.; Rezaei Kanavi, M.; Afsar Aski, S.; Tooyserkani, R. In Vivo Effect of RSH-12, a Novel Selective MMP-9 Inhibitor Peptide, in the Treatment of Experimentally Induced Dry Eye Model. *Curr Eye Res* **2021**, *46* (1), 7–13.
251. Liu, X.; Lin, Z.; Zhou, T.; Zong, R.; He, H.; Liu, Z.; Ma, J.; Liu, Z.; Zhou, Y. Anti-Angiogenic and Anti-Inflammatory Effects of SERPINA3K on Corneal Injury. *PLoS One* **2011**, *6* (1), e16712.
252. Hu, J.; Zhang, Z.; Xie, H.; Chen, L.; Zhou, Y.; Chen, W.; Liu, Z. Serine Protease Inhibitor A3K Protects Rabbit Corneal Endothelium From Barrier Function Disruption Induced by TNF- α . *Investigative Ophthalmology & Visual Science* **2013**, *54* (8), 5400.
253. Lin, Z.; Zhou, Y.; Wang, Y.; Zhou, T.; Li, J.; Luo, P.; He, H.; Wu, H.; Liu, Z. Serine Protease Inhibitor A3K Suppressed the Formation of Ocular Surface Squamous Metaplasia in a Mouse Model of Experimental Dry Eye. *Investigative Ophthalmology & Visual Science* **2014**, *55* (9), 5813.

254. Lin, Z.; Liu, X.; Zhou, T.; Wang, Y.; Bai, L.; He, H.; Liu, Z. A Mouse Dry Eye Model Induced by Topical Administration of Benzalkonium Chloride. *Mol Vis* **2011**, *17*, 257–264.
255. Steele, F. R.; Chader, G. J.; Johnson, L. v.; Tombran-Tink, J. Pigment Epithelium-Derived Factor: Neurotrophic Activity and Identification as a Member of the Serine Protease Inhibitor Gene Family. *Proceedings of the National Academy of Sciences* **1993**, *90* (4), 1526–1530.
256. Karakousis, P. C.; John, S. K.; Behling, K. C.; Surace, E. M.; Smith, J. E.; Hendrickson, A.; Tang, W. X.; Bennett, J.; Milam, A. H. Localization of Pigment Epithelium Derived Factor (PEDF) in Developing and Adult Human Ocular Tissues. *Mol Vis* **2001**, *7*, 154–163.
257. Singh, R. B.; Blanco, T.; Mittal, S. K.; Taketani, Y.; Chauhan, S. K.; Chen, Y.; Dana, R. Pigment Epithelium-Derived Factor Secreted by Corneal Epithelial Cells Regulates Dendritic Cell Maturation in Dry Eye Disease. *Ocul Surf* **2020**, *18* (3), 460–469.
258. Ma, B.; Zhou, Y.; Liu, R.; Zhang, K.; Yang, T.; Hu, C.; Gao, Y.; Lan, Q.; Liu, Y.; Yang, X.; et al. Pigment Epithelium-Derived Factor (PEDF) Plays Anti-Inflammatory Roles in the Pathogenesis of Dry Eye Disease. *Ocul Surf* **2021**, *20*, 70–85.
259. Joossen, C.; Lanckacker, E.; Zakaria, N.; Koppen, C.; Joossens, J.; Cools, N.; de Meester, I.; Lambeir, A.-M.; Delputte, P.; Maes, L.; et al. Optimization and Validation of an Existing, Surgical and Robust Dry Eye Rat Model for the Evaluation of Therapeutic Compounds. *Exp Eye Res* **2016**, *146*, 172–178.
260. Singh, R. B.; Blanco, T.; Mittal, S. K.; Alemi, H.; Chauhan, S. K.; Chen, Y.; Dana, R. Pigment Epithelium-Derived Factor Enhances the Suppressive Phenotype of Regulatory T Cells in a Murine Model of Dry Eye Disease. *Am J Pathol* **2021**, *191* (4), 720–729.
261. Saarinen, N. V. v.; Stone, V. M.; Hankaniemi, M. M.; Mazur, M. A.; Vuorinen, T.; Flodström-Tullberg, M.; Hyöty, H.; Hytönen, V. P.; Laitinen, O. H. Antibody Responses against Enterovirus Proteases Are Potential Markers for an Acute Infection. *Viruses* **2020**, *12* (1), 78.

-
262. Costanzi, E.; Kuzikov, M.; Esposito, F.; Albani, S.; Demitri, N.; Giabbai, B.; Camasta, M.; Tramontano, E.; Rossetti, G.; Zaliani, A.; et al. Structural and Biochemical Analysis of the Dual Inhibition of MG-132 against SARS-CoV-2 Main Protease (Mpro/3CLpro) and Human Cathepsin-L. *Int J Mol Sci* **2021**, *22* (21), 11779.
263. Peng, H.; Hulleman, J. D. Prospective Application of Activity-Based Proteomic Profiling in Vision Research-Potential Unique Insights into Ocular Protease Biology and Pathology. *Int J Mol Sci* **2019**, *20* (16), 3855.
264. Zhang, L.; Lin, D.; Sun, X.; Curth, U.; Drosten, C.; Sauerhering, L.; Becker, S.; Rox, K.; Hilgenfeld, R. Crystal Structure of SARS-CoV-2 Main Protease Provides a Basis for Design of Improved α -Ketoamide Inhibitors. *Science (1979)* **2020**, *368* (6489), 409–412.
265. Sperber, A. D.; Bangdiwala, S. I.; Drossman, D. A.; Ghoshal, U. C.; Simren, M.; Tack, J.; Whitehead, W. E.; Dumitrascu, D. L.; Fang, X.; Fukudo, S.; et al. Worldwide Prevalence and Burden of Functional Gastrointestinal Disorders, Results of Rome Foundation Global Study. *Gastroenterology* **2021**, *160* (1), 99–114.
266. Oka, P.; Parr, H.; Barberio, B.; Black, C. J.; Savarino, E. v.; Ford, A. C. Global Prevalence of Irritable Bowel Syndrome According to Rome III or IV Criteria: A Systematic Review and Meta-Analysis. *Lancet Gastroenterol Hepatol* **2020**, *5* (10), 908–917.
267. Palsson, O. S.; Whitehead, W.; Törnblom, H.; Sperber, A. D.; Simren, M. Prevalence of Rome IV Functional Bowel Disorders Among Adults in the United States, Canada, and the United Kingdom. *Gastroenterology* **2020**, *158* (5), 1262-1273.e3.
268. Camilleri, M. Sex as a Biological Variable in Irritable Bowel Syndrome. *Neurogastroenterology and Motility* **2020**, *32* (7).
269. Creed, F. Risk Factors for Self-Reported Irritable Bowel Syndrome With Prior Psychiatric Disorder: The Lifelines Cohort Study. *J Neurogastroenterol Motil* **2022**, *28* (3), 442–453.
270. Creed, F. Review Article: The Incidence and Risk Factors for Irritable Bowel Syndrome in Population-Based Studies. *Aliment Pharmacol Ther* **2019**, *50* (5), 507–516.

271. Chey, W. D.; Kurlander, J.; Eswaran, S. Irritable Bowel Syndrome. *JAMA* **2015**, *313* (9), 949.
272. Black, C. J. Review Article: Diagnosis and Investigation of Irritable Bowel Syndrome. *Aliment Pharmacol Ther* **2021**, *54* (S1), S33–S43.
273. Camilleri, M. Diagnosis and Treatment of Irritable Bowel Syndrome: A Review. *JAMA* **2021**, *325* (9), 865–877.
274. Anand, P.; Aziz, Q.; Willert, R.; van oudenove, L. Peripheral and Central Mechanisms of Visceral Sensitization in Man. *Neurogastroenterology & Motility* **2007**, *19* (s1), 29–46.
275. Blackshaw, L. A.; Brookes, S. J. H.; Grundy, D.; Schemann, M. Sensory Transmission in the Gastrointestinal Tract. *Neurogastroenterology & Motility* **2007**, *19* (s1), 1–19.
276. Brizuela, M.; Castro, J.; Harrington, A. M.; Brierley, S. M. Pruritogenic Mechanisms and Gut Sensation: Putting the “Irritant” into Irritable Bowel Syndrome. *Am J Physiol Gastrointest Liver Physiol* **2021**, *320* (6), G1131–G1141.
277. van Spaendonk, H.; Ceuleers, H.; Witters, L.; Patteet, E.; Joossens, J.; Augustyns, K.; Lambeir, A.-M.; de Meester, I.; de Man, J. G.; de Winter, B. Y. Regulation of Intestinal Permeability: The Role of Proteases. *World J Gastroenterol* **2017**, *23* (12), 2106.
278. Vergnolle, N. Modulation of Visceral Pain and Inflammation by Protease-Activated Receptors. *Br J Pharmacol* **2004**, *141* (8), 1264–1274.
279. Barbara, G.; Stanghellini, V.; de Giorgio, R.; Cremon, C.; Cottrell, G. S.; Santini, D.; Pasquinelli, G.; Morselli-Labate, A. M.; Grady, E. F.; Bunnett, N. W.; et al. Activated Mast Cells in Proximity to Colonic Nerves Correlate with Abdominal Pain in Irritable Bowel Syndrome. *Gastroenterology* **2004**, *126* (3), 693–702.
280. Theoharides, T. C.; Alysandratos, K. D.; Angelidou, A.; Delivanis, D. A.; Sismanopoulos, N.; Zhang, B.; Asadi, S.; Vasiadi, M.; Weng, Z.; Miniati, A.; et al. Mast Cells and Inflammation. *Biochim Biophys Acta* **2012**, *1822* (1), 21–33.
281. Aguilera-Lizarraga, J.; Florens, M. v.; Viola, M. F.; Jain, P.; Decraecker, L.; Appeltans, I.; Cuende-Estevez, M.; Fabre, N.; van Beek, K.; Perna, E.; et al. Local Immune

- Response to Food Antigens Drives Meal-Induced Abdominal Pain. *Nature* **2021**, *590* (7844), 151–156.
282. Zhao, J. H.; Dong, L.; Shi, H. T.; Wang, Z. Y.; Shi, H. Y.; Ding, H. The Expression of Protease-Activated Receptor 2 and 4 in the Colon of Irritable Bowel Syndrome Patients. *Dig Dis Sci* **2012**, *57* (1), 58–64.
283. Buhner, S.; Hahne, H.; Hartwig, K.; Li, Q.; Vignali, S.; Ostertag, D.; Meng, C.; Hörmannspenger, G.; Braak, B.; Pehl, C.; et al. Protease Signaling through Protease Activated Receptor 1 Mediate Nerve Activation by Mucosal Supernatants from Irritable Bowel Syndrome but Not from Ulcerative Colitis Patients. *PLoS One* **2018**, *13* (3).
284. Róka, R.; Rosztóczy, A.; Leveque, M.; Izbéki, F.; Nagy, F.; Molnár, T.; Lonovics, J.; Garcia-Villar, R.; Fioramonti, J.; Wittmann, T.; et al. A Pilot Study of Fecal Serine-Protease Activity: A Pathophysiologic Factor in Diarrhea-Predominant Irritable Bowel Syndrome. *Clinical Gastroenterology and Hepatology* **2007**, *5* (5), 550–555.
285. Gecse, K.; Roka, R.; Ferrier, L.; Leveque, M.; Eutamene, H.; Cartier, C.; Ait-Belgnaoui, A.; Rosztoczy, A.; Izbeki, F.; Fioramonti, J.; et al. Increased Faecal Serine Protease Activity in Diarrhoeic IBS Patients: A Colonic Luminal Factor Impairing Colonic Permeability and Sensitivity. *Gut* **2008**, *57* (5), 591–599.
286. Edogawa, S.; Edwinson, A. L.; Peters, S. A.; Sundt, W.; Graves, S.; Gurunathan, S. v.; Breen-Lyles, M.; Johnson, S.; Dyer, R.; Graham, R.; et al. Serine Proteases as Luminal Mediators of Intestinal Barrier Dysfunction and Symptom Severity in IBS. *Gut* **2020**, *69*, 62–73.
287. Vergnolle, N. Clinical Relevance of Proteinase Activated Receptors (PARs) in the Gut. *Gut* **2005**, *54* (6), 867–874.
288. Kawabata, A.; Kawao, N.; Kuroda, R.; Tanaka, A.; Shimada, C. The PAR-1-Activating Peptide Attenuates Carrageenan-Induced Hyperalgesia in Rats. *Peptides (N.Y.)* **2002**, *23* (6), 1181–1183.
289. Kawao, N.; Ikeda, H.; Kitano, T.; Kuroda, R.; Sekiguchi, F.; Kataoka, K.; Kamanaka, Y.; Kawabata, A. Modulation of Capsaicin-Evoked Visceral Pain and Referred

- Hyperalgesia by Protease-Activated Receptors 1 and 2. *Journal of Pharmacological Sciences J Pharmacol Sci* **2004**, *94*, 277–285.
290. Annaházi, A.; Gecse, K.; Dabek, M.; Ait-Belgnaoui, A.; Rosztóczy, A.; Róka, R.; Molnár, T.; Theodorou, V.; Wittmann, T.; Bueno, L.; et al. Fecal Proteases from Diarrheic-IBS and Ulcerative Colitis Patients Exert Opposite Effect on Visceral Sensitivity in Mice. *Pain* **2009**, *144* (1–2), 209–217.
291. Coelho, A.; Vergnolle, N.; Guiard, B.; Fioramonti, J.; Bueno, L. Proteinases and Proteinase-Activated Receptor 2: A Possible Role to Promote Visceral Hyperalgesia in Rats. *Gastroenterology* **2002**, *122* (4), 1035–1047.
292. Kawabata, A.; Kawao, N.; Kuroda, R.; Tanaka, A.; Itoh, H.; Nishikawa, H. Peripheral PAR-2 Triggers Thermal Hyperalgesia and Nociceptive Responses in Rats. *Neuroreport* **2001**, *12* (4), 715–719.
293. Cenac, N.; Andrews, C. N.; Holzhausen, M.; Chapman, K.; Cottrell, G.; Andrade-Gordon, P.; Steinhoff, M.; Barbara, G.; Beck, P.; Bunnett, N. W.; et al. Role for Protease Activity in Visceral Pain in Irritable Bowel Syndrome. *Journal of Clinical Investigation* **2007**, *117* (3), 636–647.
294. Wang, P.; Chen, F. X.; Du, C.; Li, C. Q.; Yu, Y. B.; Zuo, X. L.; Li, Y. Q. Increased Production of BDNF in Colonic Epithelial Cells Induced by Fecal Supernatants from Diarrheic IBS Patients. *Sci Rep* **2015**, *5*.
295. Ceuleers, H.; Hanning, N.; Heirbaut, J.; Van Remoortel, S.; Joossens, J.; Van Der Veken, P.; Francque, S. M.; De Bruyn, M.; Lambeir, A.-M.; De Man, J. G.; et al. Newly Developed Serine Protease Inhibitors Decrease Visceral Hypersensitivity in a Post-Inflammatory Rat Model for Irritable Bowel Syndrome. *Br J Pharmacol* **2018**, *175*, 3516–3533.
296. Ceuleers, H.; Hanning, N.; de bruyn, M.; de Man, J. G.; de Schepper, H. U.; Li, Q.; Liu, L.; Abrams, S.; Smet, A.; Joossens, J.; et al. The Effect of Serine Protease Inhibitors on Visceral Pain in Different Rodent Models With an Intestinal Insult. *Front Pharmacol* **2022**, *13*, 1850.

-
297. Zhao, J.; Wang, J.; Dong, L.; Shi, H.; Wang, Z.; Ding, H.; Shi, H.; Lu, X. A Protease Inhibitor against Acute Stress-Induced Visceral Hypersensitivity and Paracellular Permeability in Rats. *Eur J Pharmacol* **2011**, *654* (3), 289–294.
298. Hanning, N.; de bruyn, M.; Ceuleers, H.; Boogaerts, T.; Berg, M.; Smet, A.; de Schepper, H. U.; Joossens, J.; van Nuijs, A. L. N. N.; de Man, J. G.; et al. Local Colonic Administration of a Serine Protease Inhibitor Improves Post-Inflammatory Visceral Hypersensitivity in Rats. *Pharmaceutics* **2021**, *13* (6), 811.
299. Moussa, L.; Bézirard, V.; Salvador-Cartier, C.; Bacquié, V.; Lencina, C.; Lévêque, M.; Braniste, V.; Ménard, S.; Théodorou, V.; Houdeau, E. A Low Dose of Fermented Soy Germ Alleviates Gut Barrier Injury, Hyperalgesia and Faecal Protease Activity in a Rat Model of Inflammatory Bowel Disease. *PLoS One* **2012**, *7* (11), e49547.
300. Moussa, L.; Bézirard, V.; Salvador-Cartier, C.; Bacquié, V.; Houdeau, E.; Théodorou, V. A New Soy Germ Fermented Ingredient Displays Estrogenic and Protease Inhibitor Activities Able to Prevent Irritable Bowel Syndrome-like Symptoms in Stressed Female Rats. *Clinical Nutrition* **2013**, *32* (1), 51–58.
301. Aoyama, T.; Ino, Y.; Ozeki, M.; Oda, M.; Sato, T.; Koshiyama, Y.; Suzuki, S.; Fujita, M. Pharmacological Studies of FUT-175, Nafamstat Mesilate I. Inhibition of Protease Activity in in Vitro and in Vivo Experiments. *The Japanese Journal of Pharmacology* **1984**, *35* (3), 203–227.
302. Iwaki, M.; Ino, Y.; Motoyoshi, A.; Ozeki, M.; Sato, T.; Kurumi, M.; Aoyama, T. Pharmacological Studies of FUT-175, Nafamostat Mesilate V. Effects on the Pancreatic Enzymes and Experimental Acute Pancreatitis in Rats. *The Japanese Journal of Pharmacology* **1986**, *41* (2), 155–162.
303. Oleksyszyn, J.; Boduszek, B.; Kam, C. M.; Powers, J. C. Novel Amidine-Containing Peptidyl Phosphonates as Irreversible Inhibitors for Blood Coagulation and Related Serine Proteases. *J Med Chem* **1994**, *37* (2), 226–231.
304. Negrier, C.; Shima, M.; Hoffman, M. The Central Role of Thrombin in Bleeding Disorders. *Blood Rev* **2019**, *38*, 100582.

305. Ramos-Llorca, A.; Scarpellini, C.; Augustyns, K. Proteases and Their Potential Role as Biomarkers and Drug Targets in Dry Eye Disease and Ocular Surface Dysfunction. *Int J Mol Sci* **2022**, *23* (17), 9795.
306. Ness, T. J.; Gebhart, G. F. Colorectal Distension as a Noxious Visceral Stimulus: Physiologic and Pharmacologic Characterization of Pseudoaffective Reflexes in the Rat. *Brain Res* **1988**, *450* (1–2), 153–169.
307. Ceradini, D.; Cacivkins, P.; Ramos-Llorca, A.; Shubin, K. Improved Synthesis of the Selected Serine Protease UPA Inhibitor UAMC-00050, a Lead Compound for the Treatment of Dry Eye Disease. *Organic Process Research & Development* **2022**, *26* (10), 2937–2946.
308. Walker, B.; Wharry, S.; Hamilton, R. J.; Martin, S. L.; Healy, A.; Walker, B. J. Asymmetric Preference of Serine Proteases toward Phosphonate and Phosphinate Esters. *Biochem Biophys Res Commun* **2000**, *276* (3), 1235–1239.
309. Aykul, S.; Martinez-Hackert, E. Determination of Half-Maximal Inhibitory Concentration Using Biosensor-Based Protein Interaction Analysis. *Anal Biochem* **2016**, *508*, 97–103.
310. Gladysz, R.; Adriaenssens, Y.; de Winter, H.; Joossens, J.; Lambeir, A. M.; Augustyns, K.; van der Veken, P. Discovery and SAR of Novel and Selective Inhibitors of Urokinase Plasminogen Activator (UPA) with an Imidazo[1,2-A]Pyridine Scaffold. *J Med Chem* **2015**, *58* (23), 9238–9257.
311. Schwartz, L. B.; Bradford, T. R. Regulation of Trypsin from Human Lung Mast Cells by Heparin. Stabilization of the Active Tetramer. *Journal of Biological Chemistry* **1986**, *261* (16), 7372–7379.
312. Tanaka, T.; McRae, B. J.; Cho, K.; Cook, R.; Fraki, J. E.; Johnson, D. A.; Powers, J. C. Mammalian Tissue Trypsin-like Enzymes. Comparative Reactivities of Human Skin Trypsin, Human Lung Trypsin, and Bovine Trypsin with Peptide 4-Nitroanilide and Thioester Substrates. *Journal of Biological Chemistry* **1983**, *258* (22), 13552–13557.

313. Ono, S.; Kuwahara, S.; Takeuchi, M.; Sakashita, H.; Naito, Y.; Kondo, T. Syntheses and Evaluation of Amidinobenzofuran Derivatives as Tryptase Inhibitors. *Bioorg Med Chem Lett* **1999**, *9* (23), 3285–3290.
314. Rice, K. D.; Gangloff, A. R.; Kuo, E. Y. L.; Dener, J. M.; Wang, V. R.; Lum, R.; Newcomb, W. S.; Havel, C.; Putnam, D.; Cregar, L.; et al. Dibasic Inhibitors of Human Mast Cell Tryptase. Part 1: Synthesis and Optimization of a Novel Class of Inhibitors. *Bioorg Med Chem Lett* **2000**, *10* (20), 2357–2360.
315. Combrink, K. D.; Gülgeze, H. B.; Meanwell, N. A.; Pearce, B. C.; Zulan, P.; Bisacchi, G. S.; Roberts, D. G. M.; Stanley, P.; Seiler, S. M. 1,2-Benzisothiazol-3-One 1,1-Dioxide Inhibitors of Human Mast Cell Tryptase. *J Med Chem* **1998**, *41* (24), 4854–4860.
316. Copeland, R. A. *Evaluation of Enzyme Inhibitors in Drug Discovery A Guide for Medicinal Chemists and Pharmacologists*; Wiley, 2013.
317. McWhirter, C. Kinetic Mechanisms of Covalent Inhibition. In *Annual Reports in Medicinal Chemistry*; Academic Press Inc., 2021; Vol. 56, pp 1–31.
318. Fang, H.; Peng, B.; Ong, S. Y.; Wu, Q.; Li, L.; Yao, S. Q. Recent Advances in Activity-Based Probes (ABPs) and Affinity-Based Probes (A f BPs) for Profiling of Enzymes. *Chem Sci* **2021**, *12* (24), 8288–8310.
319. Carvalho, L. A. R. R.; Ruivo, E. F. P. P.; Lucas, S. D.; Moreira, R. Activity-Based Probes as Molecular Tools for Biomarker Discovery. *Medchemcomm* **2015**, *6* (4), 536–546.
320. Yao, T.; Xu, X.; Huang, R. Recent Advances about the Applications of Click Reaction in Chemical Proteomics. *Molecules* **2021**, *26* (17), 5368.
321. Poreba, M.; Rut, W.; Vizovisek, M.; Groborz, K.; Kasperkiewicz, P.; Finlay, D.; Vuori, K.; Turk, D.; Turk, B.; Salvesen, G. S.; et al. Selective Imaging of Cathepsin L in Breast Cancer by Fluorescent Activity-Based Probes. *Chem Sci* **2018**, *9* (8), 2113–2129.
322. Elvas, F.; vanden Berghe, T.; Adriaenssens, Y.; Vandenabeele, P.; Augustyns, K.; Staelens, S.; Stroobants, S.; van der Veken, P.; Wyffels, L. Caspase-3 Probes for PET Imaging of Apoptotic Tumor Response to Anticancer Therapy. *Org Biomol Chem* **2019**, *17* (19), 4801–4824.

323. Kallemeijn, W. W.; Li, K.-Y.; Witte, M. D.; Marques, A. R. A.; Aten, J.; Scheij, S.; Jiang, J.; Willems, L. I.; Voorn-Brouwer, T. M.; van Roomen, C. P. A. A.; et al. Novel Activity-Based Probes for Broad-Spectrum Profiling of Retaining β -Exoglucosidases In Situ and In Vivo. *Angewandte Chemie* **2012**, *124* (50), 12697–12701.
324. Yee, M.; Fas, S. C.; Stohlmeyer, M. M.; Wandless, T. J.; Cimprich, K. A. A Cell-Permeable, Activity-Based Probe for Protein and Lipid Kinases. *Journal of Biological Chemistry* **2005**, *280* (32), 29053–29059.
325. Kalesh, K. A.; Tan, L. P.; Lu, K.; Gao, L.; Wang, J.; Yao, S. Q. Peptide-Based Activity-Based Probes (ABPs) for Target-Specific Profiling of Proteintyrosine Phosphatases (PTPs). *Chem. Commun.* **2010**, *46* (4), 589–591.
326. Wang, G.; Mahesh, U.; Chen, G. Y. J.; Yao, S. Q. Solid-Phase Synthesis of Peptide Vinyl Sulfones as Potential Inhibitors and Activity-Based Probes of Cysteine Proteases. *Org Lett* **2003**, *5* (5), 737–740.
327. Kato, D.; Boatright, K. M.; Berger, A. B.; Nazif, T.; Blum, G.; Ryan, C.; Chehade, K. A. H.; Salvesen, G. S.; Bogyo, M. Activity-Based Probes That Target Diverse Cysteine Protease Families. *Nat Chem Biol* **2005**, *1* (1), 33–38.
328. Geurink, P. P.; Klein, T.; Prèly, L.; Paal, K.; Leeuwenburgh, M. A.; van der Marel, G. A.; Kauffman, H. F.; Overkleeft, H. S.; Bischoff, R. Design of Peptide Hydroxamate-Based Photoreactive Activity-Based Probes of Zinc-Dependent Metalloproteases. *European J Org Chem* **2010**, *2010* (11), 2100–2112.
329. Reihill, J. A.; Walker, B.; Hamilton, R. A.; Ferguson, T. E. G.; Elborn, J. S.; Stutts, M. J.; Harvey, B. J.; Saint-Criq, V.; Hendrick, S. M.; Martin, S. L. Inhibition of Protease–Epithelial Sodium Channel Signaling Improves Mucociliary Function in Cystic Fibrosis Airways. *Am J Respir Crit Care Med* **2016**, *194* (6), 701–710.
330. Martin, S. L.; Walker, B. Preparation of Protease-Specific Probes Containing Succinyl Moiety for Use in Complex Biological Samples for Diagnostic Applications. WO2011024006A1, 2011.

331. Breugst, M.; Reissig, H. The Huisgen Reaction: Milestones of the 1,3-Dipolar Cycloaddition. *Angewandte Chemie International Edition* **2020**, *59* (30), 12293–12307.
332. Hamilton, R.; Walker, B. J.; Walker, B. A Convenient Synthesis of N-Protected Diphenyl Phosphonate Ester Analogues of Ornithine, Lysine and Homolysine. *Tetrahedron Lett* **1993**, *34* (17), 2847–2850.
333. Ceradini, D.; Shubin, K. One-Pot Synthesis of α -Aminophosphonates by Yttrium-Catalyzed Birum–Oleksyszyn Reaction. *RSC Adv* **2021**, *11* (62), 39147–39152.
334. Borsari, C.; Keles, E.; McPhail, J. A.; Schaefer, A.; Sriramaratnam, R.; Goch, W.; Schaefer, T.; de Pascale, M.; Bal, W.; Gstaiger, M.; et al. Covalent Proximity Scanning of a Distal Cysteine to Target PI3K α . *J Am Chem Soc* **2022**, *144* (14), 6326–6342.
335. Tuley, A.; Fast, W. The Taxonomy of Covalent Inhibitors. *Biochemistry* **2018**, *57* (24), 3326–3337.
336. Benoist, C.; Mathis, D. Mast Cells in Autoimmune Disease. *Nature* **2002**, *420* (6917), 875–878.
337. Caughey, G. H. Mast Cell Proteases as Pharmacological Targets. *Eur J Pharmacol* **2016**, *778*, 44–55.
338. Pejler, G.; Åbrink, M.; Ringvall, M.; Wernersson, S. Mast Cell Proteases. In *Advances in Immunology*; Academic Press, 2007; Vol. 95, pp 167–255.
339. Le, Q. T.; Lyons, J. J.; Naranjo, A. N.; Olivera, A.; Lazarus, R. A.; Metcalfe, D. D.; Milner, J. D.; Schwartz, L. B. Impact of Naturally Forming Human α/β -Tryptase Heterotetramers in the Pathogenesis of Hereditary α -Tryptasemia. *Journal of Experimental Medicine* **2019**, *216* (10), 2348–2361.
340. Böttcher, T.; Sieber, S. A. β -Lactones as Specific Inhibitors of ClpP Attenuate the Production of Extracellular Virulence Factors of Staphylococcus Aureus. *J Am Chem Soc* **2008**, *130* (44), 14400–14401.
341. Kumar, V.; Bharate, S. B.; Vishwakarma, R. A.; Bharate, S. S. Selection of a Water-Soluble Salt Form of a Preclinical Candidate, IIIM-290: Multiwell-Plate Salt Screening and Characterization. *ACS Omega* **2018**, *3* (7), 8365–8377.

342. de la Fuente, M.; Rodríguez-Agirretxe, I.; Vecino, E.; Astigarraga, E.; Acera, A.; Barreda-Gómez, G. Elevation of Tear MMP-9 Concentration as a Biomarker of Inflammation in Ocular Pathology by Antibody Microarray Immunodetection Assays. *Int J Mol Sci* **2022**, *23* (10), 5639.
343. Walker, B.; Lynas, J. F. Strategies for the Inhibition of Serine Proteases. *Cellular and Molecular Life Sciences* **2001**, *58* (4), 596–624.

SCIENTIFIC CURRICULUM VITAE

Scientific Curriculum Vitae

Frist Name Alba
Surname Ramos Llorca
Date of birth September 22nd 1994
Place of birth Santa Coloma de Gramanet, Barcelona (Spain)

Education

2016-2018 **Master of Science in Drug Development and Safety**
Vrije Universiteit Amsterdam, Amsterdam (The Netherlands)
Final master thesis at the laboratory of Prof. dr. Rob Leurs

2016-2018 **Master of Science in Medicinal Chemistry**
University of Copenhagen, Copenhagen (Denmark)

2012-2016 **Bachelor of Science in Chemistry**
Institut Quimic de Sarria, Ramon Llull University, Barcelona (Spain)
Final bachelor thesis at the laboratory of Prof. dr. José I. Borrell

Experience

2018-2022 **PhD in Pharmaceutical Sciences**
IT-DED³ Marie Curie Sklodowdoska-Curie Actions, Horizon 2020
University of Antwerp, Antwerp (Belgium)
Laboratory of Medicinal Chemistry

2021 **Industrial secondment**
Symeres, Nijmegen (The Netherlands)

2021 **Academic secondment**
Latvian Institue of Organic Synthesis, Riga (Latvia)

Scientific publications

Alba Ramos-Llorca, Lisse Decraecker, Valerie Cacheux, Irena Zeiburlina, Michelle De bruyn, Louise Battut, Carlos Moreno-Cinos, Davide Ceradini, Eric Espinosa, Gilles Dietrich, Maya Berg, Ingrid De Meester, Pieter Van Der Veken, Guy Boeckstaens, Anne-Marie Lambeir, Alexandre Denadai-Souza and Koen Augustyns. Chemically Diverse Activity-Based Probes With Unexpected Inhibitory Mechanisms Targeting Trypsin-Like Serine Proteases. *Front. Chem.*, **2023**, *10*, 1089959.

Camilla Scarpellini, **Alba Ramos-Llorca**, Caroline Lanthier, Greta Klejborowska, Koen Augustyns. The Potential Role of Regulated Cell Death in Dry Eye Diseases and Ocular Surface Dysfunction. *Int. J. Mol. Sci.* **2023**, *24*, 731.

Davide Ceradini, Pavel Cacivkis, **Alba Ramos-Llorca**, Kirikk Shubin. Improved Synthesis of the Selected Serine Protease uPA Inhibitor UAMC-00050, a Lead Compound for the Treatment of Dry Eye Disease. *Org. Process Res. Dev.* **2022**, *26*, *10*, 2937-2946.

Alba Ramos-Llorca, Camila Scarpellini, Koen Augustyns. Proteases and Their Potential Role as Biomarkers and Drug Targets in Dry Eye Disease and Ocular Surface Dysfunction. *Int. J. Mol. Sci.* **2022**, *23*, 9795.

Maarten Sijm, Julianna Siciliano de Araújo, **Alba Ramos-Llorca**, Kristina Orrling, Lydia Stiny, An Matheeussen, Louis Maes, Iwan JP de Esch, Maria de Nazaré Correia Soeiro, Geert Jan Sterk, Rob Leurs. Identification of Phenylpyrazolone Dimers as a New Class of Anti-*Trypanosoma cruzi* Agents. *ChemMedChem* **2019**, *14*, 1662.

Oral presentations

Dry Eye Drug Development from the lab to the upscaling. Presented during the European Dry Eye Society Conference - EuDEC **2021**, Paris, France.

Synthesis and characterization of activity-based probes to identify novel therapeutic and diagnostic targets for dry eye disease and irritable bowel syndrome. Presented during the Chemistry Conference for Young Scientists - ChemCYS **2020**, Blankenberge, Belgium.

Poster presentations

Alba Ramos-Llorca, Lisse Decraecker, Valerie Cacheux, Irena Zeiburlina, Michelle De bruyn, Louise Battut, Carlos Moreno-Cinos, Davide Ceradini, Eric Espinosa, Gilles Dietrich, Maya Berg, Ingrid De Meester, Pieter Van Der Veken, Guy Boeckxstaens, Anne-Marie Lambeir, Alexandre Denadai-Souza and Koen Augustyns. Activity-based Probes Targeting Trypsin-like Serine Proteases For Target And Biomarker Discovery. Presented during the EFMC International Symposium on Medicinal Chemistry **2022**, Nice, France. (Flash Poster presentation)

Alba Ramos-Llorca, Valerie Cacheux, Carlos Moreno-Cinos, Pieter Van der Veken, Koen Augustyns. Synthesis and characterization of activity-based probes to identify novel therapeutic and diagnostic targets for dry eye disease and irritable bowel syndrome. Presented during the Chemistry Conference for Young Scientists - ChemCYS **2020**, Blankenberge, Belgium.

Alba Ramos-Llorca, Valerie Cacheux, Carlos Moreno-Cinos, Pieter Van der Veken, Koen Augustyns. Synthesis of functionalized probes to identify and validate novel therapeutic and diagnostic targets for dry eye disease and irritable bowel syndrome. Presented during the EFMC International Symposium on Advances in Synthetic and Medicinal Chemistry **2019**, Athens, Greece.

ACKNOWLEDGMENTS

Acknowledgments

Five years ago, in May 2018, when I was accepted position, I would have never imagined all the new experiences I would go through. During the last years, I have learned a lot and grown as a person and scientist. I rapidly made Antwerp my new home and found my place here, but this would not have been possible without the support of many others.

First of all, I would like to thank **Prof. Koen Augustyns** for giving me the opportunity to be part of the IT-DED³ consortium and perform my doctoral research at the University of Antwerp. **Koen**, thank you for all your support through the process. Thank you for always being reachable and for your advice and help when I struggled to get results. But also, thank you for giving me my space and freedom to make mistakes and learn from them. It was a pleasure having you as a supervisor.

I also would like to thank **Prof. Pieter Van Der Veken** for always having constructive input and many scientific discussions. Your impressive knowledge and your availability to help were of tremendous value.

To the members of my Internal Doctoral Committee, **Prof. Ingrid De Meester** and **Prof. Paul Cos**, I would like to extend my gratitude for your kind and constructive comments while developing this research and revising my thesis and the internal defense.

I want to thank the external jury members, **Prof. Rob Leurs** (VU Amsterdam) and **Prof. Steven Verhelst** (KU Leuven). Thank you for accepting the jury task and evaluating my thesis, your constructive remarks, and the green light to go to my public defense.

I would like to thank **Prof. Anne-Marie Lambeir** for your help in developing the enzymatic assays. When I reached out to you, your input and constructive comments were of utmost

help. Thank you for always sharing your remarkable knowledge in the field of enzyme kinetics with me. I have learned a lot from you.

During my first year as a PhD student, I had a warm welcome to the ABP project from **Dr. Valerie Cacheux**. Thanks to you, starting in a new lab and with new chemistry was easier. Thank you for always sharing your knowledge, your helpful guidance, and for always having a positive attitude.

I am incredibly grateful to our collaborators from the FWO-SBO TRP sensation consortium. I would like to recognize the assistance and work from **Prof. Alexandre Denadai Souza**, **Lisse Decraecker**, and **Irena Zeiburlina** from KU Leuven and **Dr. Michelle De bruyn** from UAntwerp for their support with the enzymatic assays and the labeling and visualization of the proteases with the ABPs. Moreover, I would like to extend my gratitude to the rest of the consortium for the constructive discussions during the different meetings.

Thanks also to the members of the IT-DED³ consortium for the many interesting scientific discussions. It was a pleasure sharing annual meetings and winter schools with all of you. Especially, thanks to **Dr. Davide Ceradini** for your warm welcome in Riga during my academic secondment and your contribution to this thesis. I also wish to thank **Dr. Helmus van de Langemheen** and **Dr. Peter Molenveld** for their welcome and guidance during my industrial secondment at Symeres.

During these four years at UAMC, I had the opportunity to work with many inspiring colleagues. The list is a long one, so I hope not to forget anyone, **Koen, Pieter, Hans, Sophie L., Camilla, Valerie, Karuna, Siham, Pedro, Kenneth, Rafaela, Johannes, Eduardo, Sophie V., Birgit, Muhammet, Thomas, Alejandro, Nicco, Nik, Theresa, Vanessa, Pawel, Gustavo, Roy, Roberta, Adrian, Caroline, Greta, Aaron, Henri-Philippe, Philipp, Margarida, Lorenzo, Murat, Maarten, Nikita, Magda, Louis, Nicolò, Sergei, Zunigha, Mélissa, Joep, Alan, and Olivier**, thank you for the excellent work atmosphere. Thank you for the many moments together during lunch breaks, group meetings, conferences, and “after-hours” events. I

want to give a special thanks to **Sophie Lyssens** because the lab would not work the same without you. Thanks for all your help. Thanks to **Alejandro**, gracias por estar siempre allí y hacer que UAMC estuviera un poquito más cerca de casa. And the most special thank you to **Camilla**. This PhD would not have been the same without you. It was a great support to go through it together. You are a big part of this PhD and a friend for life.

The process of the PhD has a lot of up-and-down moments. Some people outside the lab made this process easier, making the downs less downs and the ups more enjoyable.

I thank the **Jungle Gym Antwerp family** for the energy and super good atmosphere. The tough training is easier when the people around you help you. It was a great way to release tensions. Special thanks to all the coaches, **Enoch, Tom, Ilyach, Jules**, and **Stacy**, your push and motivation might be frustrating and tiring at first but always super rewarding.

My experience in Antwerp would not have been the same without my Belgian family, my friends. I want to thank **Jenny, Clara, Karina, Nath, Santi, Jeroen, Furkan** and **Zak**. You make my life in Belgium better and make me feel at home. I am happy we found each other, and we clicked. Even though we are all so different, something always unites us. Thank you for all the moments together and all those yet to come.

A very special thank you to **Maarten** for taking care of me and for your unconditional support. You are one of the best things that happened during the last years. Thank you for sharing your life with me.

L'últim i l'agraïment més important és per la **meva família** i la **Patri**. Gràcies a tots per sempre creure en mi. Sobretot gràcies a la **mama** i al **papa**. Gràcies per haver-me oferit la millor educació possible, per fer tots els esforços necessaris perquè jo estigui aquí. Sempre heu estat un gran exemple, gràcies per sempre estar al meu costat. Us estimo.

Thank you – Gracias – Gràcies – Dank u wel